ABSTRACT

Title of Dissertation: INTEGRATED THRESHOLD-ACTIVATED FEEDBACK MICROSYSTEM FOR REAL-TIME CHARACTERIZATION, SENSING AND TREATMENT OF BACTERIAL BIOFILMS

Sowmya Subramanian, Doctor of Philosophy, 2016

Dissertation directed by: Professor Reza Ghodssi, Department of Electrical and Computer Engineering, Institute for Systems Research

Biofilms are the primary cause of clinical bacterial infections and are impervious to typical amounts of antibiotics, necessitating very high doses for treatment. Therefore, it is highly desirable to develop new alternate methods of treatment that can complement or replace existing approaches using significantly lower doses of antibiotics. Current standards for studying biofilms are based on end-point studies that are invasive and destroy the biofilm during characterization. This dissertation presents the development of a novel real-time sensing and treatment technology to aid in the non-invasive characterization, monitoring and treatment of bacterial biofilms.

The technology is demonstrated through the use of a high-throughput bifurcation-based microfluidic reactor that enables simulation of flow conditions similar to indwelling medical devices. The integrated microsystem developed in this work incorporates the advantages of previous *in vitro* platforms while attempting to overcome some of their limitations.

Biofilm formation is extremely sensitive to various growth parameters that cause large variability in biofilms between repeated experiments. In this work we investigate the use of microfluidic bifurcations for the reduction in biofilm growth variance. The microfluidic flow cell designed here spatially sections a single biofilm into multiple channels using microfluidic flow bifurcation. Biofilms grown in the bifurcated device were evaluated and verified for reduced biofilm growth variance using standard techniques like confocal microscopy. This uniformity in biofilm growth allows for reliable comparison and evaluation of new treatments with integrated controls on a single device.

Biofilm partitioning was demonstrated using the bifurcation device by exposing three of the four channels to various treatments. We studied a novel bacterial biofilm treatment independent of traditional antibiotics using only small molecule inhibitors of bacterial quorum sensing (analogs) in combination with low electric fields. Studies using the bifurcation-based microfluidic flow cell integrated with real-time transduction methods and macro-scale end-point testing of the combination treatment showed a significant decrease in biomass compared to the untreated controls and well-known treatments such as antibiotics.

To understand the possible mechanism of action of electric field-based treatments, fundamental treatment efficacy studies focusing on the effect of the energy of the applied electrical signal were performed. It was shown that the total energy and not the type of the applied electrical signal affects the effectiveness of the treatment. The linear dependence of the treatment efficacy on the applied electrical energy was also demonstrated.

The integrated bifurcation-based microfluidic platform is the first microsystem that enables biofilm growth with reduced variance, as well as continuous real-time threshold-activated feedback monitoring and treatment using low electric fields. The sensors detect biofilm growth by monitoring the change in impedance across the interdigitated electrodes. Using the measured impedance change and user inputs provided through a convenient and simple graphical interface, a custom-built MATLAB control module intelligently switches the system into and out of treatment mode. Using this self-governing microsystem, *in situ* biofilm treatment based on the principles of the bioelectric effect was demonstrated by exposing two of the channels of the integrated bifurcation device to low doses of antibiotics.

INTEGRATED THRESHOLD-ACTIVATED FEEDBACK MICROSYSTEM FOR REAL-TIME CHARACTERIZATION, SENSING AND TREATMENT OF BACTERIAL BIOFILMS

By

Sowmya Subramanian

Dissertation submitted to the Faculty of the Graduate School of the
University of Maryland, College Park, in partial fulfillment
of the requirements for the degree of
Doctor of Philosophy
2016

Advisory Committee:
Professor Reza Ghodssi, Chair
Professor William Bentley
Professor Romel Gomez
Professor Agis Iliadis
Professor Ian White

Dedication

In memory of my loving father T.P. Subramanian (1952 – 2014). We miss you.

Acknowledgements

First, I would like to thank my advisor Prof. Reza Ghodssi for his constant guidance and support during this work. I would also like to thank my committee members, Prof. William Bentley, Prof. Romel Gomez, Prof. Agis Iliadis and Prof. Ian White for generously volunteering their time. I also am grateful to Prof. Romel Gomez for supporting me through my initial years in graduate school. I also acknowledge the funding agencies, Robert W. Deutsch Foundation and the National Science Foundation, without which this research would not have been possible.

I have been very fortunate in being able to work with so many supportive colleagues, some of whom have become very dear friends of mine. I acknowledge my mentors Dr. Mariana Meyer, Dr. Young Wook Kim and Dr. Konstantinos Gerasopoulos for their help during the formative years of my graduate school. I express my sincere gratitude to all the members, past and present, of the MEMS Sensors and Actuators Laboratory (MSAL) for their support in multiple ways. I especially thank Thomas Winkler, Faheng Zang, Hyun Jung, Sangwook Chu and George Banis for reviewing this manuscript and for supporting this work through thoughtful and critical discussions. I am also grateful to my undergraduate mentees Ms. Kathryn Schneider and Ms. Ekaterina Tolstaya for inspiring me to take risks in research. I also express my gratitude to Pamela White, Regina King and Vicci Barrett for patiently working with me on tedious logistics through these years.

This research would not have been possible without the continued support and collaboration of multiple facilities and laboratories. I recognize all my collaborators in the Maryland Biochip Collaborative for encouraging an amicable atmosphere for

interdisciplinary studies. I am especially grateful to Profs. William Bentley and Herman Sintim, and their students Tanya Tschirhart, Narendranath Bhokisham, Jess Terrell, Melissa Rhoads and Min Guo who welcomed me into their laboratory and helped me through my work. I truly express thanks to the Maryland NanoCenter and its Fablab staff, and also Amy Beaven and the University of Maryland Imaging Core Facility.

Finally, I would like to thank my family and friends for their support. I am extremely thankful to my parents for encouraging me to follow my dream, and my sister Sandhya and brother Shyam for being patient with me through these years. I am grateful to my in-laws for their unwavering faith in me. I am eternally indebted to my three-year old niece Twishaa, for uplifting my spirits when I needed it the most. I thank my aunt Hema and uncle Ramamurthy for being my local support system through these years. I also express thanks to my friends Sowmiya Subramanian, Filiz Yesilkoy, Timir Datta and Eduardo Arvelo for their expert technical advice and for being my moral and emotional crutch. Lastly, I would like to thank my husband Prashant, for being everything I need, wish and will ever dream of; for being the perfect companion and partner, and supporting me literally through life and death.

Thesis Contributions

1. Investigation of the use of microfluidic bifurcations for the reduction in biofilm growth variance.
2. Investigation of the effect of electrical energy on the treatment efficacy of the bioelectric effect.
3. Investigation of the synergistic effects of a combination therapy using AI-2 analog and electric fields.
4. Development of an impedimetric sensor with feedback for self-governing biofilm sensing and treatment.

Table of Contents

List of Tables

List of Figures

List of Abbreviations

AC: Alternating Current

AHL: Acyl-Homoserine Lactone

AI-1: Autoinducer-1

AI-2 Analog: Autoinducer-2 Analog

AI-2: Autoinducer-2

ANOVA: Analysis Of Variance

BE: Bioelectric Effect

CBR: CDC Biofilm Reactor

CCD: Charge Coupled Device

CFU: Colony Forming Unit

CHI: CH Instruments

DC: Direct Current

DMMB: Dimethyl Methylene Blue

DPD: 4,5-Dihydroxy-2,3-Pentanedione

ECM: Extracellular Matrix

eDNA: Extracellular DNA

EIS: Electrochemical Impedance Spectroscopy

EMA: Effective Medium Approximation

GFP: Green Fluorescence Protein

GUI: Graphical User Interface

HA: Hydroxyapatite

IDE: Interdigitated Electrodes

IM: Impedance Microbiology

KOH: Potassium Hydroxide

LB: Luria Broth/Luria Bertani

LOC: Lab-On-a-Chip

MIC: Minimum Inhibitory Concentration

MMT: Maxwell's Mixture Theory

OD: Optical Density

PBS: Phosphate Buffered Saline

PDMS: Polydimethylsiloxane

PIA: Polysaccharide Intercellular Adhesion

QS: Quorum Sensing

SAH: S-Adenosyl-L-Homocysteine

SAW: Surface Acoustic Wave

SDS: Sodium Dodecyl Sulfate

SEM: Scanning Electron Micrographs

Chapter 1. Introduction

1.1 Background and Motivation

Bacterial biofilms are a major cause of concern in the clinical field. They are the primary cause of clinical infections, commonly forming on medical devices like implants and catheters and also on respiratory tract surfaces and teeth [1,2]. It is estimated that 65% of all bacterial infections involve biofilms [3]. The high mutation rates and horizontal exchange of genetic material in biofilms promote antibiotic tolerance mechanism and result in high resistance to antibiotics [1,4-7]. It is estimated that biofilms require 500 – 5000× higher doses of antibiotics for treatment as compared to freely floating planktonic bacteria [1,6,8]. The use of such high doses of antibiotics has led to the emergence of antibiotic resistant strains [7]. Hence, there is an urgent need to develop alternate treatment methodologies that eliminate the need for such high doses of antibiotics.

While biofilms have been studied for decades [9,10], much is still unknown. Over the years, a number of *in vitro* models have been developed to not only understand the biology of biofilms but also to study the effect and biofilm response to external stimuli such as change in pH or exposure to antimicrobials [7,11-15]. However, no standard procedures have been identified for the characterization and study of biofilms. Moreover, the variability inherent to biological systems warrants the need for multiple experimental repeats in order to ensure reliability. Hence, biofilms grown *in vitro* show a high degree of growth variability both in between and within

platforms [16,17]. This prevents reliable comparison of treated biofilms to their controls.

Additionally, biofilm characterization and evaluation often rely on bulky external quantification equipment or laborious protocols that label components of the biofilm and destroy the biofilm itself [18,19]. Furthermore, maintaining the consistency of macroscale protocols is a challenge that adds to the variability of biofilms. Therefore, there is an urgent need to develop scalable and reliable systems that can quantify and characterize biofilms noninvasively. Microfluidic lab-on-a-chip (LOC) sensing platforms are an ideal solution to address this multi-faceted problem. Microfluidics provides several advantages including ease of fabrication, low reagent volumes and cost, and high throughput. Additionally, they can be readily integrated with sensing technologies that can be used to evaluate the biofilms in real time for label-free, continuous and noninvasive characterization of biofilm properties [20-52]. This doctoral research aims at developing a scalable microfluidic platform with integrated sensor-treatment modules for biofilm testing and treatment evaluation. It is anticipated that this integrated system will lay the foundation for rapid and reliable testing of clinically effective biofilm therapies.

1.2 Summary of Accomplishments

In this work we leverage the advantages of microfluidic LOC systems to develop a novel, high-throughput microfluidic platform for the rapid investigation of new alternative biofilm treatment methods that are independent of high doses of antibiotics. Specifically, this work focuses on the development of a high-throughput

microfluidic biofilm impedimetric sensor-treatment microsystem that can be used for biofilm evaluation and new treatment testing. Using this platform, a new combinatorial biofilm treatment that combines small molecule inhibitors, autoinducer-2 analog (AI-2 analog), with electric fields was evaluated. We envision that successful development of this sensor-treatment system will enable future technologies for active treatment for biofilm infections right at the onset of biofilm growth. For example, a prospective application of this technology would be integrating the sensor-treatment system into a simple indwelling medical device like a catheter. As a first step to enable this research four key objectives were investigated: development of high-throughput microfluidics, the investigation of the proposed combinatorial therapy using small molecule inhibitors and electric fields, investigation of the role of electric energy on the efficacy of the bioelectric effect (BE), and the development of the impedimetric sensor-treatment module. Each of these objectives is discussed in the following sub-sections.

1.2.1 Investigation of Biofilm Growth Variance in Bifurcation Microfluidics

For this work, an easy-to-fabricate, high-throughput PDMS based microfluidic device was developed. A PDMS mold using negative photoresist was fabricated and used to cast a simple PDMS device. The PDMS-based flow cell aided in mimicking clinical conditions, for example the flow rates observed in a urinary catheter. The microfluidics was tested for reduced biofilm growth variance, and flow rates and dimensions similar to *in vivo* models were used to allow for reliable testing of new treatments. The growth variance of the biofilms grown in these devices, as compared

to single channel microfluidics, was analyzed using traditional confocal microscopy. Biofilms grown in this platform exhibit only an 7.1% variation in thickness as compared to previously reported 68% variation in single channel microfluidics.

1.2.2 Investigation of the Effect of Electrical Energy on the Efficacy of the Bioelectric Effect

The second goal of this dissertation is to examine the effect of electrical energy on the efficacy of the bioelectric effect. The use of electric fields in combination with small doses of antibiotics for enhanced treatment of biofilms is termed the bioelectric effect (BE). Different mechanisms of action for the alternating current (AC) and direct current (DC) fields have been reported in the literature over the last two decades. In this work, we conduct the first study on the correlation between the electrical energy and the treatment efficacy of the BE on *Escherichia coli* K-12 W3110 biofilms. Our results demonstrate that the energy of the electrical signal, and not the type of electrical signal (AC or DC or SP), is the key to determine the efficacy of the BE treatment. We anticipate that this observation will pave the way for further understanding of the mechanism of action of the BE treatment method and open new doors to the use of electric fields in the treatment of bacterial biofilms.

1.2.3 Investigation of a Novel Combinatorial Therapy Using Small Molecule Inhibitors and Electric Fields

The third accomplishment of this work is to investigate a novel combinatorial therapy for bacterial biofilms. Specifically, small molecule inhibitors known as AI-2

analogs, were combined with electric fields. The efficacy of this treatment to treat mature biofilms was studied. Mature biofilms treated with this combination therapy showed a 46% decrease in biomass using a static macro-scale system and a 78% decrease in biofilm thickness using the dynamic microfluidic system, in comparison to the untreated control. Additional characterization and investigation of this therapy could lead to the development of a new bacterial biofilm treatment method that is independent of traditional antibiotics.

1.2.4 Development of an Impedimetric Sensor-Treatment System

The final objective of this research is the development of a noninvasive label-free sensing technology that allows for sensitive real-time monitoring of bacterial biofilms. An impedance sensor suitable for monitoring surface attachment events was used as the transducer in this LOC system. This impedimetric sensor was designed to operate in two modes: 1. Sensing mode (lower frequencies and volatges), and 2. Treatment mode (higher frequencies and voltages). The electrodes of the impedance sensor were used in the sensor mode to sense biofilm growth and in the treatment mode to apply electric fields in combination with antibiotics or small molecule inhibitors (analogs) to treat bacterial biofilms. A flowchart showing the feedback system is shown in Figure 1-1. The successful development of this sensor-treatment system will lay the foundation for integration of electric field-based biofilm sensors and treatments into medically relevant indwelling devices like catheters and stents.

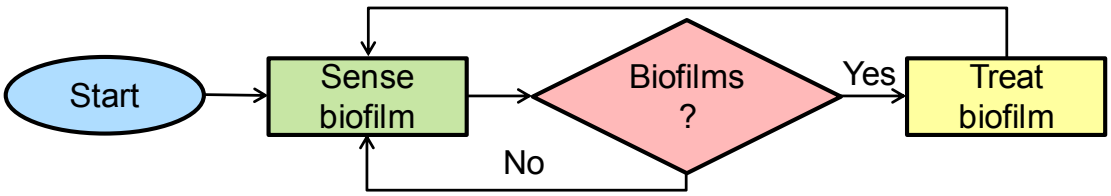

Figure 1-1 Flowchart showing the feedback to switch from sensing to treatment mode.

1.3 Literature Review

This section provides the necessary background and literature review as applicable to the presented work. First, a discussion of bacterial biofilms is presented with a focus on quorum sensing and the factors contributing to the increased severity of biofilm infections. Second, current treatment methods and new alternative methods of treatment under research are reviewed. Third, traditional methods of studying biofilms along with their advantages and disadvantages are discussed. Finally, LOC platforms with emphasis on microfluidic systems for biofilm studies are presented.

1.3.1 Bacterial Biofilms

Bacterial biofilms are complex communities of bacteria enveloped in a self-produced matrix of polysaccharides, proteins and extracellular DNA (eDNA), known as the extracellular matrix (ECM). Biofilm formation is initiated by the attachment of freely floating (otherwise known as planktonic) bacteria to surfaces. The adhesion, while initially reversible, is strengthened through the secretion of the ECM which promotes bacterial adhesion to the surface and also between the bacterial cells in the

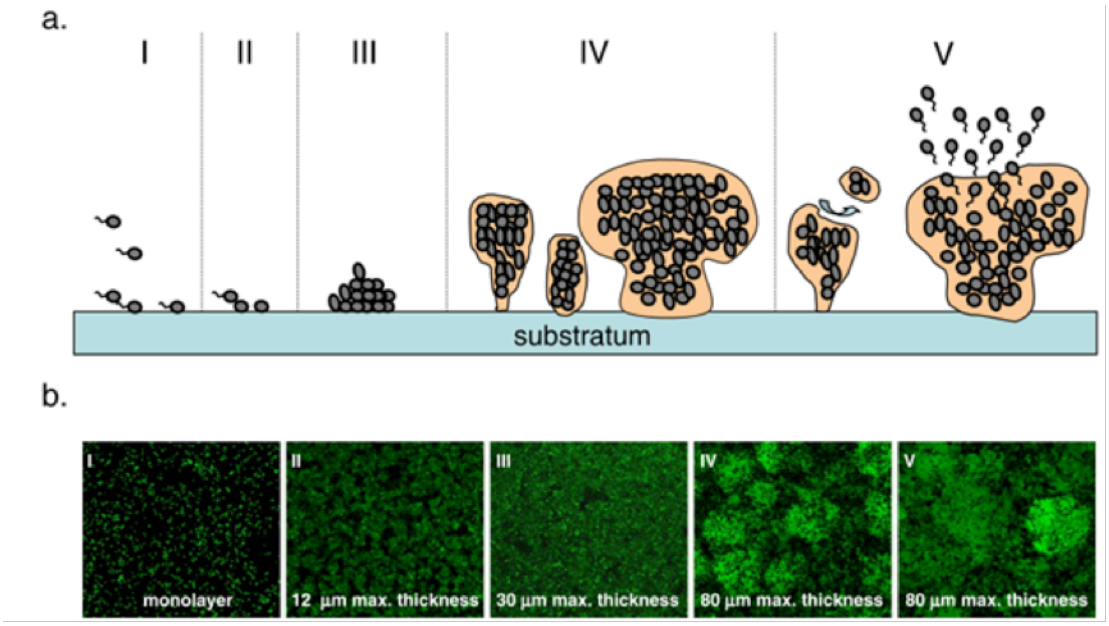

Figure 1-2 Life cycle of a biofilm. (a) Diagram of the biofilm growth cycle. (b) Pseudomonas aeruginosa PAO1 biofilms expressing green fluorescence protein (GFP) at various stages of growth. The stages of biofilm growth shown are (I) Reversible attachment, (II) Irreversible attachment, (III) Microcolony formation, (IV) 3D structure formation, and (V) Detachment or dispersion. Reproduced with permission from [53].

biofilm as shown in Figure 1-2. The ECM provides the biofilm with structural stability and also protects the bacteria from attack from the host's immune system [4,54]. It also plays a role in restricting the molecular diffusion of typical treatments like antibiotics, thereby necessitating higher doses of antibiotics for treatment [1,6]. The various stages of biofilm growth include reversible attachment (stage I), followed by irreversible attachment to the substrate (stage II). Following this, microcolonies are formed (stage III) and three-dimensional structures known as stalks and towers form as the biofilm matures (stage IV) The final stage involves the release of motile bacteria through rupture of the ECM or detachment of larger pieces of encased bacteria (stage V) [53].

Antibiotic Resistance

Bacterial biofilms are known to exhibit higher resistance to antibiotic treatment than planktonic (freely suspended) bacteria. There are a number of hypotheses concerning what mechanisms enable biofilm resistance to antibiotics [5,55]. First, the ECM itself can reduce the potency of antibiotics applied to biofilms. Antibiotics that interact with the ECM are often prevented from completely penetrating thick biofilm layers [56-58]. However, other studies have shown that slow diffusion of antibiotics through the ECM may not be a function of its composition, but rather of other factors secreted by the bacteria in the biofilm or of the type of antibiotic and bacterial species [59,60]. Second, horizontal gene transfer between the bacteria in the biofilm often promotes biofilm survival, as genes that regulate antibiotic and metal resistance are carried on plasmids that can be easily transferred between cells [61,62]. Third, the chemical environment within biofilms is believed to promote antibiotic tolerance by altering bacterial rates of metabolism and growth, thereby removing antibiotic targets [63]. Traditional antibiotics are known to target vital processes in actively growing bacteria, such as metabolism or cell wall production. Removal of these vital processes in bacteria in biofilms is thought to add to the antibiotic tolerance of biofilms. Finally, the differences in nutrient concentrations and deep anaerobic niches of the biofilm can lead to the formation of persister cells, which are inactive, dormant cells that can persist even on prolonged exposure to high doses of antibiotics. Persister cells can revert back to active cells under favorable conditions and restart the biofilm formation process [64,65].

The high antibiotic resistance of bacterial biofilms precludes the use of small doses of antibiotics for their treatment, thereby requiring significantly higher doses of

antibiotics (500 – 5000× in comparison to planktonic bacteria) for treatment [1,6]. Hence, there is an urgent need for alternate methods of treatment that can effectively and efficiently remove existing biofilms and prevent the onset of biofilm formation.

Quorum Sensing

Biofilm formation is triggered through a cell-to-cell communication mechanism known as quorum sensing (QS) [66-68]. QS molecules or autoinducers are secreted into the extracellular environment by the bacteria. Bacteria can detect the concentration of the autoinducers in the extracellular environment through nonspecific uptake of the molecule or through specific autoinducer binding receptors [69]. Once a threshold concentration of autoinducer molecules is attained, a genetic cascade regulating a number of QS genes is triggered. This is illustrated in Figure 1-3.

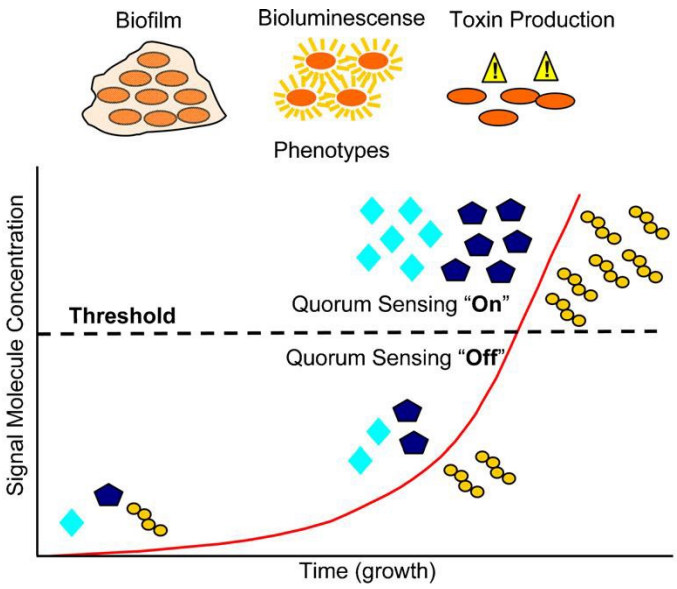

Figure 1-3 Schematic of phenotypes turned on by QS. Accumulation of greater than threshold level autoinducer molecules in the extracellular environment turns "on" QS. Reproduced with permission from [70].

QS is known to regulate numerous genes, and many of these genes control phenotypes associated with bacterial biofilm pathogenicity including toxin production and biofilm formation [69,70].

While different bacteria have different QS systems, the class of autoinducers known as autoinducer-2 or AI-2 is referred to as "universal" since its synthase, LuxS, is found in more than 70 species of bacteria [71]. AI-2 is believed to regulate the interspecies communication in many bacteria including *Vibrio harveyi, Salmonella typhimirium, Pseudomonas aeruginosa* and *Escherichia coli* [72-74]. AI-2 is synthesized intracellularly in a multi-step process. In *E. coli*, multiple enzymes are used to convert S-adenosyl-L-homocysteine (SAH) to 4,5-dihydroxy-2,3-pentanedione (DPD). DPD is then cyclized and undergoes further processing to form AI-2, which is then secreted. Once secreted, the extracellular AI-2 is imported into the cells through interactions with the AI-2 transporter as well as non-specific uptake [75]. Inside the cell, the AI-2 molecule is phosphorylated by LsrK, after which it interacts with the repressor LsrR, allowing for the transcription of the *lsr* operon, including genes regulating AI-2 uptake and processing [76].

Much work has been conducted to understand QS, as it controls a number of processes contributing to the formation of biofilms and toxin production by bacteria. *E. coli* strains that lack the AI-2 signaling regulators *lsrK* and *lsrR* have been observed to form thinner biofilms than the wild type [77]. Furthermore, addition of AI-2 to *E. coli* biofilms resulted in a 30-fold increase in biomass of the biofilm [78]. AI-2 has also been linked to cell motility and ECM production [78-80].

While AI-2 is primarily used for interspecies communication, another class of autoinducers, called autoinducer-1 (AI-1) is used for intraspecies communication. *P. aeruginosa* uses QS extensively to modulate both biofilm formation and maturation, using acyl-homoserine lactone (AHL) molecules in autoinducer-1 (AI-1) signaling. It has been shown that *P. aeruginosa* deficient in producing AHLs formed thinner biofilms that were more sensitive to detergents compared to wild-type biofilms [81]. Although *P. aeruginosa* primarily uses the AI-1 QS system and does not produce AI-2, gene expression in this species can still be regulated by extracellular AI-2 present in the surrounding environment [82]. The genes regulated by AI-2 include virulence genes implying that AI-2 is capable of altering the *P. aeruginosa* gene expression and pathogenicity [82].

An additional contributor to chronic biofilm infections are persister cells. Persisters, as discussed earlier are dormant variants of regular cells that form stochastically in microbial populations and are highly tolerant to antibiotics. Interestingly, QS does not appear to have an effect on the formation of these cells. Initial evidence suggests that presence of AI-2 does not increase or decrease the incidence of persister cells [65].

While QS in itself is not required for the growth and survival of bacteria, it is the key mechanism responsible for the severity and pathogenicity of infections. Hence, understanding this mechanism has been a key focus over the past two decades. Additionally, research involving development of methods to inhibit QS has been pursued as an alternative treatment method [83-85]. QS inhibition and other methods of biofilm treatment are discussed in the next section.

1.3.2 Biofilm Treatments

The high resistance to antibiotics renders traditional antibiotic therapy ineffective in treating biofilm infections. Hence alternate methods of treatment for both preventing and treating biofilms are being pursued by the scientific community at large. Some of these alternative treatment methods are discussed in this section.

Antimicrobial Coatings

In the pathogenesis of biofilm infection around implants, initial adhesion of bacteria onto biomaterial surfaces is believed to be a critical event [86]. For example, titanium, a biomedical implant material of choice due to its biocompatibility, is known to be susceptible to bacterial colonization and biofilm infections because of a surface protein layer that is formed under physiological conditions [87-90]. Since antibiotic treatments are ineffective in treating implant related biofilm infections, one of the major biofilm treatment methods under research is the use of antimicrobial surface coatings or surface modifications to prevent biofilm formation.

Antibiotic loaded coatings for implants have been tested in both *in vitro* and *in vivo* models as a method for preventing implant related biofilm infections. Specifically, antibiotics have been loaded into porous hydroxyapatite (HA) or sol-gel coatings on titanium implants [91,92]. The antibiotic-HA coatings show an improved prevention of infections compared to standard HA coatings in *in vivo* models, although fabrication of these coatings with clinical relevant doses of antibiotics and timely release of the antibiotics are a challenge [93-98]. Besides antibiotic-releasing coatings, there is interest in covalent bonding of drugs to the implant surface to

realize long lasting antibacterial ability. Unlike non-covalent coatings, covalently bonded antibiotics are not released from the surface during bacterial infections. This method has shown some promise as these modified surfaces exhibit prolonged prevention of biofilm formation when tested using *in vitro* models. However, a protein layer is formed on the surface under physiological conditions and the efficacy of the covalently bonded antibiotics in preventing biofilm formation *in vivo* is still under doubt [87]. Although antibiotic coatings (covalent and non-covalent) seem promising there are many outstanding issues. Apart from the challenges of fabrication and the timely release of the drug, the use of antibiotics could potentially lead to the emergence of many more antibiotic-resistant strains. Furthermore, it has been reported that some drug carriers release the antibiotics at levels below the minimum inhibitory concentration (MIC) for long after the implantation (~ 6 years) [99]. Such prolonged exposure could lead to toxic side effects including damage to DNA, proteins and lipids in human cells that may harm regular cellular functions [100,101].

To avoid the risk of emergence of antibiotic resistance strains as a result of use of antibiotic coated surfaces to treat biofilms, non-antibiotic coatings like chlorhexidine, chloroxylenol, and poly(hexamethylenebiguanide) have been investigated [102,103]. However, several studies have suggested that use of these non-antibiotic antimicrobials may cause cell damage [100]. Furthermore, effective ways to fabricate these antimicrobials and controlled elution still remain a challenge.

One of the inorganic antimicrobial agents that has shown some promise as an infection-preventing surface modification in the recent past is silver. Some of the advantages of using silver-doped surfaces are that it prevents bacterial adhesion, has

broad antibacterial spectrum to both Gram-positive and Gram-negative bacteria and most importantly is believed to be less prone to resistance development [104-107]. Initial *in vitro* studies show that silver has excellent biocompatibility without genotoxicity or cytotoxicity and *in vivo* studies have indicated that silver coatings have no local or systemic side-effects [108-110]. Additionally, fabrication of silver doped materials is easy due to the stability of the element. While other inorganic antimicrobial agents like zinc, copper, calcium, fluorine, and nitrogen have been studied, none have been as widely investigated as silver [111]. However the mechanism of antimicrobial activity of silver is still not well understood and further clarification of its bactericidal properties is much need to broaden its clinical applications. Also some research suggests that use of silver compounds can not only lead to development of bacterial resistance but also toxicity in rats [112-115]. Hence, further investigation into the potential side effects of silver as a biofilm inhibiting agent is required.

Surface Modifications

The surface characteristics like surface chemistry, surface energy, roughness, hydrophobicity, and surface potential play a crucial role in the initial adhesion of and growth of bacteria on the surface. Hence a bacterial adhesion-resistant surface can be fabricated by modifying these surface properties.

Various studies implementing different surface modifications including modification of the physical and chemical properties of the surface through UV irradiation or changing the crystalline structure of the surface oxide have been

conducted [116,117]. Anti-adhesive surface polymers have also been developed and their anti-adhesion properties were tested in both *in vitro* and *in vivo* models [118-120]. In *in vivo* systems, although the adsorption of plasma proteins encourages biofilm formation, microbial growth is strongly delayed on the coated surfaces [120]. Biofunctionalization with antibacterial bioactive polymers like chitosan and hyaluronic acid have also been performed. These polymers possess the ability to inhibit bacterial adhesion and/or kill the bacteria [121-123]. Chitosan is noted for various biological properties including biocompatibility, biodegradability into harmless products, nontoxicity, physiological inertness, remarkable affinity to proteins, and antibacterial, hemostatic, fungistatic, antitumoral, and anticholesteremic properties [124]. However, the binding affinity and bonding strength of chitosan to various materials is smaller than that reported for other coatings. Also, further *in vivo* studies to understand its performance are necessary for the widespread use of chitosan as an antimicrobial surface coating.

Surface microtopography has also been shown to play a crucial role in bacterial adhesion and biofilm formation. It has been observed that some unique patterns or certain surface microtopographies prevent microorganisms from settling and growing on the patterned surface. For example, Sharklet^{TM}, an ordered, microscopic surface pattern, inspired by the skin of sharks, is micropatterned as an anti-adhesion surface treatment [125,126]. The skin of sharks was chosen as the ideal surface topography, as the shark is the only mobile marine creature whose skin does not foul. It is hypothesized that the distinct diamond pattern with tiny riblets on the shark's skin

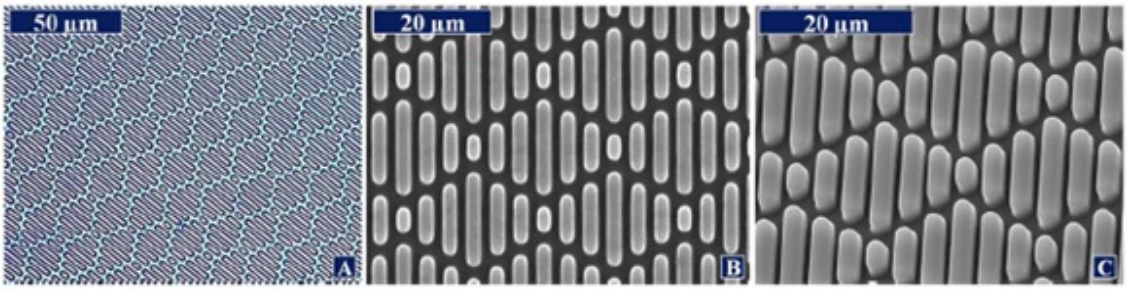

Figure 1-4 Sharklet™ topography with 2 µm feature width and spacing and 3 µm feature height. (A) Light micrograph of sharklet topography on PDMS. (B) and (C) Scanning electron micrographs (SEMs) captured at different angles. Reproduced with permission from [127].

prevents the adhesion and growth of microorganisms on it. The Sharklet™ micropattern, fabricated using PDMS shown in Figure 1-4, was observed to delay the onset of bacterial colonization. The smooth PDMS surface exhibited early-stage biofilm colonies at 7 days and mature biofilms at 14 days, while the topographically modified surface did not show evidence of early biofilm colonization until day 21. [127]. Other microtopographies for biofilm prevention are currently under investigation, as is optimization of the dimensions of the topographies [128,129].

Bioelectric Effect

Application of electric fields in combination with antibiotics has been observed to enhance the biocidal effect of the antibiotics in a phenomenon termed the bioelectric effect [130,131]. A number of hypotheses for the mechanism of action of the enhanced biocidal effect have been proposed. One of these suggests that the application of electric fields promotes the penetration of the antibiotic into the biofilm either through the application of an electrophoretic force or due to an increase in the permeability of the ECM [130,132,133]. An increased concentration of antibiotics

inside the biofilm results in an improved treatment efficacy of the antibiotic. It has also been suggested that the electrochemical generation of various oxidant species due to the application of electric fields may play a significant role in the increased efficacy of this treatment method. Also, the delivery of increased oxygen to the biofilm due to electrolysis may be the cause for this enhanced treatment efficacy [130,132,134]. Yet other research postulates that the biofilm may expand and contract depending on the polarity of an applied alternating current electric field, and thereby enhance convective transport of antibiotics into the biofilm [132].

The BE throughout literature, has been implemented by application of either an AC or DC field in combination with antibiotics. In our group, a super-imposed electrical signal was applied in combination with near-MIC levels of antibiotics [135,136]. The use of different modes of electrical energy (AC and DC) allowed for the application of higher electrical energies, at which significant inhibition was observed, using lower voltages that were below the limit for water electrolysis (0.82 V). This is an important advancement in the field of biofilm treatment, as this allowed for the application of higher energy BE without the generation of gaseous species within the solution. Previous work in our group conducted by Kim et al. further demonstrates the efficacy of the BE without any significant bulk electrolysis. While localized hydrolysis may be a contributing factor to the biofilm removal by the BE, the exact mechanism of action is still unknown. Furthermore, characterization and optimization of the electrical parameters and the antibiotic concentration needs to be performed in order to ensure that the electrochemically generated products do not

damage the surrounding microflora or host cells near the biofilm when an electric field is applied.

Quorum Sensing Inhibition

QS inhibition is considered an ideal biofilm treatment method as QS does not influence cell growth or viability. Consequently, many research groups have developed new QS inhibitors and many studies have been performed on QS inhibitors with the hypothesis that development of resistance to these inhibitors will either not occur or will be delayed. Much work has been performed in developing such inhibitors, analogs of AHLs and AI-2 [83-85]. The effect of these analogs on QS and biofilm formation has been studied and verified [137,138]. *In vitro* and *in vivo* studies show that these small molecule inhibitors or analogs prevent biofilm formation and work synergistically with antibiotics [139-141].

Since AI-2-based QS is found in over 70 species of bacteria, AI-2 analog development may have significant impact in controlling and treating biofilm infections [83]. Many AI-2 analogs have been shown to be effective QS inhibitors [73,142,143]. In previous work conducted by our collaborators, C-1 alkyl analogs of AI-2, including isobutyl-DPD, were developed and demonstrated to be highly effective broad species QS inhibitors in *E. coli, S. typhimurium* and *V. harveyi* [141,144]. An illustration of the mechanism of action of AI-2 analogs in *E. coli* is shown in Figure 1-5. Isobutyl-DPD is phosphorylated by LsrK in *E. coli* and inhibits QS-related *lsr* expression in the presence of the repressor of the circuit LsrR [143].

Gamby et al. also showed that phenyl-DPD, a different C-1 alkyl analog, inhibits QS-dependent production of pyocyanin in *P. aeruginosa* [145].

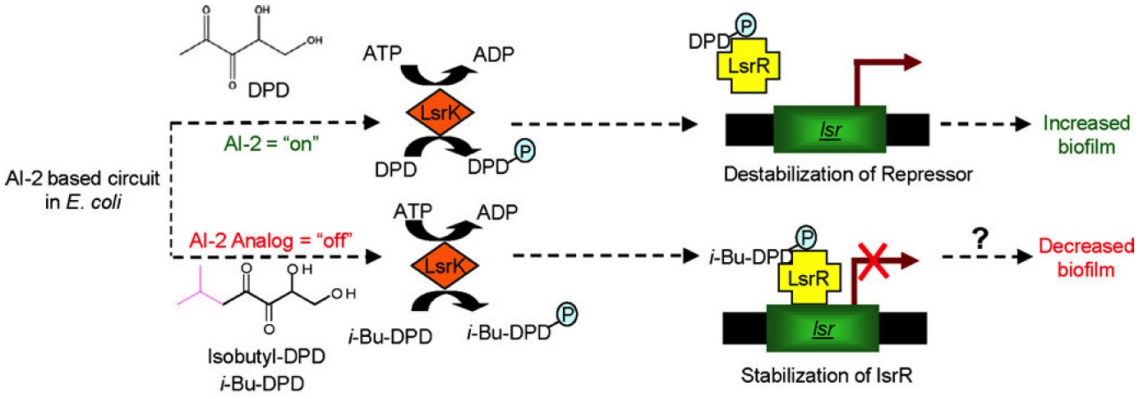

Figure 1-5 The AI-2-based circuit in *E. coli*. AI-2 (DPD) gets phosphorylated by the *E. coli* kinase LsrK. Phospho DPD binds to the repressor LsrR derepressing the lsr operon and switching on the expression of related QS genes. Phospho iso-butyl-DPD binds to the repressor LsrR repressing the lsr operon and turning off the expression of related QS genes. Reproduced with permission from [141].

While AI-2 analogs that can inhibit QS in several types of bacteria have been developed, no studies have been performed to date to investigate the efficacy of the combinatorial treatment of AI-2 analogs used in conjunction with electric fields. Such studies could lead to the development of a novel treatment for biofilm infections that is independent of traditional antibiotic therapy.

1.3.3 Evaluation of Biofilms

In developing the field of biofilm science, various new techniques and formats to evaluate biofilms have been employed by researchers through the years. This section discusses some of the most commonly employed methods used for growth and evaluation biofilms.

Macroscale Biofilm Reactors

Broadly, biofilm reactors can be divided into static biofilm reactors and flow cells. Static biofilm reactors allow for the growth of biofilms in a static environment where the media is replenished only periodically. The most common format for growing biofilms in a static environment is using microwell plates. Microwell plate readers are a staple to every microbiology and biotechnology laboratory. Furthermore, automated systems for filling and mixing reagents in microwells exist that allow for easy handling and experimentation of biofilms.

As opposed to static biofilm reactors, biofilms can also be grown under flow, which provides a continuous supply of nutrients to the biofilm in addition to aiding in continuous removal of planktonic cells, separate from the biofilm, from the system; an added advantage over static systems. Flow cells typically have one inlet, one outlet, and one channel throughout which biofilms are grown. The biofilms grown in these devices can be monitored continuously using a microscope, however this requires that the device be mounted on a transparent substrate. Some of the commonly used flow reactors are presented below.

The modified Robbin's device is a commonly used method for evaluation of biofilms. The device, shown in Figure 1-6, consists of a main channel that contains multiple specimen plugs on which biofilms can be grown. After biofilm growth, these plugs can be removed and the biofilm grown on the plugs can be subject to various experiments [15]. Although the biofilms are grown in parallel, their analysis remains serial in this configuration.

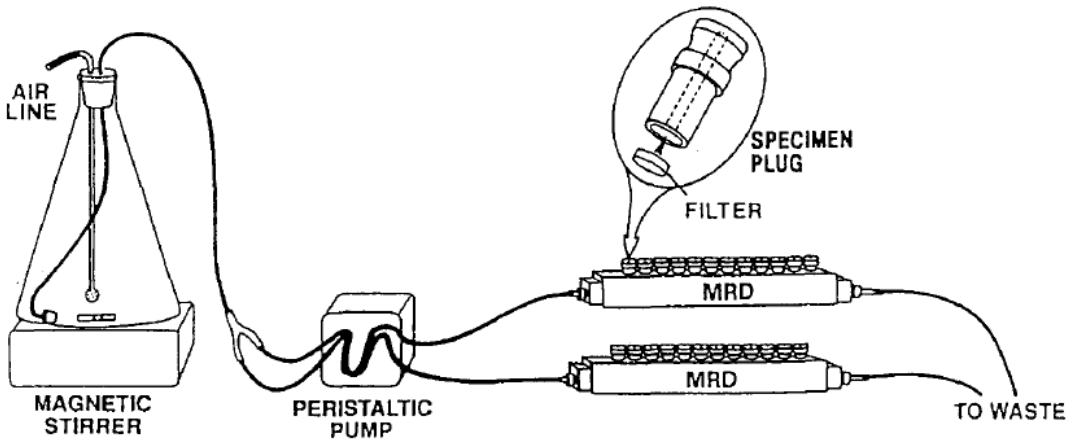

Figure 1-6 A Schematic of two parallel modified Robbin's devices showing the specimen plugs and the apparatus required to provide continuous flow of media. Reproduced with permission from [15].

The Calgary biofilm device combines the microwell plate with the ability to apply shear stress through flow as provided by the modified Robbin's device [11]. The device has two components, a pegged lid and a bottom with channels, shown in Figure 1-7. The pegs on the lid can be positioned over the channels or fitted into a traditional 96 well plate. The flow of the liquid in the channels can be directed around the pegs by placing the device on a rocking table. The biofilms grown on the pegs experience a constant amount of shear due to the flow of the fluid. They can be removed and analyzed individually as in the case of the Robbin's device or the pegged lid can be inserted in a microwell plate filled with different antibiotics or new treatments that needs to be tested. A major drawback of this device is that imaging of the biofilms on the pegs using either confocal microscopy or scanning electron microscopy requires that each peg be individually broken off the lid and manipulated.

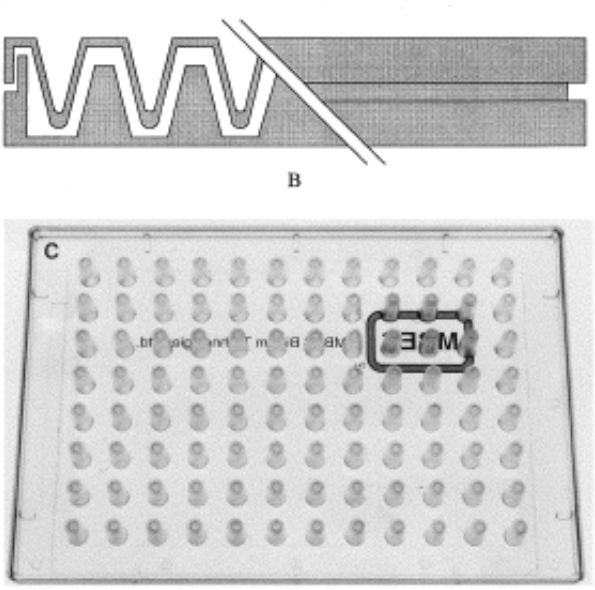

Figure 1-7 Cross-sectional (top) and top view (bottom) of a Calgary biofilm device. The figure on the top shows the pegs on which the biofilm grows as the channels below are used to flow nutrients. The bottom figure illustrates the pegs are arrayed in a 12x8 array compatible with a 96-well plate. Reproduced with permission from [11].

The CDC biofilm reactor (CBR) allows for the growth of biofilms under moderate to high fluid shear stress [146]. The reactor, shown in Figure 1-8, incorporates 24 removable biofilm growth surfaces (coupons) for sampling and analyzing the biofilm. It consists of a 1 liter glass vessel with an outlet positioned to provide about 350 ml of working fluid capacity. The polyethylene lid supports eight independent removable rods that can each house 3 coupons, an inlet port, and a gas exchange port. The entire device is usually placed on a digitally controlled stir plate to provide constant rotation of the baffled stir bar at a designated speed that controls the amount of applied fluid shear. The CBR is used as a flow cell i.e. a continuous-flow stirred-tank reactor, by constantly pumping fresh media into and out of the reactor. The primary disadvantage of this device is that it is bulky and that all 24 coupons can only be subjected to the

same treatment. Hence different treatments need to be tested serially which leads to experimental variation.

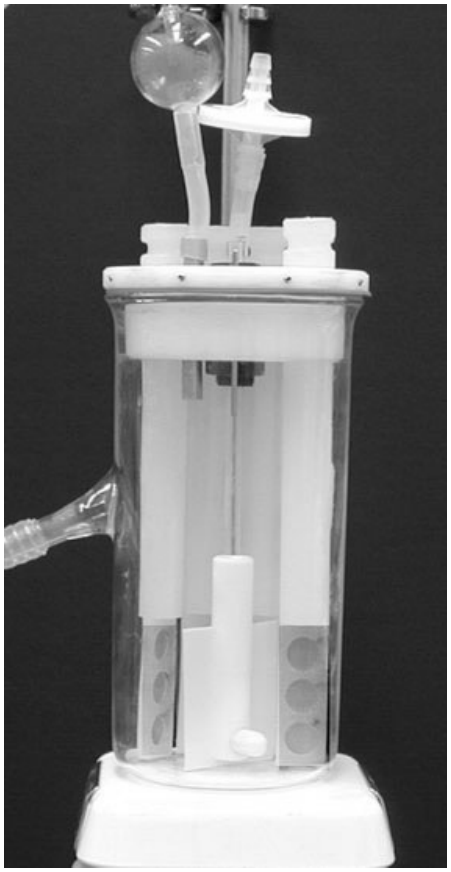

Figure 1-8 Photograph of a CDC biofilm reactor (CBR). Reproduced with permission from [146].

Microfluidics

Microscale systems are able to address many of the disadvantages and measurement challenges of their macroscale counterparts. The use of microfluidics allows for greater ease in controlling the fluidic environment and integration of microfabricated sensors or micropatterned growth substrates [147,148]. Additionally, in comparison to the macro-scale platforms like the 96 well plates, microfluidic

systems require smaller sample and reagent volumes on the order of nanoliters. While larger samples of bacterial cultures are easy to obtain, it is often difficult to obtain larger volumes of reagents, antibiotics, or new drugs under research. In the recent past, several standard macroscale methods routinely used for the analysis of biomolecules, like electrophoresis and PCR have been successfully miniaturized into microscale systems [149,150].

While the simplest microfluidic systems, single channels or chambers, are miniatures of existing macroscale platforms such as microwell plates or flow cells, complex fluid handling architectures can be integrated with arrays of channels or chambers. On-chip pumps can provide tunable flow of solutions throughout a device whereas integrated valves can direct this flow to designated locations on demand. Integrating microfluidic valves into PDMS and using a pressurized gas to control the valve orientation, also known as Quake valves, is a popular valving scheme used in much of today's microfluidic work [151-153].

Another significant advantage of using microfluidic systems is that they can be integrated with microfabricated sensors. These microfluidic LOC systems provide numerous advantages in biomedical research and clinical diagnostics and can be a valuable tool in the investigation of novel therapies. They enable functional integration with other technologies, leading to portability, and high-throughput usage. These translational technologies hold the potential to improve the resolution, regulation, sensitivity, and flexibility over more traditional approaches. Summarily, microfluidic LOC devices can provide a dense array of microfluidic channels and sensors at the micro-scale, which drastically reduce the necessary sample volumes,

along with flow conditions similar to *in vivo* systems, and can include integrated sensors, all critical elements to new drug discovery [20-52,154].

End-Point Measurement Methods

The most common method of quantifying biofilms is using the crystal violet stain [155,156]. In this method, crystal violet is applied to a biofilm, where it binds to negatively charged exopolysaccharides and molecules on bacterial cell surfaces. The excess unbound dye is rinsed out, following which the stain bound to the biofilm is solubilized into a second solution. The optical density of this solution of released dye is measured at 590 nm and directly corresponds to the biomass of the biofilm. While this is a standard method of biofilm measurement, the method suffers from variability. This is primarily due to the differences in stain penetration into the biofilm and variable binding of the dye to the cell wall.

The most common high resolution methods used for imaging biofilms are confocal microscopy and scanning electron microscopy (SEM) [18,19,157,158]. Confocal microscopy allows for the imaging of biofilms that are comprised of fluorescent bacterial cells. Fluorescence can be obtained either by using a cell line that is engineered to produce a fluorescent protein like the green fluorescent protein (GFP) or by staining the biofilms using commercially available kits like the Filmtracer™ LIVE/DEAD® Biofilm Viability Kit (Invitrogen Corp.). Given a fluorescent biofilm, confocal microscopy can generate a series of images along the z-axis, called a Z-stack. By concatenating the various images of the Z-stack using software such as Imaris (Bitplane, Inc.) or Volocity (PerkinElmer, Inc.), a complete

three-dimensional representation of the biofilm can be obtained. Quantitative analyses of the biofilm can be performed using software packages like COMSTAT, developed by Heydorn et al. [159]. This provides morphological data like average thickness, maximum thickness, surface coverage, roughness etc., which allow for measureable characterization and comparison of different biofilms. However, a major drawback of this method of measurement is that it necessitates the use of bulky and expensive equipment and also requires pre-treatment of the biofilms with stains.

SEM provides more detailed topographical information than confocal microscopy by virtue of its high resolution and independence of specific fluorescent markers. This technique can be used to evaluate the quality of the ECM and the interaction of the ECM with the cells in the biofilm [18]. Typically, biofilms are super-critically dried and coated with a metal and imaged under high vacuum conditions, thereby dehydrating the biofilm and preventing further growth. Environmental SEM or ESEM can be used to image the biofilm in a hydrated state, however imaging using ESEM requires low temperatures close to freezing and continuous interaction with the electron beam, preventing imaging through an enclosed biofilm reactor.

Noninvasive Measurement Methods

It is evident from the end-point measurement methods discussed in the previous section that the primary challenge in studying biofilms is observing the properties of the biofilm in a non-destructive manner. Although these methods are not used as commonly as the end-point measurement techniques discussed previously, a number of non-invasive methods that can be used to evaluate biofilms at any point in growth

have been developed [160]. Some of the common methods of non-invasive biofilm evaluation are discussed below.

A common method of biofilm evaluation is using their electrical properties. Both cells and the ECM within the biofilm serve as a dielectric material and thereby provide an electrical impedance that varies with time or with composition of the biofilm. The electrical impedance of the biofilm can be measured using techniques like electrochemical impedance spectroscopy (EIS) or capacitive measurement techniques [161-163]. A detailed review of the concepts of impedance based sensing of biological samples especially biofilms is provided in Chapter 2.

Another method of evaluating biofilm growth is using fiber optic sensors [160]. The biofilm can be quantified by observing its turbidity in the biofilm reactor. This can be implemented as a differential measurement system wherein one turbidity measurement is obtained from the biofilm and the other is obtained from a blank at a location where no biofilm exists [164].

The Optical density (OD) measurement technique uses the same principle as above to characterize bacterial biofilms. OD measurements have been used for detecting the cell count in bacterial suspensions for decades. Similar to OD measurements for cell suspension, the OD of biofilms can be measured at a particular wavelength at various instances in time. This can be compared to a baseline or blank measurement obtained before biofilm growth or formation [165]. This change in OD from the baseline was compared to the optical thickness. While the two were not directly correlated it was observed that as the biofilm grows the optical density increases. The change in OD is attributed to light scattering by the cells present

within the biofilm, similar to the OD measurements performed on bacterial suspensions using a spectrophotometer. Previous work by our group has demonstrated the viability of biofilm monitoring via the use of optical absorbance. Continuous optical sensing was achieved by integrating microscale flow cells with inexpensive off-the-shelf optical components like a broad band light source and a photodetector [136,166,167].

1.3.4 Microsystems for Biofilm Characterization, Sensing and Treatment

Biofilm studies have been performed for decades using macroscale setups like the modified Robbin's device and the microwell plate. However, more recently the study of biofilms using microfluidics has spawned research providing new insight on the various properties of biofilms including development of antibiotic resistance, biofilm growth characterization and the role of intercellular communication [141,157,166,168-170]. Furthermore, it has been suggested that small devices based on microfluidics will reduce the analysis time from days to the order of 2 to 4 hours with a more accurate specific recognition of the biological targets [171,172].

Biofilms grown in microfluidic devices have been observed to exhibit device-to-device variability [16]. Due to this variability, many biofilm studies are conducted to only understand the trends of growth and treatment and rarely report more than three repetitions. One solution to this problem is to perform multiple biofilm characterization experiments in parallel on the same device with an integrated control [173]. This reduces inter-device variability, along with the advantages of high throughput experimentation, thereby saving time and resources.

Although a majority of the biofilm studies performed in microfluidics utilize direct measurement of biofilm thickness using microscopy and image analysis, very few studies performed demonstrate real-time microsystem-based monitoring of bacterial biofilm during growth and treatment. Previous work conducted by our group demonstrated the sensitive real-time detection of biofilm growth using a surface acoustic wave (SAW) sensor and treatment system [154,174,175]. A schematic of the SAW sensor integrated with electrodes for BE treatment application is shown in Figure 1-9. Real-time detection of biofilms is achieved by measuring the resonant frequency of the SAW system, which is a function of the total biomass adhered to the surface of the sensor. As both biofilm growth and BE treatment cause a change in the adhered biomass, they can be measured in real-time by monitoring the resonant frequency of the system. Moreover, other studies that employ microfluidic platforms with interdigitated or parallel electrodes for impedance spectroscopy to detect biofilm formation have been performed [161,163,176]. However, the use of such a system has not expanded into the community of bacterial biofilm researchers.

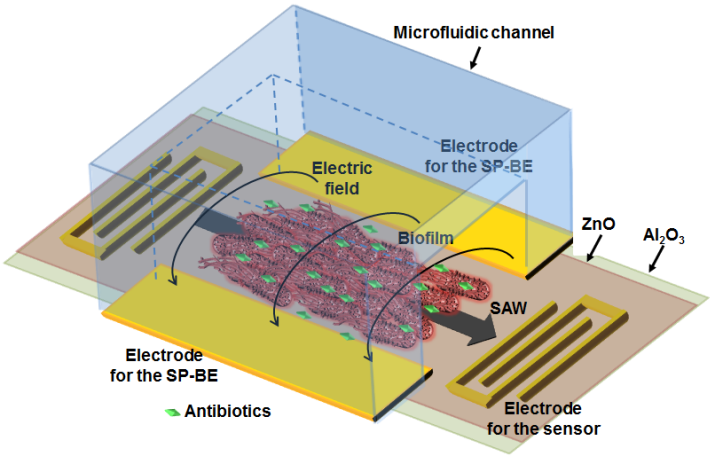

Figure 1-9 Schematic of a surface acoustic wave (SAW) sensor passivated with Al_2O_3 and integrated with BE treatment capabilities. Reproduced with permission from [175].

While microsystems have leveraged the properties of microfluidics to create environments more difficult to obtain with traditional biofilm reactors, very few real-time integrated monitoring and treatment microsystems have been developed for biofilm sensing, treatment and characterization. The development and validation of such microsystems against traditional methods of biofilm sensing and characterization will allow for easy detection of biofilm formation and evaluation of new treatments for biofilm prevention and removal in real-time.

1.4 Structure of Dissertation

The preceding chapter presented the motivation behind this research along with a brief literature review to establish context for the performed research. Chapter 2 discusses the theory and design of the microfluidic LOC system and its components. Chapters 3, 4 and 5 present the key results of this dissertation. Specifically, chapter 3 presents the design and characterization results obtained for the valveless bifurcation-based microfluidic biofilm sectioning device. Chapter 4 introduces alternate treatment therapies like the BE and its variations, alongside the results that show that the electrical energy is a key factor in determining the efficacy of the BE. Chapter 5 presents the sensing and treatment results using the designed impedimetric microfluidic LOC system and its components. Lastly, chapter 7 summarizes the research work of the dissertation and concludes with a discussion of potential future directions of this work.

Chapter 2. A Microfluidic Impedance Sensor-Treatment Platform: Theory and Design

This chapter covers the design of the microfluidic impedance sensor platform. First, the theory and design of the valve-less microfluidic device is described. This is followed by a brief review of the basics of impedance sensing followed by a description of the design and operation of the impedance sensor. The final section describes the integration of the microfluidic device with the sensor.

2.1 Bifurcation-based Microfluidic Platform

2.1.1 Principle of Bifurcation

Microfluidic systems offer significant advantages over macroscale systems including precise control and flow of fluid and particles. These particles can be rigid, immiscible liquid drops, vesicles, or biological cells. For this work, we developed a simple scheme based on the principle of bifurcation that allows for the equal distribution of the biological cells suspended in the media across all the microfluidic channels of the device. This will ensure reduced biofilm variability across the multiple channels of the device, thereby allowing more reliable comparison of the different treatment therapies within the same device.

A bifurcation is a point where a channel splits into two channels. Bifurcation based devices have been used to direct particles or fluid along preferred paths in microfluidic devices or prevent them from entering certain microchannels. In a microfluidic system, under low Reynolds numbers, the motions of liquid and freely

suspended particles are determined completely by the channel geometry and the way in which the channels are connected to each other [177]. Thus, it may be possible to control the direction of particle flow by controlling these device parameters. Since, this method of controlling suspended particles is solely dependent on the design of the channel, it is amenable to scale-up as compared to other methods of controlling particle flow, such as changing local flow rates or pressures.

Roberts and Olbricht conducted experiments to examine the effects of microchannel cross-sectional shape and the angles between the bifurcation branches [177]. Figure 2-1 shows the schematics of the two different bifurcations studied by Roberts and Olbricht. Specifically, Figure 2-1a illustrates the schematics of a Y-shaped bifurcation where the angles between the branches of the bifurcation

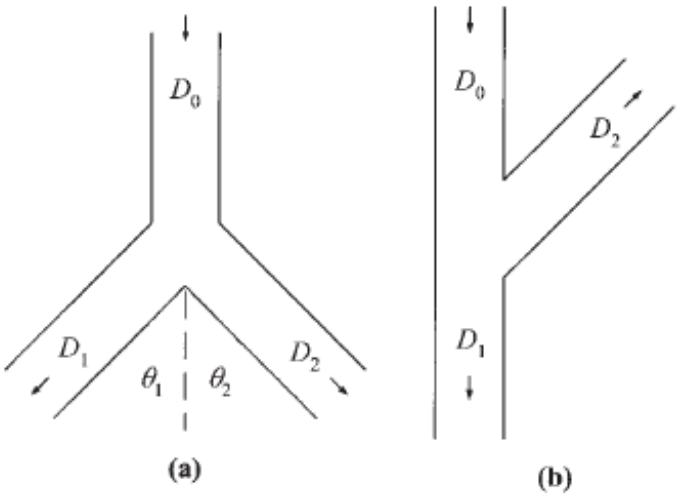

Figure 2-1 Schematic of the two bifurcations studied by Roberts and Olbricht [177]. The arrows indicate direction of fluid flow. (a) A Y-shaped bifurcation with $\Theta_1 = \Theta_2 = 45°$. (b) An oblique bifurcation with $\Theta_1 = 0°$ and $\Theta_2 = 135°$. The widths of the channels D_0, D_1, and D_2, are identical. Reproduced with permission from [177].

are equal ($\Theta_1 = \Theta_2 = 45°$) and Figure 2-1b shows the schematic of an oblique bifurcation with $\Theta_1 = 0°$ and $\Theta_2 = 135°$. All the branches of the bifurcation (one inlet and two outlets) lie in the same plane, so that the overall geometry is determined only by the angles of the two outlet branches with respect to the inlet branch.

Figure 2-2 plots the fractions of particles entering branch 1 (N_1/N_T) as a function of the fractional volumetric flow rate in branch 1 (Q_1/Q_T), for both the Y-shaped bifurcation (Figure 2-2a) and the oblique bifurcation (Figure 2-2b) for two different

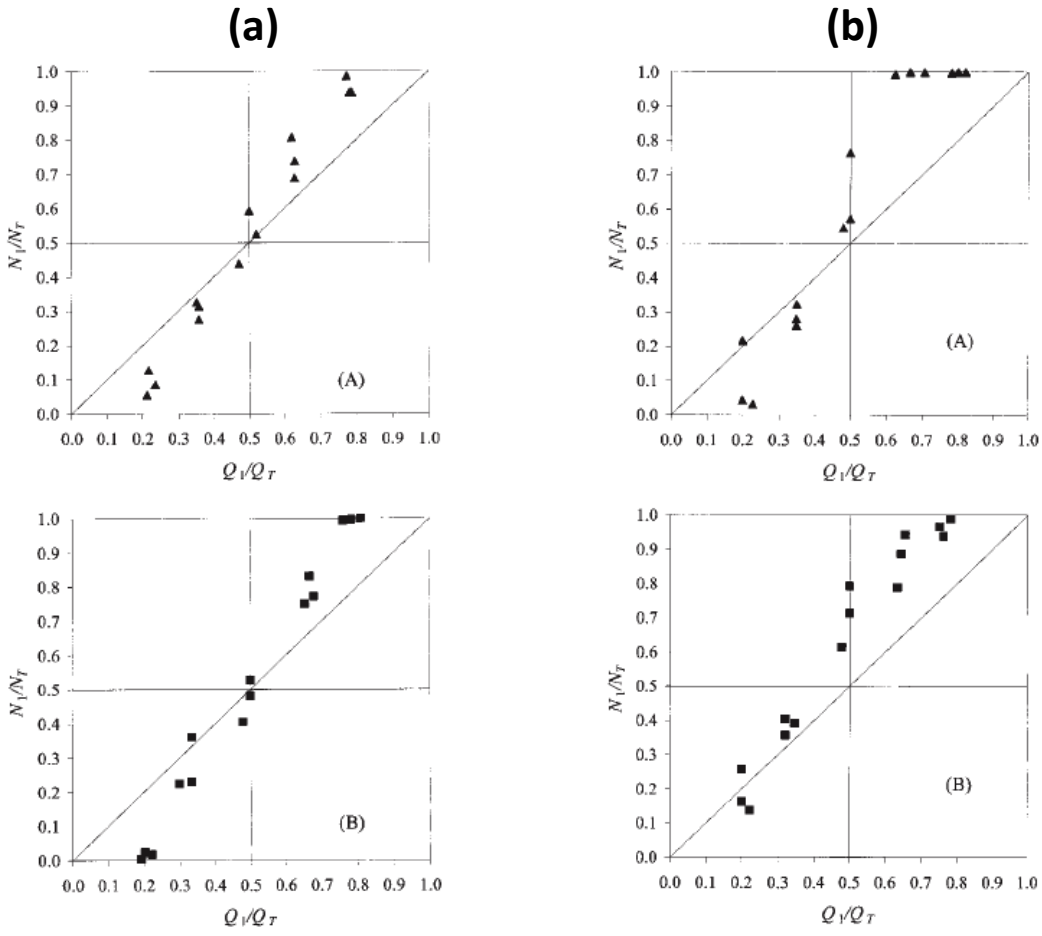

Figure 2-2 Fraction of particles entering branch 1 as a function of total volume entering branch 1 for 100 by 100 µm bifurcation (A, ▲) and a 100 by 200 µm bifurcation (B, ■) for (a) a Y-shaped bifurcation with angles of bifurcation $\Theta_1 = \Theta_2 = 45°$, and for (b) an oblique bifurcation with angles of bifurcation $\Theta_1 = 0°$ and $\Theta_2 = 135°$. Reproduced with permission from [177].

cross-sections. As seen from Figure 2-2, equal distribution of the suspended particles (N_1/N_T=0.5) occurs only when the bifurcation is symmetric, as in the case of a Y-shaped bifurcation with equal flow rates across both the outlet branches (Q_1/Q_T=0.5). Furthermore comparison of the Figure 2-2aA (top) with Figure 2-2aB (bottom), suggests that for Y-shaped bifurcations the channel-cross-sectional shape does not strongly affect particle portioning. On the other hand, comparison of Figure 2-2a and Figure 2-2b, suggests that the bifurcation angles strongly affect particle portioning. Hence, a symmetric Y-shaped bifurcation device operating with equal flow rates through the outlet branches was chosen to ensure equal distribution of freely suspended bacteria and media between the outlet branches.

2.1.2 Bifurcation Device Design

Bacterial biofilms are the primary cause of infections in medical implants and catheters. The widespread use of antibiotics to treat biofilms is leading to the emergence of antibiotic-resistant bacterial strains, necessitating the development of alternative methods of treatment. However, the experimental evaluation of new treatment techniques is strongly hindered by the stochastic nature of biofilm growth [166]. Therefore, it is required to develop microsystems that can facilitate multi-experiment studies for new treatment evaluation and also enable the growth of uniform biofilms that can be used as reliable controls.

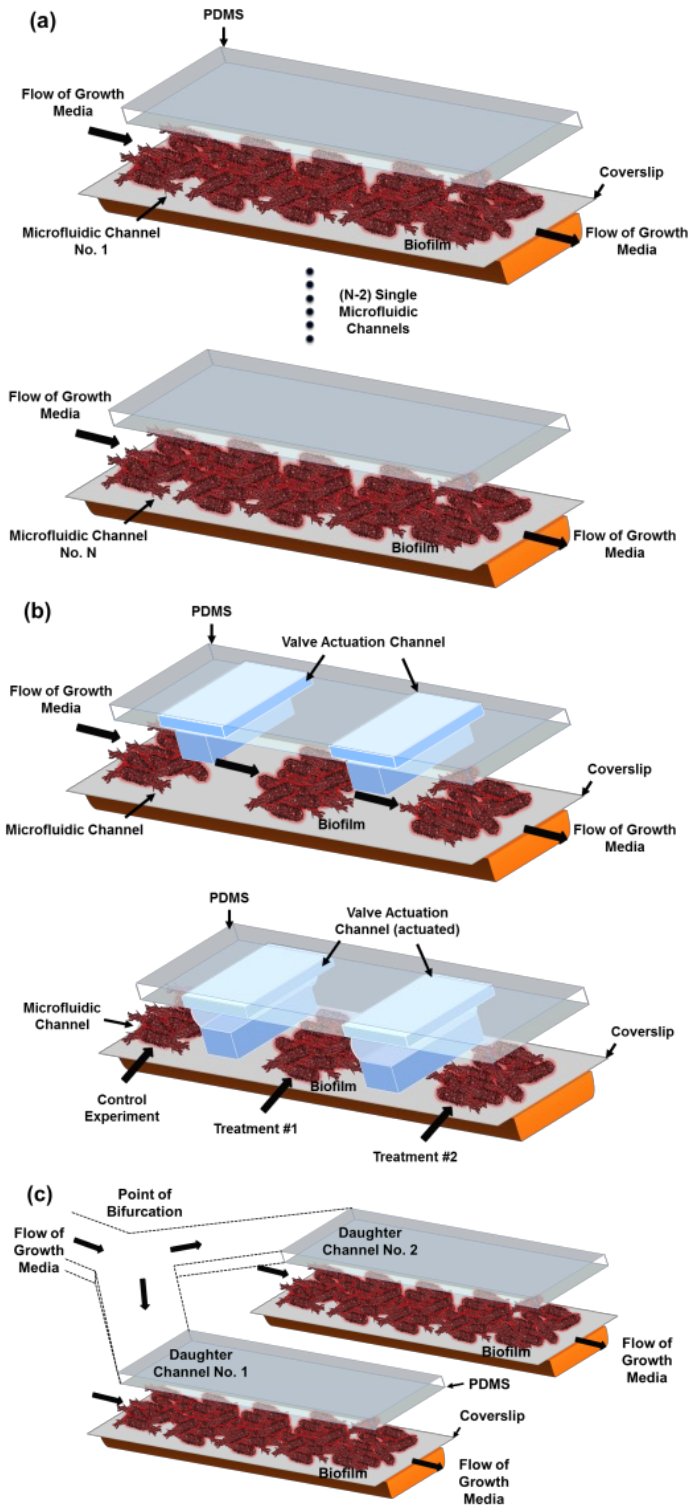

Figure 2-3 Schematic of operation of different configurations of microfluidics for biofilm characterization. (a) Biofilm growth in separate single channel devices leads to high biofilm variance between devices, (b) Biofilm growth in the open center horizontal channel and sectioning of the uniform biofilms (valves actuated), (c) Uniform biofilm growth in the spatially sectioned 21 daughter channels of the valve-less 1-level bifurcation device.

Figure 2-3 shows the schematics of different microfluidic channel configurations used for biofilm studies. While single channels (Figure 2-3a) provide an easy solution, the growth variance between the single channel devices was observed to be as high as 68% [166,178]. However, the growth variation within a single channel was observed to be less than 10% [178]. In previous work, we demonstrated an integrated microfluidic system with valve actuators to section a biofilm grown in a single horizontal channel (Figure 2-3b) [167,173]. Other complex, branched microfluidic platforms with valves have also been used for biofilm studies, but the uniformity of biofilms between channels has never been demonstrated [170]. A key challenge with these devices is the integration and fabrication of multiple microfluidic valves, which limits device scalability. Figure 2-3c shows the schematic of a valve-less device that enables biofilm sectioning using the principle of bifurcation. The device consists of a single inlet that bifurcates at 'n' levels or stages to 2^n channels. The distribution of bacteria and media between the channels is ensured to be symmetric by controlling the bifurcation angles and the flow rates as discussed in the previous section [177].

Figure 2-4 shows a simple 2-level bifurcation device that bifurcates into 4 daughter channels. During the growth phase the bacterial suspension and the media are introduced from the common source and the flow is directed from the single common inlet to the 4 outlets as shown in Figure 2-4a. Since the biofilms are grown simultaneously on the same device from the same source of bacterial suspension, the variability between the biofilms grown in the different channels of the bifurcation device is expected to be significantly lower than the variability in biofilms grown in separate single channels. After completion of biofilm growth, multiple treatments can

be tested in the different channels of the same device. During treatment, the direction of flow is reversed as shown in Figure 2-4b. Different treatments can be flowed through each channel of the bifurcation device. By using one of the channels as a reference (control), we can ensure that the results of the various experiments performed on the same device are compared to a common control. This allows for streamlined parallel experiments to be performed on one biofilm grown in the same device under uniform growth conditions using a microfluidic design that allows for an easy one step fabrication without the need for complex structures like microfluidic valves.

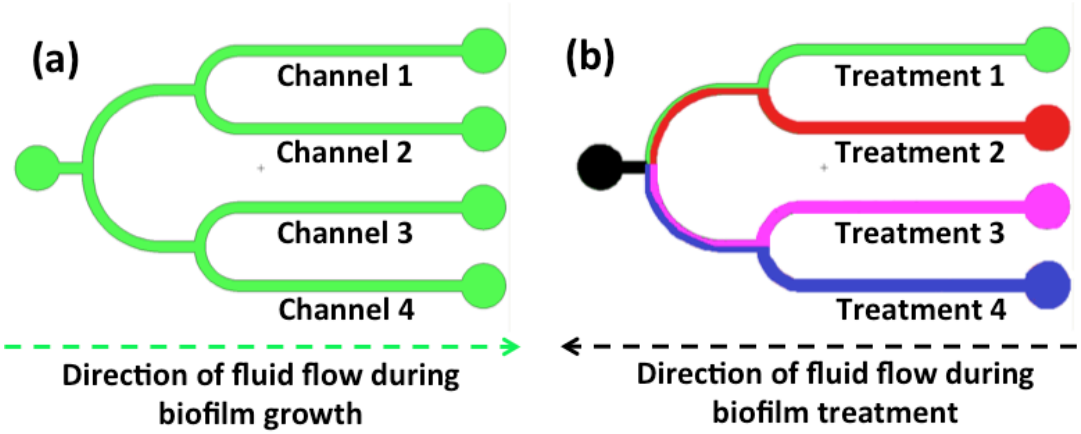

Figure 2-4 Schematic of a 2-level bifurcation device with 4 daughter channels under different modes of operation. (a) Fluid flow in the device during the biofilm growth phase. (b) Fluid flow in the device during the biofilm treatment phase.

2.2 Impedance Sensing

Impedance based techniques have been used as a method of transduction for detecting and/or quantifying bacteria. Specifically, impedance microbiology (IM) has been used for decades to detect the presence of microorganisms in samples in the

food industry, environment, health care etc. IM is based on the measurement of the change in impedance of the media or culture solution as a result of bacterial growth. However, so far the use of IM for the real-time sensing and treatment of bacterial biofilms in microfluidics has not been demonstrated. Also, the development of such a sensor with self-governing treatment capability will enable its use as a bench top platform for biofilm characterization and new treatment testing, as well as a novel technology for use in medical implants and catheters for effective biofilm management. In this section, the basic principles of impedance based sensing and the design of the impedance sensor are discussed.

2.2.1 Impedance Microbiology (IM)

A common method of evaluation of biological samples is using their electrical properties. In IM, the change in impedance is measured using a pair of electrodes that is submerged in the culture medium. This can be performed as either (i) a direct measurement, or (ii) an indirect measurement. In the direct measurement technique, the electrodes measure the change in bulk impedance of the solution with time as the bacteria grows. The impedance change is caused by the bacterial metabolism or due to ion release by the live bacteria in the medium. The ion release by the bacteria changes the ionic composition of the medium that changes its conductivity resulting in a change in the impedance. In the indirect measurement technique, the electrodes are not immersed in the growth media and hence do not directly measure the change in impedance. Instead, the electrodes are immersed in a separate solution such as

potassium hydroxide (KOH), which absorbs the gases produced by the bacteria, that decreases the conductance of the KOH solution.

To detect bacterial growth in real-time, the relative or absolute change in conductance, impedance or capacitance of the solution are measured at a given temperature. Figure 2-5a plots a typical impedance curve. At the detection time t_d, the decrease in impedance value exceeds the threshold value. This generally occurs at a bacterial count of approximately 10^6-10^7 cfu/ml [179]. Finally, the impedance growth curve plateaus when the bacteria have grown to a very high concentration. The detection time t_d is linearly related to the logarithm of the initial cell concentration (C_0) as shown in Figure 2-5b. The slope and intercept of this line depends on the type of microorganism, media, and growth conditions.

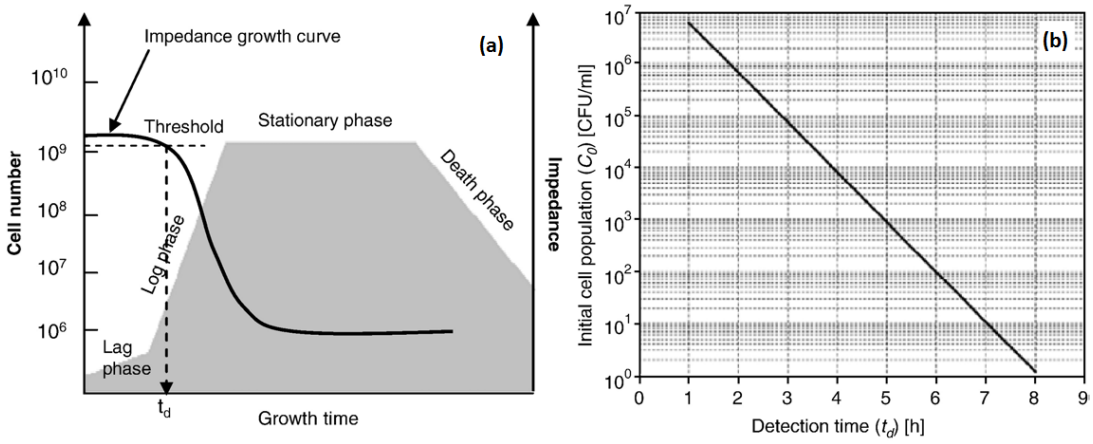

Figure 2-5 (a) A generalized impedance growth curve with the threshold and the detection time plotted along with the typical bacterial growth curve. (b) A plot showing the relationship between detection time and cell concentration. Reproduced with permissions from [179,180].

While classical impedance microbiology uses either direct or indirect measurement techniques for measuring the impedance change of the media, several

studies have found that the total impedance change during bacterial growth consists of two impedance change components that can be measured at different frequency ranges: (i) impedance change contributed by the media and (ii) impedance change contributed by the electrode/electrolyte interface, also known as electrode, or interface, or double layer impedance. The electrode impedance is dominant at lower frequencies (typically < 10 kHz) while the medium impedance is dominant at frequencies above 10 kHz. A simple equivalent circuit model can be used to understand the frequency dependence of both impedances on the total impedance. Figure 2-6b shows a simple equivalent circuit for the impedance between two electrodes of Figure 2-6a. The impedance of the circuit can be mathematically expressed as equation (2.1) below.

$$|z| = \sqrt{{R_s}^2 + \left(\frac{1}{\pi f C_{dl}}\right)^2} \qquad (2.1)$$

where R_s is the solution resistance and C_{dl} is the double layer capacitance at the electrodes. The equation explains the impedance growth curve observed (Figure 2-6c) in which the impedance always decreases as bacteria grow as a result of the decrease in the solution resistance R_s and an increase in C_{dl}. As previously discussed, R_s decreases due to the bacterial metabolism, in which large uncharged molecules are metabolized into small charged molecules. On the other hand C_{dl} increases due to the increase in ionic composition at the electrode surface because of bacterial growth.

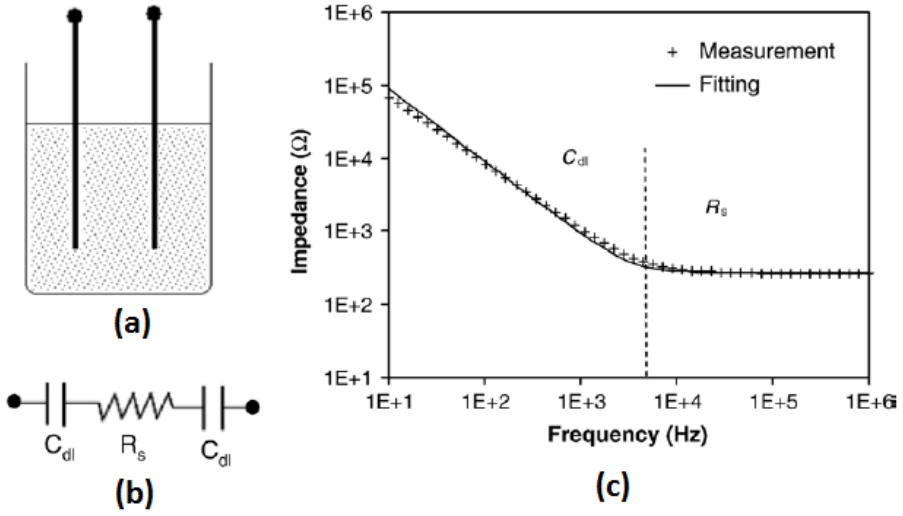

Figure 2-6 (a) Typical setup of a two-electrode system. (b) Equivalent series circuit of the two-electrode setup. (c) Plot of observed and fitted impedance versus frequency curve for *Salmonella typhimurium*. Reproduced with permission from [181].

Similarly, interdigitated microelectrodes (IDEs) have been used for sensing of biological samples. The equivalent circuit model (Figure 2-6b) is still valid for the case of the interdigitated electrodes. However, the frequency ranges over which the double layer capacitance and the medium capacitance are dominant may change with the size of the electrode spacing and width. Yang et al. demonstrated the use of IDEs for sensing growth of bacteria. Specifically, in response to bacterial growth, a 30% change in the double layer capacitance and almost no change in the medium capacitance (-0.58%) was observed [182]. In this respect, IDE based systems are different from conventional electrode systems, in that the IDE measures the change in the double layer capacitance to monitor bacterial growth. The advantages of using IDE based impedance systems include a reduction in sample volume, low resistance, high signal-to-noise ratio, and the rapid attainment of steady state [179].

Impedance biosensors have been developed for the detection of bacteria in a sample, in which an antibody specific to the target bacteria are immobilized on the IDE surface. The IDEs probe the attachment of the bacteria to the antibody. The current through the system or the sensor signal is determined by the presence of an intact cell membrane bound to the antibodies. The impedance measurement can be performed in the presence or absence of a redox probe, and is referred to as Faradaic and non-Faradaic impedance measurements, respectively. The absence of a redox probe results in the IDEs measuring the bacterial cells that are attached and growing

Table 2-1 Comparison of some current literature on detection of pathogens using impedance spectroscopy in both its variants namely Faradaic and non-Faradaic measurement techniques.

Microorganism	CFU/ml	Frequency	Parameter	Relative Change	Reference
S. epidermidis	1×10^6	10 Hz	R_s	32 %	[169]
S. typhimurium	7.6×10^1	1 MHz	R_s	30 %	[181]
S. typhimurium	4.8×10^0	10 Hz	C_{dl}	30 %	[182]
E. coli O157:H7	8×10^0	1 MHz	C_{dl}	46.5 %	[183]
P. aeruginosa	1×10^6	1 – 100 Hz	C_{dl}	15 %	[184]
P. aeruginosa	1×10^8	100 Hz	C_{dl}	10 %	[185]

on the electrode surface, primarily owing to the cell membrane that acts as an insulating layer (conductivity of the cell membrane is 10^{-7} S/m). Hence, the impedance measured is affected by changes in number, morphology and growth of the adhered bacterial cells. On the contrary, in the presence of a redox probe, the IDE

sensor measures the change in impedance due to biological events like antigen-antibody binding, oligonucleotide-DNA interaction etc. that occur on the electrode surface. Table 2-1 compares some of the current literature on pathogen detection using impedance spectroscopy techniques. Furthermore, the parameter analyzed and the relative change measured are also compared for both Faradaic and non-Faradaic measurement methods.

2.2.2 Impedance Sensing of Biofilms

In biofilms, both the cells and the ECM within the biofilm serve as a dielectric material and thereby provide the biofilm with an electrical impedance that varies with time, or composition, or metabolic state of the biofilm. Hence bacterial biofilms grown on the surface of microelectrodes can be modeled as an electrical circuit. One such equivalent electrical model is presented in Figure 2-7. Figure 2-7a presents the electrical model of a sterile culturing media that does not contain any bacteria. Figure 2-7b-c presents the series and equivalent parallel electrical models when the biofilm and ECM grows between the two electrodes. In the circuit, the parameters represent the following: C_{dl} is the double layer capacitance, R_{sol} is the resistance of the media without bacterial cells, and C_{bio} and R_{bio} are the capacitance and resistance of the biofilm, respectively. When the bacterial metabolism causes a change in the first two parameters, the impedimetric response of the culture changes proportionally [169].

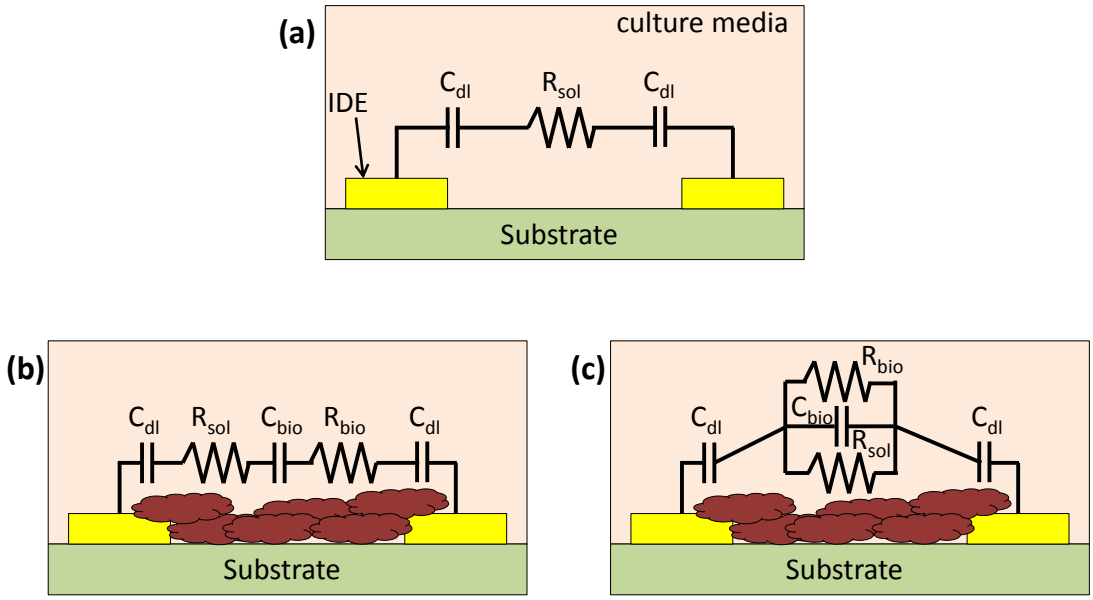

Figure 2-7 Schematic of electrical circuit model across the cross-section of a pair of interdigitated electrodes (IDE). (a) Circuit model for sterile culture media before inoculation with bacterial cells. (b) Equivalent series and (c) parallel circuit models after biofilm and ECM formation.

The magnitude of the impedance of the three electrical circuits shown in Figure 2-7 can be calculated using equations (2.2), (2.3) and (2.4) listed below. Paredes et al., calculated the numerical values of the various parameters by fitting these equations to the experimental data obtained for *Staphylococcus epidermis* biofilms [169].

$$Z_{(a)} = R_{sol} + \frac{2}{j\omega C_{dl}} \tag{2.2}$$

$$Z_{(b)} = R_{sol} + R_{bio} + \frac{2}{j\omega C_{dl}} + \frac{1}{j\omega C_{bio}} \tag{2.3}$$

$$Z_{(c)} = \frac{R_{sol}\,R_{bio}}{R_{sol} + j\omega R_{sol}R_{bio}C_{dl} + R_{bio}} + \frac{2}{j\omega C_{dl}} \tag{2.4}$$

By fitting these or other equivalent models to the experimental data, specific electrical parameters of the system can be tracked and used to accurately sense the onset of biofilm growth.

2.2.3 Impedance Sensor Design

Literature review in the field of IM suggests IDEs as the preferred electrode configuration for the accurate sensing of biological samples. As the sensitivity of the impedance sensor is dependent on the electrode surface area that is exposed to the culture media and bacteria, IDEs provide an easy way to increase the surface area while keeping the size of the device in check. IDEs provide several other advantages including higher signal to noise ratio, low resistance and faster attainment of steady state.

The distribution of the electric field or current over the electrodes is dependent primarily on the width and spacing of the fingers of the IDEs. Typically, the majority of the electric field is concentrated within a height of one-electrode spacing from the surface of the electrode. Since the designed microfluidic channels are 100 μm tall and the average thicknesses of biofilms grown in these channels are in the range of 5-30 μm, initial electrode spacings and widths of 25 μm, 50 μm and 100 μm were chosen for the IDEs. These are similar to or in the order of the widths and spacings of IDEs used previously for biofilm sensing [169,176]. However, further optimization of the electrode width and spacing needs to be performed in order to achieve higher sensitivity and lower noise while maintaining ease of fabrication and high yield.

2.3 Integrated Sensor-Treatment Platform

2.3.1 Operation of LOC Device

The goal of this research is to develop a high-throughput microfluidic platform that can reduce growth variance of *in vitro* biofilms and closely mimic the conditions encountered in a clinical indwelling device. New treatment studies are severely hampered because of the stochastic nature of biofilm growth. This platform will enable multi-experiment studies simultaneously on uniform biofilms, thus facilitating reliable comparison between different experiments performed on the same

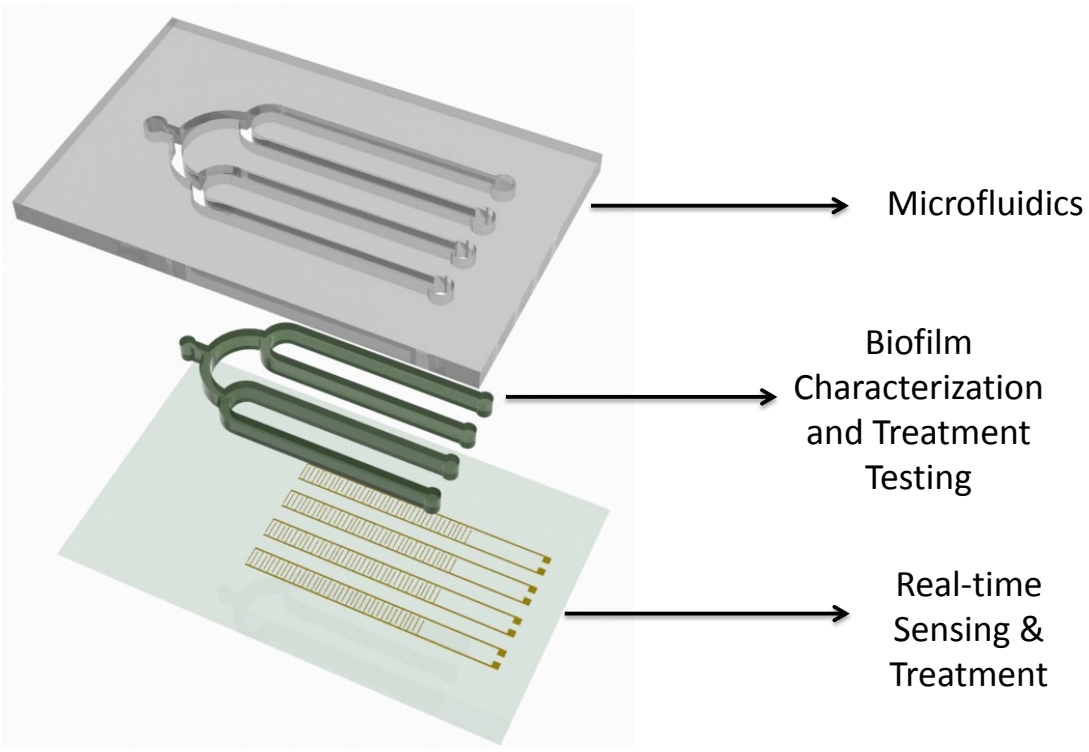

Figure 2-8 Schematic of proposed microfluidic Lab-On-a-Chip (LOC) platform designed to reduce growth variance of *in vitro* biofilms and for the reliable testing of new biofilm treatments. The platform has integrated impedimetric sensor-treatment modules for detection of onset of biofilm formation and treatment.

microfluidic device. The microfluidic LOC will be integrated with impedimetric sensor-treatment modules to accurately detect the onset of biofilm formation and perform biofilm treatment through the application of electric fields. A schematic of the proposed sensor-treatment LOC device is shown in Figure 2-8. As shown in the schematic, each channel has its individual integrated sensor-treatment module for real-time sensing and treatment within the channel.

In our previous work, we used a valved microfluidic biofilm reactor to section uniformly grown biofilms. The microfluidic device was integrated with arrays of charge coupled devices (CCDs) as optical sensors to detect long-term biofilm growth by measuring the change in optical density (OD) [167]. While the signal obtained from the CCDs does not saturate with time, this method is not sufficiently sensitive to detect the small changes in OD during onset of biofilm formation. Impedimetric sensing using interdigitated electrodes provides an efficient method for detecting the early stages of biofilm formation based on the capacitance and resistance changes between the fingers of the sensor. This method has been recently employed in our lab to conduct on-chip ELISA as well as particle counting, demonstrating the capability to accurately measure small impedance signal changes due to particle/molecule presence in the space between the sensor electrodes [186-188]. In this dissertation, we integrate an impedimetric sensing and treatment modality with high-throughput bifurcation-based microfluidics into a microsystem and demonstrate reliable, real-time, non-invasive, continuous sensing of the onset of biofilm formation. More importantly, we show for the first time, the use of the same IDEs to provide the electric field necessary for treatment of biofilms using the BE. The continuous real-

time impedance monitoring was used to provide feedback to the IDEs so as to switch the electrodes from the low frequency-low voltage sensing mode to the high frequency-high voltage treatment mode that uses the principles of the BE.

2.3.2 Expected Results and Challenges

The microfluidic LOC is designed to reduce growth variance of *in vitro* biofilms by growing biofilms in multiple channels on the same device using the same bacterial suspension. Hence it is expected that the variance in biofilm thickness between the channels of the bifurcation device is lower compared to single channel microfluidics. The integrated impedimetric sensors allow for the real-time monitoring of the biofilm growth in each channel of the device. The total impedance and the interfacial capacitance in particular are expected to increase at lower frequencies as the biofilm grows with time. This is primarily due to an increase in surface coverage by the insulating bacterial cells on the surface of the sensor. However, the ionic conductivity of the bulk solution increases, thereby decreasing the impedance at higher frequencies as a result of the change in ionic composition at the electrode surface due to the metabolically active bacteria. By measuring the change in impedance between the channels of a device and multiple devices the onset of biofilm growth can be monitored and compared.

To detect the onset of biofilm formation, a highly sensitive sensor that is capable of accurately measuring the attachment of a few cells onto the surface is required. However, increasing the sensitivity of the device could result in an increase in the background noise. Hence, methods to increase the signal-to-noise ratio may need to

be investigated. Furthermore, the sensitivity of the device depends on the active surface area of the electrodes that is exposed to the growth media. Since the proposed LOC is a microfluidic device, the active electrode area is significantly smaller when compared to macro or mm scale devices. In microfluidics, increased sensitivity is usually achieved by passivation of the IDEs using a stable dielectric; however such passivation would prevent the application of electric fields and currents through the biofilm during treatment [148]. Consequently, it is a challenge to increase the sensitivity of the system while ensuring easy and reliable application of electric field based treatment.

Some methods of improving the sensitivity of the device without the use of a dielectric include designing fine IDEs with smaller electrode widths and spacings or using three-dimensional electrodes. Both these methods increase the active area of the electrode, thereby increasing measurement sensitivity. While the use of smaller electrode width and spacing will increase the sensitivity of the device, it will adversely result in a smaller linear range of operation of the sensor. This is due to the reduced electric field strength at heights greater than one electrode spacing distance above the IDEs. A way to mitigate this problem is by using a staggered IDE scheme that has multiple electrode widths and spacings. Such a configuration is expected to provide a larger linear range of operation and increased sensitivity.

Treatment with AI-2 analogs has been previously demonstrated to reduce growth of bacterial biofilms [143,167]. Furthermore, application of novel combination therapies, including application of AI-2 analogs with small doses of antibiotics, and electric fields in combination with near MIC levels of antibiotics, to mature biofilms

have both been previously demonstrated to significantly enhance biofilm treatment [141,189]. In this work, AI-2 analogs were combined with electric fields for the treatment and prevention of mature bacterial biofilm growth. The uptake of AI-2 analog by the bacterial biofilm is currently a diffusion-limited process. It is hypothesized that the application of electric fields will provide the charged AI-2 analog molecule with the required drift component that will allow for increased penetration of the QS inhibitor by the biofilm, enhancing treatment efficacy. Furthermore, application of this combination therapy as a preventative treatment is expected to result in greatly reduced biofilm formation due to QS inhibition of the planktonic bacteria.

2.4 Chapter Summary

This chapter covers the theory and design of the components of the microfluidic LOC sensor-treatment system. The basics of microfluidic bifurcations were discussed, following which an introduction to IM was presented. Specifically, IM as applied to bacterial sensing was discussed, and the advantages and disadvantages of IM-based sensing of biofilms were presented. The design of the microfluidic LOC was introduced and the expected results and challenges were examined. The experiments and results of biofilm characterization, sensing and treatment using the designed microfluidic LOC system, as well as the characterization of the effect of electrical energy on the efficacy of BE are presented in the next two chapters.

Chapter 3. A Bifurcation-based Valveless Microfluidic Biofilm Sectioning Device

The ultimate goal of this dissertation is the development of a threshold-activated feedback biofilm sensing-treatment microfluidic system for effective treatment of biofilms right at the onset of formation. To achieve this, four individual goals introduced in chapter 1 viz., 1. Investigation of biofilm growth variance in bifurcation microfluidics, 2. Investigation of the effect of the electrical energy on the efficacy of the BE, 3. Study of a new combination treatment of AI-2 analogs with electric fields, and 4. Sensing and treatment of bacterial biofilms using the IDE-based impedance sensor were studied. The results of the first aim are presented in detail in this chapter. Here we present the results of biofilm growth and treatment using a simple microfluidic device that was designed based on the principle of bifurcation introduced in Chapter 2. I would like to acknowledge my mentor Dr. Mariana Meyer for her critical feedback and guidance without which this research would not have been possible.

3.1 Comparison with Other Microfluidic Devices

To highlight the importance of an integrated control and to assess the biofilm variability of the microfluidic bifurcation device, biofilm variability studies were performed in other microfluidic devices. Specifically, biofilm growth experiments were performed in both simple single channel microfluidics and the valved biofilm sectioning device developed in our group (Figure 2-3). A comparison of the

variability in biofilm growth between these microfluidic devices and the bifurcation device is presented below.

3.1.1 Single Channel Microfluidics

Biofilm growth experiments were performed in four simple single microfluidic channels. Each device was sterilized by flowing 70 % ethanol followed by DI at a flow rate of 100 µl/min. A culture of *E. coli* W3110, grown overnight at 37 °C at 250 rpm, was diluted to an OD_{600} of 0.25 in LB media and introduced into the channel at a flow rate of 100 µl/min. This suspension is incubated in four devices under static conditions for 2 hours at 37 °C following which, sterile LB media was introduced at a rate of 10 µl/hr for 48 hours for biofilm growth. Fresh LB media is replenished every 24 hours. Results from four devices are shown in Figure 3-1. The biofilm thicknesses obtained using the three confocal images taken for each of the four single channel devices are listed in Table 3-1.

The results of Figure 3-1 show that the variation in biofilm thickness between the four single channel devices. Confocal images were obtained at the inlet, center and the outlet of each channel. The variation in biofilm thickness within a single channel device is observed to be 15.77 % at most and 9.05 % on average. However, the average biofilm thickness of the four devices is 19.78 µm with an average variation of 13.58 µm or 68.62 %. This high inter-channel variability further illustrates the need for multiple experiments to be performed on the sections of the same biofilm grown on the same device to ensure reliable results.

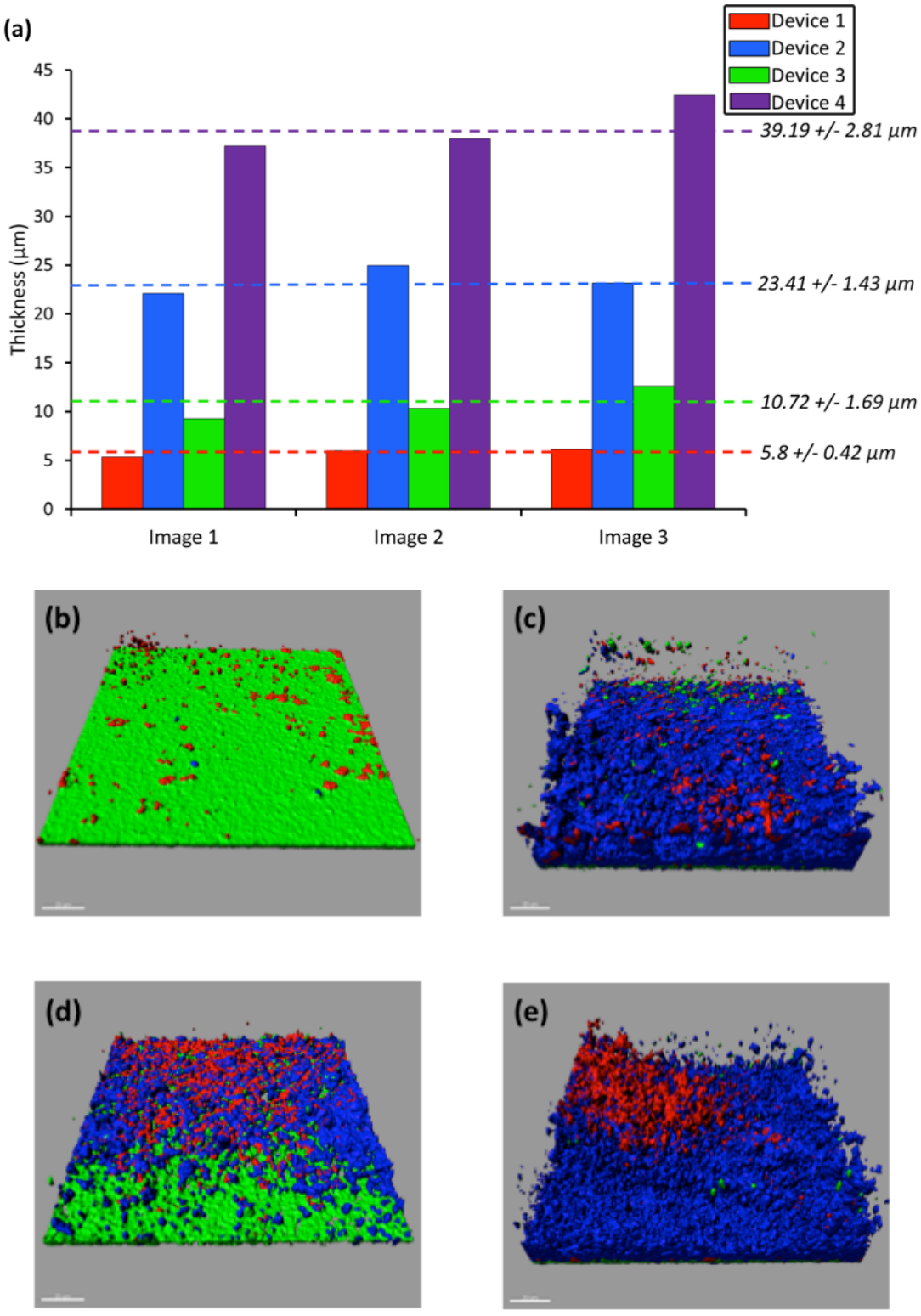

Figure 3-1 (a) Average thickness of biofilms grown in four different single channel devices. Three biofilm images were obtained per channel using confocal microscopy and were analyzed using COMSTAT [159]. (b-e) Surface rendered sample confocal images from each of the four devices. Scale bars represent a length of 20 µm.

Table 3-1 Average biofilm thickness variation across four different single channel devices. The average biofilm thickness and standard deviation of each device is calculated from the data obtained from three confocal microscopy measurements.

Device No.	Biofilm Thickness (μm)			
	Image 1	Image 2	Image 3	Average
1	5.33	5.95	6.13	5.80 ± 0.42
2	22.13	24.95	23.17	23.41 ± 1.43
3	9.28	10.30	12.58	10.72 ± 1.69
4	37.22	37.95	42.20	39.19 ± 2.81

3.1.2 Microfluidic Valved Biofilm Segmentation Device

As a solution to the biofilm variation problem, a multi-depth valved microfluidic device for biofilm segmentation was designed and fabricated in our group. The device consists of hydraulic actuated microfluidic valves (push-up and push-down configurations) that are used to section a mature biofilm into multiple (usually three or four) segments [167,173,178]. Figure 3-2a shows the schematic of a push-down three-segment valved device and its various modes of operation. It has also been previously demonstrated in our group that the total biomass of the biofilm can be indirectly measured by monitoring the change in optical density (OD) [136,166]. In order to measure biofilm growth in the sections of a four-segment valved biofilm segmentation device in real-time, a linear arrayed charge coupled device (CCD) was used (Figure 3-2a). Figure 3-2b shows the measured average change in OD during *E.*

coli biofilm growth in each of the four sections of the device with respect to the baseline OD measured at time t=0 hours. The error bars represent the spatial variation of the biofilm across the length of the microfluidic section (N = 162 pixels along length of channel). After 24 hours of growth, the change in OD in each section is observed to converge to a single point.

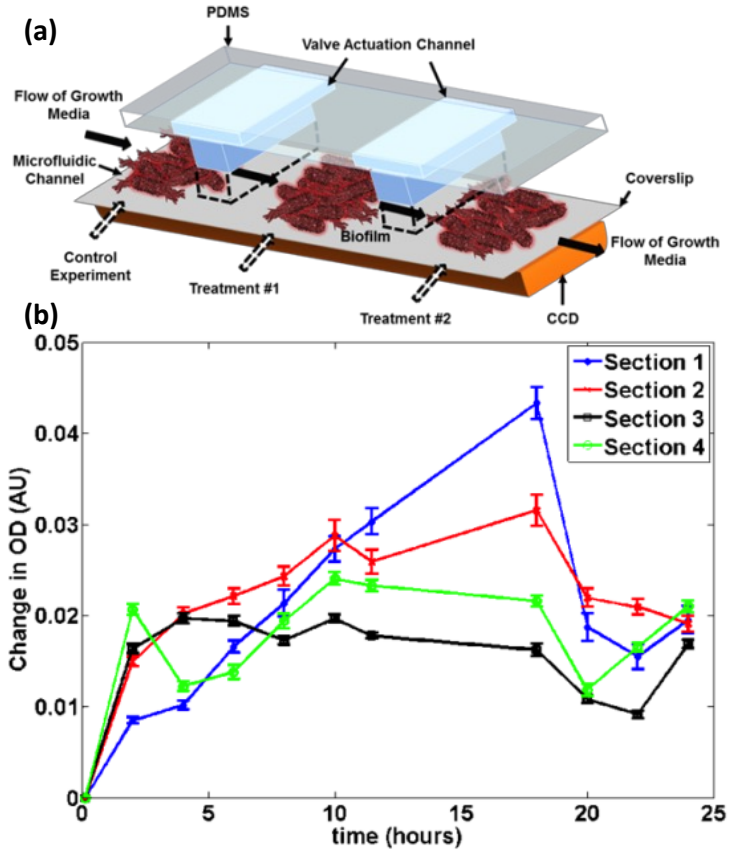

Figure 3-2 (a) Schematic of biofilm growth in center channel (solid arrows) and sectioning of biofilms for treatment (dotted arrows). (b) Biofilm growth measured as a change in optical density (OD) over 24 hours. The error bars represent the standard deviation of the OD across the length of the microfluidic channel (N = 162 pixels).

Statistical correlation was demonstrated between the OD measurements obtained for the four sections at the end of 24 hours (ANOVA, $P > 0.05$), thereby validating

the growth of a uniform biofilm across the center channel. After 24 hours of growth, the variation in biomass between the four sections was calculated to be only 9%, as compared to the 69% biomass variation seen in our previous work conducted in separate microfluidic channels. Although a sharp increase in OD, corresponding to an increase in biomass is observed around t=18 hours in some sections of the device during the biofilm growth, the OD then rapidly decreases and converges to a single point. We hypothesize that this reduction in biomass and therefore the convergence of the OD of the four sections of the device to a single point at t=24 hours is possibly a result of a self-leveling effect due to the increased shear experienced by the thick biofilms in the constricted microfluidic channels.

A further comparison of the biofilm thicknesses was made using the confocal microscope images of the *E. coli* W3110 biofilms that were grown in the central channel of three different three-segment valved devices. The biofilms were grown for 48 hours, following which they were stained and imaged using confocal microscopy following which they were analyzed using the COMSTAT software program [159]. Figure 3-3a plots the average thickness of biofilms in the three segments of the device for three different devices. The results show that the biofilms have a maximum of 2 μm thickness variation within each device (13 % of the average thickness at most and 7.2% of the average biofilm thickness on average). This is much smaller in comparison to the inter-device variability, which showed a 3.9 μm variation (23% of the average biofilm thickness). Figure 3-3b shows sample surface rendered confocal microscopy images using the Imaris software for each of the three segments of the segmentation device.

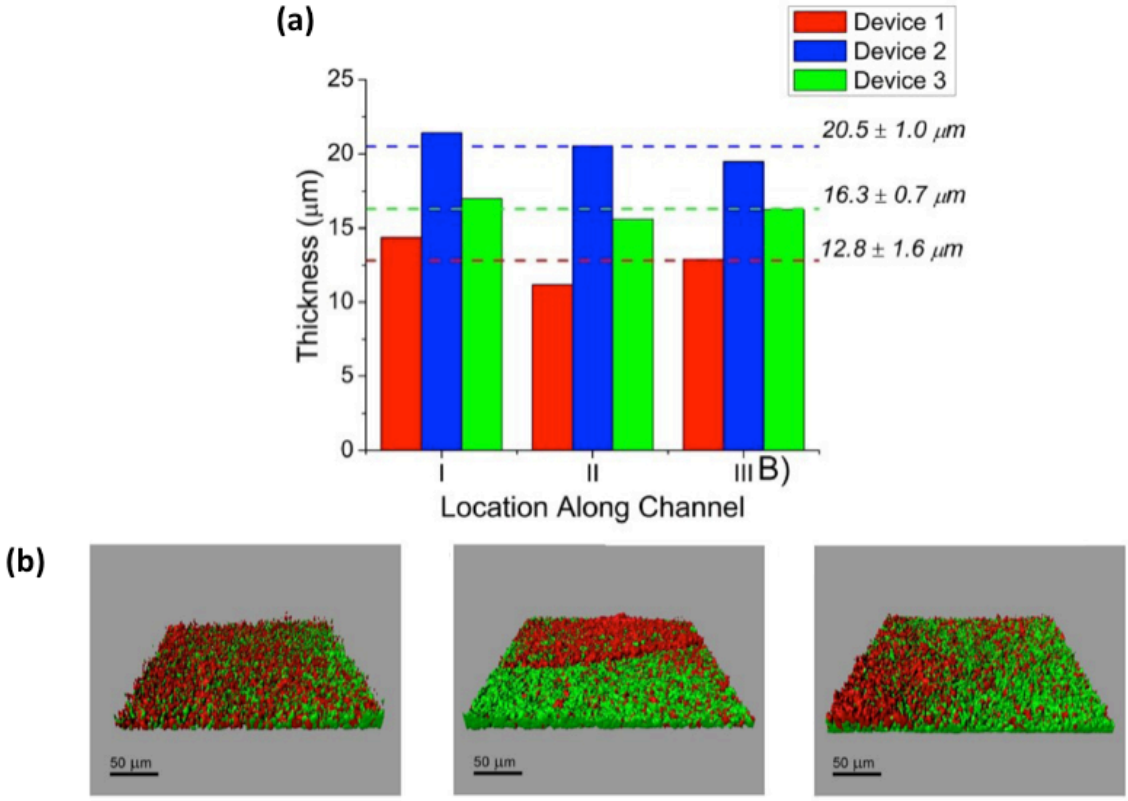

Figure 3-3 (a) Average thickness of biofilms grown in three different valved biofilm segmentation devices. The average variability in biofilm thickness between sections/segments of the same device is observed to be around 7.2%. (b) Surface rendered sample confocal images from each of the three segments from device 3. The biofilm thicknesses are 17.0 µm (segment 1), 15.6 µm (segment 2) and 16.2 µm (segment 3). Scale bars represent a length of 50 µm. The biofilm images were obtained using confocal microscopy and were analyzed using COMSTAT [159]. Reproduced with permission from [173].

Although, the average biofilm thickness variability between the sections of each of the segmentation devices (7.2 %) is very small as compared to the single channel microfluidics, a key challenge is the integration and fabrication of multiple PDMS valves for biofilm sectioning, thereby limiting scalability. However, the bifurcation device is a single-layer PDMS device that does not contain complex structures like microfluidic valves. Hence they are very easy to fabricate in comparison to the two-layer valved PDMS segmentation device. Furthermore, the bifurcation device does

not require hydraulic or pneumatic actuation to switch from biofilm growth mode to biofilm treatment mode, thus making the device more portable and easy to use.

3.2 Fabrication of the Bifurcation Device

The microfluidic bifurcation device can be fabricated using a simple two-step process. First, the mold for the device is patterned using traditional lithography techniques on a 4-inch silicon wafer using the negative photoresist KMPR 1050. PDMS (Sylgard 184, Dow Corning, USA) in the ratio of 10:1 silicone elastomer to curing agent is poured over the microfluidic mold, and cured at 60 ºC for 17 minutes. The devices are then peeled off the mold and the inlet ports are punched using a 2 mm dermatological punch. They are then irreversibly plasma bonded to a number 1 glass coverslip. Tygon tubing is connected to the inlets and outlets of the device using a tubing coupler, and the other end of the tubing is connected to a syringe pump (KDS-230, KD Scientific, USA). Figure 3-4 shows photographs of the single layer 2-level bifurcation device with one port on the left end of the device and four ports on the right end of the device. Figure 3-4a shows a photograph of the PDMS microfluidic device when used in the biofilm growth phase. As shown, in this mode the media from the single inlet is distributed to all the channels of the device. In this mode, the 4 outlets of the device are connected to the syringe pump that is operating in withdrawal mode and the direction of the fluid flow is from the single inlet on the left to the multiple outlets on the right of the device. Figure 3-4b shows a photograph of the device when used in the treatment mode. As shown in the figure, the direction of fluid flow is now reversed and the syringe pump is now operating in the infusion

mode. Use of the syringe pumps in this mode ensures a constant flow rate through each of the four channels.

Three bifurcation devices were tested for cross talk between the four channels of the device when operated in treatment mode. This was verified by flowing colored water (red and green) for three consecutive hours at a flow rate of 10 µl/hr through the four channels of the devices, as shown in Figure 3-4b. At the end of the three hours, the devices were observed to maintain laminar flow with no back-flow as evidenced by the unadulterated colored fluids in the channels. This demonstrates that the bifurcation device can be used at these flow rates or higher for testing multiple biofilm treatments in parallel.

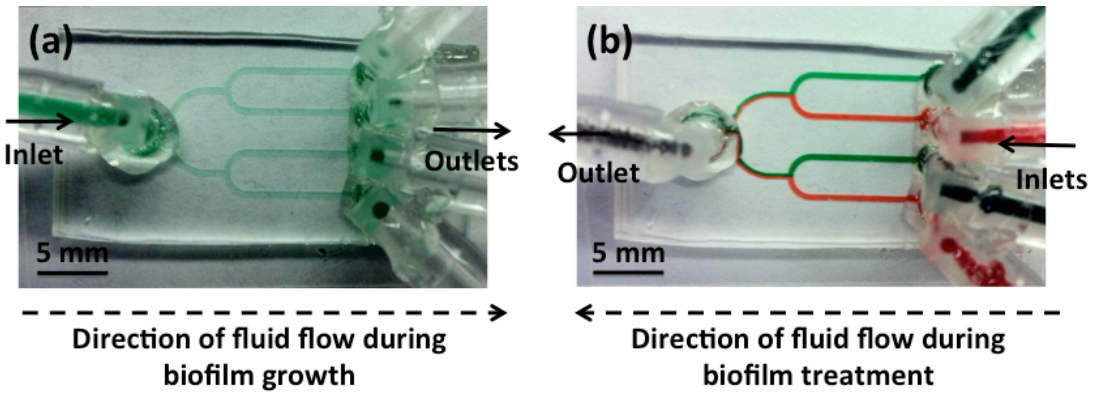

Figure 3-4 Photographs the single layer 2-level bifurcation device. (a) Device during the growth of biofilms. The single inlet serves as the common source of bacterial suspension and growth media for all four channels during the growth phase. (b) Photograph of bifurcation device during the treatment phase. Scale bar = 5 mm.

3.3 Biofilm Growth

In order to use the device for biofilm studies with integrated controls, biofilms grown in the channels of the bifurcation device must be uniform so that the control

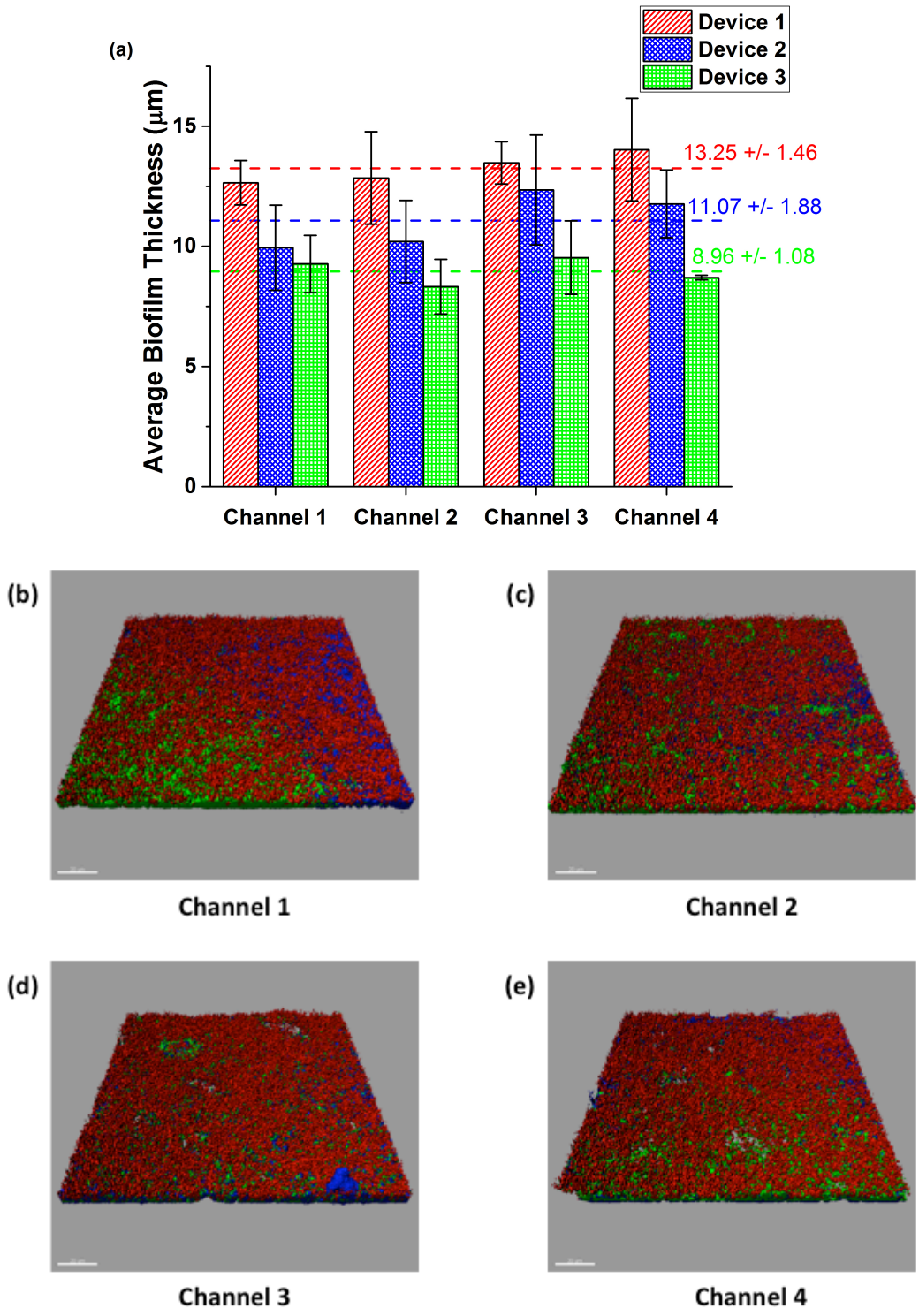

Figure 3-5 Average thickness of biofilms grown in three different bifurcation devices. The error bars represent the spatial variation of the biofilm (N = 3 images) in each channel of the bifurcation device. The average variability in biofilm thickness between the channels of the same device is observed to around 7.1%. The biofilm images were obtained using confocal microscopy and were analyzed using COMSTAT [159]. (b-e) Surface rendered sample confocal microscopy images from device 3 (scale bar = 20 µm). The thicknesses were 10.613 µm (channel 1), 8.224 µm (channel 2), 8.210 µm (channel 3) and 8.750 µm (channel 4).

Table 3-2 Average biofilm thickness variation across channels of three different bifurcation devices. The average biofilm thickness and standard deviation of each channel of each device is calculated from the data obtained from three confocal microscopy measurements.

Device No.	Average Biofilm Thickness (µm)				Average Biofilm Thickness of Device (µm)
	Channel 1	Channel 2	Channel 3	Channel 4	
1	12.65 ± 0.92	12.85 ± 1.93	13.48 ± 0.88	14.03 ± 2.14	13.25 ± 1.46
2	9.95 ± 1.77	10.20 ± 1.71	12.35 ± 2.29	11.77 ± 1.41	11.07 ± 1.88
3	9.27 ± 1.20	8.32 ± 1.14	9.53 ± 1.53	8.70 ± 0.09	8.96 ± 1.08

channel can be compared to the experimental treatment channels as reliably as possible, knowing that prior to application of the treatment, all the channels were comparable. Uniformity of biofilms was verified by performing multiple growth experiments using *E. coli* W3110 biofilms in order to quantify the variation of biofilm growth between the channels of the microfluidic bifurcation device. The biofilms were grown for 72 hours, followed by staining, imaging and analyzing the biofilm for each channel of each device.

Each device was sterilized by flowing 70 % ethanol followed by DI at a flow rate of 100 µl/min. A culture of *E. coli* W3110, grown overnight at 37 °C at 250 rpm, was diluted to an OD600 of 0.3 in Luria-Bertani (LB) media and introduced into the channels of the device set in the biofilm growth mode, at a flow rate of 100 µl/min. This suspension was incubated in the device under static conditions for 2 hours at 37 °C to allow for bacterial adhesion to the channel floor. Following this, sterile LB media was introduced at a rate of 10 µl/hr for 72 hours for biofilm growth. Fresh LB

media was replenished every 24 hours. Results from the three devices are shown in Figure 3-5a and samples of rendered confocal images are shown in Figure 3-5b-e. The colors in the image correspond to different components of the biofilm. The red represents dead cells, the green represents live cells and the blue represents the ECM of the biofilm. Specifically, the biofilm thicknesses in the various channels of three devices were compared.

The results (Figure 3-5) show that the biofilms have very small thickness variation within each device (SD < 1.2 μm, 10 % of the average thickness at the maximum, as compared to the inter-device variability of 21%). Table 3-2 lists the average biofilm thickness of each channel of each device and the average biofilm thickness across each device. Three confocal microscopy images were obtained for each channel of each device. A comparison of the average thicknesses between devices suggests that the variation between devices is large enough so that the biofilm in a device is significantly different from the biofilm in the other device (ANOVA, $P < 0.05$). The smaller intra-device variability as compared to the inter-device variability between the three devices highlights the importance of an integrated control. These results confirm that biofilm thicknesses within each device are more uniform than biofilms grown between devices. The simple microfluidic platform developed herein will now be used to test new potential biofilm treatments.

3.4 Discussion

In this work, biofilm growth in various variations of microfluidic channels was investigated. Biofilms grown in single channel microfluidics are shown to have low

variation within the channel while inter-device variability was measured to be as high as 68.62%. This device to device variability makes new treatment testing challenging in microfluidics, as comparison between channels becomes unreliable. Valved microfluidic devices provide a solution to this problem by using microfluidic valves to section a uniform biofilm grown within a single channel. Such sectioning allows for the introduction of multiple treatments into the different sections of the channel to enable true reliable comparison of the treatment efficacies.

While microfluidic valves provide a true solution to significantly reduce variability of biofilm growth, the challenges of device fabrication and microfluidic valve integration need to be addressed. As a consequence, device yield is significantly lowered when the valved devices are scaled to perform tens of experiments in parallel. To address this issue, in this work a simple valve-less biofilm sectioning device was fabricated and tested. The device worked on the principle of bifurcation and spatially sections biofilms. Using confocal image analysis the variability between the channels of the same device was shown to be similar to the variability observed in the valved microfluidic devices. The lack of valves enables a simple fabrication process and also allows for easy scalability to tens to hundreds of channels, without loss in yield, thus emphasizing the suitability of this platform for high-throughput *in vitro* characterization of both biofilm growth and treatment.

3.5 Chapter Summary

Microfluidic systems provide an efficient and convenient method for investigation of bacterial biofilms, while allowing easy integration of sensing and treatment

modules. A key challenge of using microfluidics for biofilm studies is the large variability between channels or devices. This issue was addressed through the use of a simple bifurcation-based microfluidic platform that enables spatial sectioning of the biofilms. The sectioned biofilms could then subjected to different treatments in parallel and by using one of the sections as a negative control, reliable comparison of the efficacy of the treatments was achieved.

Chapter 4. The Bioelectric Effect – An Alternate Biofilm Treatment

A promising method to increase the efficacy of antibiotics on biofilms is a combinatorial treatment based on applying electrical signals in combination with low doses of antibiotic, also termed the 'bioelectric effect' [133,190,191]. Costerton et al. [130] demonstrated improved biofilm treatment through the application of either direct or alternating current (DC or AC) electric fields [131,132,134,192-197]. Details of the fundamental mechanisms of the BE are still under investigation, and divergent hypotheses have emerged based on the type of the applied field. In the case of a DC voltage, the generation of radicals owing to media electrolysis is suggested as a principal factor [132,134,198]. In addition, some reports describe enhanced efficacy owing to improved antibiotic binding to biofilms [191,199] and enhanced biofilm detachment [200] from an external DC electrostatic force. In the case of the AC treatment, results indicate increased permeability of the exopolysaccharide matrix because of locally charged molecular vibrations [197]. Other reports note augmented effects from thermal stimuli [192] as well as electrolysis of the medium [199]. In general, investigating the mechanisms that underlie the BE on biofilms is difficult owing to their complex structures and the diverse stimuli [199].

In this chapter, we study the effect of electrical signal energy on the efficacy of the BE. This work could not have been possible without the assistance of Dr. Young Wook Kim and Dr. Konstantinos Gerasopoulos. I would like to credit Dr. Kim for performing the CFU count experiment and the bulk electrolysis quantification using a pH indicator presented in section 4.1.

4.1 Effect of Electrical Energy on Efficacy of BE Treatment

Given the divergent nature of the reports on the attributable mechanisms of action for DC and AC fields independently, a hypothesis that was examined in this work is whether their superposition could result in a synergistic treatment effect, by combining the reported benefits of both DC and AC fields, namely increased permeability of the exopolysaccharide matrix, and media electrolysis, biofilm detachment and improved antibiotic binding, respectively. To test this hypothesis, we treated biofilms with antibiotics under the application of a superpositioned (SP) field containing both AC and DC components. Interestingly, we observed that the treatment efficacy of the SP-BE was the linear sum of the individual treatment efficacies of the AC-BE and DC-BE. As the total energy of the SP-BE was the linear sum of the AC-BE and DC-BE, we investigated the effect of total electrical energy on BE treatment efficacy and established that the energy provided to the BE was the governing factor that dictated the efficacy of the treatment. Despite the number of studies of both AC and DC fields and their apparent successes, to date, no studies on the effect of the total electrical energy have been conducted.

We treated *E. coli* biofilms [201] with DC, AC and SP electric fields in combination with the antibiotic gentamicin [141]. We tested the effect of the electrical signal energy on the efficacy of the BE by applying either a DC field, an AC field or an SP field, in combination with the antibiotic gentamicin (10 μg/ml) to 24-hour mature biofilms in a macro-scale cuvette setup (Figure 4-11). Three sets of experiments were performed and the efficacy of treatment was measured: (i) the amplitudes of the three different electrical signals (AC, DC and SP) were chosen such

that the magnitude of energy of the SP signal was the sum of the magnitudes of the DC and AC signal energies, (ii) the amplitudes of the AC, DC and SP potentials were chosen such that each signal had the same magnitude of energy when applied over a period of 24 hours and (iii) increasing energies of the AC electrical signal was applied over a period of 24 hours. The effectiveness of the BE treatment was quantified by the crystal violet (CV) staining method and the live bacterial density results as measured by the colony-forming unit (CFU) assay. As the voltages selected were less than or close to 0.82 V, we were able to avoid electrolysis of the surrounding medium. The concentration of gentamicin (10 μg/ml) used in our experiments is significantly lower than what is typically necessary for biofilm treatment (500–5000 times the concentration compared with the minimum inhibitory concentration (MIC) of suspended bacteria, MIC = 2–5 μg/ml) [130]. Our experiments resulted in two key conclusions. First, we observed that biofilm BE treatment with an SP signal of higher electrical energy that was the sum of two smaller AC and DC energies resulted in a net treatment efficacy that was equivalent to the sum of the individual AC and DC treatment efficacies. Second, the application of electrical signals (DC or AC or SP) of the same energy in combination with a fixed concentration of gentamicin resulted in equivalent treatment efficacies. These results reveal that the signal energy, and not the type of electrical signal (AC or DC or SP), is the primary parameter that governs the mechanism of action of the BE. These conclusions were further confirmed when varying the BE energy, by changing the amplitude of an AC potential, resulted in a linear change in efficacy.

The results presented in this work bring to light that the mechanism of action of the BE is not different for AC or DC or SP fields for potentials <1 V, as reported previously. We hypothesize that the electrical energy applied to the treatment in the form of the DC, AC or SP signals provides the charged antibiotic molecule with additional drift that results in the enhanced efficacy of this treatment. The linear dependence of the BE on the electrical energy, enables deterministic modification to the treatment. In addition, BE dependence on the energy and not the signal type allows for more efficient utilization of nearby electronic resources. For example, in an *in vivo* BE treatment system, generation of on-chip AC signals from nearby electronics can be achieved more easily with higher efficiency as compared with generation of a pure DC potential. It also opens up the opportunity to transmit wireless power in the form of an AC signal so that future designs of *in vivo* sensor-treatment platforms can include electronics for inductive power transmission. True understanding of the mechanism of action of the BE will thus allow for more flexibility and ease of integration of the BE into various applications in both the clinical and environmental fields.

4.1.1 Electrical Amplitude Calculation

For Treatment with Equivalent Energies

To compare the effect of different types of electrical energy signals on biofilm treatment using the bioelectric effect, DC, AC and superimposed DC and AC fields of equivalent energies were applied in combination with 10 μg/ml of gentamicin to 24-

hour biofilms. The average energy E of the signals were calculated using the equation below [202]

$$E_{signal} = \frac{1}{R} \int_0^T (A + B\,sin(\omega t))^2\, dt \quad (4.1)$$

where A is the amplitude of the DC potential, B is the amplitude of the AC component of the signal, T is the duration of application of the electrical signal, R is the resistance of the system and ω is the frequency of the AC signal.

Using equation (4.1), the energy of the SP-BE treatment (0.5 V DC and 0.5 V AC at 10 MHz) can be calculated as shown in equation (4.2) below. The resistance of the system is assumed to be primarily from the glass coupon. Using the resistivity of Pyrex glass as 4 MΩ-m, the resistance of a glass coupon is calculated to be 4,000 GΩ.

$$E_{SP-BE} = \frac{1}{R} \int_0^T (0.5 + 0.5\,sin(\omega t))^2\, dt \quad (4.2)$$

The amplitudes of the pure DC signal and pure AC signal at 10 MHz can then be calculated such that equation (4.3) below was satisfied. We assume that R is constant across all the experiments.

$$E_{SP-BE} = E_{DC-BE} = E_{AC-BE} \quad (4.3)$$

The amplitudes of the DC and AC signals were calculated to be 0.613 and 0.866 V, respectively. The DC amplitude was well below the threshold of electrolysis of

0.82 V; however, the amplitude of the AC field was calculated to be slightly higher than that of 0.82 V. Nevertheless, application of an AC field of 0.866 V at 10 MHz did not result in significant electrolysis.

For Treatment with Varying Energies

To demonstrate the relationship between applied BE energy and the efficacy of treatment, increasing energies of the same type of electrical signal was applied in combination with 10 μg/ml of gentamicin to 24-hour mature biofilms. Varying amplitudes of a 10 MHz AC signal were used and the energy of the applied potential was calculated using equation (4.1). The potentials chosen were in the range of 0–0.9 V, within the limit of electrolysis, to avoid bulk electrolysis of the media. Specifically, four amplitudes of the AC signal: 0 V (control), 0.3, 0.6 and 0.866 V were applied to 24-hour mature *E. coli* biofilms in combination with 10 μg/ml of the antibiotic for 24 hours. The total biomass quantified after treatment with the varying electrical energies is normalized to the control to successfully and reliably combine multiple runs of the experiment. A linear fit of the data was performed using Origin Pro software (OriginLab Corporation, Northampton, MA, USA).

The data were inspected by an outlier checker programme (GraphPad Software, La Jolla, CA, USA, $\alpha = 0.05$) to eliminate outliers from the raw data. With the data, we performed analysis of variance (ANOVA) to investigate the significance of each experimental result. This method was applied to all the experiments.

4.1.2 Effect of Varying Energies and Field Types

Results for CFU Assay

To test the efficacy of the BE treatment, 24-hour mature *E. coli* K-12 W3110 biofilms were subjected to different fields. The concentration of the antibiotic was maintained at 10 µg/ml across all the treatments. The amplitudes of the different electrical signals—namely AC, DC and SP, used for the treatment are listed in Table 4-1. The viable cell counts of the *E. coli* K-12 W3110 biofilms exposed to the BE treatments of different energies were analyzed using the CFU assay method. The reduction in viable cells (*R*) for each of the BE treatments was then calculated by subtracting the viable cell count of the untreated control biofilms. A plot of the reduction in viable cells is plotted for the different BE samples in Figure 4-1.

It is interesting to note that the reductions in biomass as measured using the CFU count method are proportional to the net energy applied to the BE treatment. As shown in the figure, the reduction in viable cells due to the AC-BE is the lowest ($R_{AC\text{-}BE} = 7.5 \times 10^7$ CFU/ml) as it provides the lowest electrical energy during

Table 4-1 Table summarizing the voltages and energies used to test the effect of various energies of different signals on BE treatment efficacy to treat mature E. coli biofilms. Reproduced from own publication [203].

S. No	Type of BE	Concentration of Gentamicin used	Amplitude of voltage applied	Energy applied
1.	AC-BE	10 µg/ml	0.5 V at 10 MHz	2.7 nJ
2.	DC-BE	10 µg/ml	0.5 V DC	5.4 nJ
3.	SP-BE	10 µg/ml	0.5 V DC + 0.5 V at 10 MHz	8.1 nJ

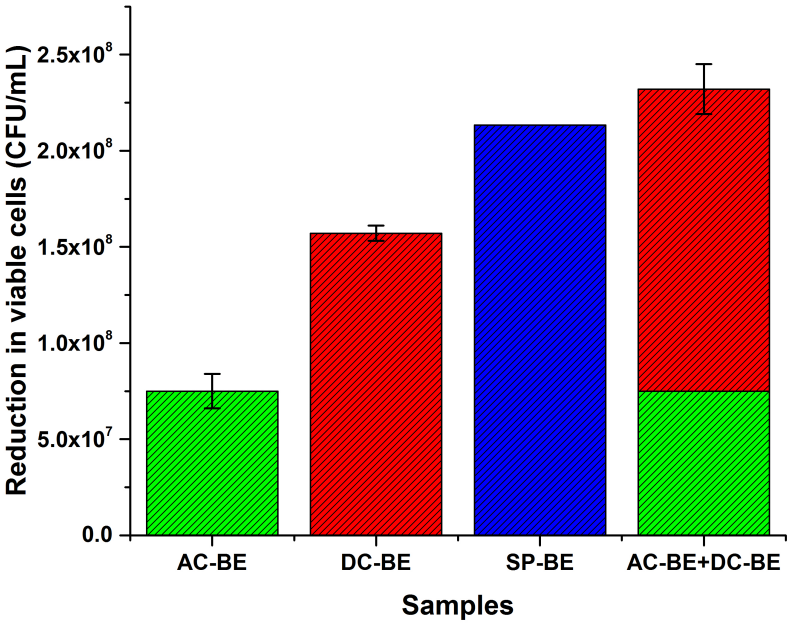

Figure 4-1 Plot showing the reduction in viable cells as measured using the colony-forming unit (CFU) assay method. Treatment with SP-BE, that has twice the energy as the AC-BE or DC-BE, results in almost twice the reduction in viable cells (N = 4 repeats for each experiment). Furthermore, the reduction in the SP-BE viable cell count is not significantly different from the linear sum of the reduction in the AC-BE and DC-BE viable cell count. The error bars represent the standard deviation across the repeats of the experiments. The error bar for the SP-BE is not large enough to be visible at this scale. AC, alternating current; BE, bioelectric effect; DC, direct current; SP, superpositioned field. Reproduced from own publication [203].

treatment. This is followed by the DC-BE, which shows a reduction of ~ 1.6×10^8 CFU/ml ($R_{DC\text{-}BE}$). Although the DC-BE has the same signal amplitude as the AC-BE (0.5 V), it provides twice the energy to the BE treatment, which results in twice the reduction in viable cells (Figure 4-1). The SP-BE, which is the superposition of the AC-BE and the DC-BE signals, results in the highest reduction in viable cells of 2.2×10^8 CFU/ml ($R_{SP\text{-}BE}$). Moreover, treatment with the SP-BE energy ($E_{SP\text{-}BE} = E_{AC\text{-}BE} + E_{DC\text{-}BE}$) results in a reduction in viable cells ($R_{SP\text{-}BE}$) that is not significantly different from the linear sum of the reduction in viable cells owing to the AC-BE ($R_{AC\text{-}BE}$) and DC-BE ($R_{DC\text{-}BE}$) or $R_{SP\text{-}BE} = R_{AC\text{-}BE} + R_{DC\text{-}BE}$ as plotted in Figure 4-1. This experiment

verified that the superposition of the AC and DC signals did not result in a synergistic treatment effect as hypothesized. However, the results suggest that the BE could depend on the energy provided to the treatment. Hence, further experiments to understand the effect of varying energy on the efficacy of the BE treatment were performed.

Results for CV Staining Method

After treatment with the different BEs for 24 hours, the biofilms were quantified using the CV staining method. Negative controls, i.e., treatment with only antibiotic (no electric field) and pure LB (no antibiotic or electric field) were also performed. The results of this experiment are shown in Figure 4-2.

Figure 4-2a plots the total biomass of the biofilms for the various treatments applied. Treatment with only antibiotics at near MIC concentrations resulted in a very small, if negligible, reduction in biomass. This is expected as biofilms are known to have increased antibiotic resistance and require at least 500–5,000 times the MIC dosage of antibiotics for effective treatment [1,6,55,60]. Treatment with the AC-BE, DC-BE and the SP-BE resulted in significant reduction in bacterial biomass as compared with the controls (ANOVA $P < 0.05$). Approximately 50% reduction in total biomass is observed when biofilms are treated with the DC-BE, as compared with the untreated controls (ANOVA $P < 0.05$). Treatment with the SP-BE that has almost 1.5 times the energy as the DC-BE resulted in a significant decrease in total biomass (ANOVA $P < 0.05$) of 50% over the DC-BE, or an overall decrease of almost 71% as compared with the untreated control.

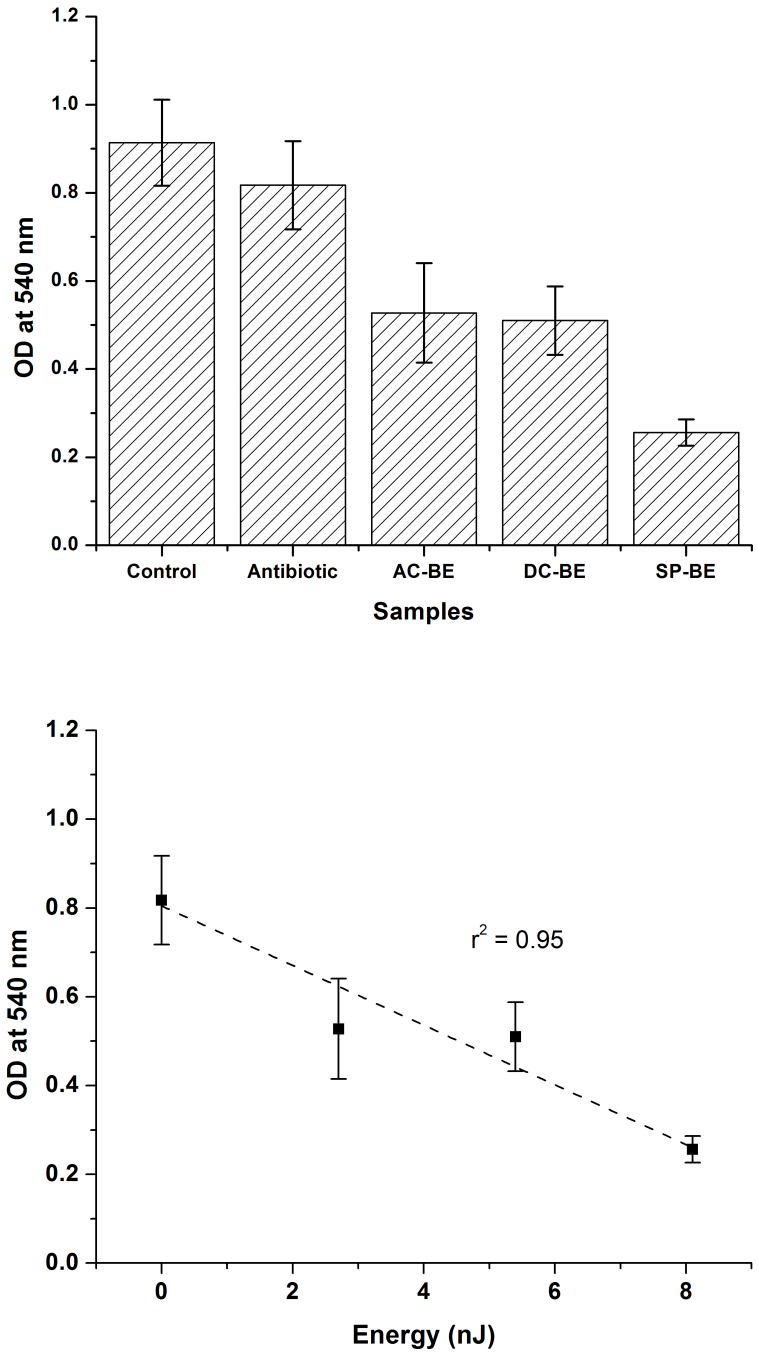

Figure 4-2 (a) Results of total biomass quantification using the crystal violet staining method. (b) Linear fit of the total biomass for the different energies provided during BE treatment. Plots show the OD at 540 nm after staining the treated biofilms with CV. Results show that the SP-BE shows a 71% reduction in bacterial biomass as compared with the untreated control (analysis of variance $P<0.05$). The SP-BE, which has higher energy as compared with the AC-BE or DC-BE is also more effective in treating biofilms. The data presented are the average OD_{540} and the error bars represent the standard deviation over repeated experiments (N = 6 repeats for each experiment). AC, alternating current; BE, bioelectric effect; DC, direct current; OD, optical density; SP, superpositioned field. Reproduced from own publication [203].

The total biomass, as measured using the CV staining method, is also plotted as a function of the total energy applied with the BE (Figure 4-2b). The biofilms treated with only 10 μg/ml of the antibiotic gentamicin is plotted as the control (treatment with no electrical energy). Again a strong linear dependence of the treatment efficacy on the applied BE energy is observed ($r^2 = 0.950$). These results further demonstrate that the super-position of the two types of fields, AC and DC, during the BE treatment does not result in a synergistic effect. Rather, the energy of the electrical signal may have a key role in determining the efficacy of the treatment.

4.1.3 Effect of Varying Field Types of Equal Energies

Results for CV Staining Method

To verify whether the electrical energy supplied to the BE treatments is the dominant factor affecting the efficacy of the BE treatment, AC-BE, DC-BE and SP-BE treatments of the same energy were applied to 24-hour mature *E. coli* biofilms over 24 hours. The energies and potentials of the AC, DC and SP signals were established using equation (4.3), and are tabulated in Table 4-2. After treatment, the biofilms were stained using the CV staining method and the OD at 540 nm was recorded. A plot of the OD_{540} for the different BE treatments and the control is shown in Figure 4-3.

As seen from Figure 4-3, the AC-BE, DC-BE and SP-BE treatments with equivalent energies result in a similar reduction in bacterial biomass (ANOVA $P > 0.05$). On average, the AC-BE resulted in an 83.57% decrease, the DC-BE treatment

Table 4-2 Table summarizing the magnitude of voltages used to test the effect of equivalent energies of different signals on BE treatment efficacy to treat mature E. coli biofilms. Reproduced from own publication [203].

S. No	Type of BE	Concentration of Gentamicin used	Amplitude of voltage applied	Energy applied
1.	AC-BE	10 µg/ml	0.866 V at 10 MHz	8.1 nJ
2.	DC-BE	10 µg/ml	0.613 V DC	8.1 nJ
3.	SP-BE	10 µg/ml	0.5 V DC + 0.5 V at 10 MHz	8.1 nJ

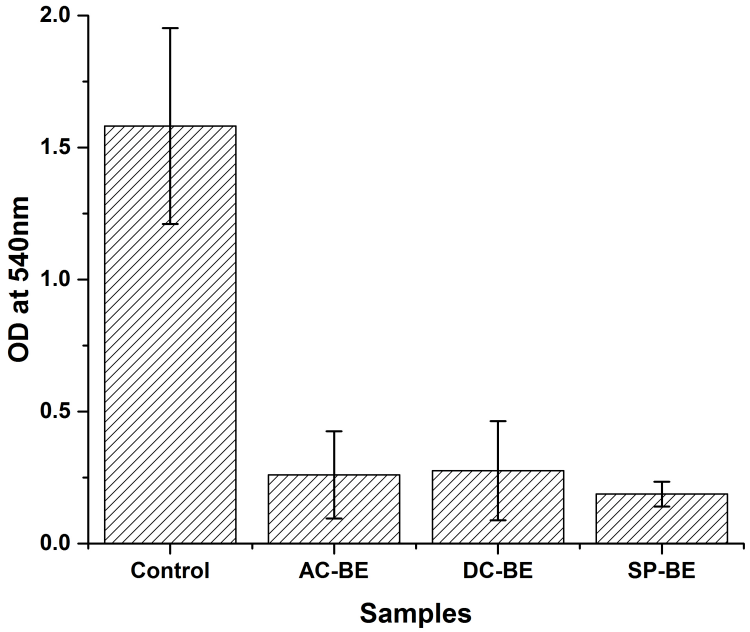

Figure 4-3 Figure plotting OD measured at 540 nm for various biofilms samples treated with BE of equivalent energies. The energy of the electrical signal dictates the efficacy of the BE as observed by the similar reduction in total biomass for the AC-BE, DC-BE and SP-BE treatments. The error bars represent the standard deviation of the experiments performed across eight samples (N = 8 repeats for each experiment). AC, alternating current; BE, bioelectric effect; DC, direct current; OD, optical density; SP, superpositioned field. Reproduced from own publication [203].

resulted in an 82.55%decrease and the SP-BE resulted in an 88.15% decrease in total biomass as compared with the untreated control. Overall, the BE treatments with

equivalent energies resulted in an 84.76 ± 5.32% average reduction of total biomass as compared with the control. This illustrates that the type of electrical signal used (AC, DC or SP) does not affect the efficacy of the BE treatment. Furthermore, these results illustrate that the BE energy applied is the prime factor in determining the treatment efficacy.

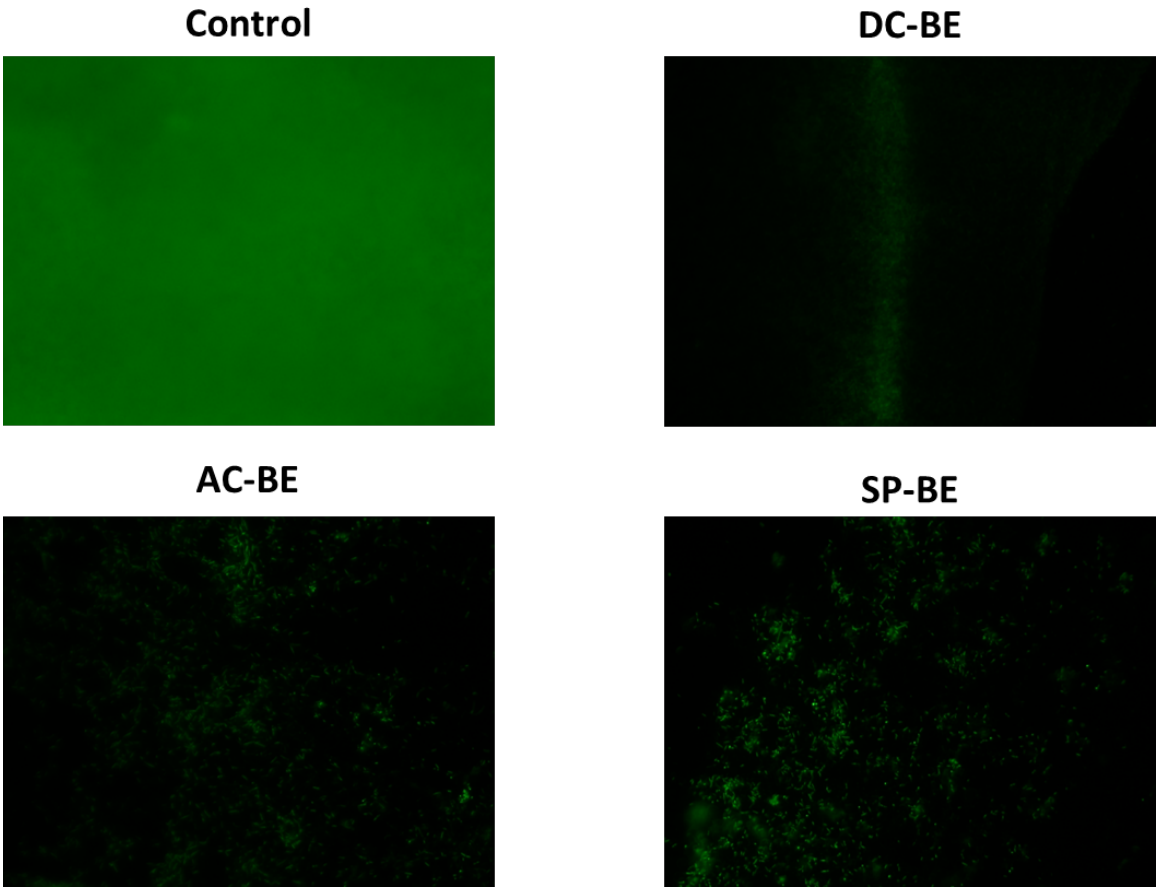

Figure 4-4 Fluorescence microscopy images of the biofilm grown on the glass coupon after treatment with DC-BE, AC-BE and SP-BE as compared with untreated biofilms (control). The BE-treated biofilms result in a similar reduction in biomass as observed from the images. AC, alternating current; BE, bioelectric effect; DC, direct current; SP, superpositioned field. Reproduced from own publication [203].

Results for Fluorescence Microscopy

To visualize the effect of the BE treatments on the biofilms, the treated biofilms were stained using Filmtracer LIVE/DEAD Biofilm Viability Kit and imaged under the fluorescence microscope. The images for the control, DC-BE, AC-BE and SP-BE biofilms are shown in Figure 4-4. The control biofilm is the densest, whereas the BE-treated samples result in almost complete removal of biofilm. Furthermore, the three BE-treated biofilms result in a similar reduction of biomass as observed from the images of Figure 4-4. This correlates very well with the end-point results obtained using the CV staining technique presented in Figure 4-3.

4.1.4 Effect of Varying Energies of Equal Field Types

To determine the relationship between the BE energy and the treatment efficacy of the BE, mature *E. coli* biofilms were treated to different electrical energies of a similar signal type. As observed from the results presented in Figure 4-3, biofilm reduction does not depend on the type of electrical signal used for the BE treatment, i.e., AC or DC or SP. Hence, for these experiments, we arbitrarily chose to use AC fields. Specifically, varying amplitudes of a 10 MHz AC signal was used in combination with 10 μg/ml of the antibiotic gentamicin. The magnitudes of the voltages used are tabulated in Table 4-3. The biofilms were then stained using the CV staining method and the OD_{540} was measured (N = 5 experimental repeats per data point).

Table 4-3 Table summarizing the magnitude of AC voltage used to test the effect of increasing energies of the same type of signal on BE treatment efficacy to treat mature E. coli biofilms. Reproduced from own publication [203].

S. No	Sample	Amplitude of 10MHz AC voltage	Energy applied
1.	Control	0 V	0 J
2.	E_1	0.3 V	1 nJ
3.	E_2	0.6 V	3.9 nJ
4.	E_3	0.866 V	8.1 nJ

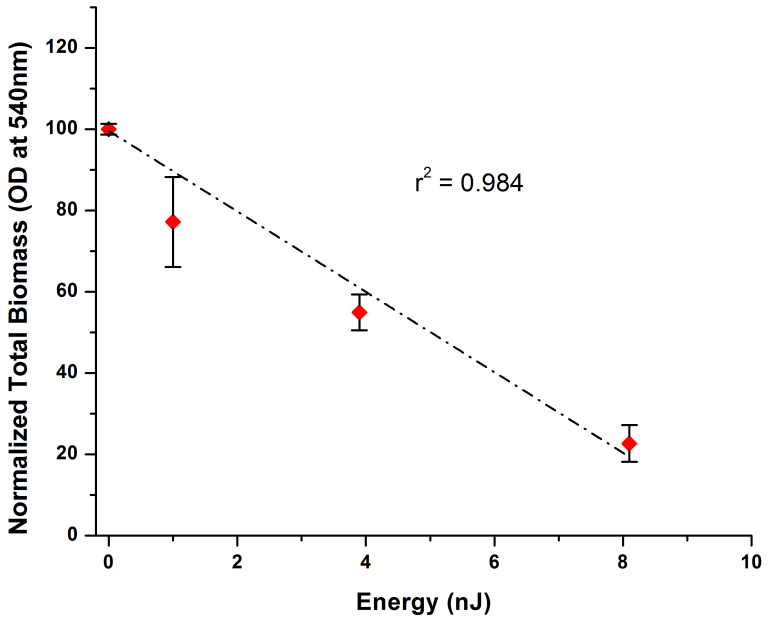

Figure 4-5 Plot showing the linear relationship between the total biomass of the biofilms as measured using CV staining method and the voltage or energy of the electrical signal applied. The error bars represent the standard deviation across the repeats (N = 5 repeats) for each experiment. AC, alternating current; BE, bioelectric effect; CV, crystal violet. Reproduced from own publication [203].

The results of increasing energy on BE treatment efficacy as measured using the CV staining method is plotted in Figure 4-5. We observe a decrease in total biomass with increasing energy supplied to the BE treatment. Specifically, the application of energy E_3 = 8.1 nJ, through the application of a 10 MHz AC voltage of 0.866 V, results in an 80 % reduction in bacterial biomass. This correlates very well with the results previously presented in Figure 4-3, wherein application of the same energy level E_3 through the use of either an AC, DC or SP voltage results in a similar decrease in total biomass. These results when taken together validate our hypothesis that the energy of the electrical signal is the primary factor in determining the efficacy of the BE treatment.

4.1.5 Discussion

In this work, the efficacy of treating biofilms with an electric field applied concurrently with antibiotic treatment was evaluated as a function of energy and type of electric signal (AC, DC or SP). We hypothesized that the superposition of DC and AC fields would enable the simultaneous application of all mechanisms previously attributed to both DC and AC currents individually. That is, a DC electric field can create a non-uniform distribution of electrolytes [199,204] and an AC field can increase biofilm permeability [197]. However, the results obtained in this work support the conclusion that the biocidal effects of the antibiotic can be improved to a similar extent when different types of electrical fields of equivalent energies are applied. Overall, our data demonstrate that the enhancement of biofilm treatment when antibiotics are combined with electric fields is primarily because of the

additional energy provided to the treatment and not owing to the type of electric signal used. Furthermore, we believe that the additional energy provided to the treatment allows for a stronger directed flow of the charged antibiotic molecule into the biofilms that results in the enhanced treatment efficacy. Hence, when higher energy is provided to the treatment either in the form of increased electrical potential or in the form of longer durations of treatment we expect to observe larger reduction in biomass.

The magnitude of the voltages applied in this work is lower than the threshold potential of biological electrolysis of the medium (0.82 V) [205]. This was done to avoid the generation of hazardous radicals [132]. Often, in previous work, the applied voltages for analyzing the BE have been above 0.82 V (typically in the range of 2–5 V/cm) [130,198,199]. In the study performed by Costerton et al. [130],5.0 times the MIC of tobramycin was used in combination with an electric field of 5 V/cm for 48 hour to treat *Pseudomonas aeruginosa* biofilms. Treatment with this high-energy combination therapy resulted in almost a complete kill of the viable cells ($<10^2$ viable cells per cm^2; ~10^6 reduction in viable cells per cm^2). In another detailed study [195], the electrical enhancement of different classes of antimicrobials (antimicrobial concentration range of 1.0–32.0 times the MIC) on various bacterial biofilms was studied. Treatment with 200 and 2,000 μA in combination with the antimicrobials resulted in ~ 10^2–$10^{4.5}$ CFU/cm^2 mean reduction in viable cells. Correspondingly, media electrolysis owing to the high external electric fields used has often been cited as one of the major contributors to the enhanced biocidal effects observed under applied DC currents [132,134,198]. Such electrolysis leads to oxidant generation and

media decomposition. These factors make the direct attribution of specific mechanisms of action difficult [190,199]. Furthermore, they make integration of such high voltage treatments in *in vivo* systems impossible. In comparison, in our work, we applied only 2.0 times the MIC of gentamicin in combination with low SP fields over 24 hours and observed a decrease of 2×10^8 CFU/ml.

In this work, we present effective treatment using voltages below those needed for electrolysis. We tested for bulk pH changes owing to electrolysis, using a pH indicator (#36828, Fluka Analytical) which changes color in the pH range of 4–10, after application of the SP-BE field to unbuffered LB media for 24 hours; results reveal no statistical difference relative to the control (no applied potential). This is in contrast to significant bulk pH change measured when the electrolysis threshold voltage of 0.82 V DC was applied (Figure 4-6, ANOVA $P < 0.05$). Samples subjected to AC or DC fields used here also exhibited no visible signs of bulk electrolysis relative to the control. We thus conclude that the application of electric fields used in this work does not induce any significant fluidic electrolysis.

We also note that thermal effects can be induced by applying external fields, which might lead to misinterpretation of data. Temperatures greater than 45 °C result in biocidal effects as enzymes and proteins essential to biofilm growth processes are denatured [206]. Several studies, however, have reported that local heating from applied AC signals with field intensities of 2 V/cm was less than 1 °C for a 24-hour treatment. This temperature change did not affect bacterial growth [192,197]. As the applied field intensity in this work was lower than previous reports (2 V/cm), we did not pursue these effects for detailed study.

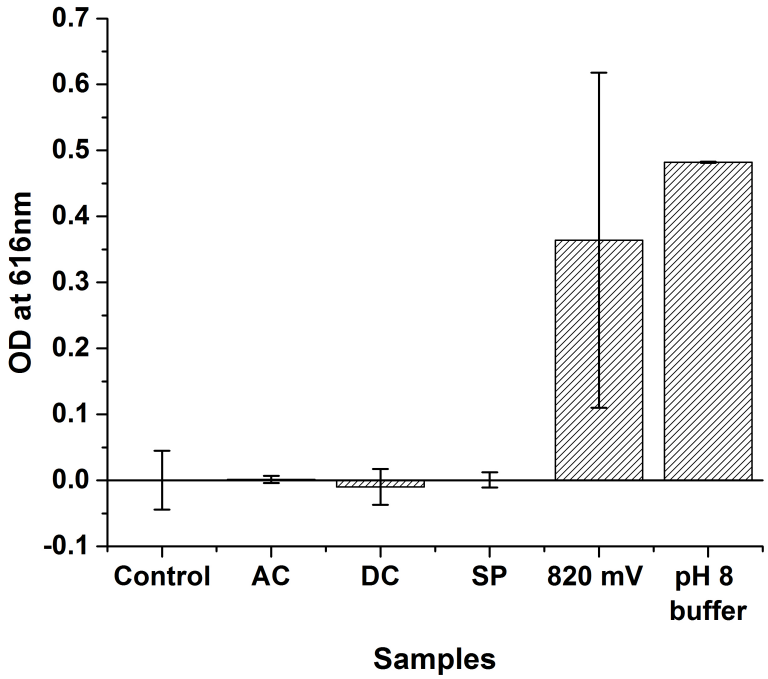

Figure 4-6 Results of bulk electrolysis quantification using a pH indicator (N = 3 repeats for each experiment). 1 mL of fresh unbuffered LB growth media was placed in the cuvette and electrical potentials (no antibiotics) were applied for 24 hours. The potentials applied are: AC: 0.5 V at 10 MHz; DC: 0.5 V; SP: 0.5 V DC + 0.5 V at 10MHz; and the electrolysis threshold voltage of 0.82 V DC. No electrical potentials were applied to the controls (pure LB media or pH 8 phosphate buffer). Since electrolysis induces the production of hydrogen gas, the solution is expected to become more basic18, 26, 34. This increase in pH is used to indirectly quantify the bulk electrolysis of the media due to application of electrical potentials. Following 24 hours of electrical potential application, two drops of the pH indicator were added to the solution and the OD spectrum was measured by the spectrophotometer. Since the peak value of the pH 8 buffer solution using the pH indicator was observed at 616 nm wavelength, OD616 was selected to quantify the electrolysis effect. As observed, only the samples to which 0.82 V was applied and the pH8 buffer positive control samples showed significantly higher OD compared to other treatments. We thus conclude that application of low energy electrical fields does not induce significant bulk electrolysis. Reproduced from own publication [203].

Finally, we note that the BE is applicable to a broad range of microorganisms; hence, it cannot be generalized. Previous studies demonstrate that the BE can be extended to different species of bacteria and various antibiotics [195,207,208]. The enhancement in efficacy of the antibiotics through the use of electrical potentials is observed to be different for different bacterial species and is known to depend on

multiple parameters like the type of antibiotic, the antibiotic concentration and the electrical energy applied [195,196,209]. However, we suggest that when all other experimental parameters (bacterial species, antibiotic and antibiotic concentration) are kept constant, for the same magnitude of electrical energy applied, irrespective of the type of electrical signal, a similar increase in efficacy of treatment is expected to be observed.

In summary, significantly improved treatment of biofilms was demonstrated by using electric fields in conjunction with the antibiotic gentamicin. It was observed that the BE supplied with higher electrical energy induced greater biofilm reduction than the BE with lower electrical energy for applied voltages less than the media electrolysis voltage. We further note that the type of electrical signal did not appear to affect the efficacy of the treatment indicating that the mechanism of action is not different for DC versus AC signals in this range of potentials (applied voltages less than 1 V). We suggest that the enhanced treatment efficacy of any BE treatment (AC, DC or SP) is primarily owing to the energy provided to the treatment that allows for either increased permeability of the membranes or the apparent improved diffusion of the charged antibiotics or both. We highlight that the intensity of the fields utilized here was below the electrolysis potential of the biological fluid. Hence, applications of this technique would minimize generating harmful radicals due to media electrolysis, enabling future integration in *in vivo* systems.

4.2 Efficacy of Alternative Treatment Therapies

Traditional treatments for biofilms include the use of high doses of antibiotics or surgical removal of the implant. However, in previous work performed in our group other alternative combinatorial treatments have been studied for the treatment of mature biofilms. The key results of these alternative therapies are presented below along with the results obtained for the new combination therapy that combines AI-2 analog with electric fields.

4.2.1 AI-2 Analog

Small molecule QS inhibitors or AI-2 analogs are of particular interest as a method of treatment for bacterial biofilms as they aid in biofilm prevention by inhibiting QS. Analogs can be tailored to target different bacteria by modifying the alkyl group attached to the DPD backbone [143]. For example, iso-butyl DPD, an AI-2 analog variant can be used to target *E. coli* biofilms. This was verified in both static and flow conditions by using a 96-well plate and a simple microfluidic flow cell. Figure 4-7 presents the results of *E. coli* W3110 and MDAI2 biofilm exposure to various concentrations of iso-butyl DPD in a microliter plate setup. The biofilms were grown in the wells of the plate for 24 hours at 37 °C, followed by treatment with various concentrations for an additional 48 hours. The AI-2 analog was diluted in LB and refreshed every 24 hours. The biofilms were stained using ECM matrix stain, Dimethyl methylene blue (DMMB), and a viable cell stain, Resazurin, as per the protocols described by Toté et al. [210]. DMMB is a cationic dye that binds to

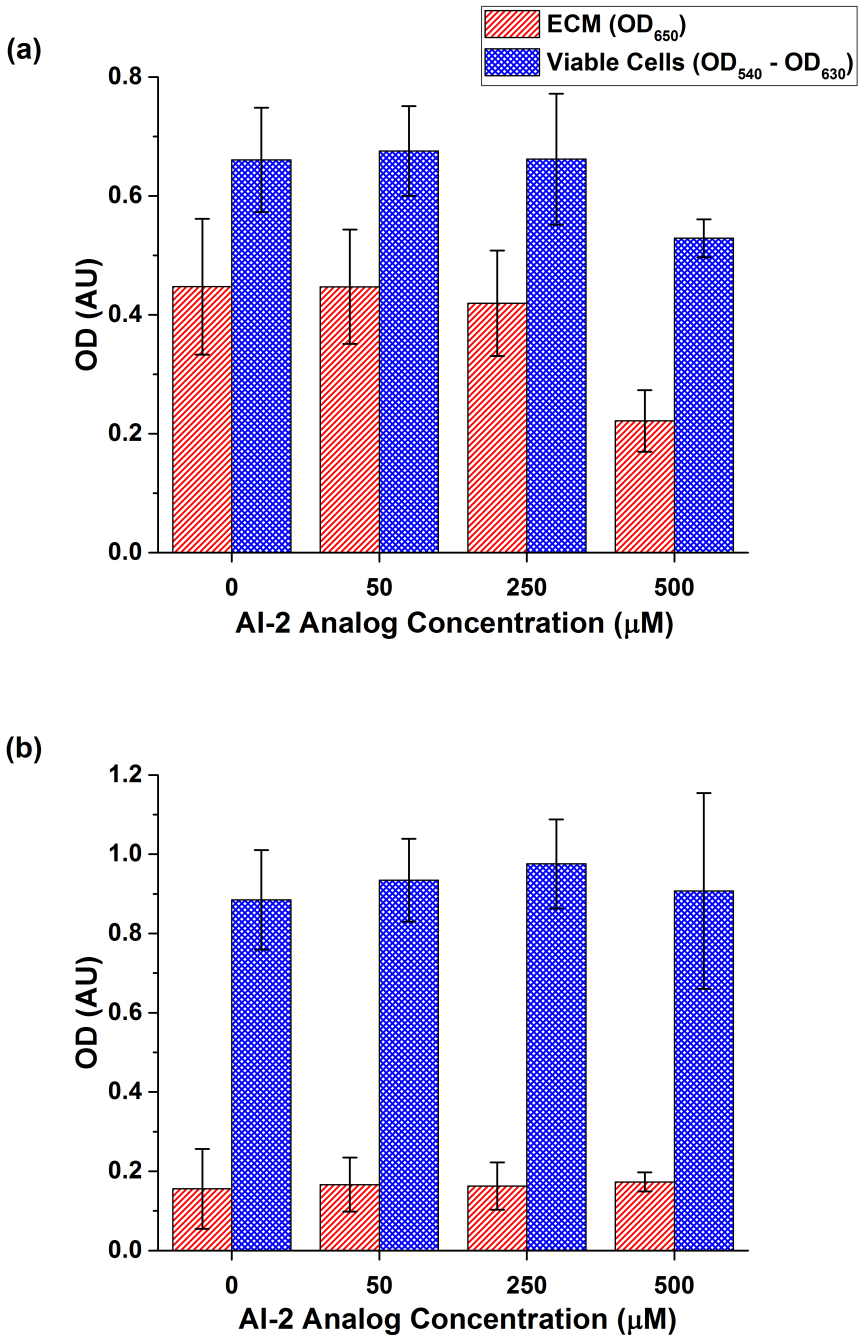

Figure 4-7 Plot of OD versus AI-2 analog concentration measured in a 96-well plate platform. (a) OD measured for AI-2-producing *E. coli* W3110 biofilms, and (b) non-AI-2-producing *E. coli* MDAI2 biofilms. The OD was measured at two different wavelengths for the stains DMMB and resazurin, which measures the amount of ECM produced by the bacterial cells and the viable cell concentration respectively. The error bars correspond to the variation in OD across six different wells of the 96 well plate.

polysaccharide intercellular adhesion (PIA) present in the ECM. Hence by measuring the amount of DMMB trapped in the ECM is directly proportional to the amount of ECM present in the sample. The redox dye resazurin, widely used for cellular viability testing, is a deep blue dye that is reduced to the pink resorufin proportionally to the amount of metabolically active cells present in the sample. Figure 4-7a plots the OD as a function of AI-2 analog concentration for *E. coli* W3110 biofilms. As seen from the figure, there is a significant decrease in the ECM produced and viable cell count with increased concentration of AI-2 analog. In contrast, Figure 4-7b plots the results for *E. coli* MDAI2 biofilms, a genetically engineered *E. coli* strain designed to not synthesize AI-2 that is critical to biofilm formation. As expected application of increased concentrations of AI-2 analog does not affect the viable cell count or the sparse ECM produced.

Varying concentrations of iso-butyl DPD were also tested on *E. coli* W3110 biofilms using a simple microfluidic flow cell (3 cm x 500 μm x 100 μm). *E. coli* biofilms were grown in the microfluidic channel for 24 hours at 37 °C, following which varying concentrations of AI-2 analog diluted in LB media was introduced at a flow rate of 10 μl/hr for 48 hours. The biofilms were then stained using Filmtracer™ LIVE/DEAD® Biofilm Viability Kit (Invitrogen Corp.) and imaged using an LSM 710 Zeiss confocal microscope. The Z-stacks obtained were then analyzed using COMSTAT computer program [159]. Figure 4-8 plots the biofilm thickness (μm) and biomass ($\mu m^3/ \mu m^2$) of the imaged Z-stacks for varying concentrations of iso-butyl DPD. The error bars represent the standard deviation of the thickness and

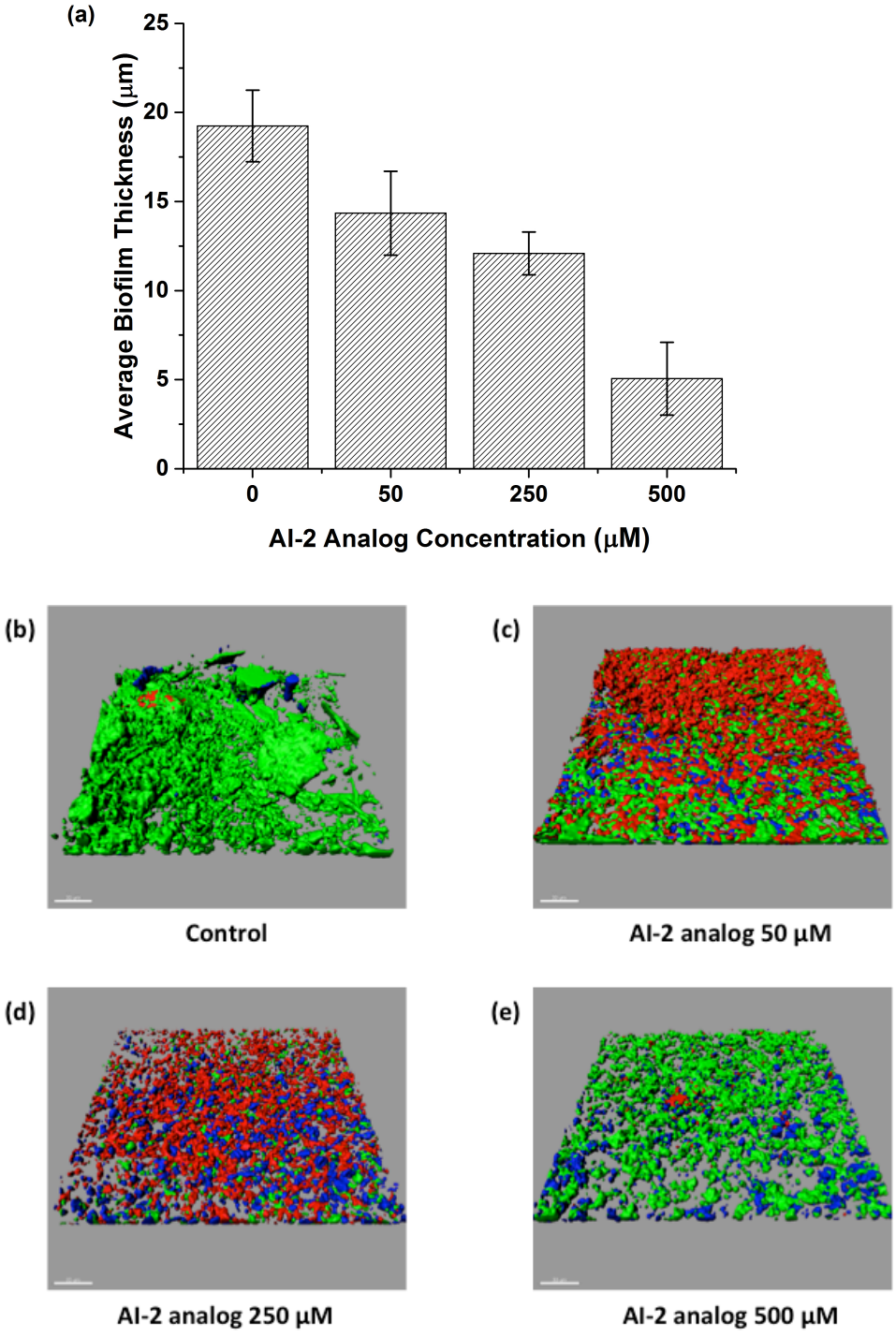

Figure 4-8 (a) Plot of biofilm thickness for various AI-2 analog concentration as tested in single channel microfluidics on E. coli W3110 biofilms. Treatment with increasing concentration of AI-2 analog results in a decrease in average biofilm thickness as measured using confocal microscopy and analyzed using COMSTAT [159]. (b-e) Surface rendered sample confocal microscopy images from the device (scale bar = 30 μm). The thicknesses were 18.47 μm (control), 16.20 μm (AI-2 analog 50 μM), 12.93 μm (AI-2 analog 250 μM) and 6.35 μm (AI-2 analog 500 μM).

biomass across three confocal images. As seen in the figure below, there is a decrease in both biofilm thickness and biomass with increasing concentration of AI-2 analog. A comparison of the results show that a reduction in biofilm thickness and biomass is observed at an analog concentration of 50 μM in the flow cell as opposed to 500 μM in the static well plate setup. The better treatment efficiency in the flow cell is attributed to the continuous replenishment of nutrients and analog.

The treatment efficacy of the AI-2 analog, iso-butyl DPD was also verified using a continuous monitoring CCD platform. *E. coli* W3110 biofilms were grown for 24 hours at 37 °C in a microfluidic biofilm sectioning device. Following the growth, the center channel was sectioned into four segments by actuating the sectioning valves. Different treatments – control (LB media, section 1), antibiotic (gentamicin, 10 μg/mL, section 2), a small molecule biofilm growth inhibitor, (AI-2 analog, iso-butyl DPD, 100 μM, section 3), and a detergent (sodium dodecyl sulfate (SDS), 0.2%, section 4) – were introduced into the four sections of the device for an additional 24 hours at the rate of 10 μl/hr. The control biofilm section was provided with LB media at the same flow rate as the other sections in order to provide a reference, thereby ensuring that the results of the treatments are compared to an integrated control. OD measurements were recorded every 8 minutes, across the length of the microfluidic channel, for each section of the device. These measurements enabled the monitoring of the spatio-temporal development of the bacterial biofilms in each section of the microfluidic device during treatment.

Figure 4-9a plots the change in OD during the 24-hour biofilm treatment. The three treatments – antibiotic (gentamicin, 10 μg/mL), the small molecule biofilm

growth inhibitor, (AI-2 analog, 100 µM), and detergent (sodium dodecyl sulfate (SDS), 0.2%) applied to sections 2, 3, and 4 respectively – showed a reduction in biofilm growth compared to the control section (pure LB media, section 1). As seen from Figure 4-9a, the section 3 treated with the AI-2 analog treatment resulted in the

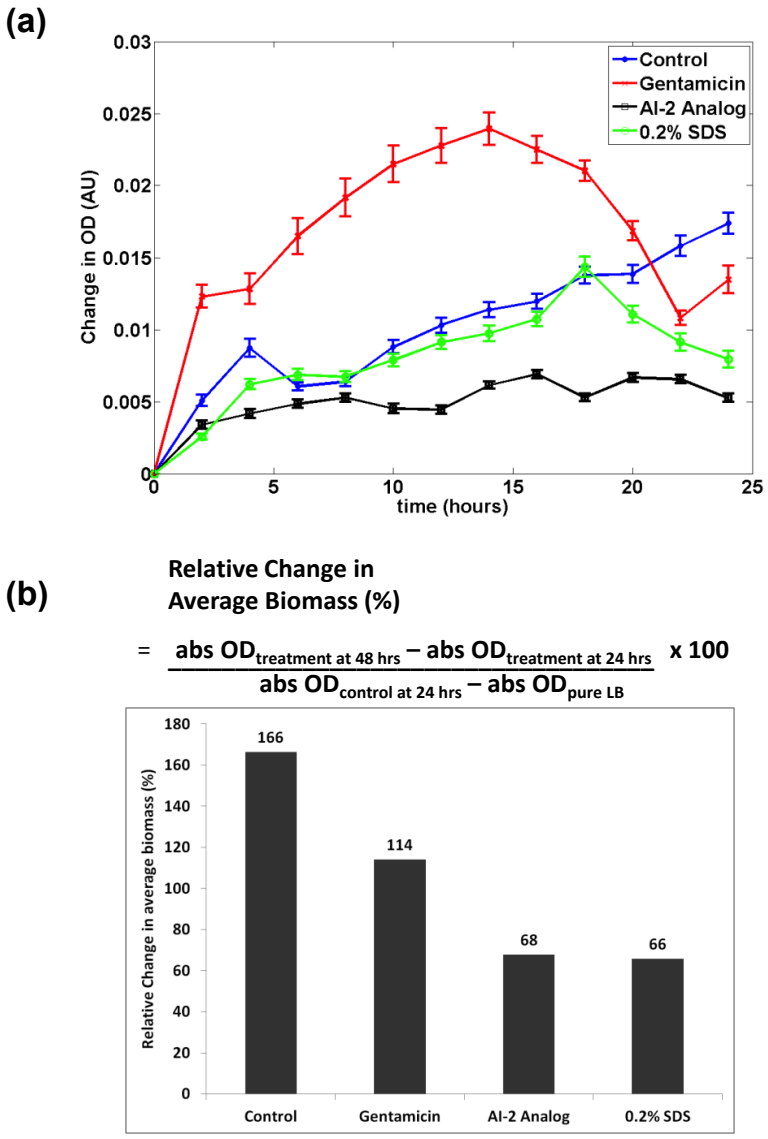

Figure 4-9 (a) Measured average change in OD across the length of each biofilm section (N = 162 pixels along length of channel section) at representative time points, during biofilm treatment in the four sections. The section treated with AI-2 analog shows the least increase in biomass. The error bars represent the spatial variation of the biofilm in each section of the microfluidic channel. (b) Relative percentage change in average biomass calculated using the OD measured after the biofilm treatment in each of the four sections of the microfluidic optical platform.

slowest growth. This correlates with previously obtained results which demonstrate the efficacy of analogs to interrupt the bacterial communication in biofilms that is required for biofilm growth, thereby reducing increase of total biomass. The percentage relative change in average biomass was also calculated for each section of the device after the 24-hour treatment. It is calculated as the ratio of the increase in biomass after treatment to the total biomass formed at the end of the initial 24-hour biofilm growth. The equation used to calculate the percentage relative change in average biomass and the calculated values for each section are plotted in Figure 4-9b. As expected, the control shows the most significant increase in biomass, with a 166% relative increase in average biomass. Treatment with gentamicin resulted in a small decrease in biomass in comparison to the control and showed a 114% increase in average biomass. The AI-2 analog and the detergent (SDS) resulted in a similar reduction in biomass growth with relative change in average biomass of 68% and 66% respectively. Specifically, the analog reduced the average biomass 88% more than the antibiotic. This further verifies the efficacy of AI-2 analogs to inhibit biofilm growth in comparison to the traditional antibiotic therapy.

4.2.2 AI-2 Analog and Antibiotics

The reliability of using the bifurcation platform as a test bed for biofilm treatment characterization and evaluation was verified by analyzing biofilms that were subjected to previously reported therapies using the protocols listed above. Presented in Figure 4-10 are the results of subjecting 24-hour *E. coli* W3110 biofilms to an

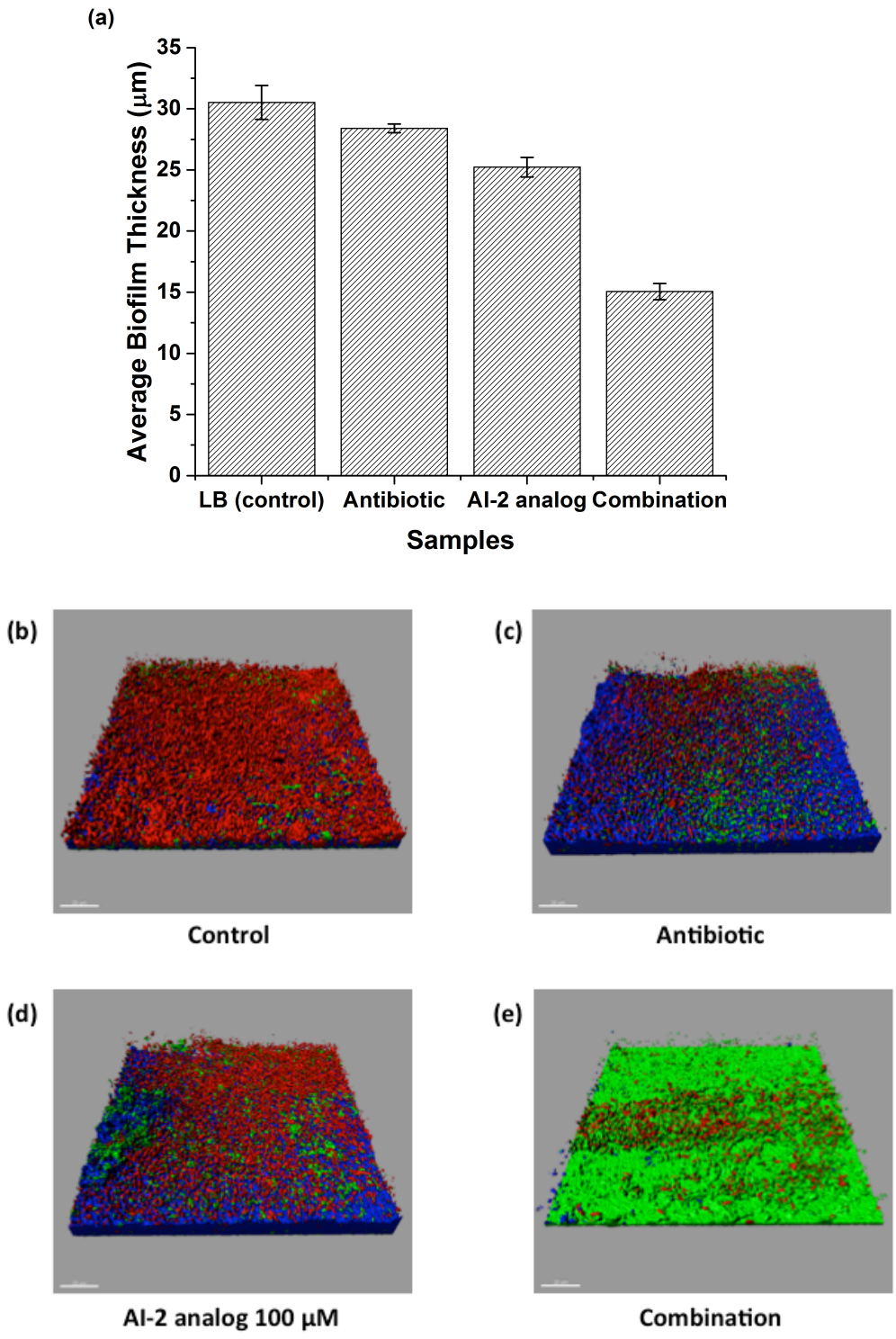

Figure 4-10 Verification of biofilm treatment testing using the bifurcation device. (a) End-point confocal microscopy of the combination treatment of the antibiotic gentamicin and AI-2 analog as applied to 24-hour E.coli W3110 biofilms, resulted in a 50.7 ± 2.2% decrease in biofilm thickness as compared to the control. This is similar to previously obtained results [141]. The error bars represent the standard deviation across three confocal images (N = 3 images) obtained in each channel of the device. (b-e) Surface rendered sample confocal microscopy images from the device (scale bar = 20 µm). The thicknesses were 29.57 µm (control), 28.62 µm (antibiotic), 26.08 µm (AI-2 analog) and 14.31 µm (combination).

antibiotic (gentamicin, 10 µl/ml), AI-2 analog (isobutyl DPD, 100 µM), and the combination of AI-2 analogs and antibiotics. As observed, the antibiotic treatment resulted in almost no change compared to the control (ANOVA, $p = 0.1$), as measured by biofilm thickness calculations using COMSTAT [159]. Treatment with 100 µM isobutyl DPD showed a slightly higher reduction of 17.4 ± 2.6% with respect to the untreated control and antibiotic treatment (ANOVA, $p = 0.0014$). However, treatment with the combination of near MIC levels gentamicin and 100 µM isobutyl DPD significantly enhanced the treatment and results in a decrease of 50.7 ± 2.2% (ANOVA, $p < 0.0001$). These correlate with previously published results [141], thereby validating the use of the bifurcation device based platform for treatment testing of biofilms.

4.2.3 AI-2 Analog and Electric Fields

Macro-scale Cuvette Test Setup

A macro-scale test setup for easy testing of electric field-based biofilm treatments was assembled as shown in Figure 4-11. Figure 4-11a presents a schematic of the macro-scale test setup. It consists of a cuvette with metal electrodes exposed to both inside and outside the cuvette for easy application of electrical voltage. A Pyrex chip 4 cm x 0.8 cm in size is placed in the center of the cuvette such that it is parallel to the electrodes. This surface provides a constant area for biofilm growth. Figure 4-11b shows a photograph of the cuvette with a Pyrex chip placed in the center. The gap between the electrodes of the cuvette is 4 mm.

Using the test setup shown in Figure 4-11, experiments to test the efficacy of the new combination therapy combining AI-2 analogs with electric fields was performed. *E. coli* W3110 cells were cultured overnight in LB media and diluted to an OD_{600} of ~ 0.25. 1 ml of the diluted suspension was pipetted into each cuvette and a Pyrex chip was placed parallel to the electrodes. The cuvettes were placed in an incubator at 37 °C for 24 hours to allow for biofilm growth on the Pyrex chip. After 24 hours, the glass chips were transferred to a new cuvette containing 1 ml of either fresh LB (for the control and electric field only cuvettes) or 100 µM of iso-butyl DPD in LB (for the AI-2 analog and combination treatment cuvettes). This concentration of AI-2 analog was chosen in order to clearly visualize if the combination treatment increased treatment efficacy, as the previous results (Figure 4-7a) showed that in a static environment even 250 µM of analog did not result in significant reduction in biofilm

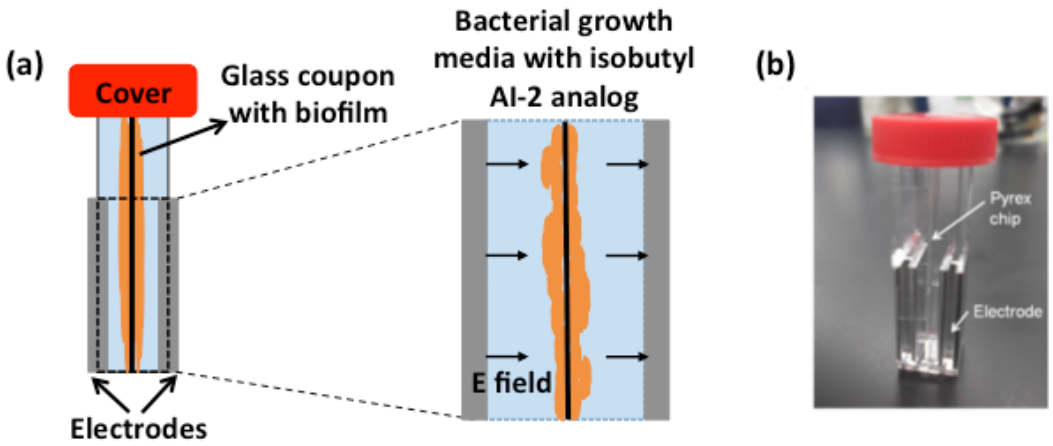

Figure 4-11 Macro-scale test setup for testing of electric field-based biofilm treatment. (a) Schematic of macro-scale biofilm treatment setup for easy application of electric fields. (b) Photograph of 1.5 ml cuvette test setup showing the position of the pyrex glass chip and the metal electrodes.

growth. An electric voltage of 0.5 V DC super-imposed on 0.5 V AC at 10 MHz was applied to the electric field only and the combination treatment cuvettes. This strength of electric field was chosen as a starting point as it was used in our previous study of BE using antibiotics [189]. After treatment for 24 hours, the glass chip from each cuvette was immersed in 1 ml of 0.1% crystal violet (CV) stain for 15 minutes. Following this the Pyrex chips were carefully rinsed in DI four times to remove any excess unbound stain. The chips were then immersed in 2 ml of the decomplexation solution (80% ethanol and 20 % acetone) for 30 minutes to allow for the absorbed CV stain to be released. The OD of this solution was then obtained at 540 nm. The results of the experiment are shown in Figure 4-12. The error bars represent the standard

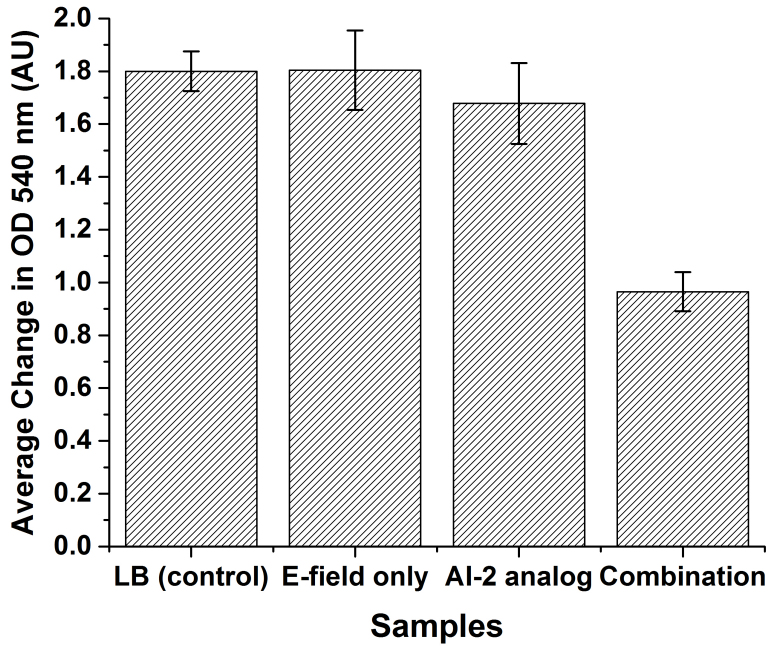

Figure 4-12 Results plotting the average total biomass after treatment with the electric field only, the AI-2 analog and the combination treatment of AI-2 analog and electric fields. The total biomass was quantified using the crystal violet staining method and the final OD was measured at 540 nm. The error bars represent the standard deviation across three experimental repeats (N = 3). The OD_{540} of the combination treatment shows a 46.5% decrease in biomass as compared to the control (ANOVA P < 0.0001).

deviation across three experimental repeats (N = 3). The OD_{540} of the combination treatment of AI-2 analog with electric fields shows a 46.5% decrease in total biomass as compared to the control (ANOVA $P < 0.0001$), whereas the AI-2 analog treatment by itself results in only a 6.76% decrease in total biomass, which correlates with the previous AI-2 analog results obtained in the microwell plate Figure 4-7a.

This is the first demonstration of an enhanced biofilm treatment without the use of any antibiotics. Further experiments to understand the effect of concentration of the analog and the effect of different types of electric fields (AC, DC and super-imposed fields) need to be performed. Additionally, the new combination treatment will also be tested as a potential method to not only treat but also prevent biofilm growth in both the macro-scale cuvette setup and in microfluidics.

Micro-scale Bifurcation Device Test Setup

E. coli biofilms were grown in the channels of the bifurcation device for 24 hours, and subsequently exposed to the four experimental conditions – control, electric fields only, AI-2 analog isobutyl DPD, and the combination of AI-2 analogs and electric fields. The respective solutions were introduced into the four channels of the device over an additional 24 hours. Both end point confocal microscopy images, and CCD-based real-time monitoring of biofilm growth and treatment were performed. These results are discussed below.

The electric field intensity used for treatment of biofilms was chosen such that no bulk electrolysis of the media occurs. Experiments previously performed on *E. coli* biofilms in Luria broth (LB) determined that AC and DC electric fields less than 1.25

V/cm can be used without inducing bulk electrolysis of the media [203]. The electrical potential used in this work was 0.125 V AC at 10 MHz offset by 0.125 V DC, significantly lower than the bulk hydrolysis potential of 0.82 V. This corresponds to an electric field of 1.25 V/cm DC field with a 1.25 V/cm AC field at 10 MHz. The frequency of the AC electric field (10 MHz) was chosen based on previous work that was shown to be effective [192,197].

End-Point Confocal Microscopy: To test the efficacy of the antibiotic-free combination therapy (AI-2 analogs and electric fields), *E. coli* biofilms were grown in the bifurcation device for 24 hours and exposed to the four treatments for an additional 24 hours. The biofilms were then stained and imaged using confocal microscopy. Figure 4-13a plots the average thickness of the biofilm after treatment. As shown, application of only an electric field results in no significant decrease in biofilm thickness (ANOVA, $p = 0.36$). Treatment with 100 μM AI-2 analog isobutyl DPD results in a 31.1 ± 10.1% decrease in average biofilm thickness as compared to the control (ANOVA, $p = 0.023$). This correlates with previously obtained data using single channel microfluidics (Figure 4-8). Treatment with the combination therapy results in a significant decrease in biofilm as measured by the 77.8 ± 6.3% (ANOVA $p = 0.0001$) decrease in average thickness as compared to the control. The larger percentage decrease in biomass following treatment using the microfluidic platform (77.8%), in contrast to the cuvette test setup (46.4%), can be attributed to the flow in the microfluidic setup. We suggest that the microfluidic flow ensures availability of

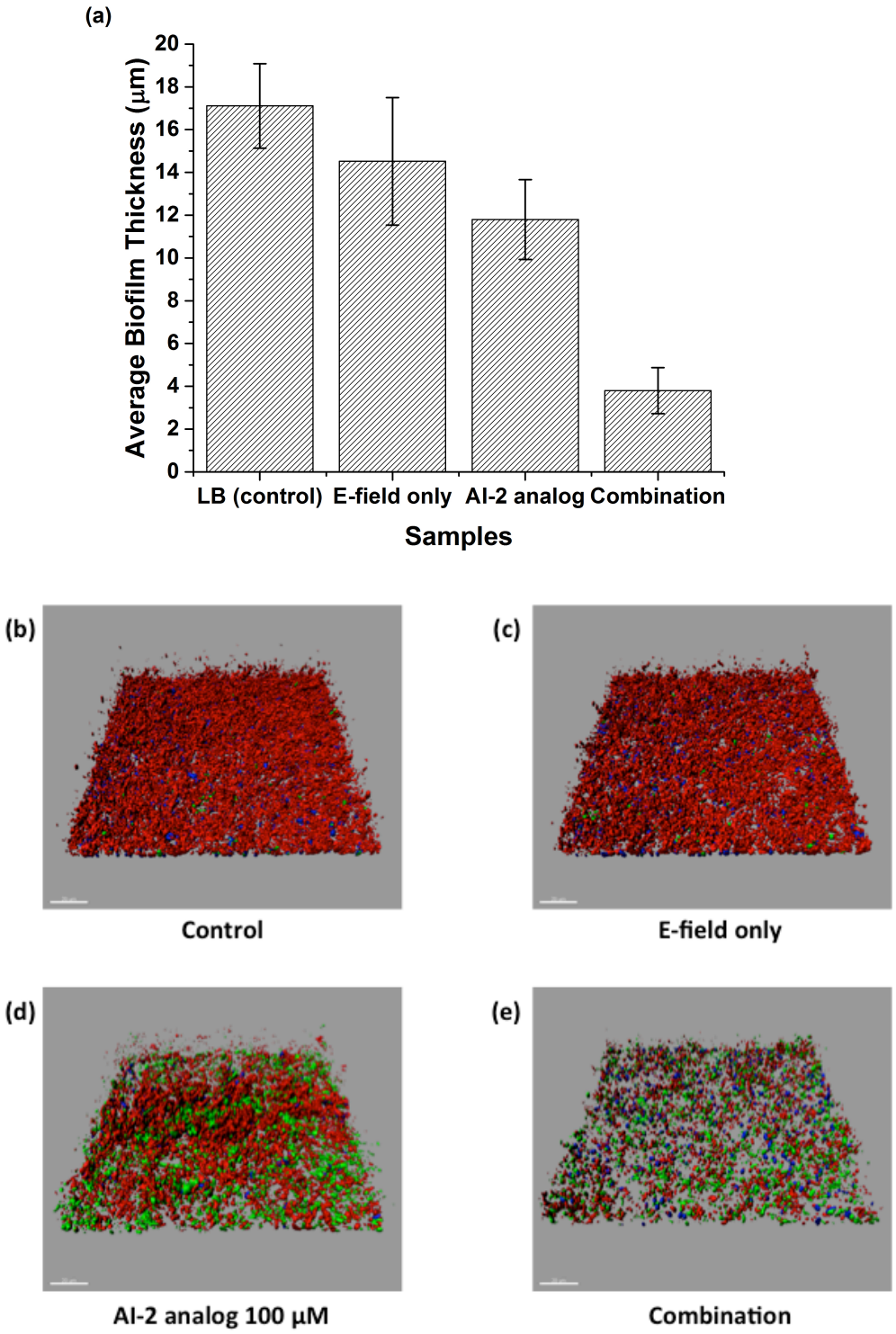

Figure 4-13 (a) Average biofilm thickness as measured using the end-point confocal microscopy technique. The combination treatment of AI-2 analogs and electric fields results in a 77.8 ± 6.3% decrease in biofilm thickness as compared to the control. The error bars represent the standard deviation across three confocal images (N = 3 images) obtained in each channel of the device. (b-e) Surface rendered sample confocal microscopy images from the device (scale bar = 20 μm). The thicknesses were 16.87 μm (control), 13.05 μm (E-field only), 10.51 μm (AI-2 analog) and 3.26 μm (combination).

fresh AI-2 analog molecules at the biofilm site. In contrast, the cuvette setup limits AI-2 analog availability at the biofilm surface to purely diffusion. Also, the better efficacy in the microfluidic device could be attributed to the shear in the channel that could add to the increased penetration of the treatment into the biofilm as well as easier removal of the biofilm.

Real-time Biofilm Monitoring: Optical density monitoring of biofilms using CCDs has been previously demonstrated [136,167] and discussed in earlier sections of the dissertation. The same CCD platform is used in conjunction with the bifurcation device to study the real-time change in OD during the treatment of mature *E. coli* biofilms with AI-2 analogs and electric fields. A schematic and photograph of bifurcation device and the platform are shown in Figure 4-14.

Figure 4-15 depicts the change in OD during the growth and treatment of *E. coli* biofilms. The high change in OD during the first few hours of growth is due to the seeding of the bacterial suspension. The OD then gradually decreases as pure LB media is pumped through the channels. Following this, small variations in OD are observed during biofilm growth and removal. We hypothesize that this is a result of the self-leveling effect experienced by thick biofilms possibly due to the increased shear observed in the microfluidic channel. Statistical correlation between the biomass in the four channels after the growth phase, as measured using the OD measurement setup was demonstrated (ANOVA, $p < 0.0001$), thus validating the growth of uniform biofilms in the channels of the device. After 24 hours of growth,

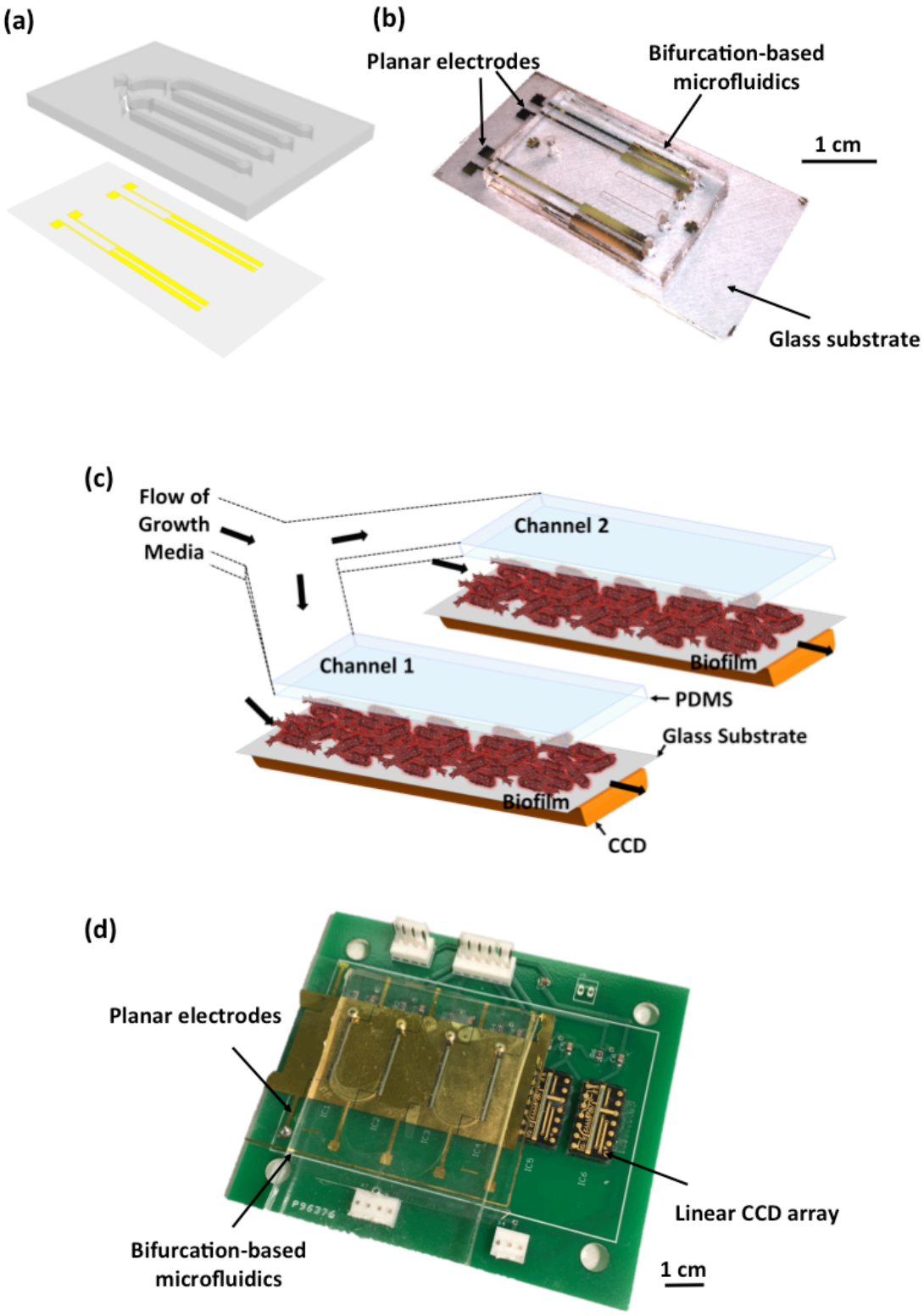

Figure 4-14 (a) Schematic of the bifurcation-based microfluidic device. (b) Photograph of fabricated microfluidic device with planar gold electrodes (scale bar = 1 cm). (c) Schematic of device integrated with the CCD monitoring platform. (d) Photograph of the CCD-based microfluidic system (scale bar = 1 cm).

the variation in biomass was observed to be 8.5% as compared to the 68% that was previously measured in single channel microfluidics [166]. This reduced biomass variance at the end of the biofilm growth period, enables reliable comparison of the various treatments. The treatments, LB, AI-2 analog, electric fields and a combination of the AI-2 analog and electric fields were applied to the channels of the device. Treatment with electric fields (pink line) resulted in no variation in total biomass in comparison to the control (black line). The AI-2 analog treatment (blue line) showed a decrease in the biomass with time. However, the combination treatment (red line)

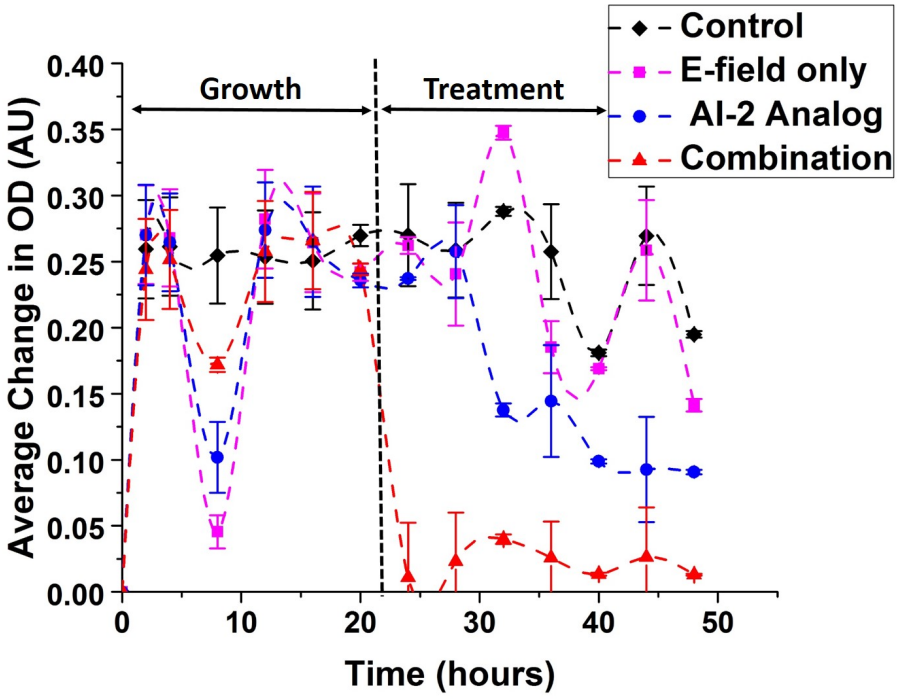

Figure 4-15 Measured average change in OD across the length of each channel (N = 186 pixels along length of channel) at representative time points during biofilm growth and treatment. The error bars represent the spatial variance of the biofilm in each of the channels of the device. The variation in OD across the four channels was observed to reduce to 8.5% (ANOVA, $p < 0.0001$) at the end of the growth period. The channel treated with AI-2 analog and electric fields shows the most significant decrease in biomass.

resulted in the most significant decrease in biomass as compared to the control. This correlates well with the end point results obtained using both the CV assay and confocal microscopy.

4.2.4 Discussion

We suggest that the AI-2 analog, when combined with electric fields permeates the biofilm more rapidly, similar to the antibiotic molecule during application of the BE. We suspect that increased permeation into the biofilm makes available more AI-2 analog molecules in the bulk of the biofilm. The rise in concentration of AI-2 analog in the biofilm, increases the probability that isobutyl DPD is imported into cells, phosphorylated by the QS kinase, LsrK, and then binds to the cognate transcriptional regulator, LsrR [143], thereby acting as a QS antagonist, quenching QS activities [68] and preventing further production of proteins necessary for biofilm ECM production. Such reduced ECM production may decrease the structural strength and stability of the biofilm, resulting in easier removal of the biofilm due to the shear experienced in the microfluidic channel. It is hypothesized that the increased shear experienced in the microfluidic channel is a contributing factor in the higher treatment efficacy observed in the microfluidic flow cell as opposed to the macro-scale cuvette setup.

The biofilm treated with AI-2 analogs and electric fields resulted in the highest reduction in biofilm thickness. Figure 4-16a plots the macro-scale CV results and the biofilm thicknesses obtained using confocal microscopy for the various treatments applied using the microfluidic bifurcation platform. As observed, small changes in

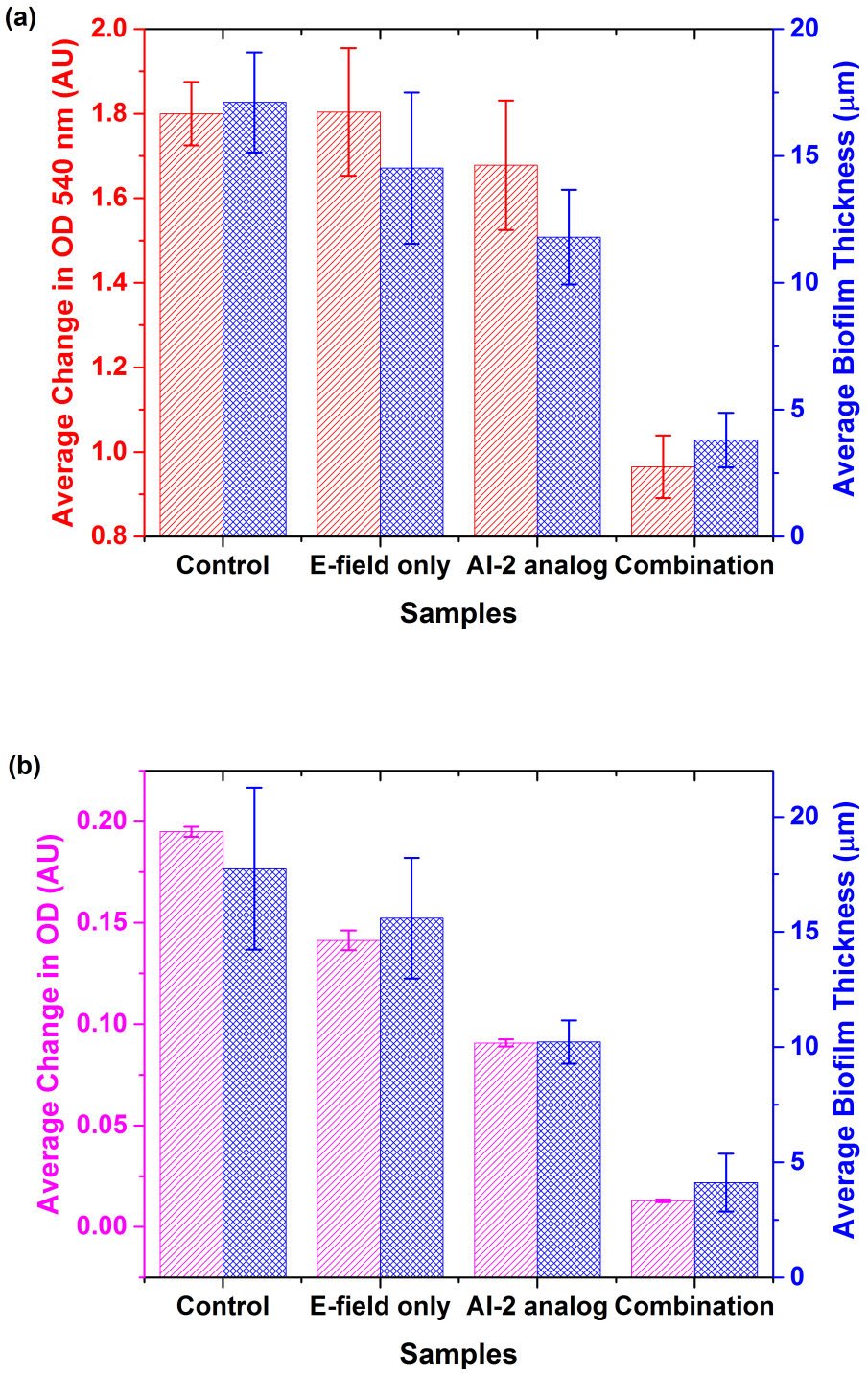

Figure 4-16 (a) Measured OD_{540} after 24 hours treatment using the CV staining method (N = 3 experimental repeats) and average biofilm thickness (N = 3 images) measured using end-point confocal microscopy measurements. (b) Measured average change in OD (N = 186 pixels) as measured using the CCD platform and average biofilm thickness (N = 2 images) measured using end-point confocal microscopy after 24 hours of treatment.

biomass are not detected with high sensitivity using the CV staining method, although the larger changes are easily measured. Due to the inherent lack in sensitivity of the CV staining method, the high resolution confocal measurements obtained using the microfluidic device do not show a very high correlation with the macro-scale measurement ($r^2 = 0.929$). This, along with the relative ease of integrating real-time sensors into the microfluidic platform make microfluidics a better choice for biofilm studies. As observed from Figure 4-16b the correlation between the measurements obtained using the CCD setup and the end-point confocal microscope are statistically significant ($r^2 = 0.980$). Even though the CCD set up cannot accurately measure very thin biofilms (<5 μm), the good correlation between the results obtained in the microfluidic device and the confocal microscopy data, combined with the low variability feature of the bifurcation design, highlight the suitability of this platform for rapid, highly paralleled *in vitro* characterization of novel biofilm treatment strategies.

4.3 Chapter Summary

To understand better the mechanism of BE, a thorough study was performed through the application of AC, DC and SP potentials on mature *E. coli* biofilms. Results showed that there is no statistical difference in treatment efficacy between the DC-, AC- and SP-based BE treatment of equivalent energies for voltages less than 1 V. We also demonstrated that the efficacy of the BE treatment as measured by the crystal violet staining method and colony-forming unit assay is proportional to the

electrical energy applied. We further verified that the treatment efficacy varies linearly with the energy of the BE treatment. Our results thus suggest that the energy of the electrical signal, and not the type of electrical signal (AC or DC or SP), is the primary factor in determining the efficacy of the BE treatment, at potentials less than the media electrolysis voltage. This suggests that at potentials below bulk media electrolysis, the mechanism of action of the BE treatment is not different for the various types of signals (AC, DC or SP), as reported previously in literature. We anticipate that this observation will pave the way for further understanding of the mechanism of action of the BE treatment method and may open new doors to the use of electric fields in the treatment of bacterial biofilms. Importantly, these findings suggest that this method is aptly suited for deployment in clinical biofilm treatment, as it enables more flexibility and ease of integration of the BE into various, especially in *in vivo* environments.

Alternate treatments to biofilm infections were studied and presented. This included efficacy studies on AI-2 analogs, as both an independent treatment and when used in combination with antibiotics or electric fields. The results suggest that even at low concentrations AI2-analogs are effective at preventing further biofilm growth. This is achieved by turning off the genetic cascade required to synthesize key proteins necessary for biofilm existence and growth. The efficacy significantly improves when combined with other treatments like antibiotics and low electric fields. The results presented in this chapter demonstrate the increased efficacy of combination therapy using AI-2 analogs and electric fields that is completely independent of traditional antibiotics; the analogs themselves target bacterial cell-cell communication, not

viability. This new treatment was tested and verified using both macro-scale and micro-scale test platforms. By integrating a real-time OD measurement system with the microfluidic device, we demonstrated that the combination of AI-2 analogs and electric fields resulted in a significant decrease in biofilm thickness. We further confirmed these results by performing end-point confocal imaging. We suggest that the increase in treatment efficacy of the AI-2 analog when combined with electric fields is due to the increased permeation of the analog into the bulk of the biofilm. It is also hypothesized that the efficacy of the treatment when using a microfluidic device is larger due to the replenishment of the AI-2 analog molecules at the site of biofilm formation due to continuous flow in the device. Importantly, this finding suggests that this method of treatment is promising as a potential treatment and prevention method against antibiotic-resistant biofilm infection formation in both the clinical and environmental settings.

Chapter 5. A Microfluidic Impedance Sensor-Treatment Platform: Characterization, Sensing and Treatment Results

This chapter presents the experimental results for impedance sensing of bacterial biofilms in microfluidic channels. The results of both single channel and bifurcation-based microfluidic devices integrated with impedance sensors are discussed. Finally the design and characterization of an impedimetric microsystem that integrates the real-time sensing and threshold-activated feedback based BE treatment of the biofilms is discussed and demonstrated. This work could not have been possible without the continuous efforts of Ms. Kathryn Schneider and Ms. Ekaterina Tolstaya.

5.1 Impedance Sensing of Biofilms in Microfluidics

In this section, we present a simple IDE-based impedance sensor that enables label-free real-time detection of bacterial biofilm growth and treatment. While impedance sensors for the detection of biofilm growth have been proposed in the past [169,176,211], they have been used to detect growth in static environments like microliter plates or petri dishes, or in macroscopic setups like the CDC reactor. The work presented here demonstrates the real-time detection of biofilm growth in microfluidic flow cells, as well as, monitoring of biofilm treatment with antibiotics. End-point fluorescence microscopy results correlate with the changes in impedance measured using our system.

5.1.1 Finite Element Modeling of Bacterial Biofilms

Effective medium approximations (EMAs) allow the theoretical modeling of the macroscopic properties of composite materials. These approximations calculate the macroscopic properties of a material by averaging the multiple values of the constituents that directly make up the composite material, although at the constituent level, these properties vary and are inhomogeneous. Given the multiple unknowns that increase the complexity of a composite medium like bacterial biofilm, precise calculation of the many constituent values is nearly impossible. However, theories have been developed that can produce acceptable approximations which in turn describe useful parameters and properties of the composite material as a whole. In this sense, EMAs are approximate descriptions of a medium (composite material) that are derived from calculations that are based on the properties and the relative fractions of its components. Presented in this section is a brief overview of one such EMA, Maxwell's mixture theory (MMT), which is most frequently employed in the analysis of biological cell suspensions, and of the simulation setup using this model to theoretically calculate the electrical properties of the biofilm.

Maxwell's Mixture Theory: Spherical Single-Shelled Model

A biological cell suspension can be modeled as a collection of differently shaped objects (the cytoplasm) covered by one or two shells (the cell membrane) and uniformly distributed in an aqueous phase (the extracellular medium). The overall dielectric properties of the suspension depend on the electrical parameters (the permittivity ε and the conductivity σ) of the individual suspension components and

their volume fractions [212-214]. Although, *E. coli* are not spherical in shape, and refinements of the model, *viz.* ellipsoidal cells have been published, the spherical model presents a sufficient first-order approximation. Thus, in this work, we calculate the dielectric properties of the biofilm by assuming it to be a collection of spherically shaped objects (the bacterial cells), covered by a single shell (their cell membrane) and uniformly distributed in a medium (the ECM) as shown in Figure 5-1.

For the single-shell spherical model, the complex dielectric constant $\varepsilon^*_{biofilm}(\omega)$ of the biofilm is given by [213]

$$\varepsilon^*_{\mathrm{biofilm}}(\omega) = \varepsilon^*_{\mathrm{mat}}(\omega)\,\frac{2(1-\varphi)\varepsilon^*_{\mathrm{med}}(\omega)+(1+2\varphi)\varepsilon^*_{\mathrm{eq}}(\omega)}{(2+\varphi)\varepsilon^*_{\mathrm{med}}(\omega)+(1-\varphi)\varepsilon^*_{\mathrm{eq}}(\omega)} \qquad (5.1)$$

Where $\varepsilon^*_{eq}(\omega)$ is the equivalent complex dielectric constant of the dispersed particles (here bacterial cells) and can be written as

$$\varepsilon^*_{\mathrm{eq}}(\omega) = \varepsilon^*_{\mathrm{mem}}(\omega)\,\frac{2(1-\vartheta)\varepsilon^*_{\mathrm{mem}}(\omega)+(1+2\vartheta)\varepsilon^*_{\mathrm{cyt}}(\omega)}{(2+\vartheta)\varepsilon^*_{\mathrm{mem}}(\omega)+(1-\vartheta)\varepsilon^*_{\mathrm{cyt}}(\omega)} \qquad (5.2)$$

Where $\varepsilon^*_{mat}(\omega) = \varepsilon_{mat} + \sigma_{mat}/(i\varepsilon_0\omega)$ is the complex permittivity of the ECM, $\varepsilon^*_{mem}(\omega) = \varepsilon_{mem} + \sigma_{mem}/(i\varepsilon_0\omega)$ is the complex permittivity of the bacterial cell membrane, and $\varepsilon^*_{cyt}(\omega) = \varepsilon_{cyt} + \sigma_{cyt}/(i\varepsilon_0\omega)$ is the complex permittivity of the cellular cytoplasm. ε_0 is the dielectric constant of free space, ω is the frequency, φ is the fractional volume of the bacterial cells. Since the bacterial cell is modeled as a sphere, it is assumed to have a radius R and a cell membrane of thickness d_{mem}. The parameter

ϑ of equation (5.2) is calculated as $\vartheta = [R/(R+d_{mem})]^3$. The values of the various parameters used to theoretically estimate the electrical properties of the biofilm are listed in Table 5-1.

Combining both equations (5.1) and (5.2) and separating the resultant complex equation into the real and imaginary part, we arrive at the permittivity $\varepsilon_{biofilm}$ and the conductivity $\sigma_{biofilm}$ of the biofilm. These calculations were performed using Mathematica (v10.2.0.0, Wolfram Research). The corresponding code is included in the appendix of this document (Appendix B).

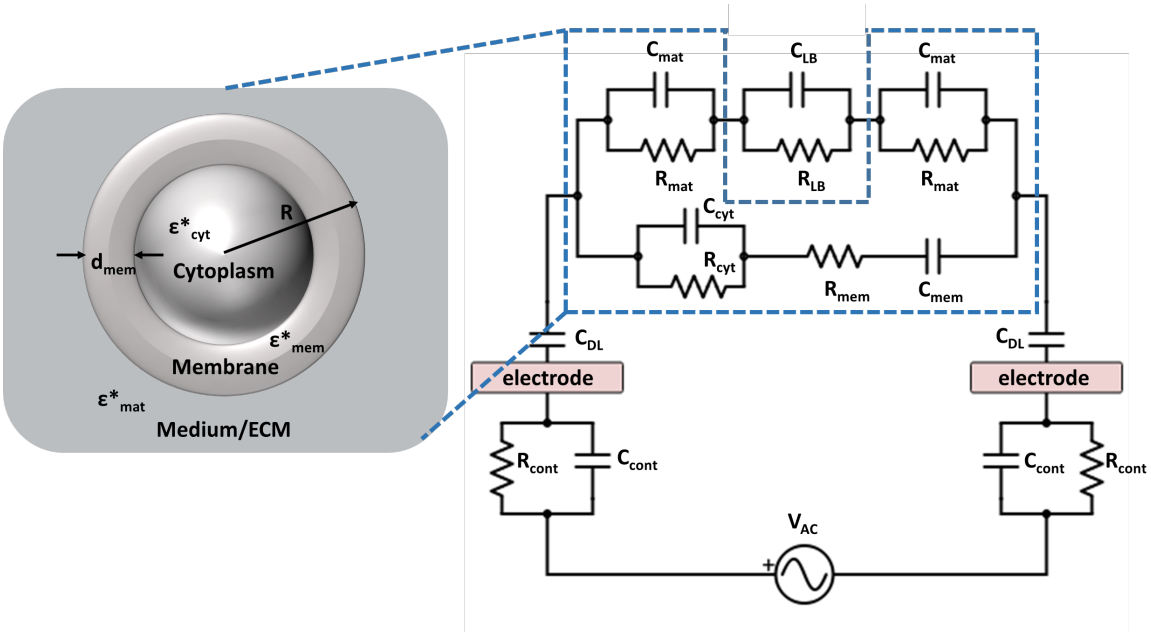

Figure 5-1 Effective medium approximation (EMA) of a bacterial cell as a single shelled sphere and the equivalent circuit of the experimental setup. The part of the equivalent circuit boxed in blue corresponds to the Maxwell's mixture theory based approximation of the biofilm, where R_{cont} and C_{cont} are the electrode contact resistance and capacitance, C_{DL} is the double layer capacitance, R_{cyt} and C_{cyt} are the cytoplasmic resistance and capacitance, R_{mem} and C_{mem} are the resistance and capacitance of the membrane, R_{mat} and C_{mat} are the extra cellular matrix (ECM) resistance and capacitance and R_{LB} and C_{LB} are the growth media (LB media) resistance and capacitance.

Table 5-1 Table listing the parameters used for the 3D electrodynamic COMSOL simulation.

	Conductivity (S/m)	**Relative Permittivity**	**Reference**
Cell cytoplasm	0.19	61	[215,216]
Cell membrane	5×10^{-8}	10.8	[215,216]
ECM	0.68	60	[217]
LB media	0.754	78	[218]

COMSOL Simulation Setup

To model the impedance system, a 3D electrodynamic simulation was setup in COMSOL Multiphysics (v4.4, COMSOL Inc.). The geometry was defined by a microfluidic channel of length 500 μm, width 50 μm and height 100 μm. Centered on the bottom of the channel is a pair of gold electrodes whose width and spacing can be varied. Three electrode widths and spacings, *viz*. 25 μm, 50 μm and 100 μm were simulated. For the ease of modeling it was assumed that a biofilm of uniform thickness (5 μm to 30 μm) grows along the entire length of the channel. The remaining channel volume was modeled to simulate LB growth media. Although the electrical characteristics of the LB media change with bacterial metabolism, for the case of this simulation it was assumed that the channel was filled with fresh LB media at all times. This represents the experimental condition in which the microfluidic flow rate is high enough to ensure that the media in the channel is replaced often and always guaranteed to be a nutrient-rich environment. The contact

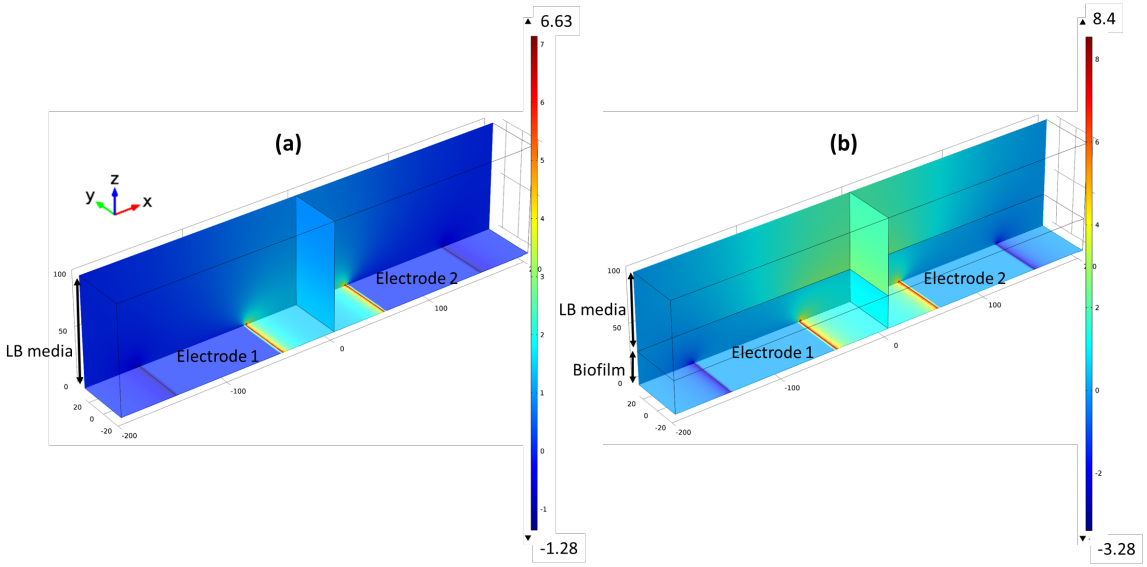

Figure 5-2 COMSOL 3D electrodynamic simulation setup plotting the current density between the two electrodes for the (a) negative control (growth media only), (b) a biofilm that grew on both electrodes. The sample simulation schematics shown are for the case of 100µm IDE finger width and spacing and a uniform biofilm thickness of 30µm.

capacitance and resistance, as well as the double layer capacitance formed at the electrodes were also included as an additional electrical circuit in the simulation. The complete equivalent circuit of the experimental setup is shown in Figure 5-1. A snapshot of the COMSOL setup for both the control and the 30µm biofilm test cases are shown in Figure 5-2a-b, respectively.

Additional simulations were performed for the test cases when the biofilm grew in only half the total surface area of the channel, namely, when a uniform biofilm grows along the entire width of the channel but only along half the length of the channel, and vice-versa.

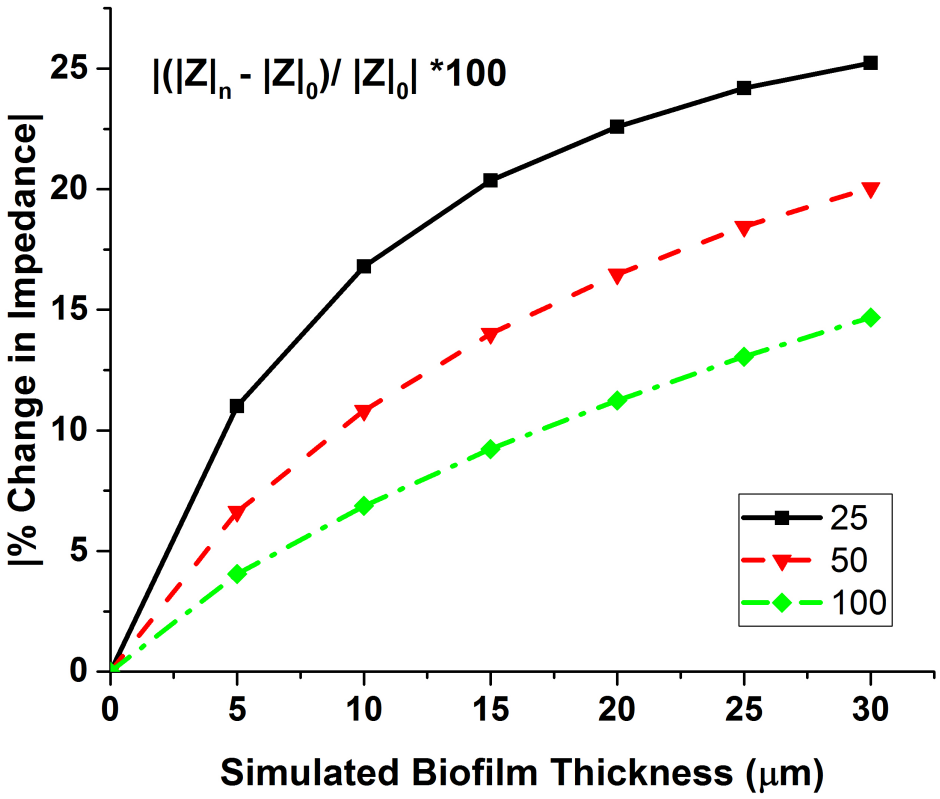

Figure 5-3 Percentage magnitude change in impedance at 100kHz for the three different electrode width and spacings with increasing biofilm thickness. The 25 μm IDE shows the highest sensitivity but the shortest time to saturation, whereas the 100 μm IDE results in the lowest sensitivity but the longest time to saturation.

The simulation results show that for IDEs with equal electrode width and spacing, the sensitivity of the sensors is inversely proportional to the width or spacing between the electrodes (Figure 5-3). Thus 25 μm IDE sensors are more sensitive than 50 μm IDE sensors, which are in turn more sensitive than the 100 μm sensors. Assuming the increase in simulated biofilm thickness is with growth time, the time to saturation of the signal is directly proportional to the electrode spacing. Thus, 100 μm IDE sensors demonstrate the largest linear range when compared to 50 μm or 25 μm IDEs. In order to balance both these aspects, 50 μm IDEs were predominantly used for demonstration of impedance sensing and treatment of biofilms.

5.1.2 Device Fabrication and Design

The impedance sensor was fabricated by patterning evaporated Cr/Au (20nm/180nm) on a Borofloat 33 or oxidized silicon wafer to form the IDE pattern. Shipley 1813 photoresist was spun on the wafer following which it was exposed and developed (Masks #4 and #5, Appendix A). The Cr/Au was then wet etched to form the IDEs after which the excess resist was stripped using acetone. IDEs of two different widths and spacings, 50 µm and 100 µm, were fabricated. Figure 5-4 shows the fabrication process flow for the IDE sensors and Figure 5-5 presents a micrograph of the 50 µm IDE sensors.

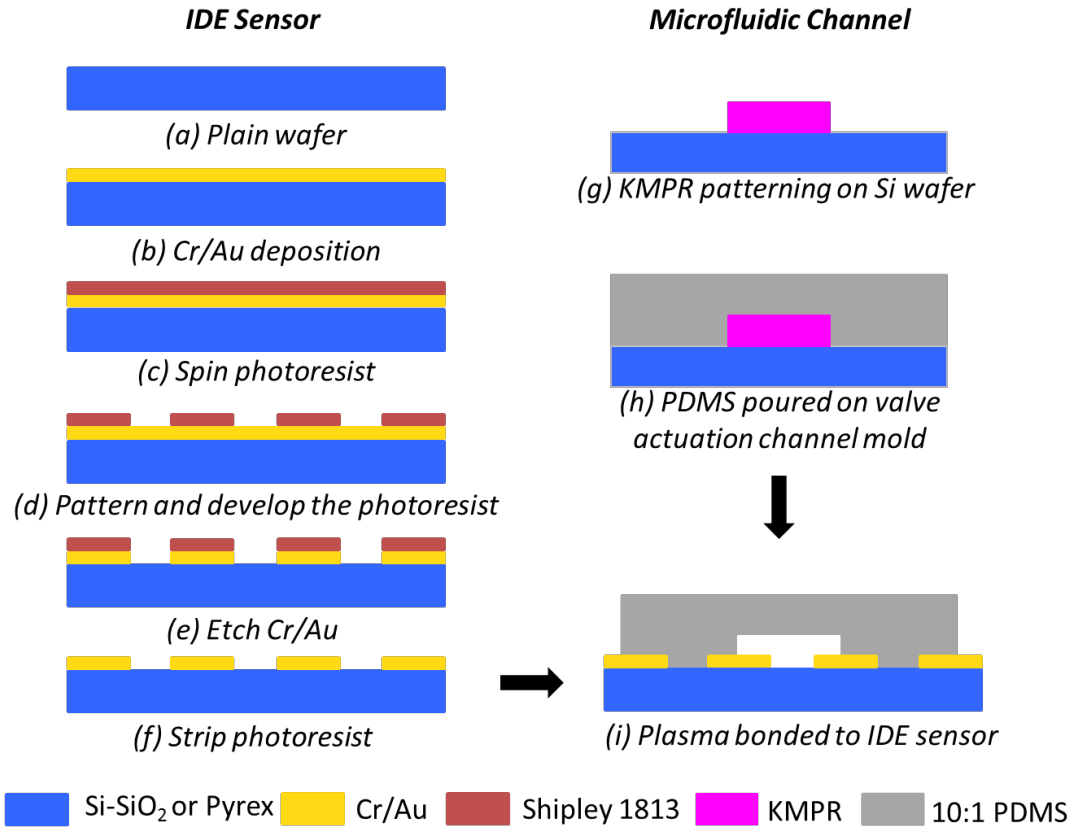

Figure 5-4 Fabrication process flow for the IDE sensors. The IDE sensors have either 50 µm or 100 µm width and spacing.

Following this, the devices were diced, cleaned by immersion in piranha solution for 1 minute, and rinsed with DI water and blow-dried. Single channel and bifurcation-based microfluidic devices were fabricated using traditional soft lithography techniques [141]. Briefly, the microfluidics is cast from polydimethylsiloxane (PDMS) (1:10 ratio of curing agent to polymer) molded by photo-patterned KMPR-1050. The microfluidic channels were 100 µm deep, 500 µm wide, and 2 cm long. Holes were punched at the inlet and outlet of each channel using a 2 mm dermatological punch. The channels were then aligned and placed over the impedance sensor and irreversibly bonded to the device.

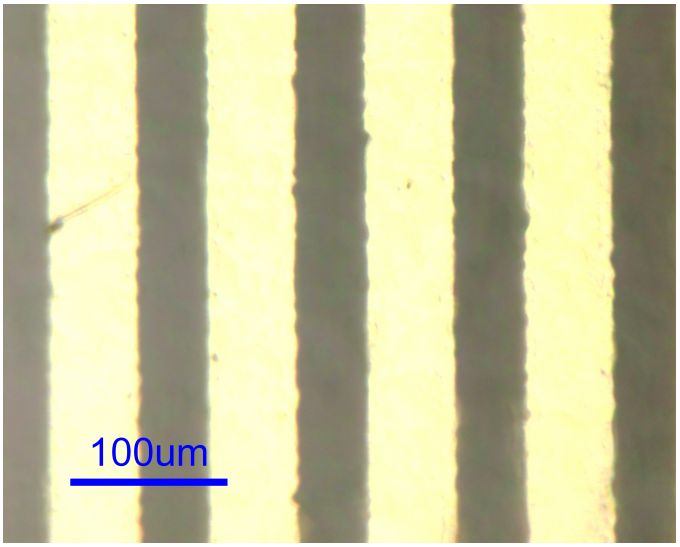

Figure 5-5 Micrograph of the IDE impedance sensor. The width and spacing of the fingers are 50 µm.

The single channel microfluidic device contained three independent IDE sensors that were located near the inlet, center and outlet of the microfluidic channel, whereas the bifurcation-based microfluidic device contained only one large sensor per

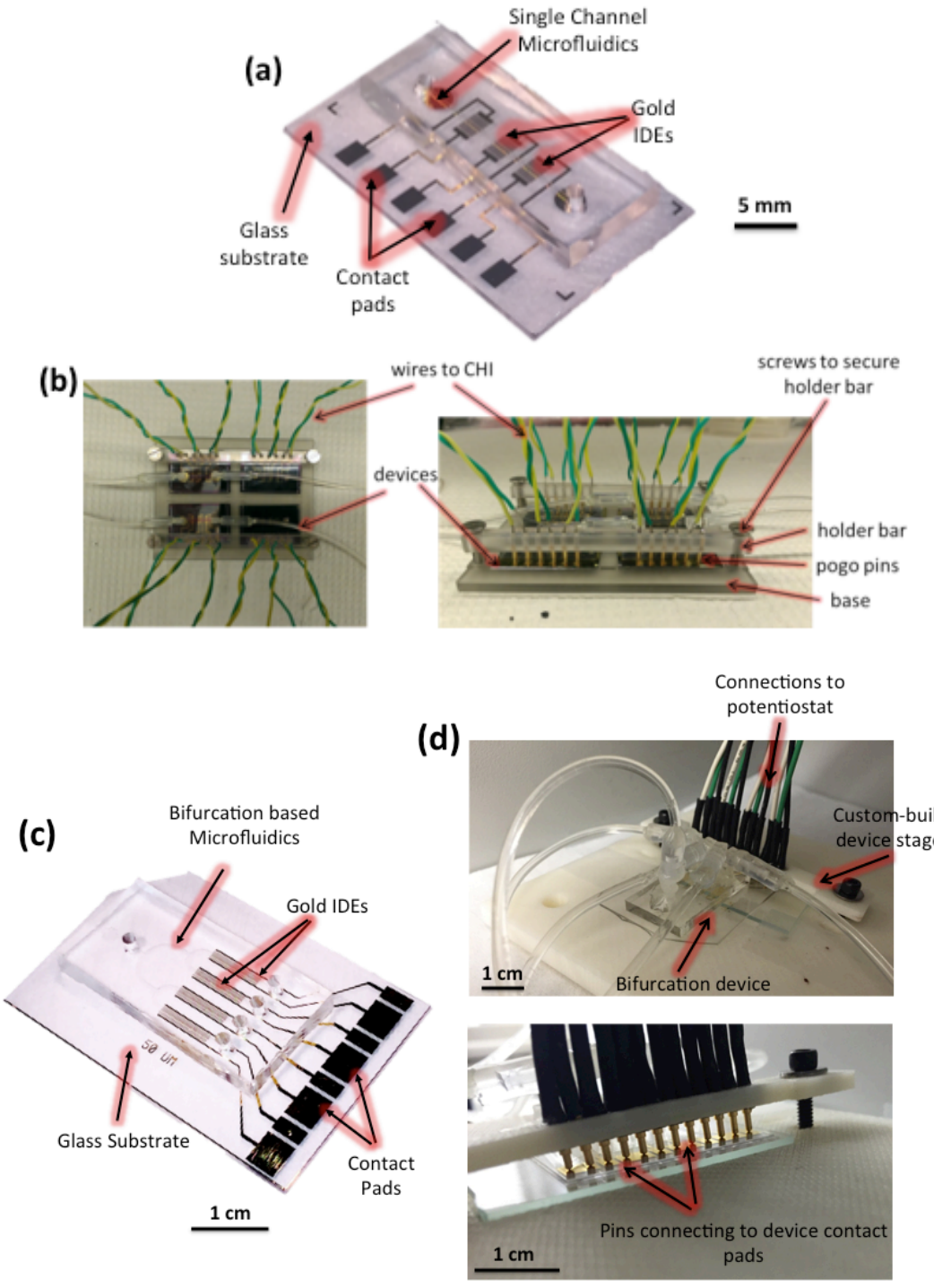

Figure 5-6 (a) Photograph of an impedimetric sensor device bonded to a simple single microfluidic channel (scale bar = 5 mm). Each device contains three IDE sensors. (b) Test setup fabricated for parallel testing of up to four single channel devices. (c) Photograph of microfluidic bifurcation device integrated with IDE sensors (scale bar = 1 cm). (d) Custom stage for interfacing up to two bifurcation devices to the potentiostat (scale bars = 1 cm).

channel. The PDMS microfluidic channels were plasma bonded to the device such that the fingers of the IDE sensor were perpendicular to the microfluidic channel (Figure 5-6a and c). To enable fluid flow, the microfluidic channels were interfaced to the external fluidic components using flexible Tygon tubing and barbed connectors (Figure 5-6). The tubing at the inlet of the single channel device was connected to a syringe pump (Cole Parmer 74901, Cole Parmer Instrument Company, LLC) operating in infusion mode at 20 μl/hr, and at the outlet, the end of the tubing is inserted into micro-centrifuge tube for waste collection. The bifurcation-based devices were operated in infusion or withdrawal mode depending on the phase of the experiment, as discussed previously. Prior to experiments, each device was sterilized by flowing 70 % ethanol for one minute and then rinsed using DI water. The entire apparatus was kept in an incubator held at 37 °C.

5.1.3 Experimental Setup

To ensure similar experimental conditions were applied to all devices at any given point in time, multiple experiments were performed in parallel. Two custom stages, shown in Figure 5-6b and d were machined, one for the single channel devices and the other for the bifurcation devices. These enabled interfacing up to twelve IDE sensors in four single channel microfluidic devices, or eight IDE sensors in two 2-level bifurcation devices, to the potentiostat (Model 600D, CH instruments Inc.). Its multiplexing capabilities (CHI684 Multiplexer, CH instruments Inc.), were used to measure the AC impedance with an applied potential of 5-50 mV for a frequency range of 10 Hz to 1 MHz for each of the interfaced IDE sensors serially every 8-10

minutes. Figure 5-7 plots the real and imaginary parts of impedance, the absolute impedance and the phase for the frequency range of 10 Hz to 1 MHz as measured using a 50 µm IDE sensor. The lines in the plots correspond to various time points during the 24-hour biofilm growth period with the solid red line corresponding to time t = 0 hrs of the biofilm growth period, followed by the solid blue, solid green, solid black, solid cyan, dashed red, dashed blue, dashed green and dashed black lines (t = 24 hrs). As observed from the plots, the impedance changes with time at any given frequency and can be used to monitor biofilm growth. On the other hand the

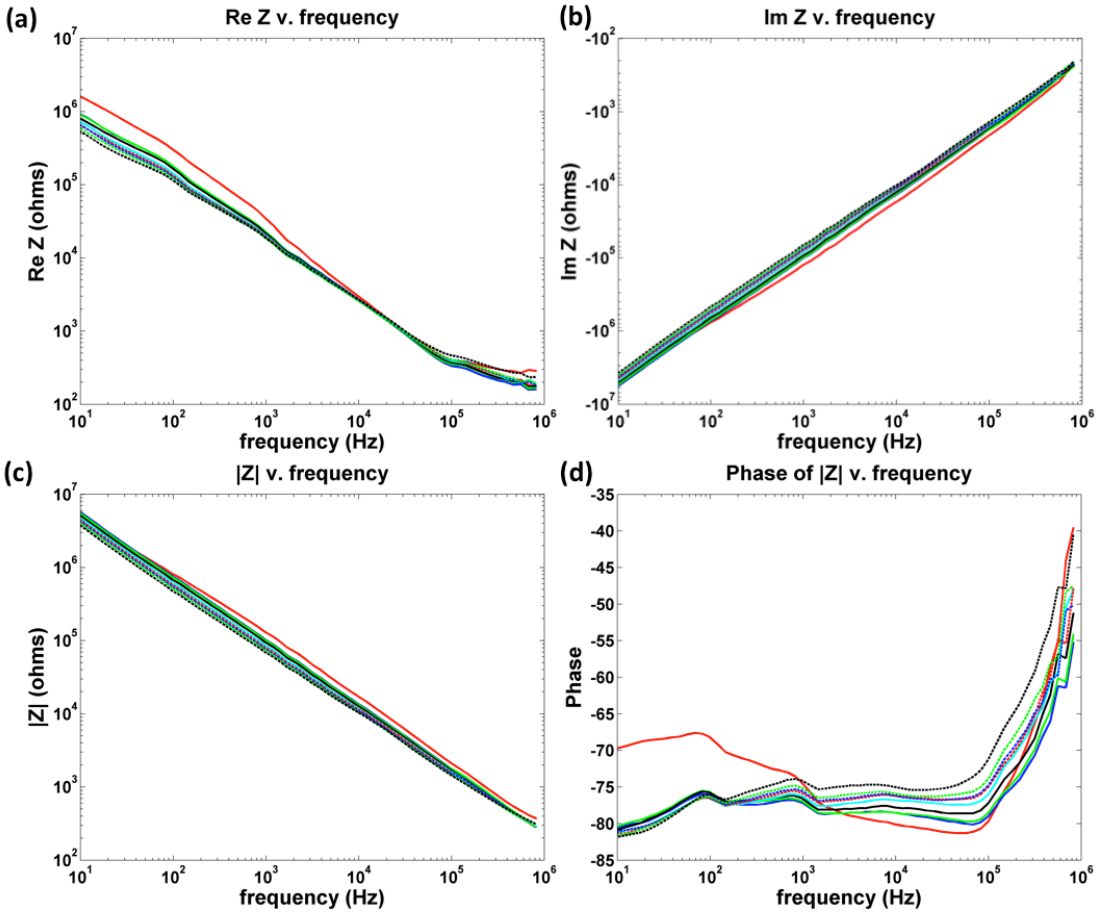

Figure 5-7 Plots showing the (a) real part of impedance, (b) imaginary part of impedance, (c) absolute impedance, and (d) phase for the frequency range of 10 Hz to 1 MHz during biofilm growth as measured by a 50 µm IDE sensor. The various lies represent different times during the 24-hour biofilm growth (the red line corresponds to t = 0 and the dashed black lines correspond to t = 24 hours).

phase remains almost constant with time at a given frequency, but changes over the frequency range as expected, with the phase being capacitive at lower frequencies and more resistive at higher frequencies.

Investigation of the recorded data revealed that the frequency of 100 Hz resulted in accurate detection of biofilm growth while maintaining a high signal to noise ratio. Thus, impedance measurements at 100 Hz was used for to analyze the results of all the experiments. Due to hardware restrictions of the potentiostat's multiplexer, only a maximum of three to four sensors could be tested in parallel.

5.1.4 Results

The results of biofilm growth and treatment in single channel microfluidics and in the bifurcation device as measured in real time using the impedance sensor are discussed in this section.

Single Channel Microfluidics

Device Pre-conditioning

Device pre-conditioning was accomplished by flowing 1× phosphate buffered saline (PBS) through the sterilized channel at 20 µl/hr for 24 hours. Any air bubbles trapped in the channel are forced to the outlet by increasing the flow to 100 µl/hr for a short period of time. The primary goal of pre-conditioning is to allow for acclimatization of the device to the change in environment from air to liquid so as to achieve a stable signal. Also, we postulate that the application of the AC potential over a 24-hour time period during pre-conditioning facilitates achievement of an

equilibrium due to electrochemical reactions occurring at the electrode surface. This process also enables removal of any excess ethanol present in the channel, tubing and connectors. Figure 5-8 shows the change in real, imaginary and absolute impedance at 100 Hz with respect to their respective overall average values for a 50 μm impedance sensor. As observed from the plots, large variation in signal is observed during the first few hours of the pre-conditioning step after which the signal stabilizes over time.

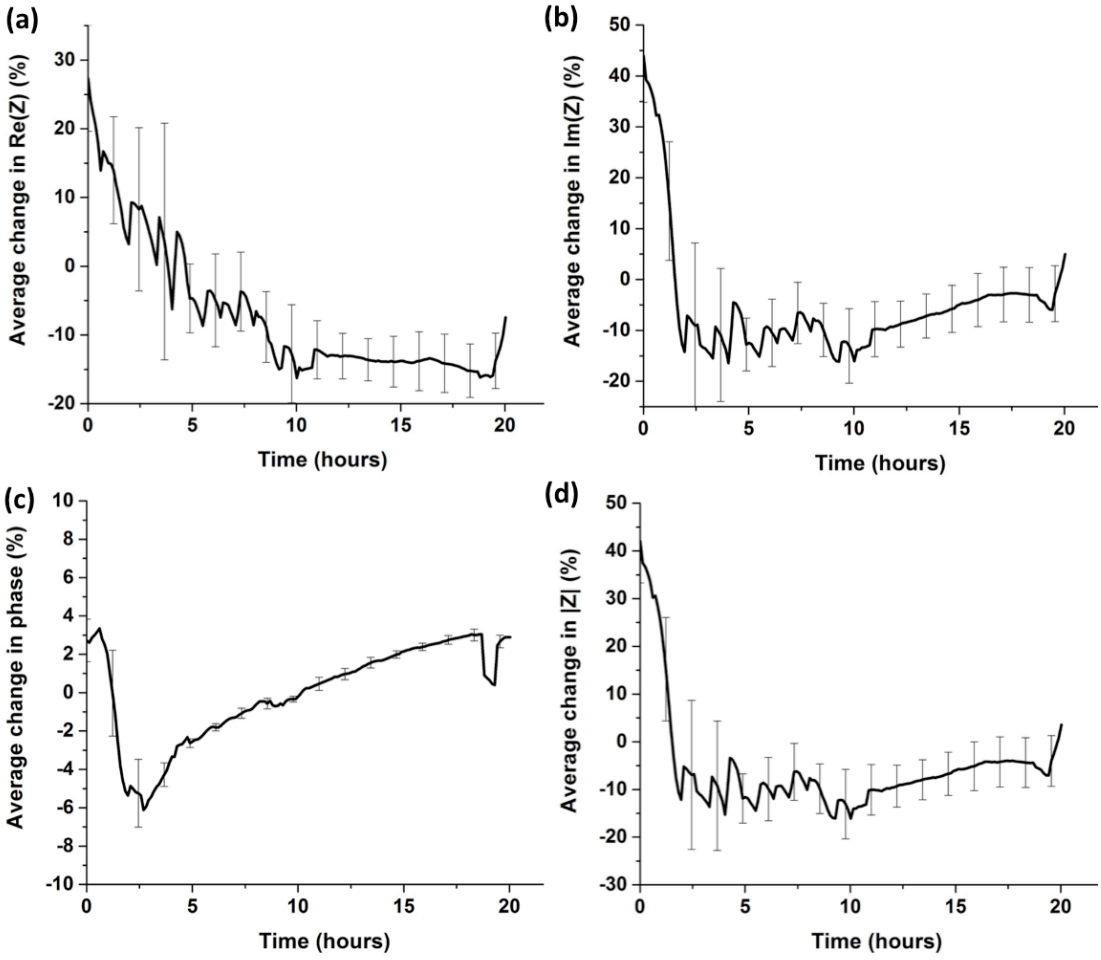

Figure 5-8 Representative plots showing the percentage relative change in (a) real part of impedance, (b) imaginary part of impedance, (c) phase, and (d) absolute impedance at 100 Hz during PBS pre-conditioning of a 50 μm IDE sensor. A large change in impedance observed during the first 3-5 hours of buffer introduction, after which the signal stabilizes. Almost no change in phase is observed during the entire duration of the conditioning. The error bars illustrate the temporal variation in signal (span = 3) at representative time points.

This preliminary change in signal is in line with the initial hypothesis and is indicative of the process of electrochemical equilibrium achievement. As time progresses the electrodes acclimatize to the new liquid environment that leads to a stable signal over time. Furthermore, as observed from the graphs the absolute change in impedance at 100 Hz almost exactly equal to the change in the imaginary part of the impedance. We attribute this to the transduction mechanism of the impedance system, in which the change in double layer and biofilm capacitance, captured by the imaginary impedance, is dominant. Thus, the absolute impedance is strongly affected and follows the imaginary component of the impedance.

Biofilm Growth

A bacterial suspension of *E. coli* K-12 W3110 [201] was prepared from a stock solution stored at −80 °C. The suspension was prepared by transferring a frozen sample of bacteria into 5 ml of LB media in a cell culture tube. The tube was then placed in an incubator-shaker (Innova 4000, New Brunswick Scientific Co. Inc.) at 250 rpm and 37°C for 18-20 hours to allow for bacterial growth. Subsequently, LB media was used to dilute the suspension to a final $OD_{600} \approx 0.25$. Prior to cell seeding, the device was pre-filled with fresh LB growth media at a flow rate of 100 µl/min per channel. Once the device was primed with LB media the flow rate was reset to 20 µl/hr per channel, and a few measurements were obtained to use as a baseline. The diluted bacterial suspension was then injected at a rate of 100 µl/min and was allowed to seed the channel for 2 hours without flow to facilitate bacterial attachment to the glass substrate. Fresh growth media (LB) was then supplied continuously to the

channel for 24 hours at the rate of 20 μl/hr. We previously characterized this flow rate and confirmed it to be sufficient to supply the needed nutrients for the formation of mature *E. coli* biofilms [136,154,166,167,175,219,220].

Figure 5-9 plots the percentage change in absolute impedance, its real and imaginary components and phase at 100 Hz during the 26 hour bacterial seeding and biofilm growth for a single 50 μm IDE sensor. It was observed that while the real and imaginary parts of impedance and the absolute impedance decreased by ~40% (Figure 5-9a, b, and d), the phase remained relatively constant (Figure 5-9c). This decrease in impedance is indicative of bacterial growth and gives a direct real-time measure of the bacterial attachment and biofilm growth on the sensor surface. The error bars plotted in the Figure 5-9 show the temporal variation of the signal (span = 3) at representative time points. However, as the variation is very small, < 2 %, the error bars are not easily discernible in the plots.

It is well documented that the low frequencies are affected by the capacitive behavior, while the higher frequencies are dominated by the resistive component [182]. Consequently, the decrease in the imaginary component of impedance at 100 Hz plotted in Figure 5-9 is caused by the increase in double-layer and biofilm capacitance as a result of biofilm attachment and planktonic bacterial growth, respectively, at the electrodes. On the other hand, as the metabolic activity of the bacteria has a direct effect on the ionic concentration and therefore on the resistance of the media, the introduction of metabolites into surrounding medium over time results in a decrease in resistance as measured by the real component of impedance. However, since the magnitude of the real part of impedance is orders of magnitude

lower than the imaginary component of impedance at low frequencies, biofilm growth results in a decrease in the absolute impedance.

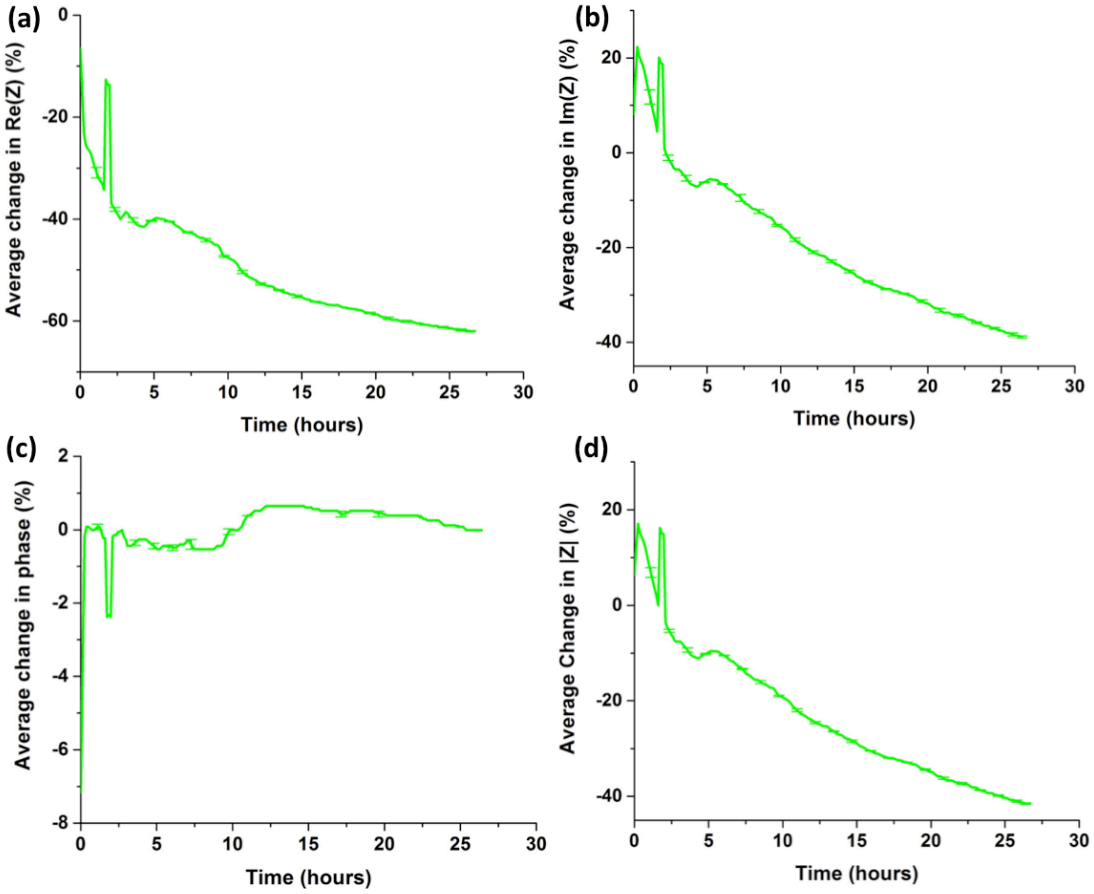

Figure 5-9 Representative plots showing the percentage relative change in (a) real part of impedance, (b) imaginary part of impedance, (c) phase, and (d) absolute impedance during biofilm growth using a 50 µm IDE sensor at 100 Hz. As observed the growth of biofilm results in a decrease in real, imaginary and absolute impedance, whereas the phase remains constant. The error bars show the temporal variation in signal (span = 3) at representative time points.

As each microfluidic channel is aligned over three similar IDE sensors, one each near the inlet, the center and the outlet of the channel, two additional impedance measurement data sets were obtained from the other two 50 µm IDE sensors aligned to the channel. The analysis revealed a similar trend for the various parameters as

plotted in Figure 5-9. The average change in absolute impedance, real and imaginary parts of the impedance and the phase after the 26 hour bacterial seeding and biofilm growth phase for all three 50 μm IDE sensors is plotted in Figure 5-10. The error bars represent the standard deviation of the average end-point impedance values across the three sensors (N = 3 experimental repeats). It can be observed from the bar graph that the average absolute impedance change and the corresponding resistance and reactance components vary by comparable amounts (ANOVA $P = 0.23$; $P > 0.05$), thus indicating that they are statistically similar, whereas there was no significant change in the phase of the measured impedance. Hence, for all future impedance sensing experiments only the change in absolute impedance was monitored and used as a direct measure of bacterial attachment and biofilm growth.

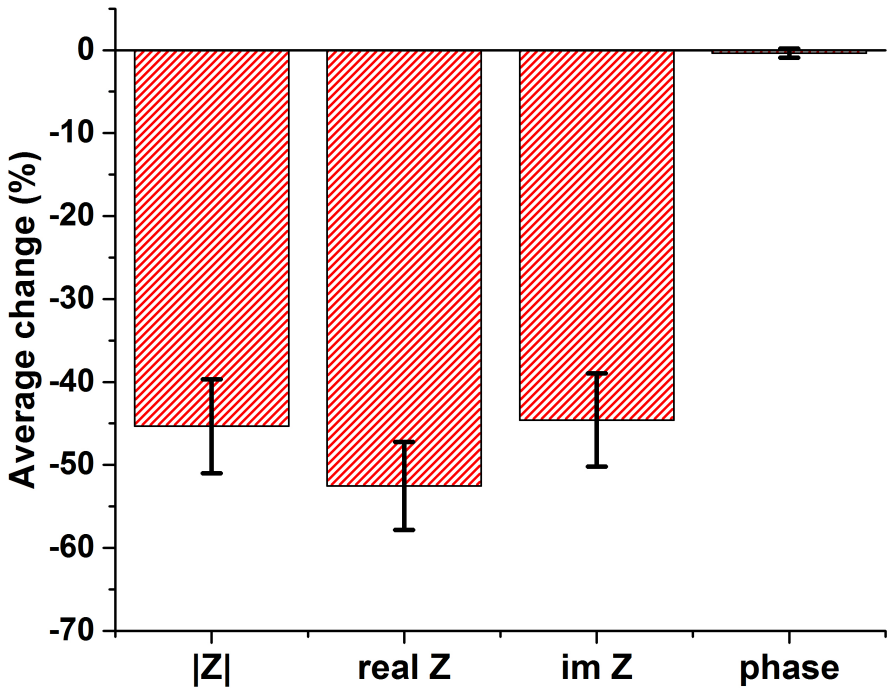

Figure 5-10 Average relative change in the absolute impedance, real impedance, imaginary impedance and the phase measured at 100 Hz across three 50 μm IDE sensors (N = 3 experimental repeats). Biofilm growth experiments were performed in parallel. The three IDE sensors were placed along the length of a single microfluidic channel.

Comparison with 100 micron IDE Sensors

Similar PBS pre-conditioning and biofilm growth experiments were conducted using 100 µm IDE sensors. Experiments were not conducted using 25 µm IDEs as the devices resulted in unstable impedance curves. The results of these experiments are shown in Figure 5-11, Figure 5-12, and Figure 5-13.

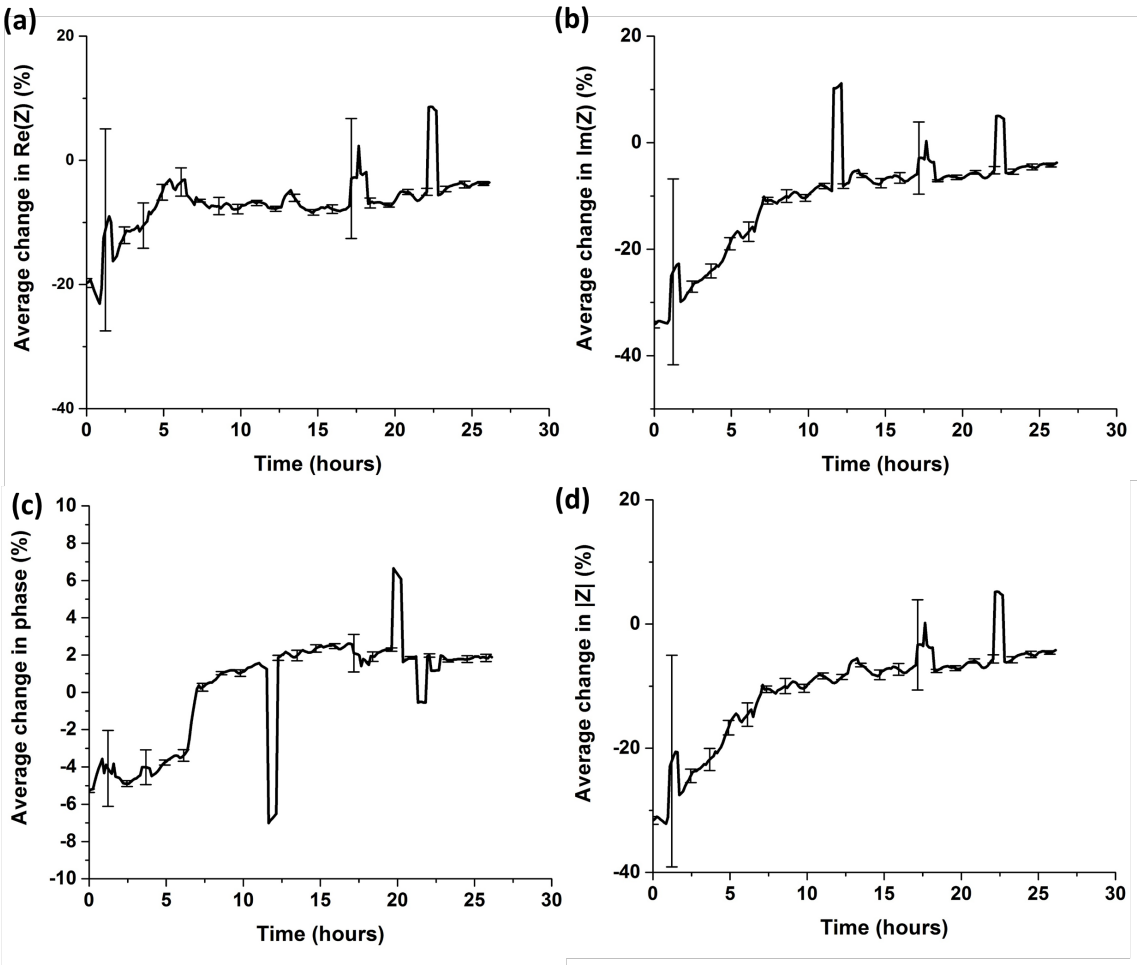

Figure 5-11 Representative plots showing the percentage relative change in (a) real part of impedance, (b) imaginary part of impedance, (c) phase, and (d) absolute impedance at 100 Hz during PBS pre-conditioning of a 100 µm IDE sensor. A large change in impedance observed during the first 3-5 hours of buffer introduction, after which the signal stabilizes. Almost no change in phase is observed during the entire duration of the conditioning. The error bars illustrate the temporal variation in signal (span = 3) at representative time points.

The buffer pre-conditioning of the devices revealed a similar trend as with the 50 µm sensors. While the impedance varies by ~20% in the first few hours (7-10 hours) of the conditioning, it stabilizes thereafter. The phase remains relatively constant through the entire period of time, with a maximum variation of 4 % during the first few hours of the buffer conditioning.

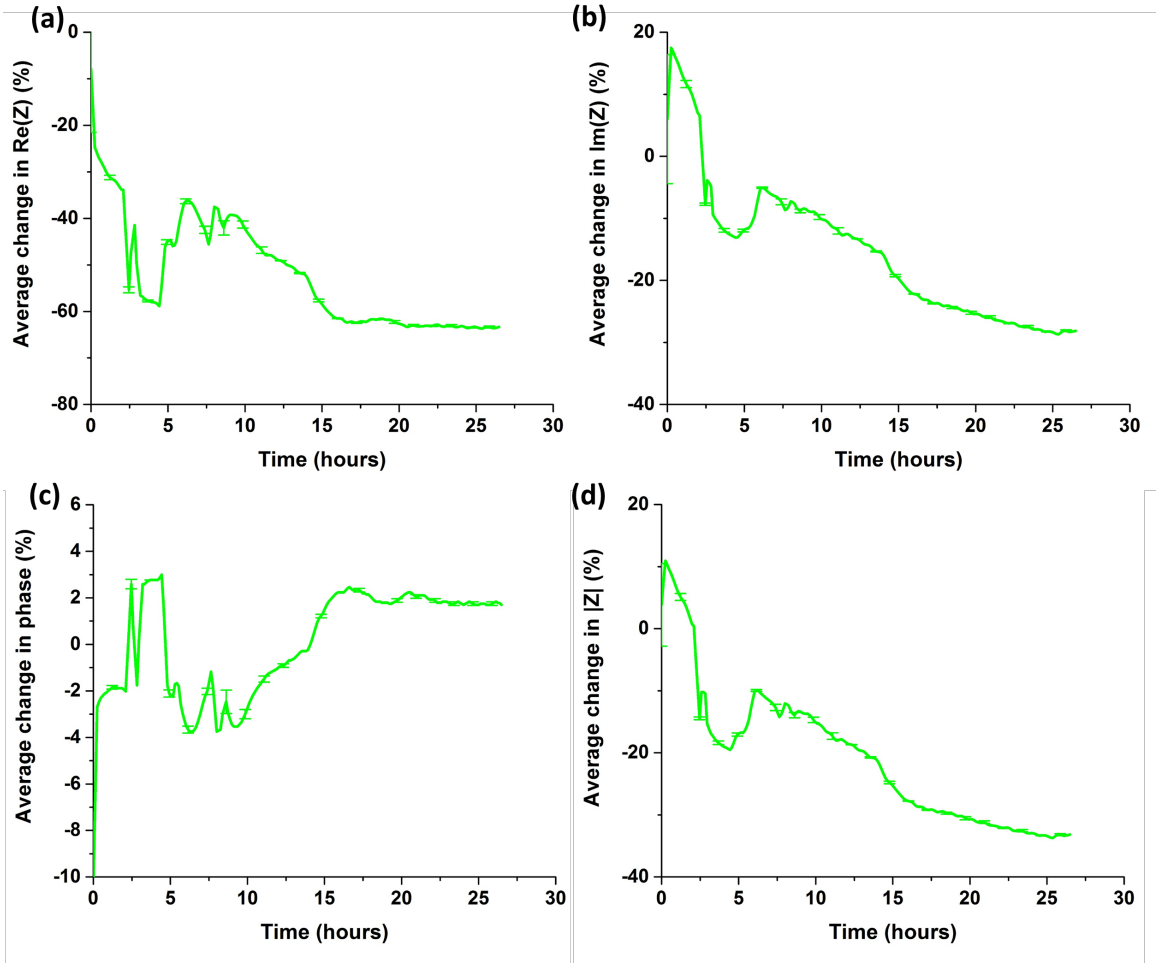

Figure 5-12 Representative plots showing the percentage relative change in (a) real part of impedance, (b) imaginary part of impedance, (c) phase, and (d) absolute impedance at 100 Hz during biofilm growth using a 100 µm IDE sensor. As observed the growth of biofilm results in a decrease in real, imaginary and absolute impedance, whereas the phase remains constant. The error bars show the temporal variation in signal (span = 3) at representative time points.

Figure 5-12 plots the change in resistance, reactance, phase and impedance during the 2-hour bacterial seeding and 24-hour biofilm growth process. As observed from the plots the change in impedance, resistance and reactance is negative indicating biofilm growth. However, a small increase in impedance is observed at the 5 hour time period. During the 5 to 15 hour time period, a shift in phase by negative 7 % is also observed. Such a change in phase was observed to occur only when small air bubble(s) were partially covering the surface of the electrode. However the general overall trend of decrease in impedance and near constant phase is observed. Moreover, we observe a saturation of the resistance signal at around the 15-hour time point. Saturation of the imaginary part of the impedance and the total impedance occurs at around t = 20 hours. Given that the 100 μm IDE sensors are theoretically known to be less sensitive to surface attachment than the 50 μm sensors, it follows that signal saturation can only occur in a 100 μm sensor when a much thicker biofilm is formed in the channel of this device as compared to the 50 μm device [178]. As discussed previously such variation in biofilms thickness is possible and very common as biofilms are extremely sensitive to environmental factors, and large variations in biofilm thickness (~68%) have been shown to occur between devices. Despite the thicker biofilm formed in the channel of the 100 μm device, the average change in impedance, resistance and reactance is comparable to the average change in these parameters measured using the 50 μm IDE sensor (Figure 5-9), proof of the lower sensitivity of the 100 μm sensors.

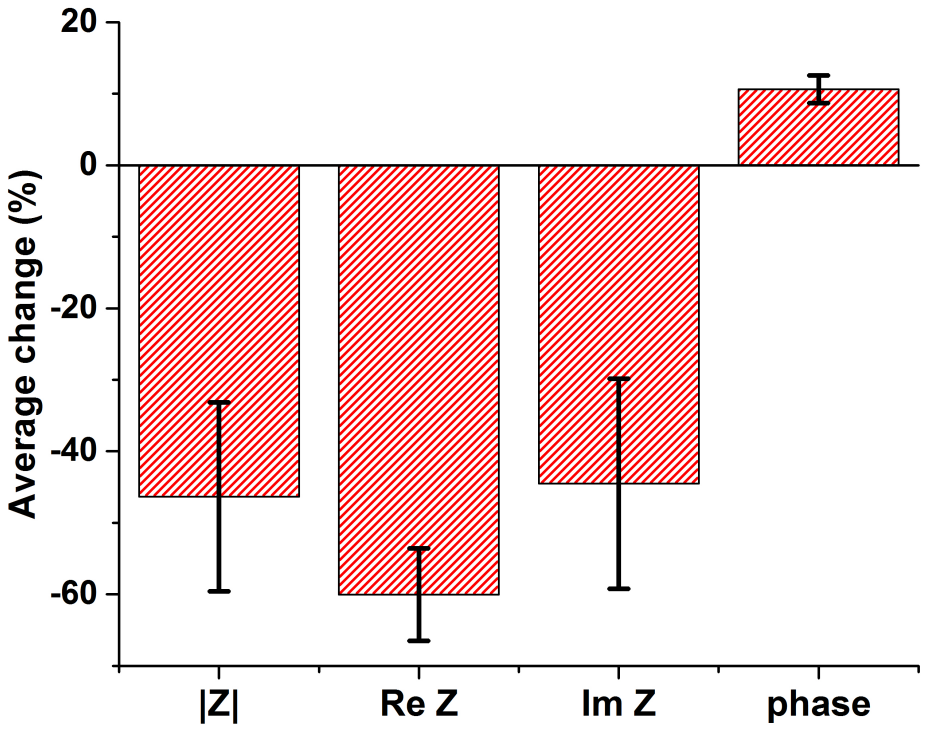

Figure 5-13 Average relative change in the absolute impedance, real impedance, imaginary impedance and the phase measured at 100 Hz across two 100 µm IDE sensors (N = 2 experimental repeats). Biofilm growth experiments were performed in parallel. The two IDE sensors were placed along the length of a single microfluidic channel.

Figure 5-13 plots the average change in resistance, reactance, impedance and phase for two 100 µm IDE sensors. While the 100 µm devices appear to show near about the same average percentage change in these values as those measured for the three 50 µm sensors, the average variation between the 100 µm devices, measured by the error bars are significantly larger than those of the 50 µm sensors. Furthermore, the 50 µm finger width and spacing is theoretically known to have a higher sensitivity than the 100 µm sensors, as the sensitivity of an impedance sensor in inversely proportional to the finger spacing, while the time to saturation is directly proportional to the finger spacing. Thus, only the 50 µm IDE sensors were used for all future impedance sensing experiments.

Bifurcation-based Microfluidics

In this work, we present the first impedimetric microsystem for real-time monitoring and treatment of bacterial biofilms in a microfluidic bifurcation device. To reliably compare various treatment efficacies in parallel, each channel of the bifurcation device was integrated with an IDE sensor. Our approach successfully utilized IDEs for both BE treatment application and monitoring biofilms through real-time impedance measurements. Our previous work with BE applied a 500 mV electrical signal during the entire treatment period [175,219], a long-term biocompatibility concern for medical devices as they on average require treatment over weeks. Additionally, the use of independent mechanical (or optical) and electrical domains for monitoring and treatment, respectively, made essential the use of auxiliary electrodes for BE application, increasing device footprint and necessitating additional bulky equipment [175,219]. Here, we demonstrate that biofilms can be accurately sensed in real-time by measuring the change in impedance across the IDEs. Treatment is performed by applying a 100 mV signal, for only ~1/7th the 24-hour treatment period, across the same IDEs in combination with small doses of antibiotic [130]. End-point optical analysis of our BE treated biofilms shows ~62% surface coverage reduction compared to the negative control, consistent with previous work [175,219]. Contrary to former systems, this integration of sensing and BE treatment capabilities into purely the electrical domain provides an elegant microsystem solution toward rapid, autonomous treatment of biofilms.

Device Pre-conditioning

The four outlets of the bifurcation device were connected to the syringe pump while the single outlet at the other end of the channels was placed in a micro-centrifuge tube that served either as a reservoir or a waste collection tube depending on the mode of operation of the device. Following the ethanol of DI rinse, PBS buffer was introduced into the channels of the device at 100 µl/min/channel (in withdrawal mode) to prime the channels. After the channels were filled with PBS and any large air bubbles in the channels were removed, the flow rate was set to 20 µl/hr/channel and the impedance of each channel of the device was obtained every 10 minutes for 20 hours by applying a 5 mV AC signal across the IDEs.

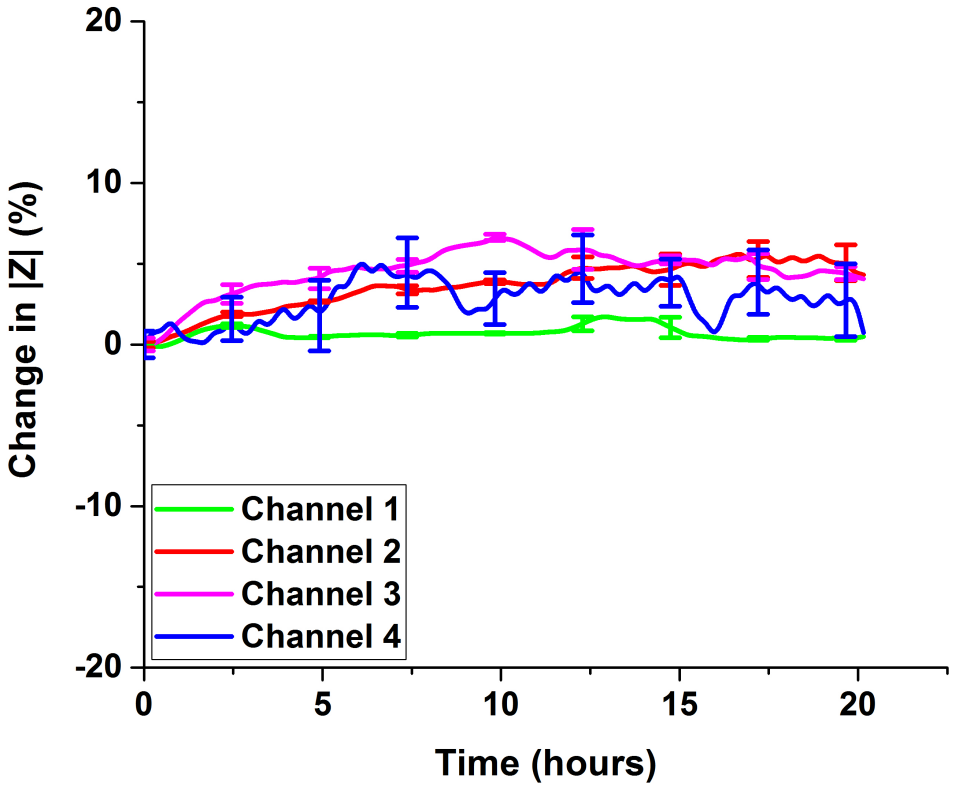

Figure 5-14 Plot showing the change in 100Hz impedance for the PBS buffer baseline for each of the four channels of the microfluidic device. The average absolute impedance remains stable around zero. The error bars plot the temporal change in absolute impedance (span = 3).

Figure 5-14 plots the measured absolute impedance at 100 Hz during the PBS buffer flow for each of the four channels of the bifurcation device. As observed from the graph the buffer flow resulted in a steady signal over time in all four channels. The variation in measured impedance is calculated to be around 2 %. The error bars represent the temporal variation in absolute impedance at 100 Hz at representative time points.

Biofilm Growth

Following the PBS conditioning, an impedance measurement of pure LB media was acquired to establish a baseline. Subsequently, all the channels of the device were seeded using an overnight culture of *E. coli* W3110 ($OD_{600} \approx 0.25$) without flow for 2 hours, after which pure LB media was introduced at a flow rate of 20 µl/hr/channel in withdrawal mode. Figure 5-15 shows the measured relative decrease in impedance during 20 hours of biofilm growth in the four channels. Compared to the steady signal when flowing buffer only (Figure 5-14), the relative decrease in absolute impedance is indicative of the attachment of bacteria and of biofilm growth. Due to a self-leveling effect in constricted channels, the variation in impedance at the end of the 20-hour growth period was observed to be only 2.35%, thereby once again validating the growth of uniform biofilms across the four channels [167].

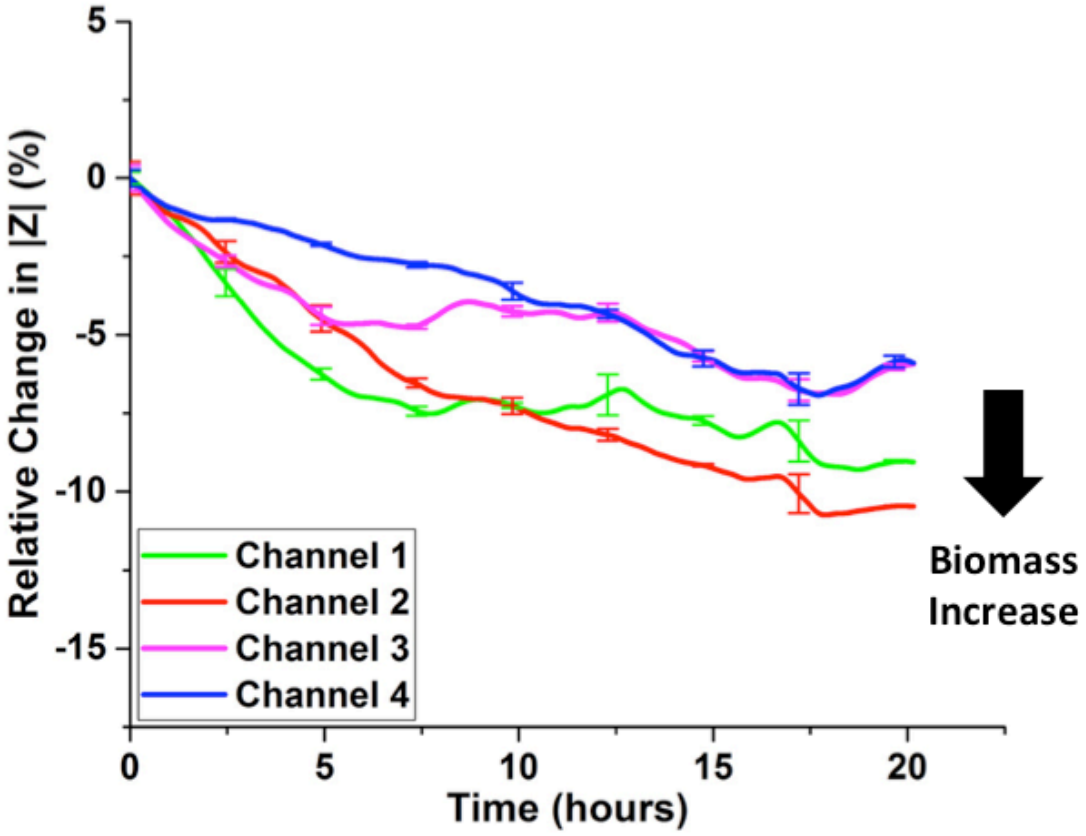

Figure 5-15 Measured change in 100Hz impedance during biofilm growth. While, the biofilm growth shows a decrease in impedance, the preceding baseline showed almost no change in measured impedance. The error bars represent the temporal variation of the biofilm (span = 3).

Biofilm Treatment

After the growth phase, different treatments were applied to the biofilms grown in the channels for an additional 24 hours. The antibiotic gentamicin, which is commonly used for treating *E. coli* infections, was diluted in LB media to a final concentration of 10µg/ml. This diluted solution of the antibiotic was introduced into two of the channels (antibiotic only and BE) and pure LB media was introduced into the remaining two channels (control and electric field only) at a flow rate of 20µl/hr. In addition to the real-time impedance measurements obtained for each channel, the

channels treated with BE and electric field only treatment were subjected to a 100 mV electrical signal for about 5 minutes per channel once every 33 minutes. Table 5-2 lists the various treatments applied to the four channels of the bifurcation device in addition to the 5 mV sensing voltage.

Table 5-2 Various experimental conditions applied to the microfluidic channels during the treatment period in addition to the 5mV sensing voltage applied.

Channel	Treatment	Experimental Conditions
1	Control	LB media only
2	E-field only	LB media + 100mV
3	Antibiotic only	10 μg/ml gentamicin in LB media
4	Bioelectric Effect (BE)	10 μg/ml gentamicin in LB media + 100mV

Figure 5-16 plots the relative change in absolute impedance measured during the application of the various treatments. The antibiotic-only (magenta line) and BE treatment (blue line) showed a reduction in biomass as measured by the increase in impedance with respect to the 20-hour growth phase. Conversely, the negative control (green line) and electric field-only treatment (red line) resulted in a continued decrease in impedance, suggesting further biofilm growth. Previous work using a SAW sensor demonstrated that the negative control and electric field-only treatments resulted in a continued increase in biomass, whereas the antibiotic-only and BE treatment resulted in a decrease in total biomass. Moreover, the BE resulted in more decrease in biomass as compared to the antibiotic-only treatment [175]. While the

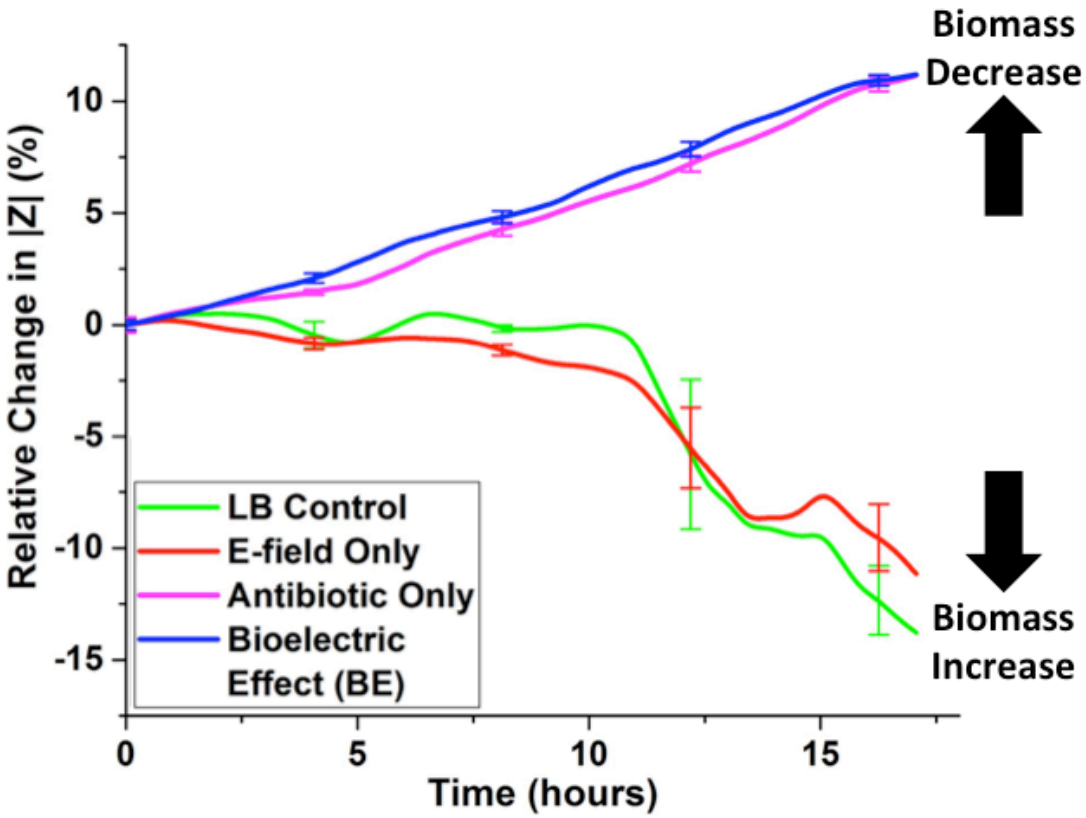

Figure 5-16 Measured change in 100Hz impedance during biofilm treatment. While biofilm growth shows a decrease in impedance, biofilm treatments (BE and antibiotic-only) result in an increase in impedance suggestive of biofilm removal. The error bars represent the temporal variation of the biofilm (span = 3).

results of the untreated negative control and the electric field only treatment presented in Figure 5-16 are consistent with the aforementioned previous outcomes, the antibiotic-only treatment showed an efficacy that is equivalent to the BE. We postulate that this equivalence and the higher than expected efficacy of the antibiotic-only treatment is a consequence of the periodic sensing voltage applied across the IDEs that also causes BE.

After the completion of 24 hours, the biofilms in the channels were stained using the Filmtracer™ LIVE/DEAD® Biofilm Viability Kit (Life Technologies Inc.), using equal proportions of SYTO9 and propidium iodide diluted in DI water, introduced at

20 µl/hr. The biofilms were then washed with DI water at the same flow rate to remove any excess stains and imaged using a fluorescent microscope (Olympus BX60, Olympus Life Science Solutions). The obtained images were analyzed using

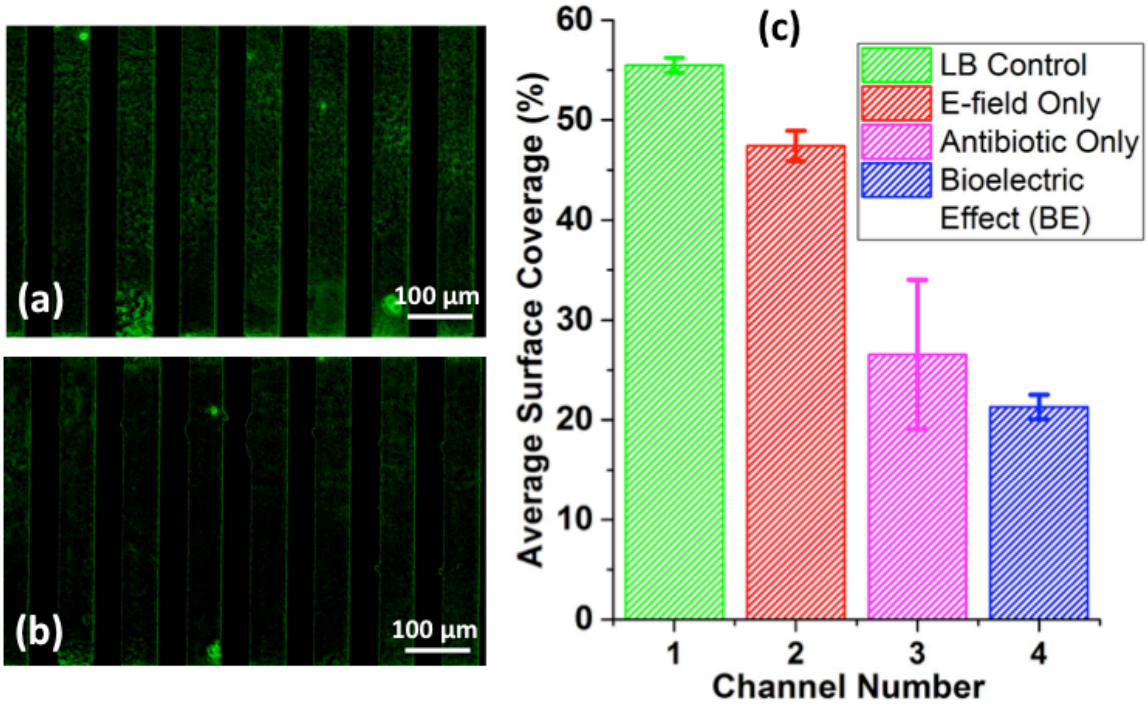

Figure 5-17 Representative micrographs of (a) untreated control, and (b) BE treated biofilm imaged after the 24-hour treatment cycle (scale bars = 100 µm). (c) Average surface coverage as measured using ImageJ (N = 2 images).

an image-processing program (Image J 1.44), which supports background subtracted image analysis facilitating an independent quantitative measurement of the biofilm surface coverage. Representative end-point optical micrographs of the control and BE-treated biofilms are presented in Figure 5-17a-b. Corresponding ImageJ analysis shows that BE treatment reduced biofilm surface coverage by ~61.6 % compared to the untreated control (Figure 5-17c).

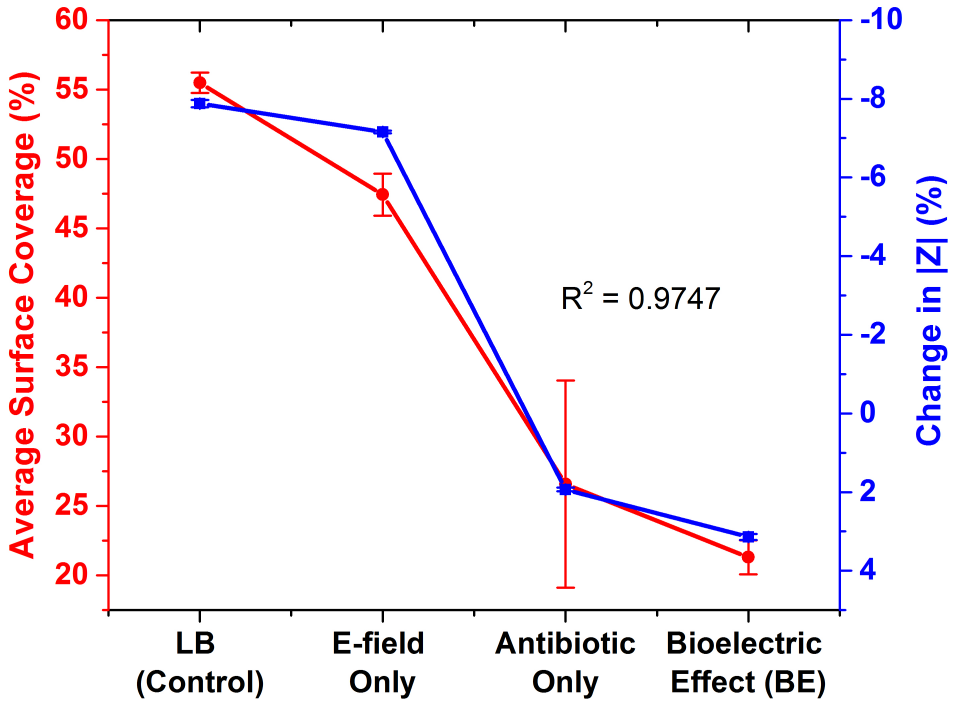

Figure 5-18 Correlation of measured average change in 100Hz impedance (span = 3) and average surface coverage (N = 2 images) calculated using ImageJ after 24-hour treatment.

Figure 5-18 plots the average change in impedance and the average biofilm surface coverage at the end of each of the four treatments. The change in impedance after 24 hours of treatment and the end-point biofilm surface coverage measurements correlate very well (R^2 = 0.97). Even though the surface coverage analysis does not measure the third dimension or thickness of the biofilms, it is a good approximation for the measurement of total biomass assuming uniform biofilm thickness.

This experiment thus demonstrates that the developed microsystem accurately detects biofilms in real-time, and also treats them using BE. The BE is applied only for a short period of the treatment cycle thus significantly lowering power utilization. The good correlation between the results obtained in the microfluidic device and the fluorescent microscopy data, combined with the low variability feature of the

bifurcation design, highlight the suitability of our platform for rapid, highly paralleled *in vitro* characterization of novel biofilm treatment strategies. This would ultimately enable threshold-activated application of BE in response to biofilm growth for rapid and effective *in situ* infection management, thus preventing post-surgery infections and significantly improving the quality of life for millions of patients.

5.1.5 Discussion

In this section we presented a simple IDE-based impedance sensor and demonstrated its ability to function not only as a sensor but also as a treatment system. The results discussed in this section successfully demonstrate that the sensor can accurately and in real-time measure the growth of biofilms. Furthermore, we show that use of the IDEs to apply the electrical signal necessary to initiate the BE treatment. Our results suggest that even the small sporadic 5 mV AC signal used for probing the impedance between the IDEs results in enhanced treatment based on the principles of BE. Thus, true de-coupling of the BE treatment from the antibiotic-only treatment is not possible using this setup.

One of the other major challenges of working with microfluidic systems is the introduction of air bubbles in the channel before or during the experiment. In the current impedance sensing microsystem removal of such air bubbles, although time consuming, is necessary in order to avoid large shifts in the measured impedance values. Thus, future generations of the microsystem will need to address this issue right at the design stage as it will avoid long periods of device priming and significantly reduce the complexity of the experiment.

As with any real-time sensing system, depending on the rate of sensing, data analyses and storage can be a challenge. For the microsystem developed as part of this dissertation no optimizations were performed for efficient data handling. The data from each channel was collected once every 8-10 minutes, yielding hundreds of data files necessitating significant memory for storage. Moreover, analyses of such large data are time consuming and require substantial compute power. Multiple experiments resulted in failure due to the lack of system memory and other processor resources. Thus, in order to truly achieve the end goal of device miniaturization towards application in a medical device, future generations of the proposed microsystem will require to address the challenge of data storage, memory usage and allocation of processor resources for data analyses so that experiments of longer time durations that are clinically relevant can be performed.

5.2 Threshold-activated Feedback Impedance Sensor-Treatment Microsystem

In the previous section, we successfully demonstrated the use of the IDEs for not only impedance based sensing but also BE based treatment of biofilms. Such integration into a single domain facilitates rapid switching between sensing and treatment. In this section, we demonstrate the use of the real-time impedimetric sensing data to accomplish self-governing treatment of biofilms using BE. We developed a MATLAB control module that uses the measured impedance across the IDEs to identify biofilm growth and based on user-defined inputs makes the decision to either switch to BE treatment or continue impedimetric sensing of biofilms. This, to the best of our knowledge, is the first integrated microsystem solution with both

sensing and self-directed treatment capabilities. We demonstrate the ability of the developed integrated microsystem using a bifurcation-based microfluidic flow cell setup. We believe that development of such threshold-activated feedback systems with sensing and self-directed treatment capabilities will pave the way towards rapid, real-time and truly autonomous management of *in situ* biofilms. Such management of biofilms on medical implants will allow for reduced revisional surgeries and greatly improve the quality of life of millions of patients.

5.2.1 Experimental Setup

We demonstrate impedimetric change-based self-governing treatment of biofilms with BE in a bifurcation device with 50 μm IDE sensors. The experimental setup to demonstrate the threshold-activated feedback sensing and treatment of biofilms is identical to the setup discussed in section 3.4.3 for the bifurcation device (Figure 5-6c). However, instead of directly gathering impedance data using the CH Instruments (CHI) control software, the potentiostat and multiplexer were controlled by a custom-built MATLAB macro that enabled real-time impedance monitoring in all four channels and also the application of E-field based treatments in any of the channels of the device based on user-defined inputs. A block schematic of our micro-total analysis system (μTAS) is shown in Figure 5-19. As shown in the schematic, the bifurcation based sensor and treatment system was placed in an incubator maintained at 37 °C. One end of the fluidics was connected to the syringe pump, while the other was connected to a micro-centrifuge tube that acted as a reservoir or a waste

collector. The device was electrically connected to the CHI multiplexer, which was in turn connected to the potentiostat.

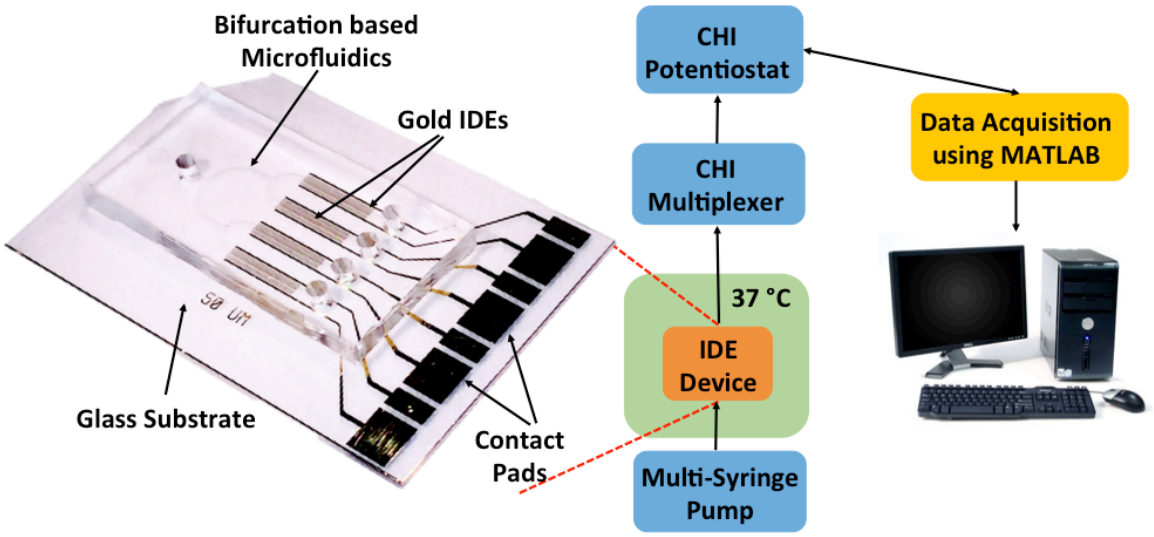

Figure 5-19 Block schematic of our µTAS concept for threshold-activated feedback biofilm treatment. Photograph of bifurcation based IDE sensor and treatment system, showing the components of the sensor and the microfluidic channels. Also shown are the electrical and/or fluidic connections between the device and other equipment.

5.2.2 MATLAB Control Macro Implementation

A graphical user interface (GUI) was created using MATLAB for the user to provide the required inputs for performing the experiment. The control macro was implemented using the libec SDK for MATLAB provided by CH Instruments, the manufacturer of the potentiostat. Other platform libraries like LabVIEW are available, however MATLAB was chosen because of the relative ease in programing and its ubiquitous use in research. The library can be downloaded from the vendor's website at http://www.chinstruments.com/libec_alpha.shtml.

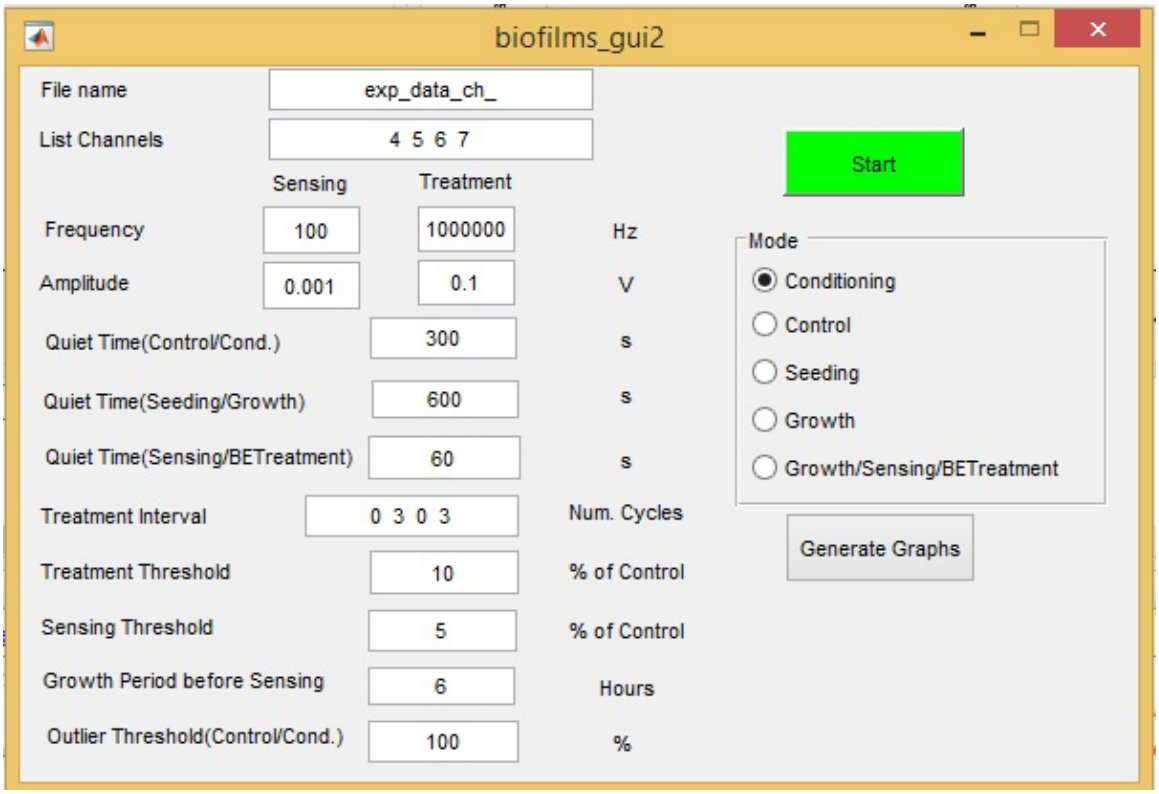

Figure 5-20 Screenshot of the MATLAB control macro graphical user interface (GUI).

Figure 5-20 presents a screenshot of the MATLAB control module GUI that appears on running the MATLAB file biofilm_gui2.m (Appendix C). On execution of the macro the library SDK is compiled using the inputs provided through the GUI to control the potentiostat. Two additional windows titled Figure 2 and Figure 3, shown in Figure 5-21, are also displayed alongside the GUI. These windows contain eight graphs in total and plot the absolute impedance and the relative change in impedance of each channel listed in *List Channels* field in real-time. A comprehensive explanation of each input to the GUI and the protocol used to successfully demonstrate threshold-activated feedback treatment are discussed in the following sub-sections.

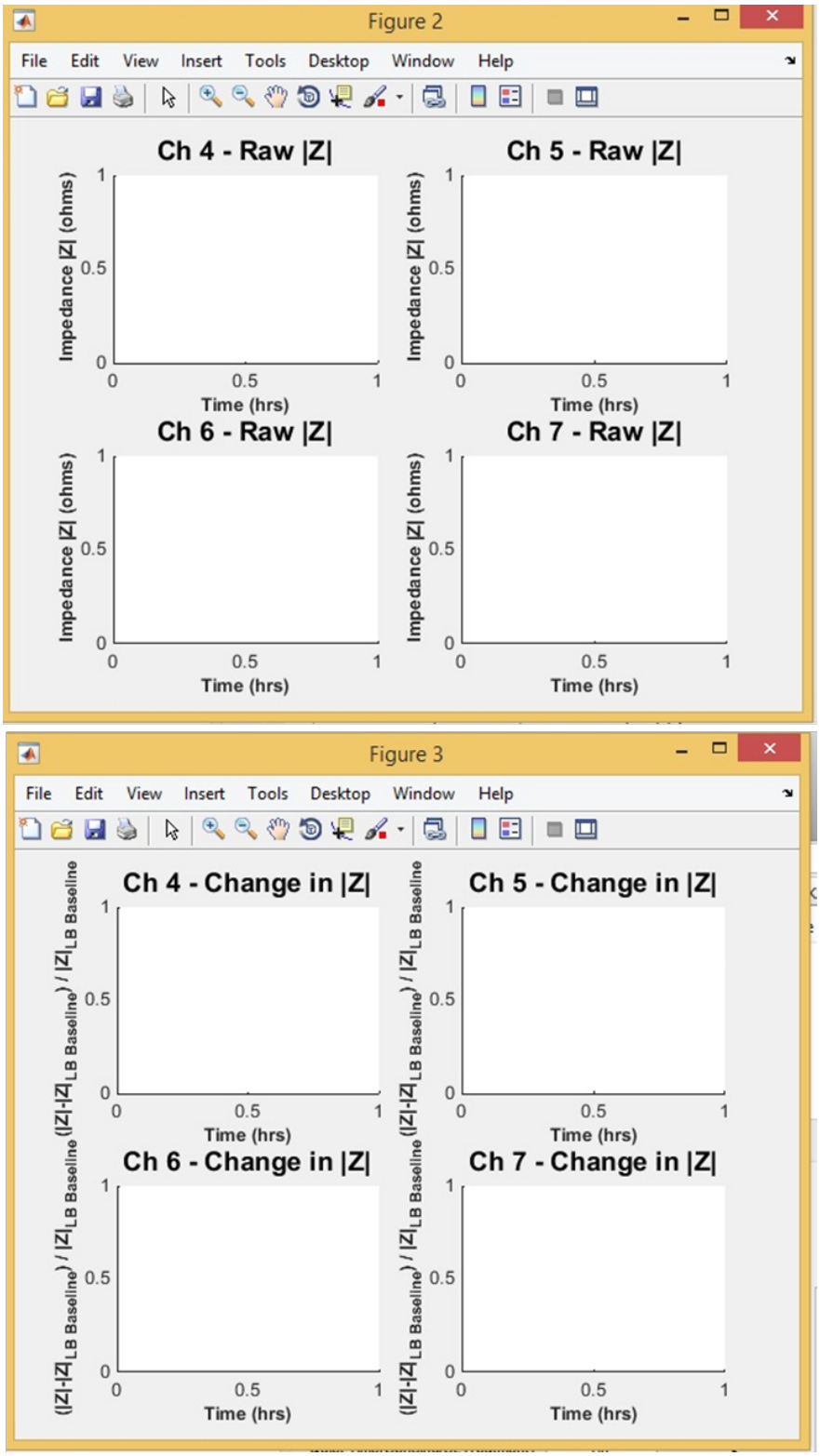

Figure 5-21 Additional windows that are displayed along with the GUI on execution of the MATLAB code biofilm_gui2.m. The window titled Figure 2 plots the absolute impedance of each channel with time while the window titled Figure 3 plots the change in impedance of each channel with time. Both sets of plots are plotted in real-time.

User Inputs

Table 5-3 lists all the inputs that are to be provided by the user using the MATLAB GUI along with a brief description of each field and their default values. A comprehensive explanation of each parameter of the GUI is discussed in this section.

Table 5-3 Table explaining the various fields of the MATLAB graphical user interface (GUI). The default values of the control macro's GUI are also listed in the table.

Field Name	Description	Default Value
File name	Prefix of the name of files that will be saved	exp_data_ch_
List channels	Array listing the physical potentiostat multiplexer channels in use	4 5 6 7
Sensing amplitude	Sensing voltage in volts	0.005 V
Sensing frequency	Sensing frequency in Hz	100 Hz
Treatment amplitude	Treatment voltage in volts	0.1 V
Treatment frequency	Treatment frequency in Hz	1 MHz
Quiet time (Control/Cond.)	Quiet time in seconds after sensing all the channels listed in "List channels" during *conditioning* and *control* mode	300 seconds
Quiet time (Seeding/Growth)	Quiet time in seconds after sensing all the channels listed in "List channels" during *seeding* and *growth* mode	600 seconds
Quiet time (Sensing/BETreatment)	Quiet time in seconds after sensing all the channels listed in "List channels" during *sensing* and *BE treatment* mode	60 seconds

Treatment interval	Array of whole numbers listing treatment mode of channels (0 – no treatment; n – treatment for 10n minutes)	0 0 3 3
Treatment threshold	Upper threshold in % at which the system must switch from sensing to treatment	20 %
Sensing threshold	Lower threshold in % at which the system must switch from treatment to sensing	15 %
Growth period before sensing	Time in hours after switching "mode" to *BE treatment* during which mode of operation continues to be *growth*	6 hours
Outlier threshold (Control/Cond.)	Threshold in % for outlier detection (used only in *conditioning* and *control* modes)	100 %
Mode	List of experimental modes (radio button list)	Conditioning
Start/Pause button	Button to start or pause data collection	NA
Generate graphs button	Button to generate all graphs in .fig and .png formats	NA

File Name

This field allows the user to enter a prefix that will be appended at the beginning of every file generated during the experiment. This includes the text files generated during the experiment and the final graphs generated at the end of the experiment.

List Channels

The multiplexer connected to the potentiostat can be programmed to serially address up to 12 channels (channel 1 to channel 12). The *List channels* field allows the user to manually enter the physical number of the various channels that needs to be addressed by the MATLAB program. The channels are listed in the order in which they are to be addressed with a space between two consecutive channels. The program is set by default to address only four channels at a time. If a different number of channels require to be addressed, the source code biofilm_gui2.m needs to be edited.

Sensing Amplitude and Frequency

The sensing amplitude and frequency refers to the AC voltage amplitude and frequency that is used to monitor the impedance across the IDEs during all modes of operation. Based on the previous experimental results presented in section 3.4, these were set to 0.001 V and 100 Hz respectively.

Treatment Amplitude and Frequency

The treatment amplitude and frequency refers to the AC voltage amplitude and frequency that will be used to apply the electric field component of the BE treatment. Since the efficacy of the BE treatment is directly proportional to the total energy applied to the treatment, a higher magnitude signal of 0.1 V at 1 MHz is set at the default. This parameter is used only during the *BE Treatment* mode of operation.

Quiet Time

Quiet time refers to the wait time that the potentiostat is temporarily inactive *i.e.* no data collection or AC application occurs, immediately after a complete set of impedance measurements are obtained from all the channels listed in the *List Channels* field. Three separate *Quiet Time* fields are listed in the GUI corresponding to the different modes of operation. The first quiet time is set to 300 seconds and is used during the *Conditioning* or *Control* mode. The second quiet time, set to 600 seconds, is used only in the *Seeding* or *Growth* mode. The wait times for the latter two modes is set to twice that of the former two modes in order to avoid electrical signal-based detachment of bacterial cells during seeding or growth. Thus, impedance data is obtained more sparsely for the *Seeding* and *Growth* modes. The final quiet time is used only during the *BE Treatment* mode.

Treatment Interval

This field allows the user to enter an array of positive whole numbers (0, 1, 2, 3,…n) and represents the number of cycles for which the electric field based treatment needs to be applied to each channel. The length of the array should be the same as the *List Channels* field array and the numbers of the field must be entered with blank spaces in between them. The number of minutes of electric field application is equal to ten times the number of cycles entered in this field. For example an entry of 0 corresponds to no electric field application to the corresponding channel, while an entry of 1, 2, 3, …, n corresponds to an electric field

application of 10, 20, 30,…, 10n minutes, respectively, across the IDEs of the corresponding channel.

Treatment and Sensing Threshold

The treatment threshold is defined as the relative percentage change in absolute impedance beyond which electric field-based treatment is initiated. The sensing threshold is defined as the relative percentage change in absolute impedance below which treatment application is terminated. Two separate thresholds were defined in order to allow for user flexibility and to account for any impedance measurement noise, which in our experiments was generally about 2-3 %.

Growth Period before Sensing

As the media and antibiotics are introduced to the channels of the bifurcation device through fluidic tubing, a fixed amount of time exists before the treatment introduced at one end of the Tygon tubing reaches the microfluidic channel of the PDMS device. The *Growth Period before Sensing* field was designed to account for this 6-8 hour time period after the change of source from growth media to treatment, during which the growth media in the Tygon tubing flows through the PDMS channels. After the mode is switched from *Growth* to *Growth/Sensing/BETreatment* a timer is set for the number of hours entered in the *Growth Period before Sensing* field and countdown is initiated. The control module does not switch from the *Growth* mode till the counter counts down to zero after which the control module switches from the *Growth* mode to the *Sensing/BETreatment* mode.

Outlier Threshold

This user-defined parameter is used to remove any outliers measured during the device *Conditioning* and *Control* modes of operation. The outlier threshold is defined as the upper limit percentage change in impedance greater than which the data obtained is considered as an outlier. The number of such outliers for each of the channels for the two modes *i.e.*, *Conditioning* and *Control*, is enumerated in a separate text file named <*File name*>*_outliers.txt*.

Mode

The GUI permits the user to select the mode of operation of the experiment from a radio-button list of five modes. The five modes are 1. *Conditioning*, 2. *Control*, 3. *Seeding*, 4. *Growth*, and 5. *Growth/Sensing/BETreatment* corresponding to the five different phases of the experimental protocol, *viz.*, PBS conditioning, LB growth media control, bacterial seeding of the microfluidic channel, biofilm growth using growth media flow, and finally the treatment by flowing antibiotic diluted in growth media. As explained in the previous paragraph, the last mode includes a brief growth phase during which the growth media in the Tygon tubing is allowed to flow through the device channels. Following this the mode changes to the sensing and the electric-field based treatment mode. The code directs the switching between these two modes based on the real-time impedance measurements collected and the sensing and treatment thresholds entered by the user.

Modes of Operation

At the end of each experimental phase the user can pause the experiment using the *Start/Pause* button, select the mode of operation from the radio-button list under the *Mode* field in the GUI and continue the experiment by pressing the *Start/Pause* button again. This section details the various modes of operation of the control module. Additionally, a comprehensive explanation of the need for each mode and each mode's functionality is discussed.

Conditioning

The *Conditioning* mode is used during the buffer conditioning of the device. This mode creates plots and data files that are independent of the other modes of operation. The data collected during this mode is plotted as black hollow circles in the Figure 2 window (Raw |Z|) of Figure 5-21. Three plots are generated for this mode per channel when the *Generate graphs* button is used. They are the raw impedance plot, the raw impedance plot with outliers removed, and the change in absolute impedance plot. These plots are saved in both MATLAB figure and portable network graphics (.png) formats.

Control

The *Control* mode is generally used during the growth media baseline data generation. This mode also plots the real time data in the Figure 2 window (Raw |Z|) of Figure 5-21 but as solid black circles. The data collected in this mode serves as the baseline for all the data collected in all other modes of operation (except the *Conditioning* mode). The *Generate graphs* option creates the three plots per channel

that are independent of the *Conditioning* mode data files. The modes discussed below append data to these plots.

Seeding

On switching modes from *Control* to *Seeding*, the change in absolute impedance is calculated and plotted in the Figure 3 window shown in Figure 5-21. The impedance values measured in this mode are plotted in real-time as absolute impedance and the change in impedance in both windows respectively. In this mode, the data points are plotted as solid magenta circles to distinguish them from the data measured in the preceding modes.

Growth

The Growth mode is used to during the growth phase of the experiment. Similar to the *Seeding* mode the *Growth* mode plots the data in real-time as absolute impedance and change in absolute impedance in both MATLAB figure windows. These are plotted as green solid spheres.

Growth, Sensing and Treatment

The final mode of operation is the *Growth/Sensing/BETreatment* mode and this is used to record impedance data once the syringe pump is switched to infuse treatment into the fluidic tubing. As the name suggests this mode is a grouping of three individual modes. The growth segment of this mode records data, in exactly the same manner as the *Growth* mode for the number of hours listed in the *Growth period*

before sensing input. This option exists to account for the growth media that has already been introduced into the Tygon tubing prior to the introduction of the treatment solutions. The *Sensing/BETreatment* modes go hand-in-hand. In the *Sensing* mode the system gathers impedance data in real-time and plots them as absolute impedance and change in impedance in both MATLAB figure windows in solid blue circles. If the average of five consecutive impedance change measurements is larger than the *Treatment threshold* set by the user, the system switches into *BETreatment* mode. During this mode the potentiostat applies the electric field-based treatment (set using the *Treatment amplitude* and *Treatment frequency*) to the appropriate channels. A red solid circle in the plots marks application of the electric field-based treatment followed by an impedance measurement at the *Sensing* amplitude and frequency. After a complete cycle of the application of electric field-based treatment to all the channels, the potentiostat switches back to the *Sensing* mode and performs five cycles of sensing across all the channels. If, for a given channel, the average change in impedance of the five consecutive sensing measurements is greater than the *Treatment threshold* the system switches once again into the *BETreatment* mode. However, if the average is less than the *Sensing threshold*, the system continues to remain in the *Sensing* mode. The system thus systematically and regularly checks for the average change in impedance and switches the system into the appropriate state based on the user-defined threshold values. This mode thus allows for the self-governing treatment based on the real-time impedance data gathered during the previous cycles.

Control Module Verification

To verify and validate the functionality of the MATLAB control module code, a simulated biofilm growth experiment was performed. Two channels (channel numbers 5 and 7) out of four channels (channel numbers 4, 5, 6, and 7) were set to switch to BE-based treatment by setting the *Treatment Interval* field to 0 3 0 3. The various settings of the MATLAB GUI are listed in Table 5-4.

Table 5-4 List of parameters values used during simulated biofilm growth experiment. The parameters not listed below were set to their default values.

Parameter Name	Parameter Value
List channels	4 5 6 7
Sensing amplitude	0.005 V
Sensing frequency	100 Hz
Treatment amplitude	0.1 V
Treatment frequency	1 MHz
Quiet time (Control/Cond.)	3 seconds
Quiet time (Seeding/Growth)	6 seconds
Quiet time (Sensing/BETreatment)	10 seconds
Treatment interval	0 3 0 3
Treatment threshold	20 %
Sensing threshold	15 %
Growth period before sensing	0.1 hours

With no device connected to the machined test stage, the first hour of measurements corresponding to the *control*, *seeding* and initial *growth* phases were obtained with an open circuit. Just before entering the *sensing* phase of the experiment, a 5 kΩ resistor was connected between the two electrodes so as to simulate the growth of a biofilm.

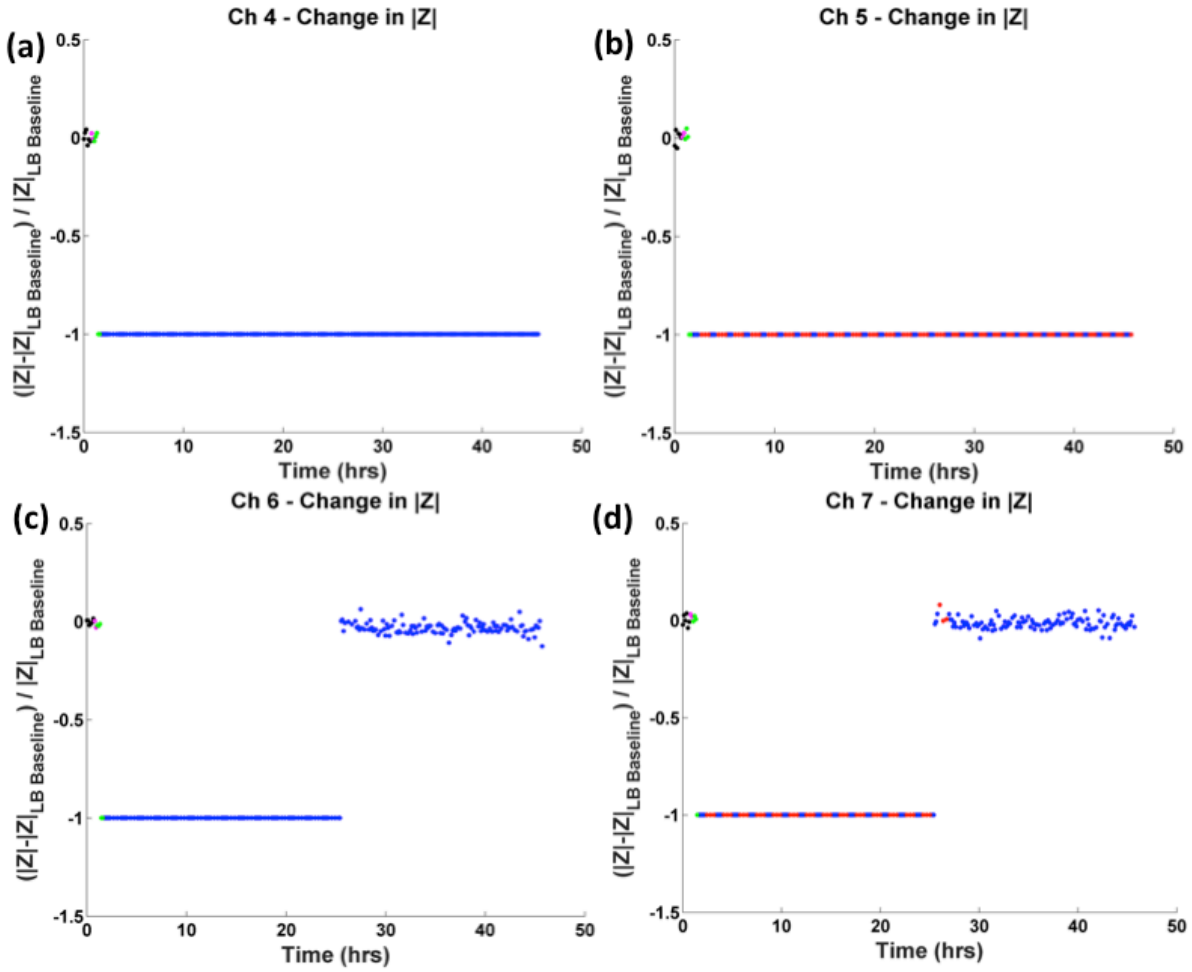

Figure 5-22 Verification of the control module code using resistors to simulate biofilm growth. As shown, the channels 5 and 7 switched into BE treatment when the average change in absolute impedance exceeded the set threshold values. Channels 4 and 6 continue in the Sensing mode despite a similar change in the absolute impedance.

Figure 5-22 presents the results of this simulated experiment. The connected resistor resulted in a large decrease in measured impedance, which after five sensing cycles triggered the *BE Treatment* in the channels 5 and 7 (red circles). Channels 4 and 6 continued in the *Sensing* mode, as indicated by the blue circles in the plots, despite a similar change in the absolute impedance. To simulate the removal of biofilm, the 5 kΩ resistor was removed from channels 6 and 7 yielding a return to the baseline in both these channels. As the now measured impedance change is less than the set *Sensing Threshold*, channel 7 returns to operate solely in *Sensing* mode (blue circles) without entering the *BETreatment cycle*. However, channel 5 continues to measure the impedance across the resistor, thus remaining above the *Treatment Threshold* and continuing to switch between the *Sensing* and *BETreatment* cycles. This simulated experiment thus validates the functionality of the macro to switch between *Sensing* and *BETreatment* modes based on the set thresholds and the real-time impedance measurements obtained during the *Sensing* mode of operation.

5.2.3 Results

With the functionality of the control macro established by means of a simulated biofilm growth experiment, a bifurcation device integrated with IDE sensors was used to demonstrate real-time sensing and threshold-activated BE treatment of *E. coli* biofilms. The various settings of the MATLAB GUI used for this experiment are listed in Table 5-5. The results at the end of the buffer conditioning, growth and treatment are discussed in this section.

Table 5-5 List of parameters values used during simulated biofilm growth experiment. The parameters not listed below were set to their default values.

Parameter Name	Parameter Value
List channels	4 5 6 7
Sensing amplitude	0.005 V
Sensing frequency	100 Hz
Treatment amplitude	0.1 V
Treatment frequency	1 MHz
Quiet time (Control/Cond.)	300 seconds
Quiet time (Seeding/Growth)	600 seconds
Quiet time (Sensing/BETreatment)	300 seconds
Treatment interval	0 3 0 3
Treatment threshold	20 %
Sensing threshold	15 %
Growth period before sensing	7 hours

PBS Conditioning

Figure 5-23 plots the change in absolute impedance for the four channels of the bifurcation device during the 24-hour buffer conditioning. Any recorded data point

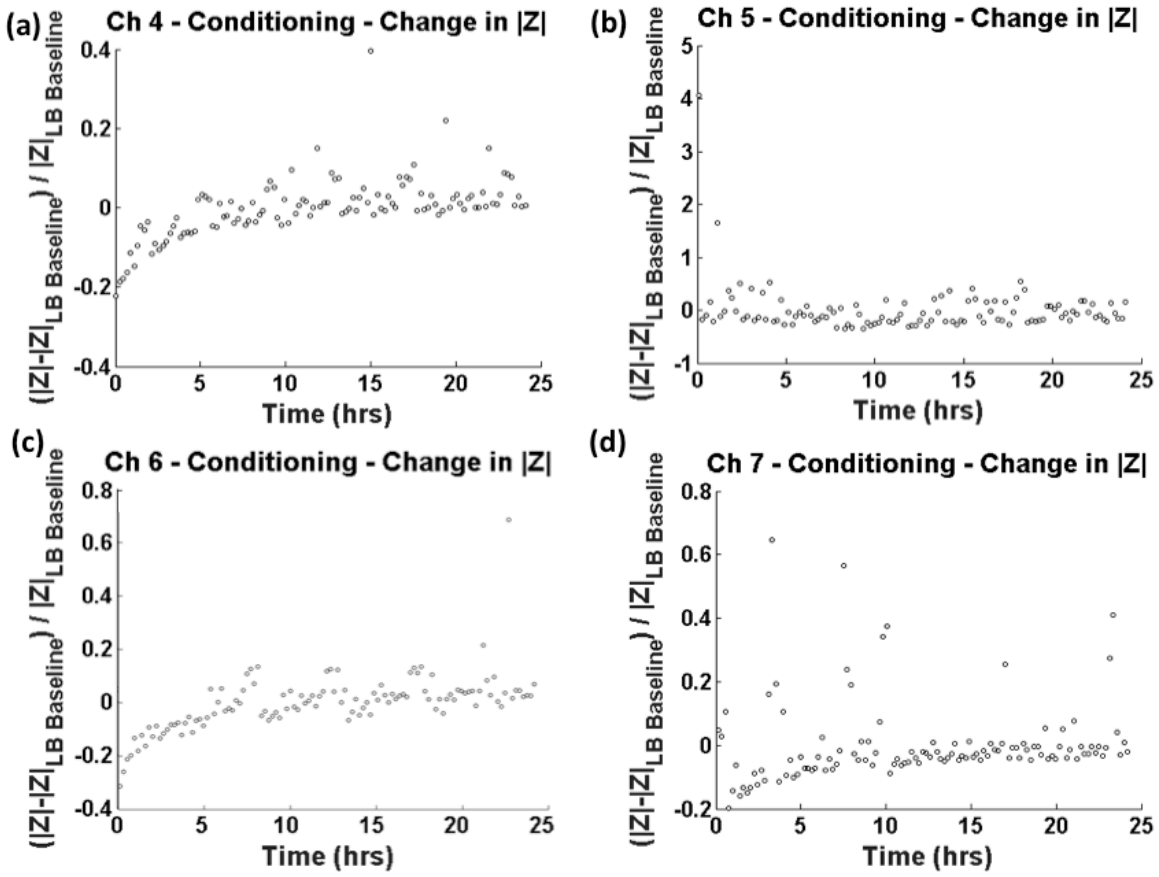

Figure 5-23 Plots showing the change in 100 Hz impedance during the 24-hour PBS conditioning measured by the IDE sensors of the four channels. All channels show an average impedance change of approximately zero. The channel numbers in the title of the subplot correspond to the physical channel address of the CH Instruments multiplexer.

greater than a 100 % change is marked an outlier and removed from the plot. In order to observe the trend in data and to remove the effect of outliers that record less than the 100 % outlier threshold, a moving average of the data is calculated (relevant MATLAB code is in Appendix C). Figure 5-24 plots the same data along with the moving average line for the four channels of the device. As observed from the plots, the average change in impedance fluctuates during the first few hours of the

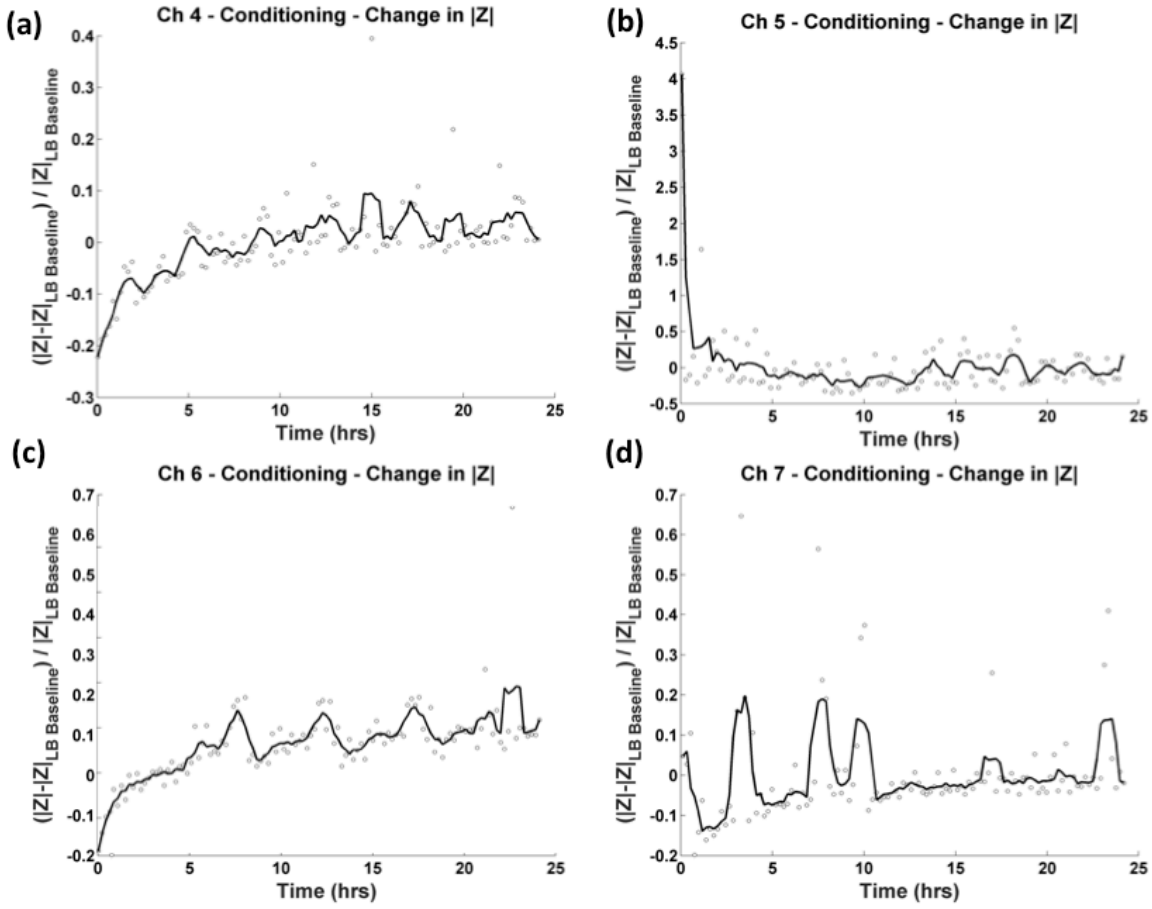

Figure 5-24 Plots showing the change in 100 Hz impedance during the 24-hour PBS conditioning measured by the IDE sensors of the four channels. All channels show an average impedance change of approximately zero. The solid line represents the moving average of the real-time data (span = 5). The channel numbers in the title of the subplot correspond to the physical channel address of the CH Instruments multiplexer.

conditioning phase but stabilizes to near zero with time. Small fluctuations in measurements, as observed by the increase in impedance, are recorded over time and it is hypothesized to be a result of either small air bubbles trapped within the microfluidic channels that are eventually removed with time, or due to the intrinsic noise of the system.

Biofilm Growth

Figure 5-25 plots the change in 100 Hz impedance and the moving average (span of moving average = 5) through the end of the biofilm growth phase of the experiment. Following the PBS buffer conditioning, pure growth media was introduced into the channels and the impedance data measured for six hours in *Control* mode. After a steady control baseline (solid black data points) is established,

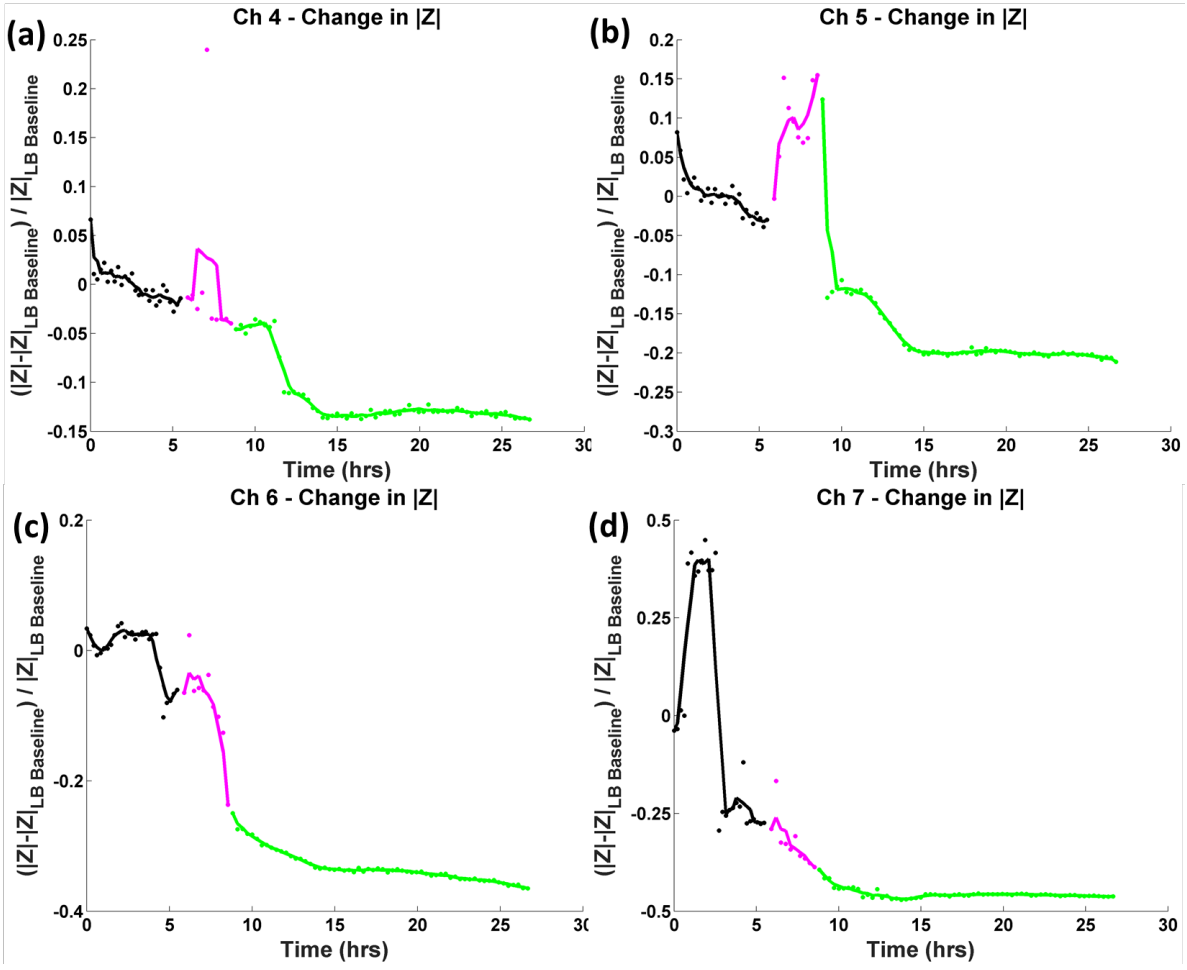

Figure 5-25 Plots showing the real-time change in absolute impedance at 100Hz, captured during growth for the four channels of the bifurcation device. The three different colors represent the three phases of the experiment, namely the LB growth media control (black), bacterial seeding (magenta) and biofilm growth (green). The line plots show the moving average (span = 5) for each of the three experimental phases for the four channels.

an overnight culture of *E. coli* W3110 suspended in growth media to a final $OD_{600} \approx 0.25$ is introduced into the device to seed the microfluidic channels and allow for bacterial attachment (no flow). The data obtained during this phase of the experiment is plotted in magenta in the plots. Subsequently, growth media is introduced into the channels at 20 µl/hr to allow for biofilm growth. The real-time change in 100 Hz impedance during growth is plotted in green.

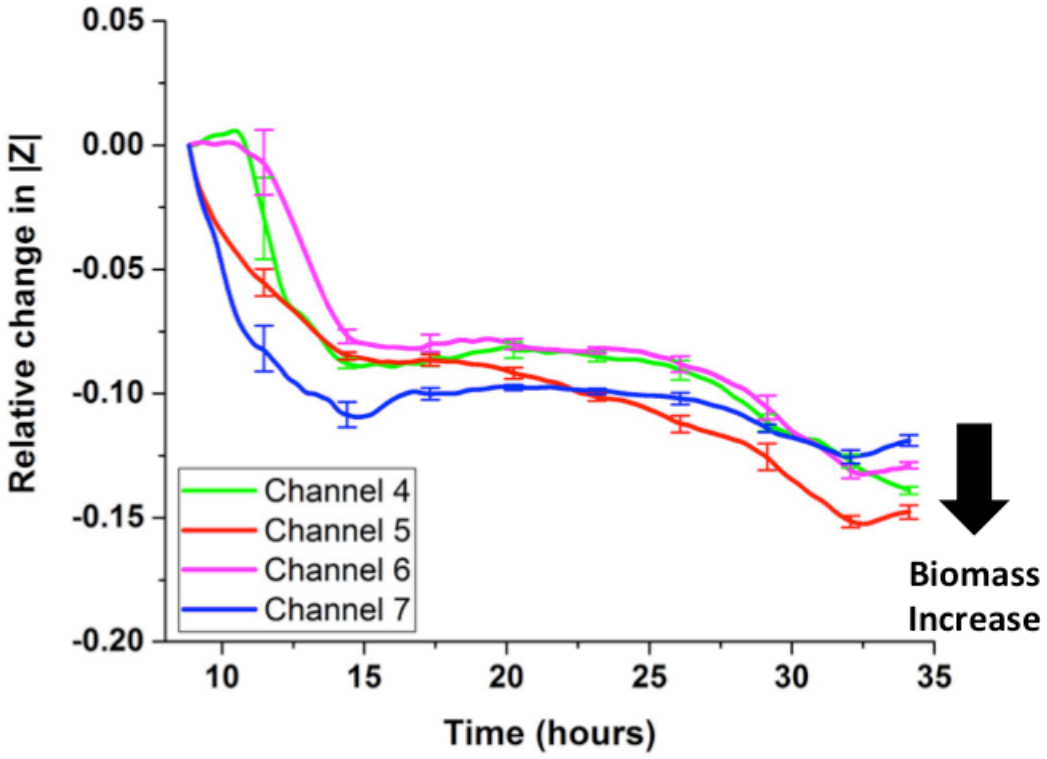

Figure 5-26 Measured real-time change in 100 Hz impedance across the four channels of the bifurcation device at the end of the growth phase. While, the biofilm growth shows a decrease in impedance, the preceding baseline showed almost no change in measured impedance. The error bars plot the temporal change in biofilm at representative time points (span = 5).

Since the plots in Figure 5-25 are plotted on different y-axis scales, the observed change in impedance between the four channels appear to be significantly different over time. This is primarily due to the large shifts observed in a few channels, *viz.*

channels 5 and 7, during the LB media control or the bacterial seeding stages, possibly due to the introduction of an air bubble in the channel. However, if these huge shifts in impedance were set aside, an equivalent net change in impedance is observed across all four channels from the start of growth to the end of growth during which a continuous supply of growth media is introduced into the microfluidic channels (Figure 5-26).

Figure 5-26 plots the relative change in impedance for each of the four channels of the device during the growth phase, from around the 9-hour time point to the 34 hour time point, with respect to first data point measured in the *Growth* mode. This plot highlights the near similar shift in impedance across all four channels of the device, which is suggestive of uniform biofilm growth in all the channels of the device. Additionally, it is worth noting that the magnitude of the change in impedance observed in Figure 5-26 is similar to that obtained in Figure 5-15, thus highlighting the reproducibility of the impedance based sensing methodology to detect biofilm growth in real-time.

Threshold-activated Biofilm Treatment

Following the growth of biofilms in all four channels of the device, different solutions, namely LB media or antibiotic (gentamicin 10 μg/ml in LB media) were introduced into the microfluidic channels. The treatments applied to the channels of the device over 24 hours are listed in Table 5-6. The channels 5 and 7 received the additional intervallic 100 mV electrical treatment in addition to the periodic 5 mV

Table 5-6 Table listing the various experimental conditions applied to the microfluidic channels during the 24-hour treatment period, over the 5mV sensing voltage applied.

Channel No.	Treatment Name	Treatment Applied
4	Control	LB media only
5	E-field Only	LB media + 0.1 V at 1MHz
6	Antibiotic	10 μg/ml gentamicin in LB media
7	Bioelectric Effect (BE)	10 μg/ml gentamicin in LB media + 0.1 V at 1MHz

sensing voltage applied to all the channels. The plots presented in Figure 5-27 show the 100 Hz change in impedance for the various channels for all the experimental phases i.e. control (black), seeding (magenta), growth (green), sensing (blue), all at 5 mV and BE treatment (red) at 100 mV.

Figure 5-27 plots the real-time change in absolute impedance at 100 Hz after the 24-hour treatment period. Even after the treatment phase the untreated control (channel 4) and the electric field-only treatment (channel 5) show a further decrease in impedance suggestive of an increase in total biomass or more biofilm growth. On the other hand, treatment with antibiotic (channel 6) and BE (channel 7) resulted in an increase in 100 Hz impedance that represents the removal or decrease in total biomass.

The change in 100 Hz impedance observed only during the treatment phase is plotted in Figure 5-28. This plot enables clear visualization and comparison of the change in 100 Hz impedance due to biofilm growth and treatment across all four

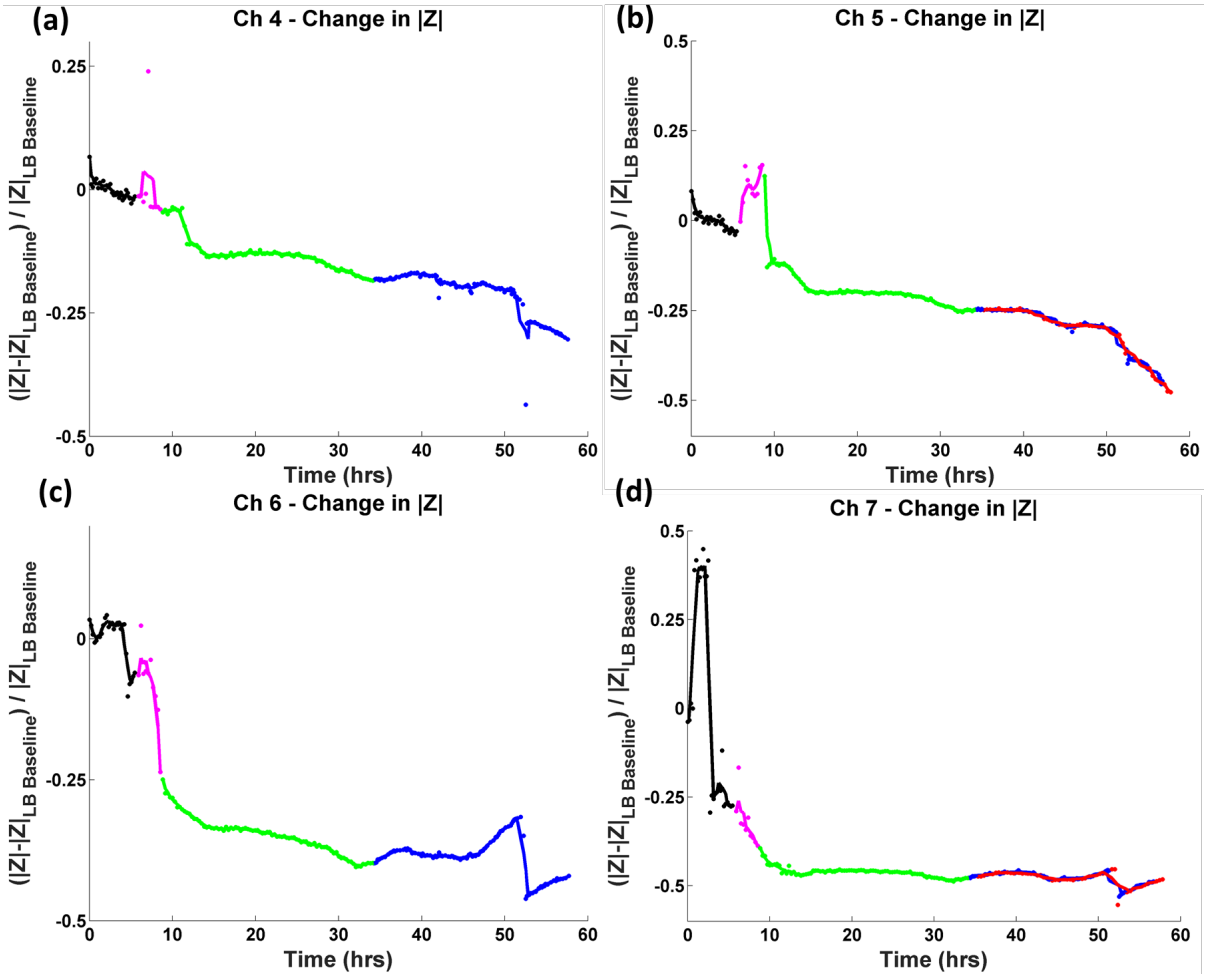

Figure 5-27 Plots showing the real-time change in absolute impedance at 100Hz, captured at the end of the treatment phase for the four channels of the bifurcation device. The different colors represent the various phases of the experiment, namely the LB growth media control (black), bacterial seeding (magenta), biofilm growth (green), biofilm sensing (blue) and biofilm treatment using BE (red). The line plots show the moving average (span = 5) for each of these experimental phases for the four channels.

channels of the device. As shown in the figure, the control (green line) and E-field only (red line) treatments continue to measure a decrease in impedance even during the treatment phase, correlating with continued biofilm growth. In contrast the antibiotic (magenta line) and the BE (blue line) exhibit a change in the opposite

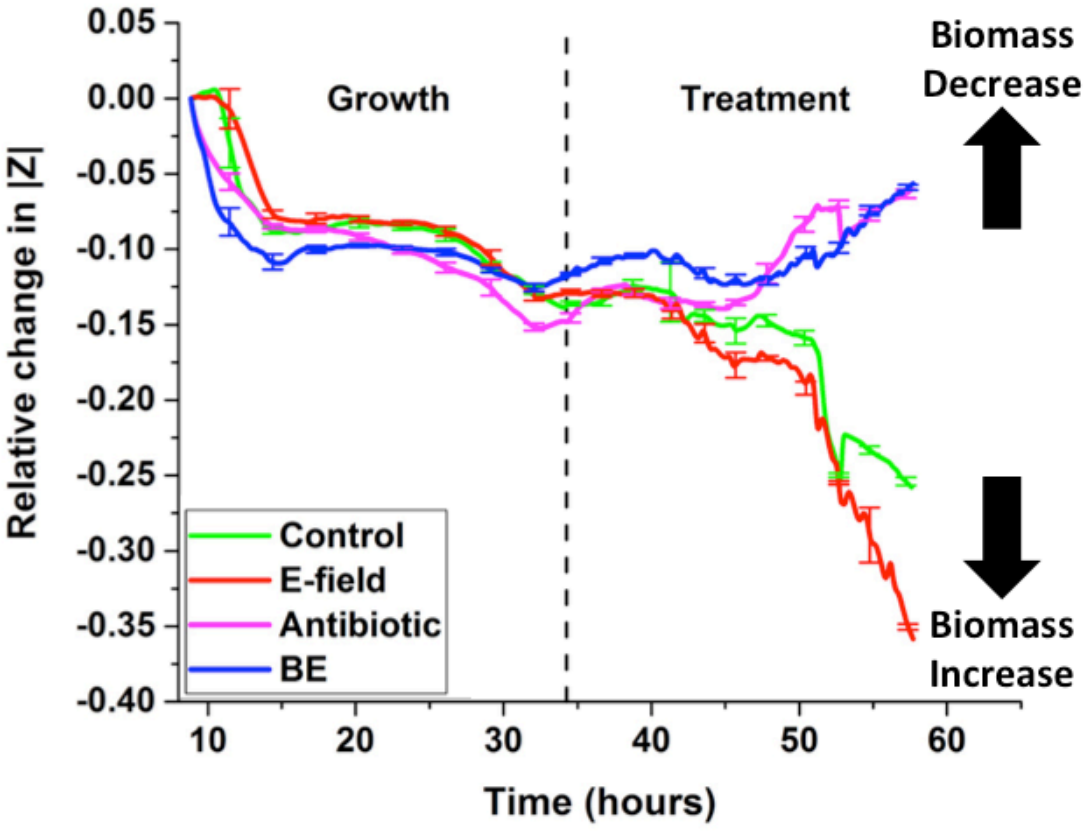

Figure 5-28 Measured real-time change in 100 Hz impedance across the four channels of the bifurcation device at the end of the treatment phase. While, the controls (control and E-field) show a decrease in impedance indicating further biofilm growth, biofilm treatments (BE and antibiotic) show an increase in impedance representing a decrease in total biomass. The error bars plot the temporal change in biofilm at representative time points (span = 5).

direction indicating a decrease in biomass. It is also worth noting that the antibiotic treatment (magenta line) appears to be as effective in treating the biofilm as the BE treatment. This is similar to previously obtained results (Figure 5-16) presented in the earlier sub-section of this chapter. As mentioned before, it is hypothesized that the similar efficacies between the antibiotic and BE treatments is due to the periodic sensing voltage applied to the antibiotic treatment (channel 6) that also causes significant BE. Hence the efficacy of the treatment applied to channel 6 is not purely

a result of only the antibiotic therapy but rather due to regular and recurring BE treatment that results in effective removal of the biofilm in the channel.

Optical Validation

To independently validate the results obtained using the impedance microsystem, analogous to section 3.4.4, end-point fluorescent images obtained for each channel of the device were analyzed using the image-processing program. Representative end-point optical micrographs of the control and BE-treated biofilms are presented in Figure 5-29a-b. ImageJ analysis shows that the antibiotic and the BE treatment reduced the average biofilm surface coverage by ~82.4 % and ~87.9 %, respectively, compared to the untreated control (Figure 5-29c).

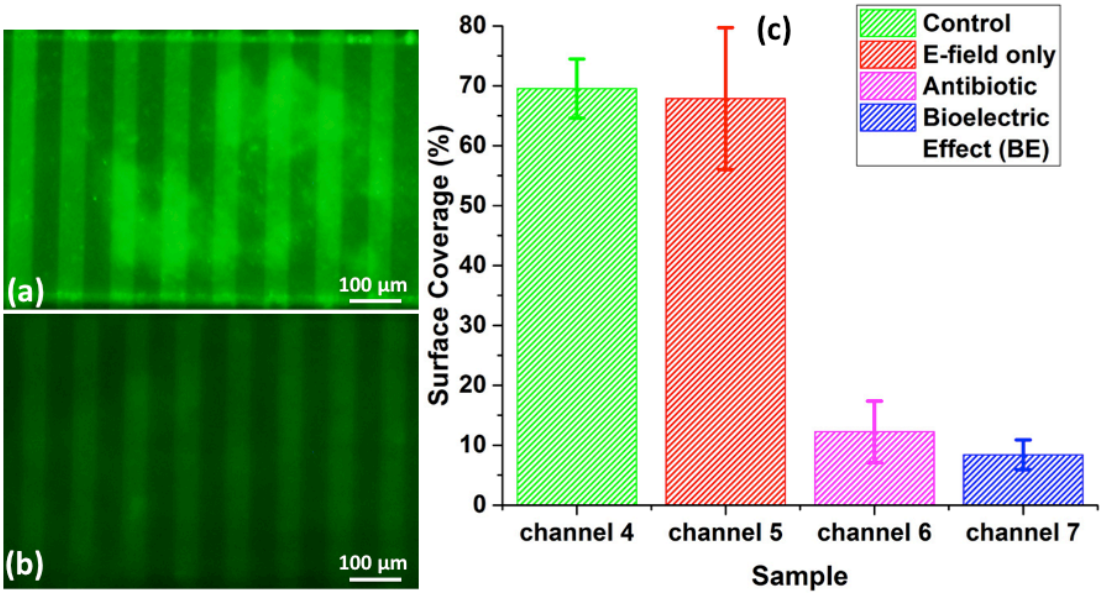

Figure 5-29 Representative micrographs of (a) untreated control, and (b) BE treated biofilm imaged after the 24-hour threshold-activated feedback treatment cycle (scale bars = 100 µm). (c) Average surface coverage as measured using ImageJ (N = 3 images). The background fluorescence exhibited by the gold IDE electrodes was subtracted during surface coverage analysis.

5.2.4 Discussion

In this section we presented a novel integrated impedance-based sensing and treatment microsystem that allowed for accurate real-time sensing and treatment of bacterial biofilms. Development of such an integrated system was not without its challenges, with the primary challenge encountered during the development of the MATLAB macro. The control macro was developed using a CHI proprietary closed-source library whose functions needed to be debugged to ensure accurate macro functionality. As the source code for the library was not openly available, efficient ways to circumvent the specific library function errors had to be implemented into the MATLAB macro using either other library functions that were experimentally determined as error-free or self-developed code. This was a time consuming process and so we envision that future designs of the microsystem will include a microprocessor coded with self-designed error-free functions to make the data acquisition control macro more efficient and if needed functionally more diverse.

Currently, the results discussed in this section successfully demonstrate that the microsystem can accurately measure the real-time change in impedance during the growth and removal of biofilms. Moreover, we showed that using a control module the sensor's IDEs can be used to perceptively apply the electrical signal necessary to initiate BE treatment. Such effective treatment, using low amplitude signals, highlights the efficiency of this microsystem to sense and treat *in situ* bacterial biofilms concurrently in time. Our results suggest that even the small periodic 5 mV AC signal used for probing the impedance between the IDEs results in enhanced treatment based on the principles of BE, leading to a two-level autonomy in

treatment. The second level of threshold-activated treatment using the MATLAB control macro can be used to help treat thicker and more mature biofilms that require much stronger BE treatment. This is a substantial advantage over our previous work with BE that applied a 500 mV electrical signal during the entire treatment period causing a long-term biocompatibility concern for medical devices as they on average require treatment over weeks. Thus, in contrast to former systems, this integration of sensing and BE treatment capabilities into purely the electrical domain provides an elegant microsystem solution for accurate threshold-activated sensing and treatment of biofilms.

5.3 Chapter Summary

A novel integration of sensing and treatment modules into an impedance-based microsystem was presented. The developed platform is the first impedimetric microsystem for real-time threshold-activated monitoring and treatment of bacterial biofilms in a microfluidic bifurcation device. It allows for accurate real-time sensing and treatment of bacterial biofilms within a single domain, thus facilitating a significant decrease in device footprint and reduction in additional bulky equipment. The IDE sensors were demonstrated to detect biofilm growth in real-time. Using the measured impedance change and user inputs, provided through a convenient and simple graphical interface, the MATLAB control module intelligently switched the system into treatment mode. Treatment was performed by applying a 100 mV signal, for only a small fraction of the total treatment period, across the same IDEs in combination with small doses of antibiotic. This microsystem provided a two-level

autonomy for treatment, by removing biofilms through periodic low energy BE treatment even while monitoring the biofilms through impedimetric measurements. Such application of BE, both during and in response to biofilm growth will ultimately enable effective rapid and autonomous *in situ* infection management, thus preventing post-surgery infections and significantly improving the quality of life for millions of patients.

Chapter 6. Conclusions

6.1 Summary

The use of high doses of antibiotics for treatment of chronic biofilm infections is resulting in the emergence of antibiotic-resistant bacterial strains, necessitating the development of new treatments that are not based on antibiotic therapies. In this work, a novel bacterial biofilm combination treatment independent of traditional antibiotics using only small molecule inhibitors of bacterial quorum sensing or AI-2 analogs with low electric fields was studied using both macro and micro-scale devices. Crystal violet staining of the macro-scale biofilms and confocal imaging of microfluidic biofilms showed a significant decrease in biomass compared to the untreated control. The enhanced treatment efficacy of this combination therapy was also demonstrated using a high-throughput bifurcation-based microfluidic biofilm analysis platform combined with different real-time transduction methods, like a linear array of charge-coupled device for monitoring change in OD. The combination treatment showed almost twice the treatment efficacy compared to antibiotic therapy alone indicating it might provide an effective alternative to traditional antibiotic therapies against bacterial biofilm infections. The use of this treatment method in both the medical and environmental fields would alleviate the need for high-dosage antibiotic therapies, thus greatly reducing the rise of antibiotic-resistant bacteria.

Secondly, this work tried to delve into the possible mechanism of action of the BE treatment. BE has been under investigation for about two decades, and researchers have shown the use of small doses of antibiotics with AC, DC and SP signals, however a true understanding of its mechanism of action is still unknown. This

dissertation tried to answer part of the complex mechanism by focusing on the energy of the electrical signal applied for potentials <1 V. We find that in this range of potentials, the type of signal does not affect the effectiveness of the treatment as once hypothesized, rather it is the total energy applied to the treatment, which could be through increased signal voltage or through extended durations of treatment time, that affects the BE treatment efficacy. We show that the success of this treatment, as measured using CFU count or biomass quantification, is linearly dependent on the energy applied, which will enable deterministic modification to the treatment. The results presented in this work, will allow for easier integration of the BE into microsystems developed for *in vivo* studies, as the dependence of BE on the energy will allow for efficient utilization of nearby electronics and to potentially transmit power wirelessly in the form of an AC signal. Consequently, true understanding of the mechanism of action of the BE will allow for more flexibility and ease of integration of the BE into various applications in both the clinical and environmental fields.

Another key goal of this work is the development of a new sensing and treatment technology designed to aid *in vitro* microfluidic biofilm investigations and perform threshold-activated sensing and treatment of *in situ* infections. While many different platforms and evaluation methods for the characterization, sensing and treatment of bacterial biofilms exist, they each come with their own set of advantages and disadvantages. The microsystem developed in this work combines the advantages of previous platforms while attempting to overcome some of their limitations.

The platform was designed to enable rapid, non-invasive, real-time biofilm monitoring and self-directed treatment. IDE impedance sensors such as previously used for macroscopic analysis of biofilms (in 96-well plates or CDC reactors), were integrated with a multi-experiment bifurcation-based microfluidic device that allowed precise control of the microenvironment within the channels. The microfluidic flow cell design addressed the high growth variation between biofilms grown in separate channels through spatially sectioning a single biofilm into separate channels using microfluidic flow bifurcation. This allowed for a more reliable comparison and evaluation of new biofilm treatments on a single device. Threshold-activated treatment, based on the principles of BE, was demonstrated using the microsystem, which will ultimately enable rapid and effective *in situ* biofilm management, preventing post-surgery infections or environmental contamination leading to significantly improved quality of life for millions.

6.2 Future Work

The research conducted as part of this dissertation raises additional questions that require further investigation. These questions fall into one of three categories – 1. technological improvements that will enhance the functionality, sensitivity or accuracy of the developed platform; 2. optimization-oriented, to develop better methods of biofilm prevention or treatment by perform optimizations of current methods; or 3. application-driven, advancing this technology into real-life clinical settings.

For the developed μTAS platform, an immediate technological advancement would be the integration with bio-recognition elements like antibodies, for target specific recognition of different pathogenic biofilm forming bacteria. Such integration will provide real-time sensing of specific pathogenic bacteria of interest in a multi-species environment.

One of the major challenges with using IDEs is the interplay between the sensitivity of the system and the dynamic range of operation. Increasing one would require compromising on the other. One potential method to optimize for this is by using graded IDEs, *i.e.* IDEs with continuously varying widths and spacings. These can be tested and optimized for sensitivity, while extending the linear range of operation of the device. Detailed impedance information obtained through such an optimized system would provide information on the long-term dynamic growth behavior of mature biofilms.

The combination treatment tested in this work used one concentration of the AI-2 analog with a fixed strength of electric field. Optimization of the analog concentration and the field strength would reduce any adverse side effects that this treatment may induce. Such optimizations also assure that the best result is obtained while minimizing usage of resources like power. Moreover, this treatment needs to be tested on co-cultured bacterial and mammalian cells. To date, no detailed studies on the adverse side effects of AI-2 analogs on mammalian cells have been shown. For this system to be applicable in a clinical setting, such toxicity studies need to be performed for the safe use of the treatment.

This system also needs to be verified for different Gram positive and Gram negative bacteria and their corresponding AI-2 analogs, for efficacy and for optimized parameters. Specifically, experiments need to be conducted with clinically relevant bacterial strains and studies demonstrating the use of this treatment to prevent the formation and growth of these biofilms using the developed lab-on-a-chip platform need to be performed. Such studies will not only provide insight into new strategies for biofilm prevention but also expand our understanding of the biofilm formation process of different bacteria while still under treatment.

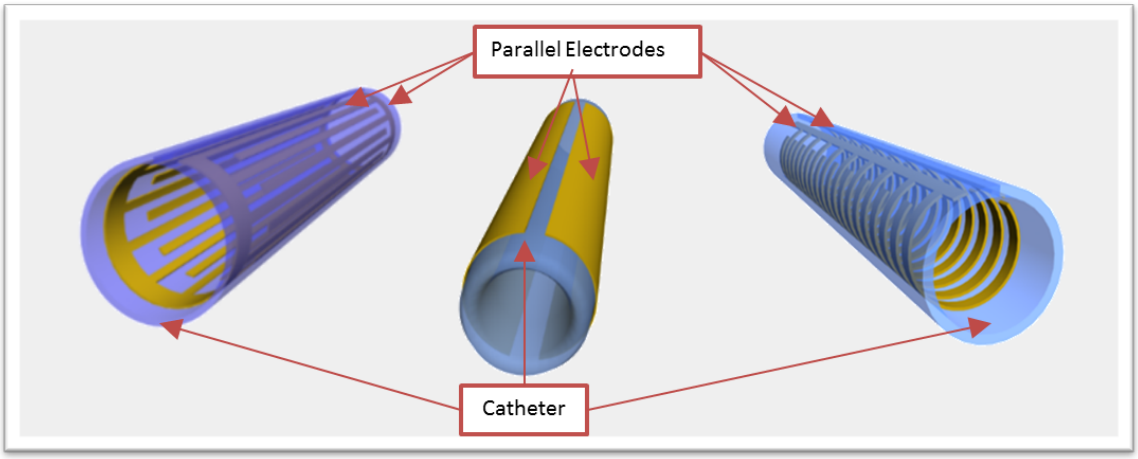

Figure 6-1 Schematic of possible future designs for flexible sensor -treatment devices that can be used in a catheter.

The work presented in this dissertation was carried out with the long-term end-goal of miniaturization for application in a clinical setting in mind. The developed system can be easily modified and fabricated on a flexible substrate for sensing and treatment of biofilms *in situ*, for example in catheters and stents as shown in Figure 6-1. Such a flexible system would also need to be tested and characterized for

sensitivity and other critical parameters. Additionally, multiple bacterial strains and bacteria-mammalian cell co-cultures would need to be tested.

Finally, to make the system fully autonomous, it is necessary to integrate this system with self-powering abilities. Wireless power transfer through inductive coupling with high efficiency rates has already been achieved. Also, easy packaging methodology into medical devices needs to be developed. Such a system level integration of the developed microsystem will enable true testing in *in vivo* models and validate the efficacy of this system and the developed treatment.

6.3 Conclusion

The rise in super-bugs and antibiotic-resistant infections due to biofilms over the last few years has created a global health challenge. This has necessitated the need for efficient tools and methods to characterize and evaluate these organisms, as well as for trying to develop sensitive methods to detect these infections *in situ* and for conceiving new antibiotic-free therapies. This dissertation addresses these needs through the development of a sensing and treatment microsystem that can be used either in conjunction with the bifurcation microfluidics as a cheap, high-throughput platform for *in vitro* evaluation of biofilm growth and new treatment testing, or as a sensitive threshold-activated sensor-treatment solution for *in situ* biofilm infection management. Additionally, the initial results presented on the novel combination treatment show promise for it to be used as an antibiotic-free method for effective biofilm treatment. Lastly, we believe that insight gained into the mechanism of action of the BE will serve as the foundation for to further comprehend the complex nature

of this organism and its treatment, and in so doing pave the way for the development of new techniques to target these persistent biofilm infections.

Appendices

Appendix A: Masks Used

Mask #1: Bifurcation Device

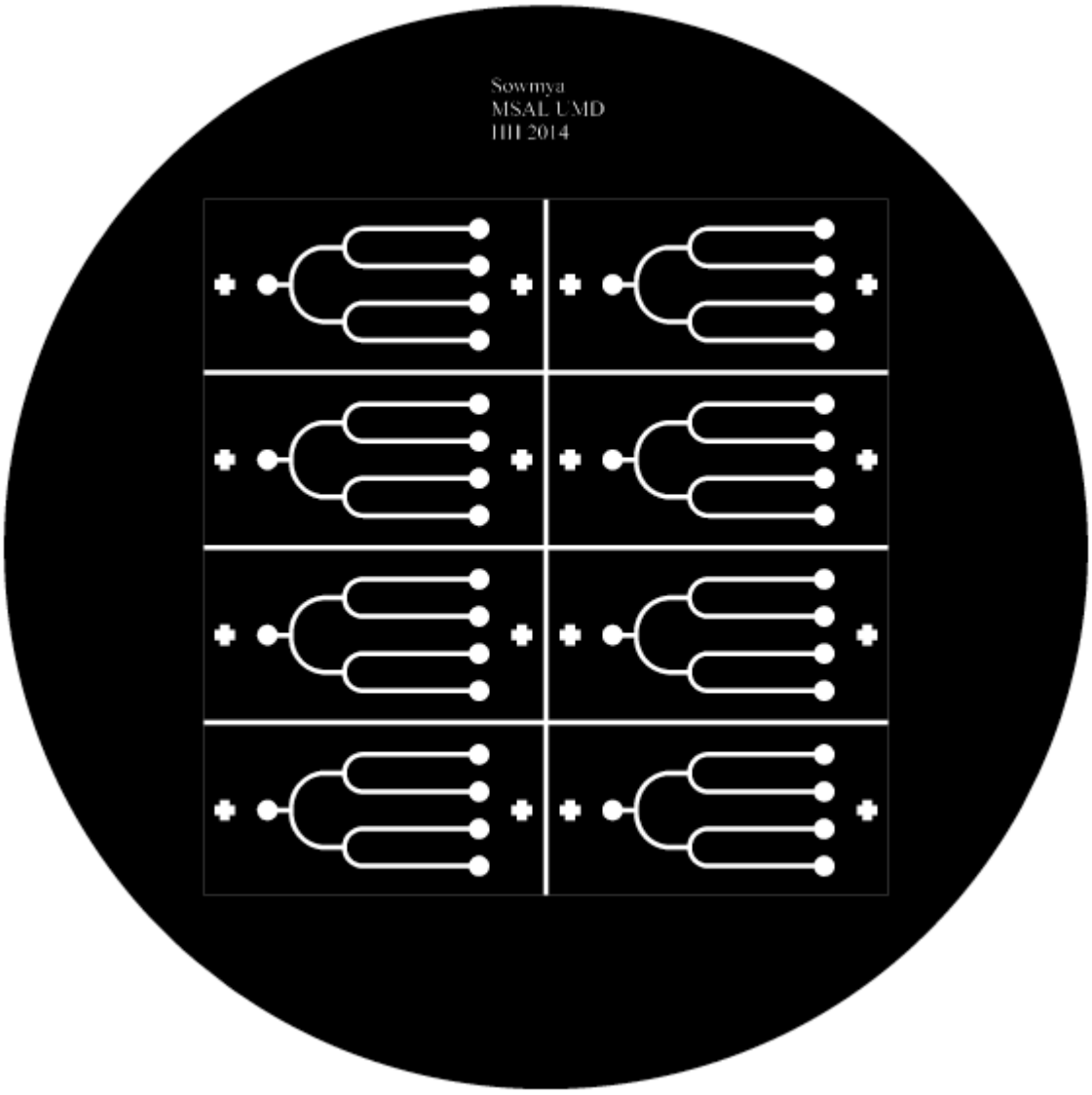

Mask #2: Modified Bifurcation Device for Integration with Micro-BOAT Setup

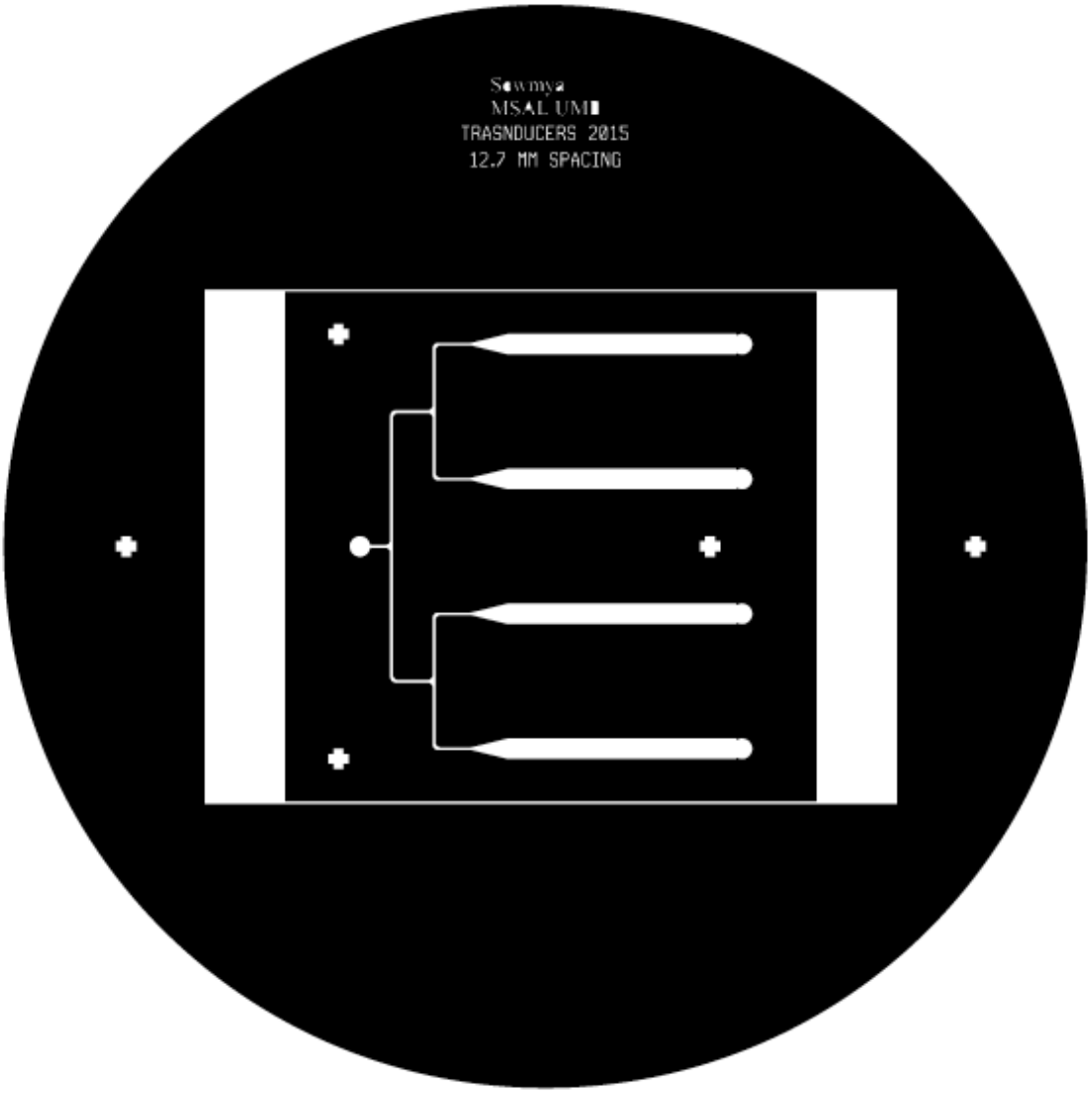

Mask #3: Co-planar Electrodes for Bifurcation Device

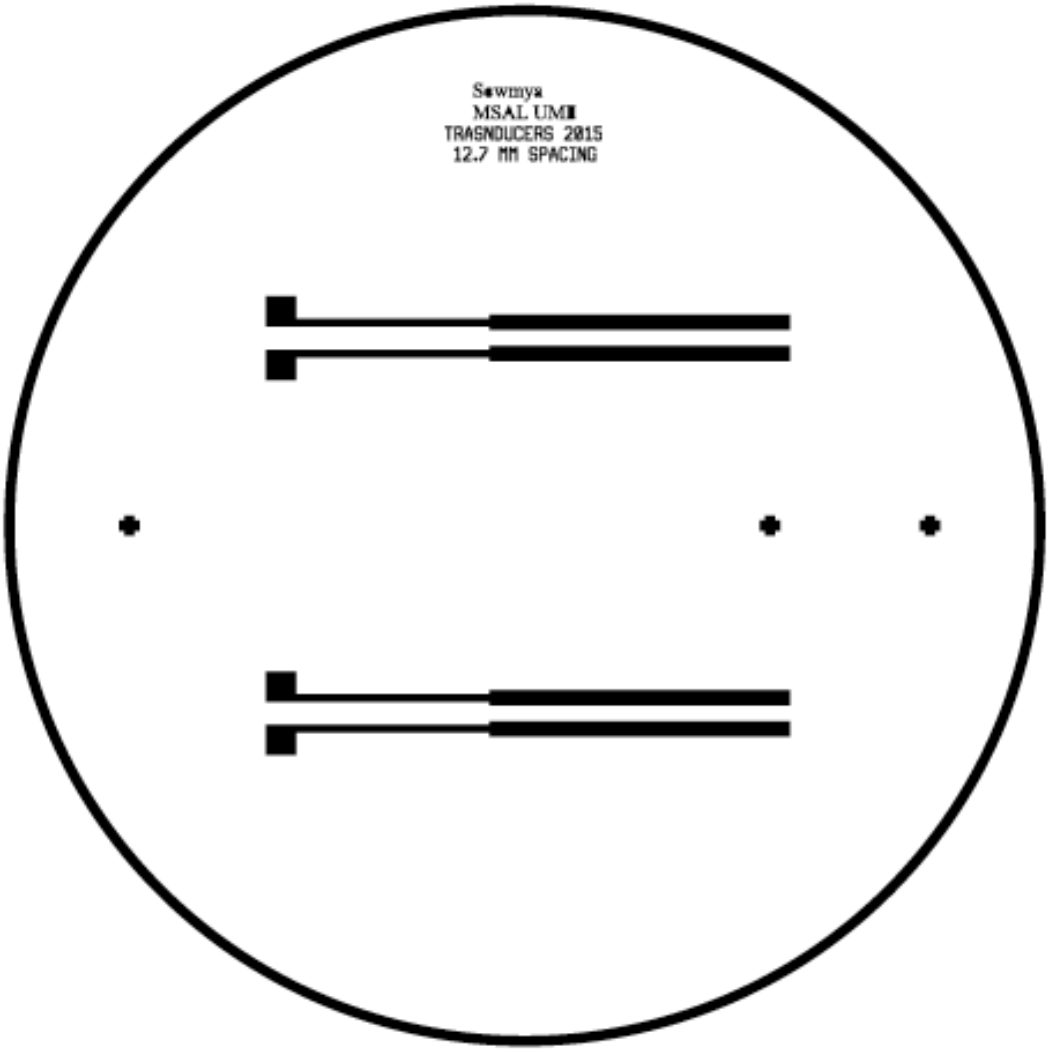

Mask #4: IDE Sensors for Single Channel Microfluidics

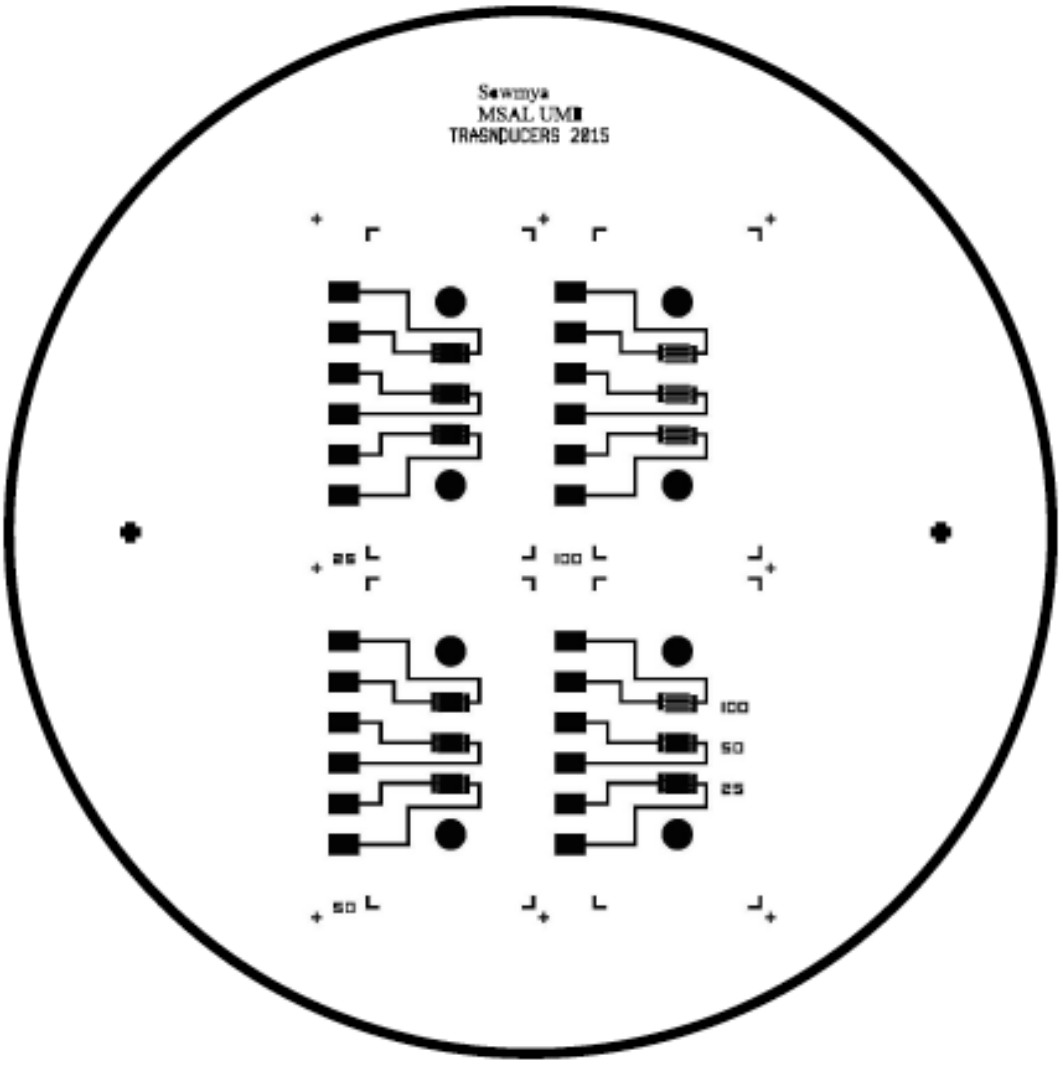

Mask #5: IDE Sensors for Bifurcation Device

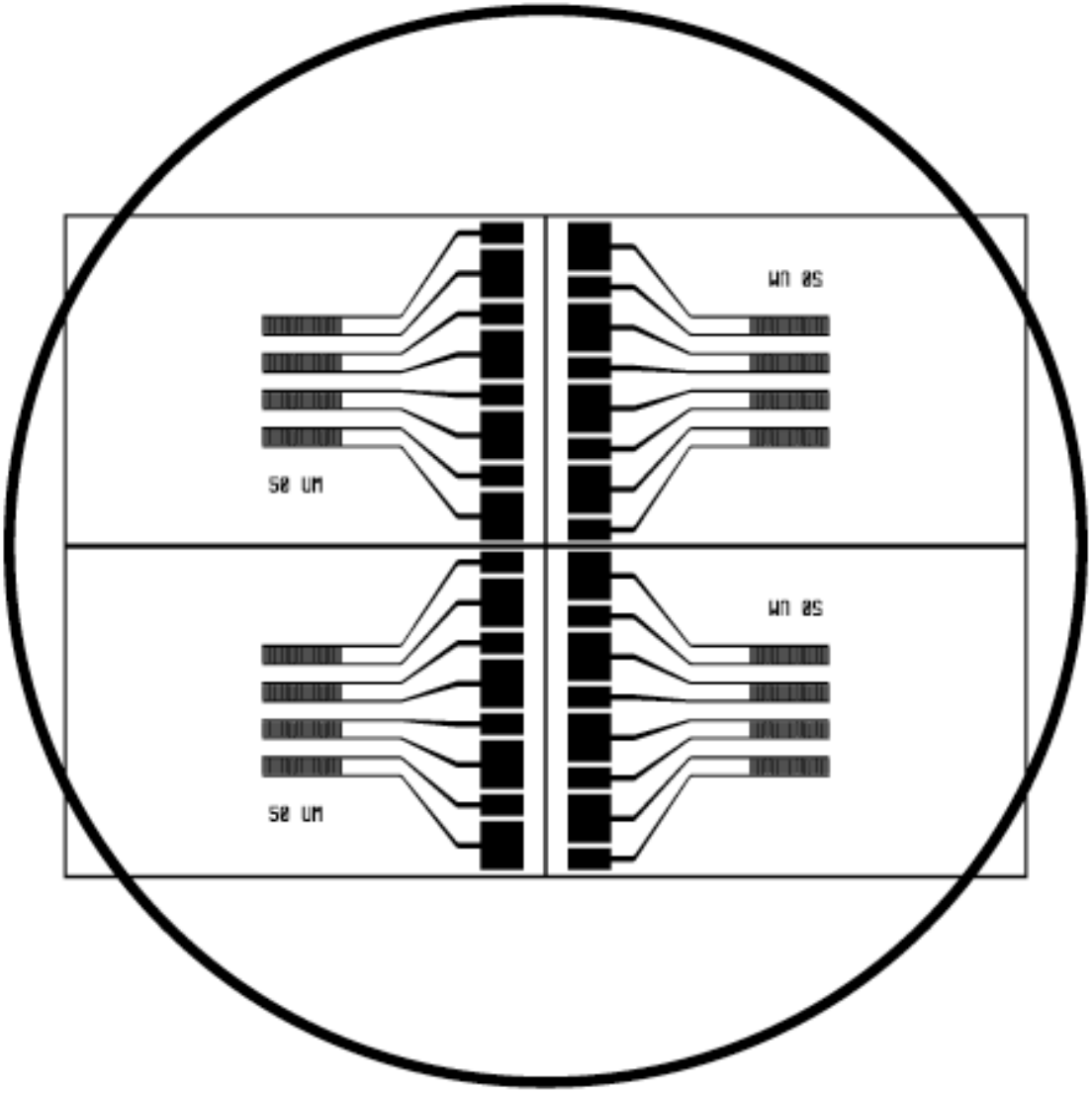

Appendix B: Mathematica Code

```
Epsmat ∈ Reals;
sigmat ∈ Reals;
ω ∈ Reals;
Epscell ∈ Reals;
sigcell ∈ Reals;
phi ∈ Reals;
EpsMat = Epsmat + I * sigmat / ω;
EpsCell = Epscell + I * sigcell / ω;
fCM = (EpsCell - EpsMat) / (EpsCell + 2 * EpsMat);
EpsBiofilm = EpsMat * (1 + 2 * phi * fCM) / (1 - phi * fCM);
Epsbiofilm = FullSimplify[ComplexExpand[Re[EpsBiofilm]]]
sigbiofilm = FullSimplify[ComplexExpand[Im[EpsBiofilm]]] * ω
```

```
(9 Epscell phi sigmat^2 - 2 Epsmat^3 (-2 + phi + phi^2) ω^2 +
    Epscell Epsmat^2 (4 + phi + 4 phi^2) ω^2 -
    Epsmat (-1 + phi) ((1 + 2 phi) sigcell^2 - 4 (-1 + phi) sigcell sigmat +
       2 (2 + phi) sigmat^2 + Epscell^2 (1 + 2 phi) ω^2)) /
  (((-1 + phi) sigcell - (2 + phi) sigmat)^2 +
    (Epscell - Epscell phi + Epsmat (2 + phi))^2 ω^2)
```

```
(ω (-sigmat (sigcell + 2 phi sigcell - 2 (-1 + phi) sigmat)
       ((-1 + phi) sigcell - (2 + phi) sigmat) +
      (9 Epsmat^2 phi sigcell - (-1 + phi)
          ((Epscell + 2 Epsmat)^2 + 2 (Epscell - Epsmat)^2 phi) sigmat) ω^2)) /
  ((sigcell - phi sigcell + (2 + phi) sigmat)^2 ω +
    (Epscell - Epscell phi + Epsmat (2 + phi))^2 ω^3)
```

Appendix C: MATLAB Code

CH Instruments Data Analysis

PBS Pre-Conditioning

```
% THIS CODE IS FOR PBS CONTROL SAMPLES ONLY

% Set MATLAB work path to folder with CHI data files

%Manually enter values of N, start and end time and date, change the
names
%of filename and filename2 to files to be analysed
filepath = '\'; % Enter your data folder path
filepath_temp = 'Z:\MSAL User\Sowmya\Biofilm impedance sensing\CHI
Data\Temp\'; %Enter filepath for temp files

startPBS = 1; % start file number of PBS
endPBS = 165; % end file number of PBS

start_date = 5; %enter start date
start_hour = 10; % enter starting hour in 24 hour format
start_min = 36; % enter starting minute

end_date = 6; %enter end date
end_hour = 6; % enter end hour in 24-hour format
end_min = 38; % enter end minute

N= endPBS-startPBS+1; % N= number of txt files/runs of the CHI
M = 60; % M = number of numeric lines in each CHI output text file

Total_time =  (end_date - start_date) * 24 * 60 * 60 + (end_hour -
start_hour)* 60 * 60 + (end_min - start_min) * 60 ; % Calculate
total time in seconds

Time_step = Total_time/(N-1); % average step time in seconds between
two consecutive runs

Time_s = 0: Time_step: Total_time; % create an array called time
Time_h = Time_s/(60*60); % row array of time in hours
Final_time = Time_h'; % column array of time in hours

Final_data = zeros(M,5*N); %size of final data array
Final_realZ = zeros(M,N); %size of final real Z data array
Final_imZ = zeros(M,N); %size of final im Z data array
Final_absZ = zeros(M,N); %size of final abs Z data array
Final_phase = zeros(M,N); %size of final phase of Z data array

j= 1; % counter
column = 1; % counter for column of final arrays
for i = startPBS:endPBS
```

```
    filename = [filepath 'imp-PBS' num2str(i) '.txt']; %give path to
files you want to analyse
    fid = fopen(filename, 'r') ;     % Open source file.
    fgetl(fid) ;                     % Read/discard line.
    fgetl(fid) ;                     % Read/discard line.
    fgetl(fid) ;                     % Read/discard line.
    fgetl(fid) ;                     % Read/discard line.
    fgetl(fid) ;                     % Read/discard line.
    fgetl(fid) ;                     % Read/discard line.
    fgetl(fid) ;                     % Read/discard line.
    fgetl(fid) ;                     % Read/discard line.
    fgetl(fid) ;                     % Read/discard line.
    fgetl(fid) ;                     % Read/discard line.
    fgetl(fid) ;                     % Read/discard line.
    fgetl(fid) ;                     % Read/discard line.
    fgetl(fid) ;                     % Read/discard line.
    fgetl(fid) ;                     % Read/discard line.
    fgetl(fid) ;                     % Read/discard line.
    fgetl(fid) ;                     % Read/discard line.
    fgetl(fid) ;                     % Read/discard line.
    fgetl(fid) ;                     % Read/discard line.
    buffer = fread(fid, Inf) ;       % Read rest of the file.
    fclose(fid);

    filename2 = [filepath_temp 'imp-PBS' num2str(i) '_TRUNC.txt'];
    fid = fopen(filename2, 'w')  ;   % Open destination file.
    fwrite(fid, buffer) ;            % Save to file without header.
    fclose(fid) ;

    %copy each file content into a temporary array named Temp
    fileID = fopen (filename2, 'r');
    formatSpec = '%f, %f, %f, %f, %f';
    sizeTemp = [5 M];
    Temp = fscanf(fileID, formatSpec, sizeTemp);
    fclose(fileID);
    Transpose_Temp = Temp';

    % Array frequency contains a column array of the frequencies at
which measurements were obtained
    for x=1:M
        Frequency(x,1) = Transpose_Temp(x,1);
        x=x+1;
    end

    %append contents of the array Temp to the final data arrays
    for x=1:M
        shift_y=j;
        for y=1:5
        Final_data(x,shift_y) = Transpose_Temp(x,y);
        y=y+1;
        shift_y=shift_y+1;
        end
    end
    j = j+5; % increment counter by 5 columns

    % Write into individual arrays
    for a=1:M
```

```
        Final_realZ(a,column)= Transpose_Temp(a,2);
        Final_imZ(a,column)= Transpose_Temp(a,3);
        Final_absZ(a,column)= Transpose_Temp(a,4);
        Final_phase(a,column) = Transpose_Temp(a,5);
        a=a+1;
    end
      column = column+1;
end

% plot figures

% Real of Z versus frequency on a log log scale
figure
loglog(Frequency,Final_realZ(:,startPBS), 'r', 'LineWidth', 2.0)
hold on
loglog(Frequency,Final_realZ(:,25),'b', 'LineWidth', 2.0)
hold on
loglog(Frequency,Final_realZ(:,50),'g', 'LineWidth', 2.0)
hold on
loglog(Frequency,Final_realZ(:,75),'k', 'LineWidth', 2.0)
hold on
loglog(Frequency,Final_realZ(:,100),'c', 'LineWidth', 2.0)
hold on
% loglog(Frequency,Final_realZ(:,125),'r--', 'LineWidth', 2.0)
% hold on
% loglog(Frequency,Final_realZ(:,150),'b--', 'LineWidth', 2.0)
% hold on
% loglog(Frequency,Final_realZ(:,175),'g--', 'LineWidth', 2.0)
% hold on
loglog(Frequency,Final_realZ(:,N),'k--', 'LineWidth', 2.0)
title('Re Z v. frequency', 'FontSize',20,'FontWeight','bold')
xlabel('frequency (Hz)', 'FontSize',20,'FontWeight','bold')
ylabel('Re Z (ohms)', 'FontSize',20,'FontWeight','bold')
set(gca,'fontsize',16,'FontWeight','bold')
print -dpng -r300 ReZ_vs_Freq
hold off

% Im of Z versus frequency on a log log scale
figure
loglog(Frequency,Final_imZ(:,1), 'r','LineWidth', 2.0)
hold on
loglog(Frequency,Final_imZ(:,25),'b','LineWidth', 2.0)
hold on
loglog(Frequency,Final_imZ(:,50),'g','LineWidth', 2.0)
hold on
loglog(Frequency,Final_imZ(:,75),'k','LineWidth', 2.0)
hold on
loglog(Frequency,Final_imZ(:,100),'c','LineWidth', 2.0)
hold on
% loglog(Frequency,Final_imZ(:,125),'r--','LineWidth', 2.0)
% hold on
% loglog(Frequency,Final_imZ(:,150),'b--','LineWidth', 2.0)
% hold on
% loglog(Frequency,Final_imZ(:,175),'g--','LineWidth', 2.0)
% hold on
loglog(Frequency,Final_imZ(:,N),'k--','LineWidth', 2.0)
```

```
title('Im Z v. frequency', 'FontSize',20,'FontWeight','bold')
xlabel('frequency (Hz)', 'FontSize',20,'FontWeight','bold')
ylabel('Im Z (ohms)', 'FontSize',20,'FontWeight','bold')
set(gca,'fontsize',16,'FontWeight','bold')
print -dpng -r300 ImZ_vs_Freq
hold off

% Abs Z versus frequency on a log log scale
figure
loglog(Frequency,Final_absZ(:,1), 'r','LineWidth', 2.0)
hold on
loglog(Frequency,Final_absZ(:,25),'b','LineWidth', 2.0)
hold on
loglog(Frequency,Final_absZ(:,50),'g','LineWidth', 2.0)
hold on
loglog(Frequency,Final_absZ(:,75),'k','LineWidth', 2.0)
hold on
loglog(Frequency,Final_absZ(:,100),'c','LineWidth', 2.0)
hold on
% loglog(Frequency,Final_absZ(:,125),'r--','LineWidth', 2.0)
% hold on
% loglog(Frequency,Final_absZ(:,150),'b--','LineWidth', 2.0)
% hold on
% loglog(Frequency,Final_absZ(:,175),'g--','LineWidth', 2.0)
% hold on
loglog(Frequency,Final_absZ(:,N),'k--','LineWidth', 2.0)
title('|Z| v. frequency', 'FontSize',20,'FontWeight','bold')
xlabel('frequency (Hz)', 'FontSize',20,'FontWeight','bold')
ylabel('|Z| (ohms)', 'FontSize',20,'FontWeight','bold')
set(gca,'fontsize',16,'FontWeight','bold')
print -dpng -r300 AbsZ_vs_Freq
hold off

% Phase versus frequency on a log log scale
figure
loglog(Frequency,Final_phase(:,1), 'r','LineWidth', 2.0)
hold on
loglog(Frequency,Final_phase(:,25),'b','LineWidth', 2.0)
hold on
loglog(Frequency,Final_phase(:,50),'g','LineWidth', 2.0)
hold on
loglog(Frequency,Final_phase(:,75),'k','LineWidth', 2.0)
hold on
loglog(Frequency,Final_phase(:,100),'c','LineWidth', 2.0)
hold on
% loglog(Frequency,Final_phase(:,125),'r--','LineWidth', 2.0)
% hold on
% loglog(Frequency,Final_phase(:,150),'b--','LineWidth', 2.0)
% hold on
% loglog(Frequency,Final_phase(:,175),'g--','LineWidth', 2.0)
% hold on
loglog(Frequency,Final_phase(:,N),'k--','LineWidth', 2.0)
title('Phase of |Z| v. frequency',
'FontSize',20,'FontWeight','bold')
xlabel('frequency (Hz)', 'FontSize',20,'FontWeight','bold')
ylabel('Phase', 'FontSize',20,'FontWeight','bold')
```

```
set(gca,'fontsize',16,'FontWeight','bold')
print -dpng -r300 Phase_vs_Freq
hold off

% Real of Z versus time
figure
plot(Time_h,Final_realZ(1,:), 'r','LineWidth', 2.0)
hold on
plot(Time_h,Final_realZ(12,:),'b','LineWidth', 2.0)
hold on
plot(Time_h,Final_realZ(24,:),'g','LineWidth', 2.0)
hold on
plot(Time_h,Final_realZ(36,:),'k','LineWidth', 2.0)
hold on
plot(Time_h,Final_realZ(48,:),'c','LineWidth', 2.0)
hold on
plot(Time_h,Final_realZ(60,:),'r--','LineWidth', 2.0)
title('Re Z v. time(hrs)', 'FontSize',20,'FontWeight','bold')
xlabel('time (hrs)', 'FontSize',20,'FontWeight','bold')
ylabel('Re Z (ohms)', 'FontSize',20,'FontWeight','bold')
legend('825 kHz', '100 kHz', '10 kHz', '1 kHz', '100 Hz', '10 Hz')
set(gca,'fontsize',16,'FontWeight','bold')
print -dpng -r300 ReZ_vs_Time
hold off

% Im of Z versus time(hrs)
figure
plot(Time_h,Final_imZ(1,:), 'r','LineWidth', 2.0)
hold on
plot(Time_h,Final_imZ(12,:),'b','LineWidth', 2.0)
hold on
plot(Time_h,Final_imZ(24,:),'g','LineWidth', 2.0)
hold on
plot(Time_h,Final_imZ(36,:),'k','LineWidth', 2.0)
hold on
plot(Time_h,Final_imZ(48,:),'c','LineWidth', 2.0)
hold on
plot(Time_h,Final_imZ(60,:),'r--','LineWidth', 2.0)
title('Im Z v. time(hrs)', 'FontSize',20,'FontWeight','bold')
xlabel('time(hrs)', 'FontSize',20,'FontWeight','bold')
ylabel('Im Z (ohms)', 'FontSize',20,'FontWeight','bold')
legend('825 kHz', '100 kHz', '10 kHz', '1 kHz', '100 Hz', '10 Hz')
set(gca,'fontsize',16,'FontWeight','bold')
print -dpng -r300 ImZ_vs_Time
hold off

% Abs Z versus time(hrs)
figure
plot(Time_h,Final_absZ(1,:), 'r','LineWidth', 2.0)
hold on
plot(Time_h,Final_absZ(12,:),'b','LineWidth', 2.0)
hold on
plot(Time_h,Final_absZ(24,:),'g','LineWidth', 2.0)
hold on
plot(Time_h,Final_absZ(36,:),'k','LineWidth', 2.0)
hold on
```

```
plot(Time_h,Final_absZ(48,:),'c','LineWidth', 2.0)
hold on
plot(Time_h,Final_absZ(60,:),'r--','LineWidth', 2.0)
title('|Z| v. time(hrs)', 'FontSize',20,'FontWeight','bold')
xlabel('time(hrs)', 'FontSize',20,'FontWeight','bold')
ylabel('|Z| (ohms)', 'FontSize',20,'FontWeight','bold')
legend('825 kHz', '100 kHz', '10 kHz', '1 kHz', '100 Hz', '10 Hz')
set(gca,'fontsize',16,'FontWeight','bold')
print -dpng -r300 AbsZ_vs_Time
hold off

% Phase versus time(hrs)
figure
plot(Time_h,Final_phase(1,:), 'r','LineWidth', 2.0)
hold on
plot(Time_h,Final_phase(12,:),'b','LineWidth', 2.0)
hold on
plot(Time_h,Final_phase(24,:),'g','LineWidth', 2.0)
hold on
plot(Time_h,Final_phase(36,:),'k','LineWidth', 2.0)
hold on
plot(Time_h,Final_phase(48,:),'c','LineWidth', 2.0)
hold on
plot(Time_h,Final_phase(60,:),'r--','LineWidth', 2.0)
title('Phase v. time(hrs)', 'FontSize',20,'FontWeight','bold')
xlabel('time(hrs)', 'FontSize',20,'FontWeight','bold')
ylabel('Phase', 'FontSize',20,'FontWeight','bold')
legend('825 kHz', '100 kHz', '10 kHz', '1 kHz', '100 Hz', '10 Hz')
set(gca,'fontsize',16,'FontWeight','bold')
print -dpng -r300 Phase_vs_Time
hold off

% Abs Z versus time(hrs) Only 100 kHz
figure
plot(Time_h,Final_absZ(12,:),'b','LineWidth', 2.0)
%hold on
%plot(Time_h,Final_absZ(24,:),'g')
title('|Z| v. time(hrs)', 'FontSize',20,'FontWeight','bold')
xlabel('time(hrs)', 'FontSize',20,'FontWeight','bold')
ylabel('|Z| (ohms)', 'FontSize',20,'FontWeight','bold')
legend( '100 kHz')
set(gca,'fontsize',16,'FontWeight','bold')
print -dpng -r300 AbsZ_100KHz_vs_Time
hold off

% Phase versus time(hrs) Only 100 kHz
figure
plot(Time_h,Final_phase(12,:),'b','LineWidth', 2.0)
%hold on
%plot(Time_h,Final_phase(24,:),'g')
title('Phase v. time(hrs)', 'FontSize',20,'FontWeight','bold')
xlabel('time(hrs)', 'FontSize',20,'FontWeight','bold')
ylabel('Phase', 'FontSize',20,'FontWeight','bold')
legend( '100 kHz')
set(gca,'fontsize',16,'FontWeight','bold')
print -dpng -r300 Phase_100KHz_vs_Time
```

```
hold off

% Change in Z with respect to baseline obtained using PBS

baseline_absZ_PBS = mean(Final_absZ, 2); %  average baseline PBS
absZ value for each frequency
baseline_imZ_PBS = mean(Final_imZ,2); %  average baseline PBS imZ
value for each frequency
baseline_realZ_PBS = mean(Final_realZ,2); %  average baseline PBS
realZ value for each frequency
baseline_phase_PBS = mean(Final_phase,2); %  average baseline PBS
phase value for each frequency


for i =1:N
    delta_absZ(:,i) = (Final_absZ(:,i) -
baseline_absZ_PBS)./baseline_absZ_PBS ;
    delta_imZ(:,i) = (Final_imZ(:,i) -
baseline_imZ_PBS)./baseline_imZ_PBS ;
    delta_realZ(:,i) = (Final_realZ(:,i) -
baseline_realZ_PBS)./baseline_realZ_PBS ;
    delta_phase(:,i) = (Final_phase(:,i) -
baseline_phase_PBS)./baseline_phase_PBS ;
    i=i+1;
end

figure
plot(Time_h,delta_realZ) % plot the change in realZ with respect to
time
title ('Change in ReZ with time','FontSize',20,'FontWeight','bold');
xlabel ('Time (hrs)', 'FontSize',20,'FontWeight','bold');
ylabel ('(ReZ-ReZ_{PBS Baseline}) / ReZ_{PBS Baseline}',
'FontSize',20,'FontWeight','bold')
set(gca,'fontsize',16,'FontWeight','bold')
print -dpng -r300 Change_ReZ_vs_Time
hold off

figure
plot(Time_h,delta_realZ(1,:), 'r', 'linewidth', 2.0)
hold on
plot(Time_h,delta_realZ(12,:),'b', 'linewidth', 2.0)
hold on
plot(Time_h,delta_realZ(24,:),'g', 'linewidth', 2.0)
hold on
plot(Time_h,delta_realZ(36,:),'k', 'linewidth', 2.0)
hold on
plot(Time_h,delta_realZ(48,:),'c', 'linewidth', 2.0)
hold on
plot(Time_h,delta_realZ(60,:),'m', 'linewidth', 2.0)
title ('Change in ReZ with time',
'FontSize',20,'FontWeight','bold');
xlabel ('Time (hrs)', 'FontSize',20,'FontWeight','bold');
ylabel ('(ReZ-ReZ_{PBS Baseline}) / ReZ_{PBS Baseline}',
'FontSize',20,'FontWeight','bold');
legend('825 kHz', '100 kHz', '10 kHz', '1 kHz', '100 Hz', '10 Hz');
set(gca,'fontsize',16,'FontWeight','bold')
```

```
print -dpng -r300 Change_ReZ_vs_Time_2
hold off

figure
plot(Time_h,delta_imZ) % plot the change in imZ with respect to
title ('Change in ImZ with time',
'FontSize',20,'FontWeight','bold');
xlabel ('Time (hrs)', 'FontSize',20,'FontWeight','bold');
ylabel ('(ImZ-ImZ_{PBS Baseline}) / ImZ_{PBS Baseline}',
'FontSize',20,'FontWeight','bold');
set(gca,'fontsize',16,'FontWeight','bold')
print -dpng -r300 Change_ImZ_vs_Time
hold off

figure
plot(Time_h,delta_imZ(1,:), 'r', 'linewidth', 2.0)
hold on
plot(Time_h,delta_imZ(12,:),'b', 'linewidth', 2.0)
hold on
plot(Time_h,delta_imZ(24,:),'g', 'linewidth', 2.0)
hold on
plot(Time_h,delta_imZ(36,:),'k', 'linewidth', 2.0)
hold on
plot(Time_h,delta_imZ(48,:),'c', 'linewidth', 2.0)
hold on
plot(Time_h,delta_imZ(60,:),'m', 'linewidth', 2.0)
title ('Change in ImZ with time',
'FontSize',20,'FontWeight','bold');
xlabel ('Time (hrs)', 'FontSize',20,'FontWeight','bold');
ylabel ('(ImZ-ImZ_{PBS Baseline}) / ImZ_{PBS Baseline}',
'FontSize',20,'FontWeight','bold');
legend('825 kHz', '100 kHz', '10 kHz', '1 kHz', '100 Hz', '10 Hz');
set(gca,'fontsize',16,'FontWeight','bold')
print -dpng -r300 Change_ImZ_vs_Time_2
hold off


figure
plot(Time_h,delta_absZ) % plot the change in absZ with respect to
title ('Change in |Z| with time',
'FontSize',20,'FontWeight','bold');
xlabel ('Time (hrs)', 'FontSize',20,'FontWeight','bold');
ylabel ('(|Z|-|Z|_{PBS Baseline}) / |Z|_{PBS Baseline}',
'FontSize',20,'FontWeight','bold');
set(gca,'fontsize',16,'FontWeight','bold')
print -dpng -r300 Change_absZ_vs_Time
hold off

figure
plot(Time_h,delta_absZ(1,:), 'r', 'linewidth', 2.0)
hold on
plot(Time_h,delta_absZ(12,:),'b', 'linewidth', 2.0)
hold on
plot(Time_h,delta_absZ(24,:),'g', 'linewidth', 2.0)
hold on
plot(Time_h,delta_absZ(36,:),'k', 'linewidth', 2.0)
```

```
hold on
plot(Time_h,delta_absZ(48,:),'c', 'linewidth', 2.0)
hold on
plot(Time_h,delta_absZ(60,:),'m', 'linewidth', 2.0)
title ('Change in |Z| with time',
'FontSize',20,'FontWeight','bold');
xlabel ('Time (hrs)', 'FontSize',20,'FontWeight','bold');
ylabel ('(|Z|-|Z|_{PBS Baseline}) / |Z|_{PBS Baseline}',
'FontSize',20,'FontWeight','bold');
legend('825 kHz', '100 kHz', '10 kHz', '1 kHz', '100 Hz', '10 Hz');
set(gca,'fontsize',16,'FontWeight','bold')
print -dpng -r300 Change_absZ_vs_Time_2
hold off

figure
plot(Time_h,delta_phase) % plot the change in absZ with respect to
title ('Change in phase with time',
'FontSize',20,'FontWeight','bold');
xlabel ('Time (hrs)', 'FontSize',20,'FontWeight','bold');
ylabel ('(Phase-Phase_{PBS Baseline}) / Phase_{PBS Baseline}',
'FontSize',20,'FontWeight','bold');
set(gca,'fontsize',16,'FontWeight','bold')
print -dpng -r300 Change_phase_vs_Time
hold off

figure
plot(Time_h,delta_phase(1,:), 'r', 'linewidth', 2.0)
hold on
plot(Time_h,delta_phase(12,:),'b', 'linewidth', 2.0)
hold on
plot(Time_h,delta_phase(24,:),'g', 'linewidth', 2.0)
hold on
plot(Time_h,delta_phase(36,:),'k', 'linewidth', 2.0)
hold on
plot(Time_h,delta_phase(48,:),'c', 'linewidth', 2.0)
hold on
plot(Time_h,delta_phase(60,:),'m', 'linewidth', 2.0)
title ('Change in phase with time',
'FontSize',20,'FontWeight','bold');
xlabel ('Time (hrs)', 'FontSize',20,'FontWeight','bold');
ylabel ('(phase-phase_{PBS Baseline}) / phase_{PBS Baseline}',
'FontSize',20,'FontWeight','bold');
legend('825 kHz', '100 kHz', '10 kHz', '1 kHz', '100 Hz', '10 Hz');
set(gca,'fontsize',16,'FontWeight','bold')
print -dpng -r300 Change_phase_vs_Time_2
hold off

%Plotting phase, real, imaginary and absolute relative change in Z
for 100Hz
figure
plot(Time_h,delta_phase(48,:),'c', 'linewidth', 2.0)
title ('Change in Phase with time',
'FontSize',20,'FontWeight','bold');
xlabel ('Time (hrs)', 'FontSize',20,'FontWeight','bold');
ylabel ('(Phase-Phase_{PBS Baseline}) / Phase_{PBS Baseline}',
'FontSize',20,'FontWeight','bold');
```

```
legend( '100 Hz');
set(gca,'fontsize',16,'FontWeight','bold')
print -dpng -r300 Change_Phase_100Hz_vs_Time
hold off

figure
plot(Time_h,delta_realZ(48,:),'c', 'linewidth', 2.0)
title ('Change in ReZ with time',
'FontSize',20,'FontWeight','bold');
xlabel ('Time (hrs)', 'FontSize',20,'FontWeight','bold');
ylabel ('(ReZ-ReZ_{PBS Baseline}) / ReZ_{PBS Baseline}',
'FontSize',20,'FontWeight','bold');
legend( '100 Hz');
set(gca,'fontsize',16,'FontWeight','bold')
print -dpng -r300 Change_ReZ_100Hz_vs_Time
hold off

figure
plot(Time_h,delta_imZ(48,:),'c', 'linewidth', 2.0)
title ('Change in ImZ with time',
'FontSize',20,'FontWeight','bold');
xlabel ('Time (hrs)', 'FontSize',20,'FontWeight','bold');
ylabel ('(ImZ-ImZ_{PBS Baseline}) / ImZ_{PBS Baseline}',
'FontSize',20,'FontWeight','bold');
legend('100 Hz');
set(gca,'fontsize',16,'FontWeight','bold')
print -dpng -r300 Change_ImZ_100Hz_vs_Time
hold off

figure
plot(Time_h,delta_absZ(48,:),'c', 'linewidth', 2.0)
title ('Change in |Z| with time',
'FontSize',20,'FontWeight','bold');
xlabel ('Time (hrs)', 'FontSize',20,'FontWeight','bold');
ylabel ('(|Z|-|Z|_{PBS Baseline}) / |Z|_{PBS Baseline}',
'FontSize',20,'FontWeight','bold');
legend( '100 Hz');
set(gca,'fontsize',16,'FontWeight','bold')
print -dpng -r300 Change_absZ_100Hz_vs_Time
hold off

%Plotting phase, real, imaginary and absolute relative change in Z
for 100kHz
figure
plot(Time_h,delta_phase(12,:),'b', 'linewidth', 2.0)
title ('Change in phase with time',
'FontSize',20,'FontWeight','bold');
xlabel ('Time (hrs)', 'FontSize',20,'FontWeight','bold');
ylabel ('(Phase-Phase_{PBS Baseline}) / Phase_{PBS Baseline}',
'FontSize',20,'FontWeight','bold');
legend('100 kHz');
set(gca,'fontsize',16,'FontWeight','bold')
print -dpng -r300 Change_Phase_100kHz_vs_Time
hold off

figure
```

```
plot(Time_h,delta_realZ(12,:),'b', 'linewidth', 2.0)
title ('Change in ReZ with time',
'FontSize',20,'FontWeight','bold');
xlabel ('Time (hrs)', 'FontSize',20,'FontWeight','bold');
ylabel ('(ReZ-ReZ_{PBS Baseline}) / ReZ_{PBS Baseline}',
'FontSize',20,'FontWeight','bold');
legend('100 kHz');
set(gca,'fontsize',16,'FontWeight','bold')
print -dpng -r300 Change_ReZ_100kHz_vs_Time
hold off

figure
plot(Time_h,delta_imZ(12,:),'b', 'linewidth', 2.0)
title ('Change in ImZ with time',
'FontSize',20,'FontWeight','bold');
xlabel ('Time (hrs)', 'FontSize',20,'FontWeight','bold');
ylabel ('(ImZ-ImZ_{PBS Baseline}) / ImZ_{PBS Baseline}',
'FontSize',20,'FontWeight','bold');
legend('100 kHz');
set(gca,'FontSize',20,'FontWeight','bold')
print -dpng -r300 Change_ImZ_100kHz_vs_Time
hold off

figure
plot(Time_h,delta_absZ(12,:),'b', 'linewidth', 2.0)
title ('Change in |Z| with time',
'FontSize',20,'FontWeight','bold');
xlabel ('Time (hrs)', 'FontSize',20,'FontWeight','bold');
ylabel ('(|Z|-|Z|_{PBS Baseline}) / |Z|_{PBS Baseline}',
'FontSize',20,'FontWeight','bold');
legend( '100 kHz');
set(gca,'fontsize',16,'FontWeight','bold')
print -dpng -r300 Change_absZ_100kHz_vs_Time
hold off

%Time in hours for each of the three steps of the experiment
PBSControl_Time = (N-1) * Time_step/(60*60)

%delete the _TRUNC temp files in the TEMP folder
 delete('Z:\MSAL User\Sowmya\Biofilm impedance sensing\CHI
Data\Temp\*_TRUNC.txt');
```

Biofilm Growth and Treatment

```
% THIS CODE IS FOR BIOFILM GROWTH AND BE TREATMENT RUNS ONLY. THE
RUNS WILL HAVE A LB WITH
% GENTAMICIN/LB ONLY CONTROL, SEEDING, BIOFILM GROWTH, BIOFILM
GROWTH-PRETREATMENT AND BIOFILM TREATMENT
% PHASES

% Set MATLAB work path to folder with CHI data files

%Manually enter values of N, start and end time and date, change the
name
% of filename and filename2 to files to be analysed
filepath = '\'; % Enter your data folder path
filepath_temp = 'Z:\MSAL User\Sowmya\Biofilm impedance sensing\CHI
Data\Temp\'; %Enter filepath for temp files

startLB = 1; % start file number of LB
endLB = 25; % end file number of LB
startSeed = 1; % start file number of Seeding
endSeed = 11; % end file number of Seeding
startGrowth = 1; % start file number of Growth
endGrowth = 100; % end file number of Growth
startPreTreat = 1; % start file number of Pre-Treatment
endPreTreat = 41; % end file number of Pre-Treatment
startTreat = 1; % start file number of Treatment
endTreat = 63; % end file number of Treatment

start_date = 3; %enter start date
start_hour = 15; % enter starting hour in 24 hour format
start_min = 18; % enter starting minute

end_PreTreat_date = 5; %enter end Pre-Treat date
end_PreTreat_hour = 10; % enter end Pre-Treat hour in 24 hour format
end_PreTreat_min = 36; % enter end Pre-Treat minute

end_date = 6; %enter end Treat date
end_hour = 12; % enter end Treat hour in 24-hour format
end_min = 18; % enter end Treat minute

M = 60; % M = number of numeric lines in each CHI output text file
Treatment_buffer = 0 ; % Enter number of hours before completion of
the 24 hour-growth phase that you start treatment

N1 = endLB - startLB + 1; % N1= number of txt files/runs of the CHI
for LB control
N2 = endSeed - startSeed + 1; % N2= number of txt files/runs of the
CHI for Seeding
N3 = endGrowth - startGrowth + 1; % N3= number of txt files/runs of
the CHI for Bioilfm growth
N4 = endPreTreat - startPreTreat + 1; % N4= number of txt files/runs
of the CHI for Bioilfm Pre-Treatment
N5 = endTreat - startTreat + 1; % N5= number of txt files/runs of
the CHI for Bioilfm Treatment
```

```
N_sense = N1+N2+N3+N4; % Total number of files with equal times of
sensing
N = N1+N2+N3+N4+N5; % Total number of files
Total_time_sense =  (end_PreTreat_date - start_date) * 24 * 60 * 60
+ (end_PreTreat_hour - start_hour)* 60 * 60 + (end_PreTreat_min -
start_min) * 60 ; % Calculate total time in seconds during sensing
Total_time_treat =  (end_date - end_PreTreat_date) * 24 * 60 * 60 +
(end_hour - end_PreTreat_hour)* 60 * 60 + (end_min -
end_PreTreat_min) * 60 ; % Calculate total time in seconds during
treatment

Time_step_sense = Total_time_sense/(N_sense-1); % average step time
in seconds between two consecutive runs during sensing
Time_step_treat = Total_time_treat/(N5-1); % average step time in
seconds between two consecutive runs during treatment

Time_s_sense = 0: Time_step_sense: Total_time_sense; % create an
array called time_s_sense
Time_h_sense = Time_s_sense/(60*60); % row array of time in hours
during sensing
Final_time_sense = Time_h_sense'; % column array of time in hours
during sensing

Time_s_treat = Total_time_sense+Time_step_treat: Time_step_treat:
Total_time_sense + Total_time_treat+Time_step_treat; % create an
array called time_s_treat
Time_h_treat = Time_s_treat/(60*60); % row array of time in hours
during treatment
Final_time_treat = Time_h_treat'; % column array of time in hours
during treatment

Time_h = cat(2, Time_h_sense, Time_h_treat); % Concatenate both time
arrays to Time_h in one row
Final_time = Time_h'; % column array of total time in hours

Final_data = zeros(M,5*N); %size of final data array
Final_realZ = zeros(M,N); %size of final real Z data array
Final_imZ = zeros(M,N); %size of final im Z data array
Final_absZ = zeros(M,N); %size of final abs Z data array
Final_phase = zeros(M,N); %size of final phase of Z data array

j= 1; % counter
column = 1; % counter for column of final arrays

% Analyze LB control files
for i = startLB:endLB
    filename = [filepath 'imp-LB' num2str(i) '.txt']; %give path to
files you want to analyse
    fid = fopen(filename, 'r') ;    % Open source file.
    fgetl(fid) ;                    % Read/discard line.
    fgetl(fid) ;                    % Read/discard line.
    fgetl(fid) ;                    % Read/discard line.
    fgetl(fid) ;                    % Read/discard line.
    fgetl(fid) ;                    % Read/discard line.
    fgetl(fid) ;                    % Read/discard line.
```

```
    fgetl(fid) ;                    % Read/discard line.
    fgetl(fid) ;                    % Read/discard line.
    fgetl(fid) ;                    % Read/discard line.
    fgetl(fid) ;                    % Read/discard line.
    fgetl(fid) ;                    % Read/discard line.
    fgetl(fid) ;                    % Read/discard line.
    fgetl(fid) ;                    % Read/discard line.
    fgetl(fid) ;                    % Read/discard line.
    fgetl(fid) ;                    % Read/discard line.
    fgetl(fid) ;                    % Read/discard line.
    fgetl(fid) ;                    % Read/discard line.
    buffer = fread(fid, Inf) ;      % Read rest of the file.
    fclose(fid);

    filename2 = [filepath_temp 'imp-LB' num2str(i) '_TRUNC.txt'];
    fid = fopen(filename2, 'w')  ;   % Open destination file.
    fwrite(fid, buffer) ;            % Save to file without header.
    fclose(fid);

    %copy each file content into a temporary array named Temp
    fileID = fopen (filename2, 'r');
    formatSpec = '%f, %f, %f, %f, %f';
    sizeTemp = [5 M];
    Temp = fscanf(fileID, formatSpec, sizeTemp);
    fclose(fileID);
    Transpose_Temp = Temp';

    % Array frequency contains a column array of the frequencies at
which measurements were obtained
    for x=1:M
        Frequency(x,1) = Transpose_Temp(x,1);
        x=x+1;
    end

    %append contents of the array Temp to the final data arrays
    for x=1:M
        shift_y=j;
        for y=1:5
        Final_data(x,shift_y) = Transpose_Temp(x,y);
        y=y+1;
        shift_y=shift_y+1;
        end
    end
    j = j+5; % increment counter by 5 columns

    % Write into individual arrays
    for a=1:M
        Final_realZ(a,column)= Transpose_Temp(a,2);
        Final_imZ(a,column)= Transpose_Temp(a,3);
        Final_absZ(a,column)= Transpose_Temp(a,4);
        Final_phase(a,column) = Transpose_Temp(a,5);
        a=a+1;
    end
      column = column+1;
end
```

```
%Analyse seeding files
for i = startSeed:endSeed
    filename = [filepath 'imp-Seeding' num2str(i) '.txt']; %give
path to files you want to analyse
    fid = fopen(filename, 'r') ;     % Open source file.
    fgetl(fid) ;                     % Read/discard line.
    fgetl(fid) ;                     % Read/discard line.
    fgetl(fid) ;                     % Read/discard line.
    fgetl(fid) ;                     % Read/discard line.
    fgetl(fid) ;                     % Read/discard line.
    fgetl(fid) ;                     % Read/discard line.
    fgetl(fid) ;                     % Read/discard line.
    fgetl(fid) ;                     % Read/discard line.
    fgetl(fid) ;                     % Read/discard line.
    fgetl(fid) ;                     % Read/discard line.
    fgetl(fid) ;                     % Read/discard line.
    fgetl(fid) ;                     % Read/discard line.
    fgetl(fid) ;                     % Read/discard line.
    fgetl(fid) ;                     % Read/discard line.
    fgetl(fid) ;                     % Read/discard line.
    fgetl(fid) ;                     % Read/discard line.
    fgetl(fid) ;                     % Read/discard line.
    fgetl(fid) ;                     % Read/discard line.
    buffer = fread(fid, Inf) ;       % Read rest of the file.
    fclose(fid);

    filename2 = [filepath_temp 'imp-Seeding' num2str(i)
'_TRUNC.txt'];
    fid = fopen(filename2, 'w')  ;   % Open destination file.
    fwrite(fid, buffer) ;            % Save to file without header.
    fclose(fid) ;

    %copy each file content into a temporary array named Temp
    fileID = fopen (filename2, 'r');
    formatSpec = '%f, %f, %f, %f, %f';
    sizeTemp = [5 M];
    Temp = fscanf(fileID, formatSpec, sizeTemp);
    fclose(fileID);
    Transpose_Temp = Temp';

    % Array frequency contains a column array of the frequencies at
which measurements were obtained
%     for x=1:M
%         Frequency(x,1) = Transpose_Temp(x,1);
%         x=x+1;
%     end

    %append contents of the array Temp to the final data arrays
    for x=1:M
        shift_y=j;
        for y=1:5
        Final_data(x,shift_y) = Transpose_Temp(x,y);
        y=y+1;
        shift_y=shift_y+1;
        end
    end
    j = j+5; % increment counter by 5 columns
```

```
    % Write into individual arrays
    for a=1:M
        Final_realZ(a,column)= Transpose_Temp(a,2);
        Final_imZ(a,column)= Transpose_Temp(a,3);
        Final_absZ(a,column)= Transpose_Temp(a,4);
        Final_phase(a,column) = Transpose_Temp(a,5);
        a=a+1;
    end
      column = column+1;
end


% Analyze Growth files
for i = startGrowth:endGrowth
    filename = [filepath 'imp-Growth' num2str(i) '.txt']; %give path
to files you want to analyse
    fid = fopen(filename, 'r') ;     % Open source file.
    fgetl(fid) ;                     % Read/discard line.
    fgetl(fid) ;                     % Read/discard line.
    fgetl(fid) ;                     % Read/discard line.
    fgetl(fid) ;                     % Read/discard line.
    fgetl(fid) ;                     % Read/discard line.
    fgetl(fid) ;                     % Read/discard line.
    fgetl(fid) ;                     % Read/discard line.
    fgetl(fid) ;                     % Read/discard line.
    fgetl(fid) ;                     % Read/discard line.
    fgetl(fid) ;                     % Read/discard line.
    fgetl(fid) ;                     % Read/discard line.
    fgetl(fid) ;                     % Read/discard line.
    fgetl(fid) ;                     % Read/discard line.
    fgetl(fid) ;                     % Read/discard line.
    fgetl(fid) ;                     % Read/discard line.
    fgetl(fid) ;                     % Read/discard line.
    fgetl(fid) ;                     % Read/discard line.
    fgetl(fid) ;                     % Read/discard line.
    buffer = fread(fid, Inf) ;       % Read rest of the file.
    fclose(fid);

    filename2 = [filepath_temp 'imp-Growth' num2str(i)
'_TRUNC.txt'];
    fid = fopen(filename2, 'w')  ;   % Open destination file.
    fwrite(fid, buffer) ;            % Save to file without header.
    fclose(fid) ;

    %copy each file content into a temporary array named Temp
    fileID = fopen (filename2, 'r');
    formatSpec = '%f, %f, %f, %f, %f';
    sizeTemp = [5 M];
    Temp = fscanf(fileID, formatSpec, sizeTemp);
    fclose(fileID);
    Transpose_Temp = Temp';

    % Array frequency contains a column array of the frequencies at
which measurements were obtained
%     for x=1:M
%         Frequency(x,1) = Transpose_Temp(x,1);
```

```
%          x=x+1;
%      end

    %append contents of the array Temp to the final data arrays
    for x=1:M
        shift_y=j;
        for y=1:5
        Final_data(x,shift_y) = Transpose_Temp(x,y);
        y=y+1;
        shift_y=shift_y+1;
        end
    end
    j = j+5; % increment counter by 5 columns

    % Write into individual arrays
    for a=1:M
        Final_realZ(a,column)= Transpose_Temp(a,2);
        Final_imZ(a,column)= Transpose_Temp(a,3);
        Final_absZ(a,column)= Transpose_Temp(a,4);
        Final_phase(a,column) = Transpose_Temp(a,5);
        a=a+1;
    end
      column = column+1;
end

% Analyze Pre-Treatment files
for i = startPreTreat:endPreTreat
    filename = [filepath 'imp-GrowthPreTreat' num2str(i) '.txt'];
%give path to files you want to analyse
    fid = fopen(filename, 'r') ;     % Open source file.
    fgetl(fid) ;                     % Read/discard line.
    fgetl(fid) ;                     % Read/discard line.
    fgetl(fid) ;                     % Read/discard line.
    fgetl(fid) ;                     % Read/discard line.
    fgetl(fid) ;                     % Read/discard line.
    fgetl(fid) ;                     % Read/discard line.
    fgetl(fid) ;                     % Read/discard line.
    fgetl(fid) ;                     % Read/discard line.
    fgetl(fid) ;                     % Read/discard line.
    fgetl(fid) ;                     % Read/discard line.
    fgetl(fid) ;                     % Read/discard line.
    fgetl(fid) ;                     % Read/discard line.
    fgetl(fid) ;                     % Read/discard line.
    fgetl(fid) ;                     % Read/discard line.
    fgetl(fid) ;                     % Read/discard line.
    fgetl(fid) ;                     % Read/discard line.
    fgetl(fid) ;                     % Read/discard line.
    fgetl(fid) ;                     % Read/discard line.
    buffer = fread(fid, Inf) ;       % Read rest of the file.
    fclose(fid);

    filename2 = [filepath_temp 'imp-GrowthPreTreat' num2str(i)
'_TRUNC.txt'];
    fid = fopen(filename2, 'w')  ;   % Open destination file.
    fwrite(fid, buffer) ;            % Save to file without header.
    fclose(fid) ;
```

```
    %copy each file content into a temporary array named Temp
    fileID = fopen (filename2, 'r');
    formatSpec = '%f, %f, %f, %f, %f';
    sizeTemp = [5 M];
    Temp = fscanf(fileID, formatSpec, sizeTemp);
    fclose(fileID);
    Transpose_Temp = Temp';

    % Array frequency contains a column array of the frequencies at
which measurements were obtained
%     for x=1:M
%         Frequency(x,1) = Transpose_Temp(x,1);
%         x=x+1;
%     end

    %append contents of the array Temp to the final data arrays
    for x=1:M
        shift_y=j;
        for y=1:5
        Final_data(x,shift_y) = Transpose_Temp(x,y);
        y=y+1;
        shift_y=shift_y+1;
        end
    end
    j = j+5; % increment counter by 5 columns

    % Write into individual arrays
    for a=1:M
        Final_realZ(a,column)= Transpose_Temp(a,2);
        Final_imZ(a,column)= Transpose_Temp(a,3);
        Final_absZ(a,column)= Transpose_Temp(a,4);
        Final_phase(a,column) = Transpose_Temp(a,5);
        a=a+1;
    end
      column = column+1;
end

% Analyze Treatment files
for i = startTreat:endTreat
    filename = [filepath 'imp-Treat' num2str(i) '.txt']; %give path
to files you want to analyse
    fid = fopen(filename, 'r') ;     % Open source file.
    fgetl(fid) ;                     % Read/discard line.
    fgetl(fid) ;                     % Read/discard line.
    fgetl(fid) ;                     % Read/discard line.
    fgetl(fid) ;                     % Read/discard line.
    fgetl(fid) ;                     % Read/discard line.
    fgetl(fid) ;                     % Read/discard line.
    fgetl(fid) ;                     % Read/discard line.
    fgetl(fid) ;                     % Read/discard line.
    fgetl(fid) ;                     % Read/discard line.
    fgetl(fid) ;                     % Read/discard line.
    fgetl(fid) ;                     % Read/discard line.
    fgetl(fid) ;                     % Read/discard line.
    fgetl(fid) ;                     % Read/discard line.
    fgetl(fid) ;                     % Read/discard line.
    fgetl(fid) ;                     % Read/discard line.
    fgetl(fid) ;                     % Read/discard line.
```

```
    fgetl(fid) ;                    % Read/discard line.
    fgetl(fid) ;                    % Read/discard line.
    fgetl(fid) ;                    % Read/discard line.
    buffer = fread(fid, Inf) ;      % Read rest of the file.
    fclose(fid);

    filename2 = [filepath_temp 'imp-Treat' num2str(i) '_TRUNC.txt'];
    fid = fopen(filename2, 'w')  ;   % Open destination file.
    fwrite(fid, buffer) ;            % Save to file without header.
    fclose(fid) ;

    %copy each file content into a temporary array named Temp
    fileID = fopen (filename2, 'r');
    formatSpec = '%f, %f, %f, %f, %f';
    sizeTemp = [5 M];
    Temp = fscanf(fileID, formatSpec, sizeTemp);
    fclose(fileID);
    Transpose_Temp = Temp';

    % Array frequency contains a column array of the frequencies at
which measurements were obtained
%     for x=1:M
%         Frequency(x,1) = Transpose_Temp(x,1);
%         x=x+1;
%     end

    %append contents of the array Temp to the final data arrays
    for x=1:M
        shift_y=j;
        for y=1:5
        Final_data(x,shift_y) = Transpose_Temp(x,y);
        y=y+1;
        shift_y=shift_y+1;
        end
    end
    j = j+5; % increment counter by 5 columns

    % Write into individual arrays
    for a=1:M
        Final_realZ(a,column)= Transpose_Temp(a,2);
        Final_imZ(a,column)= Transpose_Temp(a,3);
        Final_absZ(a,column)= Transpose_Temp(a,4);
        Final_phase(a,column) = Transpose_Temp(a,5);
        a=a+1;
    end
      column = column+1;
end

% plot figures
% Real of Z versus frequency on a log log scale
figure
loglog(Frequency,Final_realZ(:,1), 'r', 'LineWidth', 2.0)
hold on
loglog(Frequency,Final_realZ(:,25),'b', 'LineWidth', 2.0)
hold on
loglog(Frequency,Final_realZ(:,50),'g', 'LineWidth', 2.0)
```

```
hold on
loglog(Frequency,Final_realZ(:,75),'k', 'LineWidth', 2.0)
hold on
loglog(Frequency,Final_realZ(:,100),'c', 'LineWidth', 2.0)
hold on
loglog(Frequency,Final_realZ(:,125),'r--', 'LineWidth', 2.0)
hold on
loglog(Frequency,Final_realZ(:,150),'b--', 'LineWidth', 2.0)
hold on
loglog(Frequency,Final_realZ(:,175),'g--', 'LineWidth', 2.0)
hold on
loglog(Frequency,Final_realZ(:,N),'k--', 'LineWidth', 2.0)
title('Re Z v. frequency', 'FontSize',20,'FontWeight','bold')
xlabel('frequency (Hz)', 'FontSize',20,'FontWeight','bold')
ylabel('Re Z (ohms)', 'FontSize',20,'FontWeight','bold')
set(gca,'fontsize',16,'FontWeight','bold')
print -dpng -r300 ReZ_vs_Freq
hold off

% Im of Z versus frequency on a log log scale
figure
loglog(Frequency,Final_imZ(:,1), 'r', 'linewidth', 2.0)
hold on
loglog(Frequency,Final_imZ(:,25),'b', 'linewidth', 2.0)
hold on
loglog(Frequency,Final_imZ(:,50),'g', 'linewidth', 2.0)
hold on
loglog(Frequency,Final_imZ(:,75),'k', 'linewidth', 2.0)
hold on
loglog(Frequency,Final_imZ(:,100),'c', 'linewidth', 2.0)
hold on
loglog(Frequency,Final_imZ(:,125),'r--', 'linewidth', 2.0)
hold on
loglog(Frequency,Final_imZ(:,150),'b--', 'linewidth', 2.0)
hold on
loglog(Frequency,Final_imZ(:,175),'g--', 'linewidth', 2.0)
hold on
loglog(Frequency,Final_imZ(:,N),'k--', 'linewidth', 2.0)
title('Im Z v. frequency', 'FontSize',20,'FontWeight','bold')
xlabel('frequency (Hz)', 'FontSize',20,'FontWeight','bold')
ylabel('Im Z (ohms)', 'FontSize',20,'FontWeight','bold')
set(gca,'fontsize',16,'FontWeight','bold')
print -dpng -r300 ImZ_vs_Freq
hold off

% Abs Z versus frequency on a log log scale
figure
loglog(Frequency,Final_absZ(:,1), 'r', 'linewidth', 2.0)
hold on
loglog(Frequency,Final_absZ(:,25),'b', 'linewidth', 2.0)
hold on
loglog(Frequency,Final_absZ(:,50),'g', 'linewidth', 2.0)
hold on
loglog(Frequency,Final_absZ(:,75),'k', 'linewidth', 2.0)
hold on
loglog(Frequency,Final_absZ(:,100),'c', 'linewidth', 2.0)
```

```
hold on
loglog(Frequency,Final_absZ(:,125),'r--', 'linewidth', 2.0)
hold on
loglog(Frequency,Final_absZ(:,150),'b--', 'linewidth', 2.0)
hold on
loglog(Frequency,Final_absZ(:,175),'g--', 'linewidth', 2.0)
hold on
loglog(Frequency,Final_absZ(:,N),'k--', 'linewidth', 2.0)
title('|Z| v. frequency', 'FontSize',20,'FontWeight','bold')
xlabel('frequency (Hz)', 'FontSize',20,'FontWeight','bold')
ylabel('|Z| (ohms)', 'FontSize',20,'FontWeight','bold')
set(gca,'fontsize',16,'FontWeight','bold')
print -dpng -r300 AbsZ_vs_Freq
hold off

% Phase versus frequency on a log log scale
figure
loglog(Frequency,Final_phase(:,1), 'r','LineWidth', 2.0)
hold on
loglog(Frequency,Final_phase(:,25),'b','LineWidth', 2.0)
hold on
loglog(Frequency,Final_phase(:,50),'g','LineWidth', 2.0)
hold on
loglog(Frequency,Final_phase(:,75),'k','LineWidth', 2.0)
hold on
loglog(Frequency,Final_phase(:,100),'c','LineWidth', 2.0)
hold on
% loglog(Frequency,Final_phase(:,125),'r--','LineWidth', 2.0)
% hold on
% loglog(Frequency,Final_phase(:,150),'b--','LineWidth', 2.0)
% hold on
% loglog(Frequency,Final_phase(:,175),'g--','LineWidth', 2.0)
% hold on
loglog(Frequency,Final_phase(:,N),'k--','LineWidth', 2.0)
title('Phase of |Z| v. frequency',
'FontSize',20,'FontWeight','bold')
xlabel('frequency (Hz)', 'FontSize',20,'FontWeight','bold')
ylabel('Phase', 'FontSize',20,'FontWeight','bold')
set(gca,'fontsize',16,'FontWeight','bold')
print -dpng -r300 Phase_vs_Freq
hold off

% Real of Z versus time
figure
plot(Time_h,Final_realZ(1,:), 'r', 'linewidth', 2.0)
hold on
plot(Time_h,Final_realZ(12,:),'b', 'linewidth', 2.0)
hold on
plot(Time_h,Final_realZ(24,:),'g', 'linewidth', 2.0)
hold on
plot(Time_h,Final_realZ(36,:),'k', 'linewidth', 2.0)
hold on
plot(Time_h,Final_realZ(48,:),'c', 'linewidth', 2.0)
hold on
plot(Time_h,Final_realZ(60,:),'m', 'linewidth', 2.0)
title('Re Z v. time(hrs)', 'FontSize',20,'FontWeight','bold')
```

```
xlabel('time (hrs)', 'FontSize',20,'FontWeight','bold')
ylabel('Re Z (ohms)', 'FontSize',20,'FontWeight','bold')
legend('825 kHz', '100 kHz', '10 kHz', '1 kHz', '100 Hz', '10 Hz')
set(gca,'fontsize',16,'FontWeight','bold')
print -dpng -r300 ReZ_vs_Time
hold off

% Im of Z versus time(hrs)
figure
plot(Time_h,Final_imZ(1,:), 'r', 'linewidth', 2.0)
hold on
plot(Time_h,Final_imZ(12,:),'b', 'linewidth', 2.0)
hold on
plot(Time_h,Final_imZ(24,:),'g', 'linewidth', 2.0)
hold on
plot(Time_h,Final_imZ(36,:),'k', 'linewidth', 2.0)
hold on
plot(Time_h,Final_imZ(48,:),'c', 'linewidth', 2.0)
hold on
plot(Time_h,Final_imZ(60,:),'m', 'linewidth', 2.0)
title('Im Z v. time(hrs)', 'FontSize',20,'FontWeight','bold')
xlabel('time(hrs)', 'FontSize',20,'FontWeight','bold')
ylabel('Im Z (ohms)', 'FontSize',20,'FontWeight','bold')
legend('825 kHz', '100 kHz', '10 kHz', '1 kHz', '100 Hz', '10 Hz')
set(gca,'fontsize',16,'FontWeight','bold')
print -dpng -r300 ImZ_vs_Time
hold off

% Abs Z versus time(hrs)
figure
plot(Time_h,Final_absZ(1,:), 'r', 'linewidth', 2.0)
hold on
plot(Time_h,Final_absZ(12,:),'b', 'linewidth', 2.0)
hold on
plot(Time_h,Final_absZ(24,:),'g', 'linewidth', 2.0)
hold on
plot(Time_h,Final_absZ(36,:),'k', 'linewidth', 2.0)
hold on
plot(Time_h,Final_absZ(48,:),'c', 'linewidth', 2.0)
hold on
plot(Time_h,Final_absZ(60,:),'m', 'linewidth', 2.0)
title('|Z| v. time(hrs)', 'FontSize',20,'FontWeight','bold')
xlabel('time(hrs)', 'FontSize',20,'FontWeight','bold')
ylabel('|Z| (ohms)', 'FontSize',20,'FontWeight','bold')
legend('825 kHz', '100 kHz', '10 kHz', '1 kHz', '100 Hz', '10 Hz')
set(gca,'fontsize',16,'FontWeight','bold')
print -dpng -r300 AbsZ_vs_Time
hold off

% Phase versus time(hrs)
figure
plot(Time_h,Final_phase(1,:), 'r','LineWidth', 2.0)
hold on
plot(Time_h,Final_phase(12,:),'b','LineWidth', 2.0)
hold on
plot(Time_h,Final_phase(24,:),'g','LineWidth', 2.0)
```

```
hold on
plot(Time_h,Final_phase(36,:),'k','LineWidth', 2.0)
hold on
plot(Time_h,Final_phase(48,:),'c','LineWidth', 2.0)
hold on
plot(Time_h,Final_phase(60,:),'r--','LineWidth', 2.0)
title('Phase v. time(hrs)', 'FontSize',20,'FontWeight','bold')
xlabel('time(hrs)', 'FontSize',20,'FontWeight','bold')
ylabel('Phase', 'FontSize',20,'FontWeight','bold')
legend('825 kHz', '100 kHz', '10 kHz', '1 kHz', '100 Hz', '10 Hz')
set(gca,'fontsize',16,'FontWeight','bold')
print -dpng -r300 Phase_vs_Time
hold off

% Abs Z versus time(hrs) Only 100 kHz
figure
plot(Time_h,Final_absZ(12,:),'b', 'linewidth', 2.0)
%hold on
%plot(Time_h,Final_absZ(24,:),'g')
title('|Z| v. time(hrs)', 'FontSize',20,'FontWeight','bold')
xlabel('time(hrs)', 'FontSize',20,'FontWeight','bold')
ylabel('|Z| (ohms)', 'FontSize',20,'FontWeight','bold')
legend( '100 kHz')
set(gca,'fontsize',16,'FontWeight','bold')
print -dpng -r300 AbsZ_100KHz_vs_Time
hold off

% Phase versus time(hrs) Only 100 kHz
figure
plot(Time_h,Final_phase(12,:),'b','LineWidth', 2.0)
%hold on
%plot(Time_h,Final_phase(24,:),'g')
title('Phase v. time(hrs)', 'FontSize',20,'FontWeight','bold')
xlabel('time(hrs)', 'FontSize',20,'FontWeight','bold')
ylabel('Phase', 'FontSize',20,'FontWeight','bold')
legend( '100 kHz')
set(gca,'fontsize',16,'FontWeight','bold')
print -dpng -r300 Phase_100KHz_vs_Time
hold off

% Change in Z with respect to baseline obtained using LB
for i=1:N1
    LB_absZ(:,i) = Final_absZ(:,i);
    LB_imZ(:,i) = Final_imZ(:,i);
    LB_realZ(:,i) = Final_realZ(:,i);
    LB_phase(:,i) = Final_phase(:,i);
    i=i+1;
end

baseline_absZ_LB = mean(LB_absZ, 2); %  average baseline LB absZ
value for each frequency
baseline_imZ_LB = mean(LB_imZ,2); %  average baseline LB imZ value
for each frequency
baseline_realZ_LB = mean(LB_realZ,2); %  average baseline LB realZ
value for each frequency
```

```
baseline_phase_LB = mean(LB_phase,2); %  average baseline LB phase
value for each frequency

for i =1:N
    delta_absZ(:,i) = (Final_absZ(:,i) -
baseline_absZ_LB)./baseline_absZ_LB ;
    delta_imZ(:,i) = (Final_imZ(:,i) -
baseline_imZ_LB)./baseline_imZ_LB ;
    delta_realZ(:,i) = (Final_realZ(:,i) -
baseline_realZ_LB)./baseline_realZ_LB ;
    delta_phase(:,i) = (Final_phase(:,i) -
baseline_phase_LB)./baseline_phase_LB ;
    i=i+1;
end

figure
plot(Time_h,delta_realZ) % plot the change in realZ with respect to
title ('Change in ReZ with time','FontSize',20,'FontWeight','bold');
xlabel ('Time (hrs)', 'FontSize',20,'FontWeight','bold');
ylabel ('(ReZ-ReZ_{LB}) / ReZ_{LB}',
'FontSize',20,'FontWeight','bold')
set(gca,'fontsize',16,'FontWeight','bold')
print -dpng -r300 Change_ReZ_vs_Time
hold off

figure
plot(Time_h,delta_realZ(1,:), 'r', 'linewidth', 2.0)
hold on
plot(Time_h,delta_realZ(12,:),'b', 'linewidth', 2.0)
hold on
plot(Time_h,delta_realZ(24,:),'g', 'linewidth', 2.0)
hold on
plot(Time_h,delta_realZ(36,:),'k', 'linewidth', 2.0)
hold on
plot(Time_h,delta_realZ(48,:),'c', 'linewidth', 2.0)
hold on
plot(Time_h,delta_realZ(60,:),'m', 'linewidth', 2.0)
title ('Change in ReZ with time',
'FontSize',20,'FontWeight','bold');
xlabel ('Time (hrs)', 'FontSize',20,'FontWeight','bold');
ylabel ('(ReZ-ReZ_{LB}) / ReZ_{LB}',
'FontSize',20,'FontWeight','bold');
legend('825 kHz', '100 kHz', '10 kHz', '1 kHz', '100 Hz', '10 Hz');
set(gca,'fontsize',16,'FontWeight','bold')
print -dpng -r300 Change_ReZ_vs_Time_2
hold off

figure
plot(Time_h,delta_imZ) % plot the change in imZ with respect to
title ('Change in ImZ with time',
'FontSize',20,'FontWeight','bold');
xlabel ('Time (hrs)', 'FontSize',20,'FontWeight','bold');
ylabel ('(ImZ-ImZ_{LB}) / ImZ_{LB}',
'FontSize',20,'FontWeight','bold');
set(gca,'fontsize',16,'FontWeight','bold')
print -dpng -r300 Change_ImZ_vs_Time
```

```
hold off

figure
plot(Time_h,delta_imZ(1,:), 'r', 'linewidth', 2.0)
hold on
plot(Time_h,delta_imZ(12,:),'b', 'linewidth', 2.0)
hold on
plot(Time_h,delta_imZ(24,:),'g', 'linewidth', 2.0)
hold on
plot(Time_h,delta_imZ(36,:),'k', 'linewidth', 2.0)
hold on
plot(Time_h,delta_imZ(48,:),'c', 'linewidth', 2.0)
hold on
plot(Time_h,delta_imZ(60,:),'m', 'linewidth', 2.0)
title ('Change in ImZ with time',
'FontSize',20,'FontWeight','bold');
xlabel ('Time (hrs)', 'FontSize',20,'FontWeight','bold');
ylabel ('(ImZ-ImZ_{LB}) / ImZ_{LB}',
'FontSize',20,'FontWeight','bold');
legend('825 kHz', '100 kHz', '10 kHz', '1 kHz', '100 Hz', '10 Hz');
set(gca,'fontsize',16,'FontWeight','bold')
print -dpng -r300 Change_ImZ_vs_Time_2
hold off


figure
plot(Time_h,delta_absZ) % plot the change in absZ with time
title ('Change in |Z| with time',
'FontSize',20,'FontWeight','bold');
xlabel ('Time (hrs)', 'FontSize',20,'FontWeight','bold');
ylabel ('(|Z|-|Z|_{LB}) / |Z|_{LB}',
'FontSize',20,'FontWeight','bold');
set(gca,'fontsize',16,'FontWeight','bold')
print -dpng -r300 Change_absZ_vs_Time
hold off

figure
plot(Time_h,delta_absZ(1,:), 'r', 'linewidth', 2.0)
hold on
plot(Time_h,delta_absZ(12,:),'b', 'linewidth', 2.0)
hold on
plot(Time_h,delta_absZ(24,:),'g', 'linewidth', 2.0)
hold on
plot(Time_h,delta_absZ(36,:),'k', 'linewidth', 2.0)
hold on
plot(Time_h,delta_absZ(48,:),'c', 'linewidth', 2.0)
hold on
plot(Time_h,delta_absZ(60,:),'m', 'linewidth', 2.0)
title ('Change in |Z| with time',
'FontSize',20,'FontWeight','bold');
xlabel ('Time (hrs)', 'FontSize',20,'FontWeight','bold');
ylabel ('(|Z|-|Z|_{LB}) / |Z|_{LB}',
'FontSize',20,'FontWeight','bold');
legend('825 kHz', '100 kHz', '10 kHz', '1 kHz', '100 Hz', '10 Hz');
set(gca,'fontsize',16,'FontWeight','bold')
print -dpng -r300 Change_absZ_vs_Time_2
```

```
hold off

figure
plot(Time_h,delta_phase) % plot the change in phase with time
title ('Change in phase with time',
'FontSize',20,'FontWeight','bold');
xlabel ('Time (hrs)', 'FontSize',20,'FontWeight','bold');
ylabel ('(Phase-Phase_{LB}) / Phase_{LB}',
'FontSize',20,'FontWeight','bold');
set(gca,'fontsize',16,'FontWeight','bold')
print -dpng -r300 Change_phase_vs_Time
hold off

figure
plot(Time_h,delta_phase(1,:), 'r', 'linewidth', 2.0)
hold on
plot(Time_h,delta_phase(12,:),'b', 'linewidth', 2.0)
hold on
plot(Time_h,delta_phase(24,:),'g', 'linewidth', 2.0)
hold on
plot(Time_h,delta_phase(36,:),'k', 'linewidth', 2.0)
hold on
plot(Time_h,delta_phase(48,:),'c', 'linewidth', 2.0)
hold on
plot(Time_h,delta_phase(60,:),'m', 'linewidth', 2.0)
title ('Change in phase with time',
'FontSize',20,'FontWeight','bold');
xlabel ('Time (hrs)', 'FontSize',20,'FontWeight','bold');
ylabel ('(phase-phase_{LB}) / phase_{LB}',
'FontSize',20,'FontWeight','bold');
legend('825 kHz', '100 kHz', '10 kHz', '1 kHz', '100 Hz', '10 Hz');
set(gca,'fontsize',16,'FontWeight','bold')
print -dpng -r300 Change_phase_vs_Time_2
hold off

%Plotting phase, real, imaginary and absolute relative change in Z
for 100Hz

figure
plot(Time_h,delta_phase(48,:),'c', 'linewidth', 2.0)
title ('Change in Phase with time',
'FontSize',20,'FontWeight','bold');
xlabel ('Time (hrs)', 'FontSize',20,'FontWeight','bold');
ylabel ('(Phase-Phase_{LB}) / Phase_{LB}',
'FontSize',20,'FontWeight','bold');
legend( '100 Hz');
set(gca,'fontsize',16,'FontWeight','bold')
print -dpng -r300 Change_Phase_100Hz_vs_Time
hold off

figure
plot(Time_h,delta_realZ(48,:),'c', 'linewidth', 2.0)
title ('Change in ReZ with time',
'FontSize',20,'FontWeight','bold');
xlabel ('Time (hrs)', 'FontSize',20,'FontWeight','bold');
```

```
ylabel ('(ReZ-ReZ_{LB Baseline}) / ReZ_{LB Baseline}',
'FontSize',20,'FontWeight','bold');
legend( '100 Hz');
set(gca,'fontsize',16,'FontWeight','bold')
print -dpng -r300 Change_ReZ_100Hz_vs_Time
hold off

figure
plot(Time_h,delta_imZ(48,:),'c', 'linewidth', 2.0)
title ('Change in ImZ with time',
'FontSize',20,'FontWeight','bold');
xlabel ('Time (hrs)', 'FontSize',20,'FontWeight','bold');
ylabel ('(ImZ-ImZ_{LB Baseline}) / ImZ_{LB Baseline}',
'FontSize',20,'FontWeight','bold');
legend('100 Hz');
set(gca,'fontsize',16,'FontWeight','bold')
print -dpng -r300 Change_ImZ_100Hz_vs_Time
hold off

figure
plot(Time_h,delta_absZ(48,:),'c', 'linewidth', 2.0)
title ('Change in |Z| with time',
'FontSize',20,'FontWeight','bold');
xlabel ('Time (hrs)', 'FontSize',20,'FontWeight','bold');
ylabel ('(|Z|-|Z|_{LB Baseline}) / |Z|_{LB Baseline}',
'FontSize',20,'FontWeight','bold');
legend( '100 Hz');
set(gca,'fontsize',16,'FontWeight','bold')
print -dpng -r300 Change_absZ_100Hz_vs_Time
hold off


%Plotting real, imaginary and absolute relative change in Z for
100kHz
figure
plot(Time_h,delta_phase(12,:),'b', 'linewidth', 2.0)
title ('Change in phase with time',
'FontSize',20,'FontWeight','bold');
xlabel ('Time (hrs)', 'FontSize',20,'FontWeight','bold');
ylabel ('(Phase-Phase_{LB}) / Phase_{LB}',
'FontSize',20,'FontWeight','bold');
legend('100 kHz');
set(gca,'fontsize',16,'FontWeight','bold')
print -dpng -r300 Change_Phase_100kHz_vs_Time
hold off

figure
plot(Time_h,delta_realZ(12,:),'b', 'linewidth', 2.0)
title ('Change in ReZ with time',
'FontSize',20,'FontWeight','bold');
xlabel ('Time (hrs)', 'FontSize',20,'FontWeight','bold');
ylabel ('(ReZ-ReZ_{LB Baseline}) / ReZ_{LB Baseline}',
'FontSize',20,'FontWeight','bold');
legend('100 kHz');
set(gca,'fontsize',16,'FontWeight','bold')
print -dpng -r300 Change_ReZ_100kHz_vs_Time
```

```
hold off

figure
plot(Time_h,delta_imZ(12,:),'b', 'linewidth', 2.0)
title ('Change in ImZ with time',
'FontSize',20,'FontWeight','bold');
xlabel ('Time (hrs)', 'FontSize',20,'FontWeight','bold');
ylabel ('(ImZ-ImZ_{LB Baseline}) / ImZ_{LB Baseline}',
'FontSize',20,'FontWeight','bold');
legend('100 kHz');
set(gca,'fontsize',16,'FontWeight','bold')
print -dpng -r300 Change_ImZ_100kHz_vs_Time
hold off

figure
plot(Time_h,delta_absZ(12,:),'b', 'linewidth', 2.0)
title ('Change in |Z| with time',
'FontSize',20,'FontWeight','bold');
xlabel ('Time (hrs)', 'FontSize',20,'FontWeight','bold');
ylabel ('(|Z|-|Z|_{LB Baseline}) / |Z|_{LB Baseline}',
'FontSize',20,'FontWeight','bold');
legend( '100 kHz');
set(gca,'fontsize',16,'FontWeight','bold')
print -dpng -r300 Change_absZ_100kHz_vs_Time
hold off


%Time in hours for each of the three steps of the experiment
LBControl_Time = (N1-1) * Time_step_sense/(60*60)
Seeding_Time = LBControl_Time + N2 * Time_step_sense/(60*60)
Growth_Time = Seeding_Time + N3 * Time_step_sense/(60*60) + N4 *
Time_step_sense/(60*60)
Treat_Time = Growth_Time + (N5-1) * Time_step_treat/(60*60) +
Time_step_treat/(60*60)

%delete the _TRUNC temp files in the TEMP folder
 delete('Z:\MSAL User\Sowmya\Biofilm impedance sensing\CHI
Data\Temp\*_TRUNC.txt');
```

Real-time Threshold-activated Sensing-Treatment

```
% Last edited on : 2/1/2015 13:00
% Installation Notes:
% MUST use 32 bit install of Matlab!! 64 bit WILL NOT WORK!
% No LabVIEW install necessary!

% Copy folder, including all files, from MSAL server - \MSAL
User\MSAL Undergrad\Kate\libec.windows
% Add to Matlab path (when running biofilms_gui2.m)

% Necessary files(must be in same folder):
% biofilms_gui2.m, biofilms_gui2.fig

% Library files(must be in same folder):
% libec.dll
% Qt*.dll
% Microsoft.VC90.CRT (folder)
% *.h
% plotoptions
% msvc*.dll
%%%%%%%%%%%%%%%%%%%%%%%%%%%%%%%%%%%%%%%%%%%%%%%%%%%%%%%%%%%%%%%%%%%%%%%%
%%%%%%%
% Execution Notes:
% CHANGE num_channels in code! Cannot be changes in GUI

% Output file header(not included in file)
% ExperimentTime(s) ReZ(Ohm) ImZ(Ohm) |Z|(Ohm) Phase(Rad) Mode(See
below)

% Data values separated by \t (tab) character
% 1 file per channel

% Modes: 1-Control, 2-Seeding, 3-Sensing, 4-Treatment, 5-
Conditioning, 6-Growth
%%%%%%%%%%%%%%%%%%%%%%%%%%%%%%%%%%%%%%%%%%%%%%%%%%%%%%%%%%%%%%%%%%%%%%%%
%%%%%%%
% Development Resources:
% http://www.chinstruments.com/libec_alpha.shtml
% http://sourceforge.net/p/libec-vi-
repo/discussion/general/thread/dbd93430/
% http://www.mathworks.com/matlabcentral/fileexchange/29618-spspj
%
http://www.mathworks.com/matlabcentral/newsreader/view_thread/143621

function varargout = biofilms_gui2(varargin)
% Initialization of GUI elements - DO NOT EDIT
gui_Singleton = 1;
gui_State = struct('gui_Name',       mfilename, ...
                   'gui_Singleton',  gui_Singleton, ...
                   'gui_OpeningFcn', @biofilms_gui2_OpeningFcn, ...
                   'gui_OutputFcn',  @biofilms_gui2_OutputFcn, ...
                   'gui_LayoutFcn',  [] , ...
                   'gui_Callback',   []);
if nargin && ischar(varargin{1})
```

```
    gui_State.gui_Callback = str2func(varargin{1});
end

if nargout
    [varargout{1:nargout}] = gui_mainfcn(gui_State, varargin{:});
else
    gui_mainfcn(gui_State, varargin{:});
end
% End initialization code - DO NOT EDIT

% --- Executes just before biofilms_gui2 is made visible.
function biofilms_gui2_OpeningFcn(hObject, eventdata, handles,
varargin)
% Choose default command line output for biofilms_gui2
handles.output = hObject;

% Update handles structure
guidata(hObject, handles);

% Load Libec library

if ~libisloaded('libec')
   loadlibrary('libec.dll', 'labview.h')
end

% Declares global variables. Allows tool to share variables between
all
% functions
global channels;
global num_channels;
global treatment_cycles;
global exp_cycles_est;
global exp_data;
global mode;
global tech;
global ei_sens;
global fl_sens;
global fh_sens;
global amp_sens;
global ei_treat;
global fl_treat;
global fh_treat;
global amp_treat;
%global start_time;
global started;
global qt;
global sens_thresh;
global treat_thresh;
global baseline;
%global fileID;
global cycle;
global treat_cycles;
global filename;
global num_outliers;
global num_outliers_cond;
global M;
```

```
global growth_hours;
global qt_growth;
global qt_treat;
global outlier_thresh;

global temp_growth_mode;

% Initialize default values for experiment parameters

%%%%%%%%%%%%%%%%%%%% MODIFY NUM CHANNELS HERE
%%%%%%%%%%%%%%%%%%%%%%%%%%
num_channels = 4;
%%%%%%%%%%%%%%%%%%%%%%%%%%%%%%%%%%%%%%%%%%%%%%%%%%%%%%%%%%%%%%%%%%%%%%%%%%%%
%%%%%%%
% DO NOT USE CHANNEL 1
channels = 4:(num_channels + 3); % default channel #s
treat_cycles = zeros(1,num_channels);
if(num_channels>=2)
    for ch = num_channels/2+1:num_channels
        treat_cycles(ch) = 3; % set half of channels to 3 cycles for
treatment
    end
end
%treat_cycles = [0,0,3,3]; Default treatment cycles
started = 0; % flag if experiment has started
filename = 'exp_data_ch_';
outlier_thresh = 100; % 1x or 100% percent different from previous
value
num_outliers = zeros(num_channels,1); % Stores the number of
outliers so far
num_outliers_cond = zeros(num_channels,1); % Stores the number of
outliers so far
temp_growth_mode = zeros(num_channels,1);

% Default experiment parameters
fl_sens =  100; % sensing frequency (Hz)
fh_sens = fl_sens;
fh_treat = 1000000;
fl_treat = fh_treat/10; % treatment frequency (Hz)


amp_sens = 0.005; % sensing amplitude (V)
amp_treat = 0.1; % treatment amplitude (V)

qt = 300; % quiet time between measurments (s)
qt_growth = 600;
qt_treat = 60;

sens_thresh = 5; % sensing threshold in %
treat_thresh = 10; % treatment threshold in %
growth_hours = 6;

treatment_cycles = 20; % Num of cycles of treatment between every
switch to sensing
```

```
exp_cycles_est = 10000; % Max expected num of cycles in experiment -
pre-allocate storage, more efficient

tech = 14; % impedance sensing is technique #14 for CHI
ei_sens = 0; % DC bias sensing
ei_treat = 0; % DC bias treatment

% Preallocate data array
% 5 values per time point - time, raw |Z|, im, mag, phase, mode, |Z|
no
% outlier, |Z| processed
exp_data = Inf*zeros(num_channels,exp_cycles_est, 8);
mode= 5*ones(num_channels,1); % Mode for each channel: 1 - control,
2 - seeding, 3 - growth, 4 - treat
baseline = zeros(num_channels,1); % Baseline calculated based on
Control experiment data

cycle = 1; % current cycle

% Set up Raw data figure
figure(2);
for ch = 1:num_channels
    subplot(2,num_channels/2,ch);
    title(['Ch ' num2str(channels(ch)) ' - Raw |Z|'],
'FontSize',14,'FontWeight','bold');
    xlabel ('Time (hrs)', 'FontSize',10,'FontWeight','bold');
    ylabel ('Impedance |Z| (ohms)',
'FontSize',10,'FontWeight','bold');
end

% Set up graph for normalized data
figure(3);
for ch = 1:num_channels
    subplot(2,num_channels/2,ch);
    title(['Ch ' num2str(channels(ch)) ' - Change in |Z|'],
'FontSize',14,'FontWeight','bold');
    xlabel ('Time (hrs)', 'FontSize',10,'FontWeight','bold');
    ylabel ('(|Z|-|Z|_{LB Baseline}) / |Z|_{LB Baseline}',
'FontSize',10,'FontWeight','bold');
    %line1 = refline([0 sens_thresh/100]);
    %set(line1,'LineStyle',':', 'Color', 'k', 'LineWidth', 2);
    %line2 = refline([0 treat_thresh/100]);
    %set(line2,'LineStyle',':', 'Color', 'k', 'LineWidth', 2);
end

% filename2 = 'exp1_12032015_4-cond.txt';
% M = dlmread(filename2,'\t');

% UIWAIT makes biofilms_gui2 wait for user response (see UIRESUME)
% uiwait(handles.figure1);


% --- Outputs from this function are returned to the command line.
function varargout = biofilms_gui2_OutputFcn(hObject, eventdata,
handles)
```

```
varargout{1} = handles.output;

% Start/stop experiment button
function togglebutton1_Callback(hObject, eventdata, handles)
global run_exp;
global start_time;
global started;
get(hObject,'Value')
if (get(hObject,'Value') == get(hObject,'Max')) % if experiment
started
    set(hObject,'String','Pause');
    set(hObject,'BackgroundColor','yellow');
    run_exp = 1;
    if ~started % set start time
        started = 1;
        start_time = clock;
    end
    run_Experiment(); % start experiment
end
if (get(hObject,'Value') == get(hObject,'Min')) % if experiment
stopped
    set(hObject,'String','Start');
    set(hObject,'BackgroundColor','green');
    run_exp = 0;
end
% Hint: get(hObject,'Value') returns toggle state of togglebutton1


% get sensing Frequency from text box
function edit1_Callback(hObject, eventdata, handles)
global fl_sens;
global fh_sens;
fl_sens = str2num(get(hObject,'String'));
fh_sens = fl_sens;


% set sensing frequency text box to default
function edit1_CreateFcn(hObject, eventdata, handles)
global fl_sens;
set(hObject, 'String',num2str(fl_sens))
if ispc && isequal(get(hObject,'BackgroundColor'),
get(0,'defaultUicontrolBackgroundColor'))
    set(hObject,'BackgroundColor','white');
end

% get Treatment Frequency from text box
function edit2_Callback(hObject, eventdata, handles)
global fh_treat;
global fl_treat;
fh_treat = str2num(get(hObject,'String'));
fl_treat = fh_treat/10;
%fh_treat = fl_treat;

% set treatment frequency to default
function edit2_CreateFcn(hObject, eventdata, handles)
```

```
global fh_treat;
set(hObject, 'String',num2str(fh_treat))
if ispc && isequal(get(hObject,'BackgroundColor'),
get(0,'defaultUicontrolBackgroundColor'))
    set(hObject,'BackgroundColor','white');
end

%get Sensing Amplitude from text box
function edit3_Callback(hObject, eventdata, handles)
global amp_sens;
amp_sens = str2num(get(hObject,'String'));

%set sensing amplitude to default
function edit3_CreateFcn(hObject, eventdata, handles)
global amp_sens;
set(hObject, 'String',num2str(amp_sens))
if ispc && isequal(get(hObject,'BackgroundColor'),
get(0,'defaultUicontrolBackgroundColor'))
    set(hObject,'BackgroundColor','white');
end

% get Treatment Amplitude from text box
function edit4_Callback(hObject, eventdata, handles)
global amp_treat;
amp_treat = str2num(get(hObject,'String'));

% set treatment amplitude to default
function edit4_CreateFcn(hObject, eventdata, handles)
global amp_treat;
set(hObject, 'String',num2str(amp_treat))
if ispc && isequal(get(hObject,'BackgroundColor'),
get(0,'defaultUicontrolBackgroundColor'))
    set(hObject,'BackgroundColor','white');
end

% get Quiet Time from text box
function edit6_Callback(hObject, eventdata, handles)
global qt;
qt = str2num(get(hObject,'String'));


% set quiet time to text box
function edit6_CreateFcn(hObject, ~, handles)
global qt;
set(hObject, 'String',num2str(qt))
if ispc && isequal(get(hObject,'BackgroundColor'),
get(0,'defaultUicontrolBackgroundColor'))
    set(hObject,'BackgroundColor','white');
end

% get Treatment Interval from text box, for each channel. 0 for no
treatment
function edit7_Callback(hObject, eventdata, handles)
global treat_cycles;
treat_cycles = str2num(get(hObject,'String'));
```

```
% set treatment interval to default
function edit7_CreateFcn(hObject, eventdata, handles)
global treat_cycles;
set(hObject, 'String',num2str(treat_cycles))
if ispc && isequal(get(hObject,'BackgroundColor'),
get(0,'defaultUicontrolBackgroundColor'))
    set(hObject,'BackgroundColor','white');
end

% get Treatment Threshold from textbox
function edit8_Callback(hObject, eventdata, handles)
global treat_thresh;
treat_thresh = str2num(get(hObject,'String'));

% set treatment threshold to default
function edit8_CreateFcn(hObject, eventdata, handles)
global treat_thresh;
set(hObject, 'String',num2str(treat_thresh))
if ispc && isequal(get(hObject,'BackgroundColor'),
get(0,'defaultUicontrolBackgroundColor'))
    set(hObject,'BackgroundColor','white');
end

% get Sensing threshold from textbox
function edit9_Callback(hObject, eventdata, handles)
global sens_thresh;
sens_thresh = str2num(get(hObject,'String'));

% set sensing threshold to default
function edit9_CreateFcn(hObject, eventdata, handles)
global sens_thresh;
set(hObject, 'String',num2str(sens_thresh))
if ispc && isequal(get(hObject,'BackgroundColor'),
get(0,'defaultUicontrolBackgroundColor'))
    set(hObject,'BackgroundColor','white');
end

% get list of Channel numbers from textbox
function edit10_Callback(hObject, eventdata, handles)
global channels;
global num_channels
channels = str2num(get(hObject,'String'));
for ch = 1:num_channels % Update plot titles
    figure(2);
    subplot(2,num_channels/2,ch);
    title(['Channel ' num2str(channels(ch))]);
    figure(3);
    subplot(2,num_channels/2,ch);
    title(['Channel ' num2str(channels(ch))]);
end

% set list of channel numbers to default
function edit10_CreateFcn(hObject, eventdata, handles)
global channels;
```

```
set(hObject,'String',num2str(channels));
%num_channels = length(channels);

if ispc && isequal(get(hObject,'BackgroundColor'),
get(0,'defaultUicontrolBackgroundColor'))
    set(hObject,'BackgroundColor','white');
end

% get file name from text box
function edit11_Callback(hObject, eventdata, handles)
global filename;
filename = (get(hObject,'String'));

% set default file name
function edit11_CreateFcn(hObject, eventdata, handles)
global filename;
set(hObject,'String',filename);
if ispc && isequal(get(hObject,'BackgroundColor'),
get(0,'defaultUicontrolBackgroundColor'))
    set(hObject,'BackgroundColor','white');
end

function edit13_Callback(hObject, eventdata, handles)
global qt_growth;
qt_growth = str2num(get(hObject,'String'));


% set quiet time to text box
function edit13_CreateFcn(hObject, ~, handles)
global qt_growth;
set(hObject, 'String',num2str(qt_growth))
if ispc && isequal(get(hObject,'BackgroundColor'),
get(0,'defaultUicontrolBackgroundColor'))
    set(hObject,'BackgroundColor','white');
end



function edit14_Callback(hObject, eventdata, handles)
global outlier_thresh;
outlier_thresh = str2num(get(hObject,'String'));


% set quiet time to text box
function edit14_CreateFcn(hObject, ~, handles)
global outlier_thresh;
set(hObject, 'String',num2str(outlier_thresh))
if ispc && isequal(get(hObject,'BackgroundColor'),
get(0,'defaultUicontrolBackgroundColor'))
    set(hObject,'BackgroundColor','white');
end


% --- Executes on button press in checkbox1.
```

```
function checkbox1_Callback(hObject, eventdata, handles)

% Execute mode change based on selection
function uipanel1_SelectionChangeFcn(hObject, eventdata, handles)
global mode;
global num_channels;
global baseline;
global exp_data;
global cycle;
global filename;
global channels;
global growth_start;
global temp_growth_mode;
global fh_sens;
curr_mode =  get(hObject,'String');
if strcmp(curr_mode,'Control')
    mode = ones(num_channels,1);

    for ch = 1:num_channels % calculate the baseline for every
channel
        baseline_cond = mean(exp_data(ch,(exp_data(ch,:,6) ==
5),7));
        if baseline_cond~=0  % If baseline set, replot control data
            f = fopen([filename num2str(channels(ch)) '-cond-
proc.txt'],'a');
            for c = 1:cycle-1

%fprintf(f,'%d\t%d\t%d\n',exp_data(ch,c,1),exp_data(ch,c,8),
exp_data(ch,c,6));

fprintf(f,'%d\t%d\t%d\t%d\n',exp_data(ch,c,1),(exp_data(ch,c,7)-
baseline_cond)/baseline_cond, exp_data(ch,c,6),fh_sens);
            end
            fclose(f);
        end
    end
elseif strcmp(curr_mode,'Seeding') % Calculate baseline
    mode = 2 * ones(num_channels,1);
    for ch = 1:num_channels % calculate the baseline for every
channel
        baseline(ch) = mean(exp_data(ch,(exp_data(ch,:,6) == 1),7));
        if baseline (ch)~=0  % If baseline set, replot control data
            figure(3);
            subplot(2,num_channels/2,ch);
            hold on; % control
            plot(exp_data(ch,(exp_data(ch,:,6) ==
1),1),(exp_data(ch,(exp_data(ch,:,6) == 1),7)-
baseline(ch))/baseline(ch),'ok','MarkerSize',4,'MarkerFaceColor','k'
);
            hold off;
            drawnow

            f = fopen([filename num2str(channels(ch)) '-
proc.txt'],'a');
            start_cycle = sum(exp_data(ch,:,6) == 5)+1; %% skip the
conditioning cycles
```

```
            %start_cycle = max(1,start_cycle); % ensure start cycle
is at least 1

            for c = start_cycle:cycle-1
                exp_data(ch,c,8) = (exp_data(ch,c,7)-
baseline(ch))/baseline(ch);

fprintf(f,'%d\t%d\t%d\t%d\n',exp_data(ch,c,1),exp_data(ch,c,8),
exp_data(ch,c,6),fh_sens);

%fprintf('%d\t%d\t%d\n',exp_data(ch,c,1),(exp_data(ch,c,4)-
baseline(ch))/baseline(ch), exp_data(ch,c,6));
            end
            fclose(f);
        end
    end

elseif strcmp(curr_mode, 'Growth/Sensing/BETreatment')
    temp_growth_mode = ones(num_channels,1);
    growth_start = clock;
    mode = 6 * ones(num_channels,1);
elseif strcmp(curr_mode, 'Conditioning')
    mode = 5 * ones(num_channels,1);
elseif strcmp(curr_mode, 'Growth')
    mode = 6 * ones(num_channels,1);
end



% --- Executes on button press in pushbutton2. ---- %GENERATE
FIGURES
function pushbutton2_Callback(hObject, eventdata, handles)
global baseline;
global num_channels;
global exp_data;
global filename;
global channels;
global num_outliers;
global num_outliers_cond;
global sens_thresh;
global treat_thresh;
% hObject    handle to pushbutton2 (see GCBO)
% eventdata  reserved - to be defined in a future version of MATLAB
% handles    structure with handles and user data (see GUIDATA)

% Generate the outlier reports
    outlier_report = fopen([filename '_outliers.txt'],'w'); %
Overwrite last report
    fprintf(outlier_report,'Conditioning Outliers (per channel): ');
    fprintf(outlier_report,'%d\t',num_outliers_cond);
    fprintf(outlier_report,'\nControl Outliers (per channel): ');
    fprintf(outlier_report,'%d\t',num_outliers);
    fclose(outlier_report);
```

```
for ch = 1:num_channels % calculate the baseline for every channel

    %%%%%%%%%%%%%%%%%%%%%%  PLOT RAW EXP DATA
%%%%%%%%%%%%%%%%%%%%%%%%%%%%%
    mode = 1;
    idx = find(exp_data(ch,:,6) == mode,1,'first'); % Find start
time of experiment
    if idx > 0
        exp_start_time = exp_data(ch,idx,1);
    else
        exp_start_time = 0;
    end

    fig = figure();
    hold on;
    mode = 1;
    plot(exp_data(ch,(exp_data(ch,:,6) == mode),1)-
exp_start_time,exp_data(ch,(exp_data(ch,:,6) ==
mode),4),'ok','MarkerSize',4,'MarkerFaceColor','k');
    mode = 2;
    plot(exp_data(ch,(exp_data(ch,:,6) == mode),1)-
exp_start_time,exp_data(ch,(exp_data(ch,:,6) ==
mode),4),'om','MarkerSize',4,'MarkerFaceColor','m');
    mode = 3;
    plot(exp_data(ch,(exp_data(ch,:,6) == mode),1)-
exp_start_time,exp_data(ch,(exp_data(ch,:,6) ==
mode),4),'ob','MarkerSize',4,'MarkerFaceColor','b');
    mode = 4;
    plot(exp_data(ch,(exp_data(ch,:,6) == mode),1)-
exp_start_time,exp_data(ch,(exp_data(ch,:,6) ==
mode),4),'or','MarkerSize',4,'MarkerFaceColor','r');
    %mode = 5; % do not plot conditioning data
    %plot(exp_data(ch,(exp_data(ch,:,6) ==
mode),1),exp_data(ch,(exp_data(ch,:,6) ==
mode),4),'ok','MarkerSize',4,'MarkerFaceColor','k');
    mode = 6;
    plot(exp_data(ch,(exp_data(ch,:,6) == mode),1)-
exp_start_time,exp_data(ch,(exp_data(ch,:,6) ==
mode),4),'og','MarkerSize',4,'MarkerFaceColor','g');

    title(['Ch ' num2str(channels(ch)) ' - Raw |Z|'],
'FontSize',20,'FontWeight','bold');
    xlabel ('Time (hrs)', 'FontSize',20,'FontWeight','bold');
    ylabel ('|Z| (ohms)', 'FontSize',20,'FontWeight','bold');
    set(gca,'FontSize',16,'FontWeight','bold')
    graphname = strcat(filename,'_rawZ_',int2str(channels(ch)));
    print (fig, '-dpng', '-r300',graphname);
    strcat(graphname,'.fig')
    savefig(strcat(graphname,'.fig'))
    hold off;

    %%%%%%%%%%%%%%%%%%%%%%  PLOT NOOUTLIER EXP DATA
%%%%%%%%%%%%%%%%%%%%%%%%%%%%%
    fig = figure();
    hold on;
    mode = 1;
```

```
    plot(exp_data(ch,(exp_data(ch,:,6) == mode),1)-
exp_start_time,exp_data(ch,(exp_data(ch,:,6) ==
mode),7),'ok','MarkerSize',4,'MarkerFaceColor','k');
    mode = 2;
    plot(exp_data(ch,(exp_data(ch,:,6) == mode),1)-
exp_start_time,exp_data(ch,(exp_data(ch,:,6) ==
mode),7),'om','MarkerSize',4,'MarkerFaceColor','m');
    mode = 3;
    plot(exp_data(ch,(exp_data(ch,:,6) == mode),1)-
exp_start_time,exp_data(ch,(exp_data(ch,:,6) ==
mode),7),'ob','MarkerSize',4,'MarkerFaceColor','b');
    mode = 4;
    plot(exp_data(ch,(exp_data(ch,:,6) == mode),1)-
exp_start_time,exp_data(ch,(exp_data(ch,:,6) ==
mode),7),'or','MarkerSize',4,'MarkerFaceColor','r');
    %mode = 5;% do not plot conditioning data
    %plot(exp_data(ch,(exp_data(ch,:,6) ==
mode),1),exp_data(ch,(exp_data(ch,:,6) ==
mode),7),'ok','MarkerSize',4,'MarkerFaceColor','k');
    mode = 6;
    plot(exp_data(ch,(exp_data(ch,:,6) == mode),1)-
exp_start_time,exp_data(ch,(exp_data(ch,:,6) ==
mode),7),'og','MarkerSize',4,'MarkerFaceColor','g');

    title(['Ch ' num2str(channels(ch)) ' - |Z| [No Outliers]'],
'FontSize',20,'FontWeight','bold');
    xlabel ('Time (hrs)', 'FontSize',20,'FontWeight','bold');
    ylabel ('|Z| (ohms)', 'FontSize',20,'FontWeight','bold');
    set(gca,'FontSize',16,'FontWeight','bold')
    graphname =
strcat(filename,'_noOutliersZ_',int2str(channels(ch)));
    print (fig, '-dpng', '-r300',graphname);
    savefig(strcat(graphname,'.fig'))
    hold off;

    if baseline (ch)~=0  % If baseline set, replot control data
        fig = figure();
        hold on;
        mode = 1;
        plot(exp_data(ch,(exp_data(ch,:,6) == mode),1)-
exp_start_time,(exp_data(ch,(exp_data(ch,:,6) == mode),7)-
baseline(ch))/baseline(ch),'ok','MarkerSize',4,'MarkerFaceColor','k'
);
        mode = 2;
        plot(exp_data(ch,(exp_data(ch,:,6) == mode),1)-
exp_start_time,(exp_data(ch,(exp_data(ch,:,6) == mode),7)-
baseline(ch))/baseline(ch),'om','MarkerSize',4,'MarkerFaceColor','m'
);
        mode = 3;
        plot(exp_data(ch,(exp_data(ch,:,6) == mode),1)-
exp_start_time,(exp_data(ch,(exp_data(ch,:,6) == mode),7)-
baseline(ch))/baseline(ch),'ob','MarkerSize',4,'MarkerFaceColor','b'
);
        mode = 4;
        plot(exp_data(ch,(exp_data(ch,:,6) == mode),1)-
exp_start_time,(exp_data(ch,(exp_data(ch,:,6) == mode),7)-
```

```
baseline(ch))/baseline(ch),'or','MarkerSize',4,'MarkerFaceColor','r'
);
        %mode = 5; % do not plot exp data
        %plot(exp_data(ch,(exp_data(ch,:,6) ==
mode),1),(exp_data(ch,(exp_data(ch,:,6) == mode),4)-
baseline(ch))/baseline(ch),'ok','MarkerSize',4,'MarkerFaceColor','k'
);
        mode = 6;
        plot(exp_data(ch,(exp_data(ch,:,6) == mode),1)-
exp_start_time,(exp_data(ch,(exp_data(ch,:,6) == mode),7)-
baseline(ch))/baseline(ch),'og','MarkerSize',4,'MarkerFaceColor','g'
);

        title(['Ch ' num2str(channels(ch)) ' - Change in |Z|'],
'FontSize',20,'FontWeight','bold');
        xlabel ('Time (hrs)', 'FontSize',20,'FontWeight','bold');
        ylabel ('(|Z|-|Z|_{LB Baseline}) / |Z|_{LB Baseline}',
'FontSize',20,'FontWeight','bold');
        set(gca,'FontSize',16,'FontWeight','bold')

        line1 = refline([0 sens_thresh/100]);
        set(line1,'LineStyle',':', 'Color', 'k', 'LineWidth', 2);
        line2 = refline([0 treat_thresh/100]);
        set(line2,'LineStyle',':', 'Color', 'k', 'LineWidth', 2);

        graphname =
strcat(filename,'_changeZ_',int2str(channels(ch)));
        print (fig, '-dpng', '-r300',graphname);
        savefig(strcat(graphname,'.fig'))
        hold off;
        %clf(4)
    end

    %%%%%%%%%%%%%%%%%%%%%% PLOT BASELINE COND DATA
%%%%%%%%%%%%%%%%%%%%%%%%%%%%
    baseline_cond = mean(exp_data(ch,(exp_data(ch,:,6) == 5),7));
    if baseline_cond ~= 0
        fig = figure();
        hold on;
        mode = 5;
        plot(exp_data(ch,(exp_data(ch,:,6) ==
mode),1),(exp_data(ch,(exp_data(ch,:,6) == mode),7)-
baseline_cond)/baseline_cond,'ok','MarkerSize',4,'MarkerFaceColor','
w');

        title(['Ch ' num2str(channels(ch)) ' - Conditioning - Change
in |Z|'], 'FontSize',20,'FontWeight','bold');
        xlabel ('Time (hrs)', 'FontSize',20,'FontWeight','bold');
        ylabel ('(|Z|-|Z|_{LB Baseline}) / |Z|_{LB Baseline}',
'FontSize',20,'FontWeight','bold');
        set(gca,'FontSize',16,'FontWeight','bold')
        graphname =
strcat(filename,'_cond_changeZ_',int2str(channels(ch)));
        print (fig, '-dpng', '-r300',graphname);
        savefig(strcat(graphname,'.fig'))
        hold off;
```

```
    end

    %%%%%%%%%%%%%%%%%%%%%%% PLOT NOOUTLIER COND DATA
%%%%%%%%%%%%%%%%%%%%%%%%%%%%
    fig = figure();
    hold on;
    mode = 5;
    plot(exp_data(ch,(exp_data(ch,:,6) ==
mode),1),exp_data(ch,(exp_data(ch,:,6) ==
mode),7),'ok','MarkerSize',4,'MarkerFaceColor','w');

    title(['Ch ' num2str(channels(ch)) ' - Conditioning - |Z| [No
outliers]'], 'FontSize',20,'FontWeight','bold');
    xlabel ('Time (hrs)', 'FontSize',20,'FontWeight','bold');
    ylabel ('|Z| (ohms)', 'FontSize',20,'FontWeight','bold');
    set(gca,'FontSize',16,'FontWeight','bold')
    graphname =
strcat(filename,'_cond_noOutliersZ_',int2str(channels(ch)));
    print (fig, '-dpng', '-r300',graphname);
    savefig(strcat(graphname,'.fig'))
    hold off;


        %%%%%%%%%%%%%%%%%%%%%% PLOT RAW COND DATA
%%%%%%%%%%%%%%%%%%%%%%%%%%%
    fig = figure();
    hold on;
    mode = 5;
    plot(exp_data(ch,(exp_data(ch,:,6) ==
mode),1),exp_data(ch,(exp_data(ch,:,6) ==
mode),4),'ok','MarkerSize',4,'MarkerFaceColor','w');

    title(['Ch ' num2str(channels(ch)) ' - Conditioning - Raw |Z|
'], 'FontSize',20,'FontWeight','bold');
    xlabel ('Time (hrs)', 'FontSize',20,'FontWeight','bold');
    ylabel ('|Z| (ohms)', 'FontSize',20,'FontWeight','bold');
    set(gca,'FontSize',16,'FontWeight','bold')
    graphname =
strcat(filename,'_cond_rawZ_',int2str(channels(ch)));
    print (fig, '-dpng', '-r300',graphname);
    savefig(strcat(graphname,'.fig'))
    hold off;

    fprintf('Graphs for channel %d generated.\n', channels(ch));
    % save figure
    % clear figure
end
fprintf('Finished generating graphs.\n');

% Growth (hours)
function edit12_Callback(hObject, eventdata, handles)
global growth_hours;
growth_hours = str2num(get(hObject,'String'));

function edit12_CreateFcn(hObject, eventdata, handles)
```

```
global growth_hours;
set(hObject, 'String',num2str(growth_hours))
if ispc && isequal(get(hObject,'BackgroundColor'),
get(0,'defaultUicontrolBackgroundColor'))
    set(hObject,'BackgroundColor','white');
end

function edit15_Callback(hObject, eventdata, handles)
global qt_treat;
qt_treat = str2num(get(hObject,'String'));


% set quiet time to text box
function edit15_CreateFcn(hObject, ~, handles)
global qt_treat;
set(hObject, 'String',num2str(qt_treat))
if ispc && isequal(get(hObject,'BackgroundColor'),
get(0,'defaultUicontrolBackgroundColor'))
    set(hObject,'BackgroundColor','white');
end


function run_Experiment()
global run_exp;
global num_channels;
global channels;
global tech;
global mode;
global exp_data;
global qt;
global cycle;
global fileID;
global fileID_processed;
global fileID_condition;
global ei_sens;
global fl_sens;
global fh_sens;
global amp_sens;
global ei_treat;
global fl_treat;
global fh_treat;
global amp_treat;
global start_time;
global treat_cycles;
global sens_thresh;
global treat_thresh;
global baseline;
global filename;
global num_outliers;
global num_outliers_cond;
global outlier_thresh;
global growth_start;
global growth_hours;
global temp_growth_mode;
global qt_growth;
global qt_treat;
```

```
global M;
% Open files for writing
for ch = 1:num_channels
    fileID(ch) = fopen([filename num2str(channels(ch)) '.txt'],'a');
    fileID_processed(ch) = fopen([filename num2str(channels(ch)) '-
proc.txt'],'a');
    fileID_condition(ch) = fopen([filename num2str(channels(ch)) '-
cond.txt'],'a');
end

while (run_exp == 1)
    for ch = 1:num_channels
        %Set CHI parameters
        calllib('libec', 'CHI_set_mch', channels(ch)-1);
        calllib('libec', 'CHI_setTechnique', tech); % 14 - impedance
sensing

        if mode (ch)== 4 %treatment
            n = 50;
            disp 'treatment'
            calllib('libec', 'CHI_setParameter', 'm_iP1M', n)
            calllib('libec', 'CHI_setParameter', 'm_iP100K', n)
            calllib('libec', 'CHI_setParameter', 'm_iP10K', n)

            calllib('libec', 'CHI_setParameter', 'm_ei', ei_treat);
            calllib('libec', 'CHI_setParameter', 'm_fl', fl_treat);
            calllib('libec', 'CHI_setParameter', 'm_fh', fh_treat);
            calllib('libec', 'CHI_setParameter', 'm_amp',
amp_treat);
            calllib('libec', 'CHI_runExperiment'); % non-blocking

            %n = 50; %
            x = zeros(n, 1);
            y = zeros(n, 1);
            y2 = zeros(n, 1);
            py2 = libpointer('singlePtr',y2);

            px= libpointer('singlePtr', x);
            py= libpointer('singlePtr', y);

            while calllib('libec', 'CHI_experimentIsRunning')
               disp 'Treating...' % <- call CHI_getExperimentData()
in real time
               pause(5)
            end
            calllib('libec', 'CHI_getExperimentData_2channel', px,
py, py2, n)
            px.value
            py.value
            py2.value
        end

       % if mode(ch) == 1 || mode(ch) == 2 || mode(ch) == 3 ||
mode(ch) == 5 ||mode(ch) == 6%sensing
        n = 25;
```

```
        disp 'measuring at sensing frequency'
%         calllib('libec', 'CHI_setParameter', 'm_iP1M', n)
%         calllib('libec', 'CHI_setParameter', 'm_iP100K', n)
%         calllib('libec', 'CHI_setParameter', 'm_iP10K', n)

        calllib('libec', 'CHI_setParameter', 'm_ei', ei_sens);
        calllib('libec', 'CHI_setParameter', 'm_fl', fl_sens);
        calllib('libec', 'CHI_setParameter', 'm_fh', fh_sens);
        calllib('libec', 'CHI_setParameter', 'm_amp', amp_sens);

        %Collect data point
        calllib('libec', 'CHI_runExperiment'); % non-blocking

        %n = 1; % should be a single data point b/c only one
frequency
        x = zeros(n, 1);
        y = zeros(n, 1);
        y2 = zeros(n, 1);
        py2 = libpointer('singlePtr',y2);

        px= libpointer('singlePtr', x);
        py= libpointer('singlePtr', y);

        while calllib('libec', 'CHI_experimentIsRunning')
           disp 'Sensing...' % <- call CHI_getExperimentData() in
real time
           pause(5)
        end
        calllib('libec', 'CHI_getExperimentData_2channel', px, py,
py2, n)
        px.value
        py.value
        py2.value
        actual_freq = px.value(12);
        exp_data(ch,cycle,2) = py.value(12); %Re Z
        exp_data(ch,cycle,3) = py2.value(12); %Im Z

        current_time = clock;
        exp_data(ch,cycle,1) = etime(current_time, start_time)/3600;
% time elapsed since start of experiment
        exp_data(ch,cycle,4) = norm([exp_data(ch,cycle,2)
exp_data(ch,cycle,3)]); %|Z|
        if (mode(ch) == 3)
           exp_data(ch,cycle,4) = exp_data(ch,cycle,4);
        end
        exp_data(ch,cycle,5) =
angle(exp_data(ch,cycle,2)+1i*exp_data(ch,cycle,3)); % Phase
        exp_data(ch,cycle,6) = mode(ch); % Mode
        %exp_data(ch,cycle,7) = px.value;

        %%%%%%%%%%%%%%%%%%%%%% Test Code
%         measure = M(cycle,2);
%         if mode(ch) == 3
%             measure = measure * 1.5;
%         end
```

```
%
%         exp_data(ch,cycle,1) = M(cycle,1);
%         exp_data(ch,cycle,2) = measure;
%         exp_data(ch,cycle,3) = measure;
%         exp_data(ch,cycle,4) = measure;
%         exp_data(ch,cycle,5) = measure;
%         exp_data(ch,cycle,6) = mode(ch);
        %%%%%%%%%%%%%%%%%%%%%%%%%%%%%%%%


        % Outlier detection - compare |Z| to previous cycle, if same
mode
        ref_value = 0;
        if cycle >= 6
            ref_value = mean (exp_data(ch,cycle-5:cycle-1,7));
        end

        if ref_value > 0 && sum(exp_data(ch,cycle-5:cycle,6)) == 5*6
&& abs((exp_data(ch,cycle,4)-ref_value)/ref_value*100) >
outlier_thresh
            exp_data(ch,cycle,7) = exp_data(ch,cycle-1,7); % outlier
- replace with last data
            num_outliers_cond(ch) = num_outliers_cond(ch)+1;
            fprintf('Outlier Detected. Total number of outliers
removed for Ch %d: %d\n',channels(ch),num_outliers_cond(ch));
        elseif ref_value > 0 && sum(exp_data(ch,cycle-5:cycle,6)) ==
1*6 && abs((exp_data(ch,cycle,4)-ref_value)/ref_value*100) >
outlier_thresh
            exp_data(ch,cycle,7) = exp_data(ch,cycle-1,7); % outlier
- replace with last data
            num_outliers(ch) = num_outliers(ch)+1;
            fprintf('Outlier Detected. Total number of outliers
removed for Ch %d: %d\n',channels(ch),num_outliers(ch));
        else
            exp_data(ch,cycle,7) = exp_data(ch,cycle,4); % Not an
outlier - current data
        end

        figure(2);
        subplot(2,num_channels/2,ch);
        hold on;
        % Plot data point in correct color, depending on mode
        if mode(ch)== 1

plot(exp_data(ch,cycle,1),exp_data(ch,cycle,4),'ok','MarkerSize',4,'
MarkerFaceColor','k'); % Control - black
        elseif mode (ch) == 2

plot(exp_data(ch,cycle,1),exp_data(ch,cycle,4),'om','MarkerSize',4,'
MarkerFaceColor','m'); % Seeding - blue
        elseif mode(ch) == 3

plot(exp_data(ch,cycle,1),exp_data(ch,cycle,4),'ob','MarkerSize',4,'
MarkerFaceColor','b'); % Sensing - green
        elseif mode(ch) == 4
```

```
plot(exp_data(ch,cycle,1),exp_data(ch,cycle,4),'or','MarkerSize',4,'
MarkerFaceColor','r'); % Treatment - red
        elseif mode(ch) == 5

plot(exp_data(ch,cycle,1),exp_data(ch,cycle,4),'ok','MarkerSize',4,'
MarkerFaceColor','w'); % Conditioning
        elseif mode(ch) == 6

plot(exp_data(ch,cycle,1),exp_data(ch,cycle,4),'og','MarkerSize',4,'
MarkerFaceColor','g'); % Growth
        end
        hold off;
        drawnow

        % If baseline has been set, plot channels relative to
baseline in
        % plot 3
        if baseline(ch) ~= 0
            exp_data(ch,cycle,8) = (exp_data(ch,cycle,7)-
baseline(ch))/baseline(ch);

            figure(3);
            subplot(2,num_channels/2,ch);

            hold on;
            if mode(ch)== 1

plot(exp_data(ch,cycle,1),exp_data(ch,cycle,8),'ok','MarkerSize',4,'
MarkerFaceColor','k');
            elseif mode (ch) == 2

plot(exp_data(ch,cycle,1),exp_data(ch,cycle,8),'om','MarkerSize',4,'
MarkerFaceColor','m');
            elseif mode(ch) == 3 % sensing

plot(exp_data(ch,cycle,1),exp_data(ch,cycle,8),'ob','MarkerSize',4,'
MarkerFaceColor','b');

            elseif mode(ch) == 4 %&& fl_sens == fl_treat

plot(exp_data(ch,cycle,1),exp_data(ch,cycle,8),'or','MarkerSize',4,'
MarkerFaceColor','r');
                % do not plot conditioning
            elseif mode(ch) == 6

plot(exp_data(ch,cycle,1),exp_data(ch,cycle,8),'og','MarkerSize',4,'
MarkerFaceColor','g'); % Growth
            end
            hold off;

            if mod(cycle,20) == 0 % Replot baseline every 20 cycles
                hold on;
                line1 = refline([0 sens_thresh/100]);
                set(line1,'LineStyle',':', 'Color', 'k',
'LineWidth', 2);
```

```
                line2 = refline([0 treat_thresh/100]);
                set(line2,'LineStyle',':', 'Color', 'k',
'LineWidth', 2);
                hold off;
            end
            drawnow
            % Generate processed file containing: Time, Relative
Impedance, Mode


fprintf(fileID_processed(ch),'%d\t%d\t%d\t%d\n',exp_data(ch,cycle,1)
,exp_data(ch,cycle,8), actual_freq);
        end

        % Write data to file
        if mode(ch) == 5

fprintf(fileID_condition(ch),'%d\t%d\t%d\t%d\t%d\t%d\t%d\t%d\n',exp_
data(ch,cycle,1:5),exp_data(ch,cycle,7),exp_data(ch,cycle,6),actual_
freq);
        else

fprintf(fileID(ch),'%d\t%d\t%d\t%d\t%d\t%d\t%d\t%d\n',exp_data(ch,cy
cle,1:5),exp_data(ch,cycle,7),exp_data(ch,cycle,6),actual_freq);
        end
        now = clock;
        % Logic for changing modes sensing/treatment
        % if in growth mode & past 5 cycles are also growth

         if treat_cycles(ch)>0 && mode(ch) == 3 && baseline(ch) ~= 0
&& cycle >= 6 && sum(exp_data(ch,cycle-4:cycle,6)) == 3*5
            % Use below if only + change threshold range should
trigger treatment
            % avg = (double(mean(exp_data(ch,cycle-4:cycle,4))) -
baseline(ch))/baseline(ch);

            % Use below if both +/- change threshold range should
trigger treatment
             avg = abs((double(mean(exp_data(ch,cycle-4:cycle,4)))
- baseline(ch))/baseline(ch));

            % Use below if only - change threshold range should
trigger treatment
            % avg = -((double(mean(exp_data(ch,cycle-4:cycle,4))) -
baseline(ch))/baseline(ch));

            if exp_data(ch,cycle-5,6)== 3 && avg * 100 >
treat_thresh %if not previously in treatment, must be above
treat_tresh
                mode(ch) = 4 % go to treatment from sensing
            elseif exp_data(ch,cycle-5,6)== 4 && avg * 100 >
sens_thresh %if previously in treatment mode (before 5 sensing
samples), must be above sens_thresh
                mode(ch) = 4 % go back to treatment after 5 samples
in sensing
            end
```

```
        elseif mode(ch) == 4 && cycle >= treat_cycles(ch) &&
sum(exp_data(ch,cycle -(treat_cycles(ch)-1):cycle,6)) ==
4*treat_cycles(ch)
            mode(ch) = 3
        elseif mode(ch) == 6 && temp_growth_mode(ch) == 1 &&
abs(etime(growth_start,now))/3600 >= growth_hours % switch from
growth to treatment
            mode(ch) = 3
        end

        if ch == num_channels && (mode(ch) == 6 || mode(ch) == 2) %
seeding/growth
            fprintf('Quiet time started\n');
            pause(qt_growth);
        elseif ch == num_channels && (mode(ch) == 3 || mode(ch)==
4) % at least 1 channel is in treatment
            fprintf('Quiet time started\n');
            pause(qt_treat);
        elseif ch == num_channels % control/sensing
           fprintf('Quiet time started\n');
           pause(qt);
        else
           pause(1);
        end
    end
    cycle = cycle + 1; % increment cycle
    fprintf('Quiet time complete\n');

end

% close data files
for ch = 1: num_channels
   fclose(fileID(ch));
   fclose(fileID_processed(ch));
   fclose(fileID_condition(ch));
end
fprintf('Paused. Select next mode now.\n');
```

Smoothing Function

```
%THIS CODE EXTRACTS DATA FROM A .FIG FILE AND PERFORMS MOVING
AVERAGE
%SMOOTHING WITH THE DEFAULT SPAN OF 5
filename = exp_data_ch__cond_changeZ_4'; % Enter name (no extension)
of .fig whose data you want to extract
filename2 = strcat(filename,'.fig');
open(filename2);

% Extract data from .fig file
h = gcf; %current figure handle
axesObjs = get(h, 'Children');  %axes handles
dataObjs = get(axesObjs, 'Children'); %handles to low-level graphics
objects in axes
objTypes = get(dataObjs, 'Type');  %type of low-level graphics
object
xdata = get(dataObjs, 'XData');  %data from low-level grahics
objects
ydata = get(dataObjs, 'YData');
zdata = get(dataObjs, 'ZData');

%Perform moving average smoothing and save as new plot
yy = smooth(ydata);
plot(xdata, yy, 'k', 'LineWidth', 2.0)
graphname = strcat(filename,'_smooth');
print ('-dpng', '-r300',graphname);
```

Bibliography

1. Costerton, J. W., Stewart, P. S., and Greenberg, E. P., Bacterial Biofilms: A Common Cause of Persistent Infections, *Science*, 1999, **284** (5418), p: 1318.
2. Høiby, N., Ciofu, O., Johansen, H. K., Song, Z. J., Moser, C., Jensen, P. Ø., Molin, S., Givskov, M., Tolker-Nielsen, T., and Bjarnsholt, T., The Clinical Impact of Bacterial Biofilms, *International Journal of Oral Science*, 2011, **3** (2), p: 55.
3. Potera, C., Forging a Link between Biofilms and Disease, *Science*, 1999, **283** (5409), p: 1837.
4. Fux, C. A., Stoodley, P., Shirtliff, M., and Costerton, J. W., The Functional Resistance of Bacterial Biofilms, in *Antimicrobial Drug Resistance*, 2009, Springer. p: 121.
5. Richards, J. J., and Melander, C., Controlling Bacterial Biofilms, *Chembiochem*, 2009, **10** (14), p: 2287.
6. Anwar, H., Dasgupta, M. K., and Costerton, J. W., Testing the Susceptibility of Bacteria in Biofilms to Antibacterial Agents, *Antimicrobial agents and chemotherapy*, 1990, **34** (11), p: 2043.
7. Olson, M. E., Ceri, H., Morck, D. W., Buret, A. G., and Read, R. R., Biofilm Bacteria: Formation and Comparative Susceptibility to Antibiotics, *Can J Vet Res*, 2002, **66** (2), p: 86.
8. Davies, D., Understanding Biofilm Resistance to Antibacterial Agents, *Nature reviews Drug discovery*, 2003, **2** (2), p: 114.

9. Donlan, R. M., Biofilms and Device-Associated Infections, *Emerg Infect Dis*, 2001, **7** (2), p: 277.

10. Donlan, R. M., Biofilms: Microbial Life on Surfaces, *Emerging Infectious Diseases*, 2002, **8** (9), p: 881.

11. Ceri, H., Olson, M. E., Stremick, C., Read, R. R., Morck, D., and Buret, A., The Calgary Biofilm Device: New Technology for Rapid Determination of Antibiotic Susceptibilities of Bacterial Biofilms, *Journal of Clinical Microbiology*, 1999, **37** (6), p: 1771.

12. Crusz, S. A., Popat, R., Rybtke, M. T., Cámara, M., Givskov, M., Tolker-Nielsen, T., Diggle, S. P., and Williams, P., Bursting the Bubble on Bacterial Biofilms: A Flow Cell Methodology, *Biofouling*, 2012, **28** (8), p: 835.

13. Gilmore, B. F., Hamill, T. M., Jones, D. S., and Gorman, S. P., Validation of the Cdc Biofilm Reactor as a Dynamic Model for Assessment of Encrustation Formation on Urological Device Materials, *Journal of Biomedical Materials Research Part B: Applied Biomaterials*, 2010, **93** (1), p: 128.

14. Williams, D. L., Woodbury, K. L., Haymond, B. S., Parker, A. E., and Bloebaum, R. D., A Modified Cdc Biofilm Reactor to Produce Mature Biofilms on the Surface of Peek Membranes for an in Vivo Animal Model Application, *Current Microbiology*, 2011, **62** (6), p: 1657.

15. Kharazmi, A., Giwercman, B., and Høiby, N., Robbins Device in Biofilm Research, *Methods in enzymology*, 1998, **310**, p: 207.

16. Heydorn, A., Ersbøll, B. K., Hentzer, M., Parsek, M. R., Givskov, M., and Molin, S., Experimental Reproducibility in Flow-Chamber Biofilms, *Microbiology*, 2000, **146** (10), p: 2409.

17. Roeselers, G., Zippel, B., Staal, M., Van Loosdrecht, M., and Muyzer, G., On the Reproducibility of Microcosm Experiments–Different Community Composition in Parallel Phototrophic Biofilm Microcosms, *FEMS microbiology ecology*, 2006, **58** (2), p: 169.

18. Palmer Jr, R. J., and Sternberg, C., Modern Microscopy in Biofilm Research: Confocal Microscopy and Other Approaches, *Current Opinion in Biotechnology*, 1999, **10** (3), p: 263.

19. Hannig, C., Follo, M., Hellwig, E., and Al-Ahmad, A., Visualization of Adherent Micro-Organisms Using Different Techniques, *J Med Microbiol*, 2010, **59** (Pt 1), p: 1.

20. Hong, J., Edel, J. B., and Demello, A. J., Micro-and Nanofluidic Systems for High-Throughput Biological Screening, *Drug Discovery Today*, 2009, **14** (3), p: 134.

21. Yang, W., and Woolley, A. T., Integrated Multiprocess Microfluidic Systems for Automating Analysis, *Journal of the Association for Laboratory Automation*, 2010, **15** (3), p: 198.

22. Craighead, H., Future Lab-on-a-Chip Technologies for Interrogating Individual Molecules, *Nature*, 2006, **442** (7101), p: 387.

23. Dittrich, P. S., and Manz, A., Lab-on-a-Chip: Microfluidics in Drug Discovery, *Nature Reviews Drug Discovery*, 2006, **5** (3), p: 210.

24. Dutse, S. W., and Yusof, N. A., Microfluidics-Based Lab-on-Chip Systems in DNA-Based Biosensing: An Overview, *Sensors*, 2011, **11** (6), p: 5754.

25. Figeys, D., and Pinto, D., Lab-on-a-Chip: A Revolution in Biological and Medical Sciences, *Analytical Chemistry*, 2000, **72** (9), p: 330 A.

26. Ghanim, M., and Abdullah, M., Integrating Amperometric Detection with Electrophoresis Microchip Devices for Biochemical Assays: Recent Developments, *Talanta*, 2011, **85** (1), p: 28.

27. Haeberle, S., and Zengerle, R., Microfluidic Platforms for Lab-on-a-Chip Applications, *Lab on a Chip*, 2007, **7** (9), p: 1094.

28. Jiang, H., Weng, X., and Li, D., Microfluidic Whole-Blood Immunoassays, *Microfluidics and Nanofluidics*, 2011, **10** (5), p: 941.

29. Pollack, M. G., Pamula, V. K., Srinivasan, V., and Eckhardt, A. E., Applications of Electrowetting-Based Digital Microfluidics in Clinical Diagnostics, *Expert Review of Molecular Diagnostics*, 2011, **11** (4), p: 393.

30. Trietsch, S., Hankemeier, T., and Van der Linden, H., Lab-on-a-Chip Technologies for Massive Parallel Data Generation in the Life Sciences: A Review, *Chemometrics and Intelligent Laboratory Systems*, 2011, **108** (1), p: 64.

31. Uhlen, M., and Svahn, H. A., Affinity Reagents for Lab on Chips, *Lab on a Chip*, 2011, **11** (8), p: 1417.

32. Mir, M., Homs, A., and Samitier, J., Integrated Electrochemical DNA Biosensors for Lab−on−a−Chip Devices, *ELECTROPHORESIS*, 2009, **30** (19), p: 3386.

33. Mark, D., Haeberle, S., Roth, G., von Stetten, F., and Zengerle, R., Microfluidic Lab-on-a-Chip Platforms: Requirements, Characteristics and Applications, *Chemical Society Reviews*, 2010, **39** (3), p: 1153.

34. Rodrigues Ribeiro Teles, F. S., Pires de Távora Tavira, L. A., and Pina da Fonseca, L. J., Biosensors as Rapid Diagnostic Tests for Tropical Diseases, *Critical reviews in clinical laboratory sciences*, 2010, **47** (3), p: 139.

35. Rosen, Y., and Gurman, P., Mems and Microfluidics for Diagnostics Devices, *Current pharmaceutical biotechnology*, 2010, **11** (4), p: 366.

36. Lin, C.-C., Wang, J.-H., Wu, H.-W., and Lee, G.-B., Microfluidic Immunoassays, *Journal of the Association for Laboratory Automation*, 2010, **15** (3), p: 253.

37. Focke, M., Kosse, D., Müller, C., Reinecke, H., Zengerle, R., and von Stetten, F., Lab-on-a-Foil: Microfluidics on Thin and Flexible Films, *Lab on a Chip*, 2010, **10** (11), p: 1365.

38. Varghese, S. S., Zhu, Y., Davis, T. J., and Trowell, S. C., Fret for Lab-on-a-Chip Devices—Current Trends and Future Prospects, *Lab on a Chip*, 2010, **10** (11), p: 1355.

39. Liu, K.-K., Wu, R.-G., Chuang, Y.-J., Khoo, H. S., Huang, S.-H., and Tseng, F.-G., Microfluidic Systems for Biosensing, *Sensors*, 2010, **10** (7), p: 6623.

40. Gupta, K., Kim, D.-H., Ellison, D., Smith, C., Kundu, A., Tuan, J., Suh, K.-Y., and Levchenko, A., Lab-on-a-Chip Devices as an Emerging Platform for Stem Cell Biology, *Lab on a Chip*, 2010, **10** (16), p: 2019.

41. Huo, D.-Q., Liu, Z., Hou, C.-J., Yang, J., Luo, X.-G., Fa, H.-B., Dong, J.-L., Zhang, Y.-C., Zhnag, G.-P., and Li, J.-J., Recent Advances on Optical Detection Methods and Techniques for Cell-Based Microfluidic Systems, *Chinese Journal of Analytical Chemistry*, 2010, **38** (9), p: 1357.

42. Wlodkowic, D., and Cooper, J. M., Tumors on Chips: Oncology Meets Microfluidics, *Current opinion in chemical biology*, 2010, **14** (5), p: 556.

43. Simon, E., Biological and Chemical Sensors for Cancer Diagnosis, *Measurement Science and Technology*, 2010, **21** (11), p: 112002.

44. Didar, T. F., and Tabrizian, M., Adhesion Based Detection, Sorting and Enrichment of Cells in Microfluidic Lab-on-Chip Devices, *Lab on a Chip*, 2010, **10** (22), p: 3043.

45. Koev, S., Dykstra, P., Luo, X., Rubloff, G., Bentley, W., Payne, G., and Ghodssi, R., Chitosan: An Integrative Biomaterial for Lab-on-a-Chip Devices, *Lab on a Chip*, 2010, **10** (22), p: 3026.

46. Lim, Y. C., Kouzani, A. Z., and Duan, W., Lab-on-a-Chip: A Component View, *Microsystem Technologies*, 2010, **16** (12), p: 1995.

47. Hrnčiřík, P., and Náhlík, J., Novel Micro-Scale Analytical Devices for on-Line Bioprocess Monitoring: A Review, *Chemical and Biochemical Engineering Quarterly*, 2010, **24** (4), p: 489.

48. Weddemann, A., Albon, C., Auge, A., Wittbracht, F., Hedwig, P., Akemeier, D., Rott, K., Meißner, D., Jutzi, P., and Hütten, A., How to Design Magneto-Based Total Analysis Systems for Biomedical Applications, *Biosensors and Bioelectronics*, 2010, **26** (4), p: 1152.

49. Webster, A., Greenman, J., and Haswell, S. J., Development of Microfluidic Devices for Biomedical and Clinical Application, *Journal of Chemical Technology and Biotechnology*, 2011, **86** (1), p: 10.

50. Mohammed, M.-I., and Desmulliez, M. P., Lab-on-a-Chip Based Immunosensor Principles and Technologies for the Detection of Cardiac Biomarkers: A Review, *Lab on a Chip*, 2011, **11** (4), p: 569.

51. Jang, A., Zou, Z., Lee, K. K., Ahn, C. H., and Bishop, P. L., State-of-the-Art Lab Chip Sensors for Environmental Water Monitoring, *Measurement Science and Technology*, 2011, **22** (3), p: 032001.

52. Sharma, H., Nguyen, D., Chen, A., Lew, V., and Khine, M., Unconventional Low-Cost Fabrication and Patterning Techniques for Point of Care Diagnostics, *Annals of biomedical engineering*, 2011, **39** (4), p: 1313.

53. Wagner, V. E., and Iglewski, B. H., P. Aeruginosa Biofilms in Cf Infection, *Clinical reviews in allergy & immunology*, 2008, **35** (3), p: 124.

54. Bordi, C., and de Bentzmann, S., Hacking into Bacterial Biofilms: A New Therapeutic Challenge, *Annals of intensive care*, 2011, **1** (1), p: 1.

55. Mah, T.-F. C., and O'Toole, G. A., Mechanisms of Biofilm Resistance to Antimicrobial Agents, *Trends in microbiology*, 2001, **9** (1), p: 34.

56. Kumon, H., Tomochika, K. i., Matunaga, T., Ogawa, M., and Ohmori, H., A Sandwich Cup Method for the Penetration Assay of Antimicrobial Agents through Pseudomonas Exopolysaccharides, *Microbiology and immunology*, 1994, **38** (8), p: 615.

57. Bose, S., and Ghosh, A. K., Biofilms: A Challenge to Medical Science, *Journal of Clinical and Diagnostic Research [serial online]*, 2013, **5** (1), p: 127.

58. Walters, M. C., Roe, F., Bugnicourt, A., Franklin, M. J., and Stewart, P. S., Contributions of Antibiotic Penetration, Oxygen Limitation, and Low Metabolic Activity to Tolerance of Pseudomonas Aeruginosa Biofilms to Ciprofloxacin and Tobramycin, *Antimicrobial agents and chemotherapy*, 2003, **47** (1), p: 317.

59. Anderl, J. N., Franklin, M. J., and Stewart, P. S., Role of Antibiotic Penetration Limitation in Klebsiella Pneumoniae Biofilm Resistance to Ampicillin and Ciprofloxacin, *Antimicrobial agents and chemotherapy*, 2000, **44** (7), p: 1818.

60. Anderson, G. G., and O'toole, G. A., Innate and Induced Resistance Mechanisms of Bacterial Biofilms, in *Bacterial Biofilms*, 2008, Springer. p: 85.

61. Wuertz, S., Okabe, S., and Hausner, M., Microbial Communities and Their Interactions in Biofilm Systems: An Overview, *Water Science & Technology*, 2004, **49** (11-12), p: 327.

62. Ghigo, J.-M., Natural Conjugative Plasmids Induce Bacterial Biofilm Development, *Nature*, 2001, **412** (6845), p: 442.

63. Schembri, M. A., Kjærgaard, K., and Klemm, P., Global Gene Expression in Escherichia Coli Biofilms, *Molecular microbiology*, 2003, **48** (1), p: 253.

64. Keren, I., Kaldalu, N., Spoering, A., Wang, Y., and Lewis, K., Persister Cells and Tolerance to Antimicrobials, *FEMS microbiology letters*, 2004, **230** (1), p: 13.

65. Lewis, K., Persister Cells, *Annual review of microbiology*, 2010, **64**, p: 357.

66. Fuqua, W. C., Winans, S. C., and Greenberg, E. P., Quorum Sensing in Bacteria: The Luxr-Luxi Family of Cell Density-Responsive Transcriptional Regulators, *Journal of Bacteriology*, 1994, **176** (2), p: 269.

67. Miller, M. B., and Bassler, B. L., Quorum Sensing in Bacteria, *Annual Reviews in Microbiology*, 2001, **55** (1), p: 165.

68. Waters, C. M., and Bassler, B. L., Quorum Sensing: Cell-to-Cell Communication in Bacteria, *Annual Review of Cell and Developmental Biology*, 2005, **21**, p: 319.

69. Vendeville, A., Winzer, K., Heurlier, K., Tang, C. M., and Hardie, K. R., Making'sense'of Metabolism: Autoinducer-2, Luxs and Pathogenic Bacteria, *Nature Reviews Microbiology*, 2005, **3** (5), p: 383.

70. Roy, V., Adams, B. L., and Bentley, W. E., Developing Next Generation Antimicrobials by Intercepting Ai-2 Mediated Quorum Sensing, *Enzyme and microbial technology*, 2011, **49** (2), p: 113.

71. Sun, J., Daniel, R., Wagner-Döbler, I., and Zeng, A.-P., Is Autoinducer-2 a Universal Signal for Interspecies Communication: A Comparative Genomic and Phylogenetic Analysis of the Synthesis and Signal Transduction Pathways, *BMC Evolutionary Biology*, 2004, **4** (1), p: 36.

72. Hooshangi, S., and Bentley, W. E., From Unicellular Properties to Multicellular Behavior: Bacteria Quorum Sensing Circuitry and Applications, *Current Opinion in Biotechnology*, 2008, **19** (6), p: 550.

73. Lowery, C. A., Park, J., Kaufmann, G. F., and Janda, K. D., An Unexpected Switch in the Modulation of Ai-2-Based Quorum Sensing Discovered through Synthetic 4,5-Dihydroxy-2,3-Pentanedione Analogues, *Journal of the American Chemical Society*, 2008, **130** (29), p: 9200.

74. Surette, M. G., Miller, M. B., and Bassler, B. L., Quorum Sensing in Escherichia Coli, Salmonella Typhimurium, and Vibrio Harveyi: A New Family of Genes Responsible for Autoinducer Production, *Proceedings of the National Academy of Sciences*, 1999, **96** (4), p: 1639.

75. Wang, L., Hashimoto, Y., Tsao, C.-Y., Valdes, J. J., and Bentley, W. E., Cyclic Amp (Camp) and Camp Receptor Protein Influence Both Synthesis and Uptake of Extracellular Autoinducer 2 in Escherichia Coli, *Journal of Bacteriology*, 2005, **187** (6), p: 2066.

76. Xavier, K. B., and Bassler, B. L., Regulation of Uptake and Processing of the Quorum-Sensing Autoinducer Ai-2 in Escherichia Coli, *Journal of Bacteriology*, 2005, **187** (1), p: 238.

77. Li, J., Attila, C., Wang, L., Wood, T. K., Valdes, J. J., and Bentley, W. E., Quorum Sensing in Escherichia Coli Is Signaled by Ai-2/Lsrr: Effects on Small Rna and Biofilm Architecture, *Journal of Bacteriology*, 2007, **189** (16), p: 6011.

78. Barrios, A. F. G., Zuo, R., Hashimoto, Y., Yang, L., Bentley, W. E., and Wood, T. K., Autoinducer 2 Controls Biofilm Formation in Escherichia Coli through a Novel Motility Quorum-Sensing Regulator (Mqsr, B3022), *Journal of Bacteriology*, 2006, **188** (1), p: 305.

79. Herzberg, M., Kaye, I. K., Peti, W., and Wood, T. K., Ydgg (Tqsa) Controls Biofilm Formation in Escherichia Coli K-12 through Autoinducer 2 Transport, *Journal of Bacteriology*, 2006, **188** (2), p: 587.

80. Beloin, C., Roux, A., and Ghigo, J.-M., Escherichia Coli Biofilms, in *Bacterial Biofilms*, 2008, Springer. p: 249.

81. Davies, D. G., Parsek, M. R., Pearson, J. P., Iglewski, B. H., Costerton, J., and Greenberg, E., The Involvement of Cell-to-Cell Signals in the Development of a Bacterial Biofilm, *Science*, 1998, **280** (5361), p: 295.

82. Duan, K., Dammel, C., Stein, J., Rabin, H., and Surette, M. G., Modulation of Pseudomonas Aeruginosa Gene Expression by Host Microflora through Interspecies Communication, *Molecular microbiology*, 2003, **50** (5), p: 1477.

83. Guo, M., Gamby, S., Zheng, Y., and Sintim, H. O., Small Molecule Inhibitors of Ai-2 Signaling in Bacteria: State-of-the-Art and Future Perspectives for Anti-Quorum Sensing Agents, *International journal of molecular sciences*, 2013, **14** (9), p: 17694.

84. Rasmussen, T. B., and Givskov, M., Quorum Sensing Inhibitors: A Bargain of Effects, *Microbiology*, 2006, **152** (4), p: 895.

85. Rasmussen, T. B., and Givskov, M., Quorum-Sensing Inhibitors as Anti-Pathogenic Drugs, *International Journal of Medical Microbiology*, 2006, **296** (2–3), p: 149.

86. Busscher, H. J., and van Der Mei, R. B. H. C., Initial Microbial Adhesion Is a Determinant for the Strength of Biofilm Adhesion, *FEMS Microbiology Letters*, 1995, **128** (3), p: 229.

87. Zhao, L., Chu, P. K., Zhang, Y., and Wu, Z., Antibacterial Coatings on Titanium Implants, *Journal of Biomedical Materials Research Part B: Applied Biomaterials*, 2009, **91B** (1), p: 470.

88. Hetrick, E. M., and Schoenfisch, M. H., Reducing Implant-Related Infections: Active Release Strategies, *Chemical Society Reviews*, 2006, **35** (9), p: 780.

89. Harris, L. G., and Richards, R. G., Staphylococci and Implant Surfaces: A Review, *Injury*, 2006, **37** (2, Supplement), p: S3.

90. Dunne, W. M., Bacterial Adhesion: Seen Any Good Biofilms Lately?, *Clinical Microbiology Reviews*, 2002, **15** (2), p: 155.

91. Jahoda, D., Nyc, O., Pokorny, D., Landor, I., and Sosna, A., Antibiotic Treatment for Prevention of Infectious Complications in Joint Replacement, *Acta Chir Orthop Traumatol Cech*, 2006, **73** (2), p: 108.

92. Engesaeter, L. B., Lie, S. A., Espehaug, B., Furnes, O., Vollset, S. E., and Havelin, L. I., Antibiotic Prophylaxis in Total Hip Arthroplasty: Effects of Antibiotic Prophylaxis Systemically and in Bone Cement on the Revision Rate of 22,170 Primary Hip Replacements Followed 0-14 Years in the Norwegian Arthroplasty Register, *Acta Orthop Scand*, 2003, **74** (6), p: 644.

93. Alt, V., Bitschnau, A., Österling, J., Sewing, A., Meyer, C., Kraus, R., Meissner, S. A., Wenisch, S., Domann, E., and Schnettler, R., The Effects of Combined Gentamicin–Hydroxyapatite Coating for Cementless Joint Prostheses on the Reduction of Infection Rates in a Rabbit Infection Prophylaxis Model, *Biomaterials*, 2006, **27** (26), p: 4627.

94. Radin, S., Campbell, J. T., Ducheyne, P., and Cuckler, J. M., Calcium Phosphate Ceramic Coatings as Carriers of Vancomycin, *Biomaterials*, 1997, **18** (11), p: 777.

95. Yamamura, K., Iwata, H., and Yotsuyanagi, T., Synthesis of Antibiotic-Loaded Hydroxyapatite Beads and in Vitro Drug Release Testing, *Journal of Biomedical Materials Research*, 1992, **26** (8), p: 1053.

96. Stigter, M., Bezemer, J., de Groot, K., and Layrolle, P., Incorporation of Different Antibiotics into Carbonated Hydroxyapatite Coatings on Titanium Implants, Release and Antibiotic Efficacy, *Journal of Controlled Release*, 2004, **99** (1), p: 127.

97. Stigter, M., de Groot, K., and Layrolle, P., Incorporation of Tobramycin into Biomimetic Hydroxyapatite Coating on Titanium, *Biomaterials*, 2002, **23** (20), p: 4143.

98. Radin, S., and Ducheyne, P., Controlled Release of Vancomycin from Thin Sol–Gel Films on Titanium Alloy Fracture Plate Material, *Biomaterials*, 2007, **28** (9), p: 1721.

99. Wahlig, H., and Dingeldein, E., Antibiotics and Bone Cements: Experimental and Clinical Long-Term Observations, *Acta Orthopaedica*, 1980, **51** (1-6), p: 49.

100. Ince, A., Schutze, N., Hendrich, C., Jakob, F., Eulert, J., and Lohr, J. F., Effect of Polyhexanide and Gentamycin on Human Osteoblasts and Endothelial Cells, *Swiss Med Wkly*, 2007, **137** (9-10), p: 139.

101. Naal, F., Salzmann, G., von Knoch, F., Tuebel, J., Diehl, P., Gradinger, R., and Schauwecker, J., The Effects of Clindamycin on Human Osteoblasts in Vitro, *Archives of Orthopaedic and Trauma Surgery*, 2008, **128** (3), p: 317.

102. Campbell, A. A., Song, L., Li, X. S., Nelson, B. J., Bottoni, C., Brooks, D. E., and DeJong, E. S., Development, Characterization, and Anti-Microbial Efficacy of Hydroxyapatite-Chlorhexidine Coatings Produced by Surface-Induced Mineralization, *Journal of Biomedical Materials Research*, 2000, **53** (4), p: 400.

103. Darouiche, R. O., Green, G., and Mansouri, M. D., Antimicrobial Activity of Antiseptic-Coated Orthopaedic Devices, *International Journal of Antimicrobial Agents*, 1998, **10** (1), p: 83.

104. Berger, T. J., Spadaro, J. A., Chapin, S. E., and Becker, R. O., Electrically Generated Silver Ions: Quantitative Effects on Bacterial and Mammalian Cells, *Antimicrobial agents and chemotherapy*, 1976, **9** (2), p: 357.

105. Melaiye, A., and Youngs, W. J., Silver and Its Application as an Antimicrobial Agent, *Expert Opinion on Therapeutic Patents*, 2005, **15** (2), p: 125.

106. Li, J. X., Wang, J., Shen, L. R., Xu, Z. J., Li, P., Wan, G. J., and Huang, N., The Influence of Polyethylene Terephthalate Surfaces Modified by Silver Ion Implantation on Bacterial Adhesion Behavior, *Surface and Coatings Technology*, 2007, **201** (19–20), p: 8155.

107. Percival, S. L., Bowler, P. G., and Russell, D., Bacterial Resistance to Silver in Wound Care, *Journal of Hospital Infection*, 2005, **60** (1), p: 1.

108. Bosetti, M., Massè, A., Tobin, E., and Cannas, M., Silver Coated Materials for External Fixation Devices: In Vitro Biocompatibility and Genotoxicity, *Biomaterials*, 2002, **23** (3), p: 887.

109. Hardes, J., Ahrens, H., Gebert, C., Streitbuerger, A., Buerger, H., Erren, M., Gunsel, A., Wedemeyer, C., Saxler, G., Winkelmann, W., and Gosheger, G., Lack of Toxicological Side-Effects in Silver-Coated Megaprostheses in Humans, *Biomaterials*, 2007, **28** (18), p: 2869.

110. Gosheger, G., Hardes, J., Ahrens, H., Streitburger, A., Buerger, H., Erren, M., Gunsel, A., Kemper, F. H., Winkelmann, W., and von Eiff, C., Silver-Coated Megaendoprostheses in a Rabbit Model—an Analysis of the Infection Rate and Toxicological Side Effects, *Biomaterials*, 2004, **25** (24), p: 5547.

111. Kim, J., Pitts, B., Stewart, P. S., Camper, A., and Yoon, J., Comparison of the Antimicrobial Effects of Chlorine, Silver Ion, and Tobramycin on Biofilm, *Antimicrobial agents and chemotherapy*, 2008, **52** (4), p: 1446.

112. Silver, S., Bacterial Silver Resistance: Molecular Biology and Uses and Misuses of Silver Compounds, *FEMS Microbiology Reviews*, 2003, **27** (2-3), p: 341.

113. Hussain, S. M., Hess, K. L., Gearhart, J. M., Geiss, K. T., and Schlager, J. J., In Vitro Toxicity of Nanoparticles in Brl 3a Rat Liver Cells, *Toxicology in Vitro*, 2005, **19** (7), p: 975.

114. Burd, A., Kwok, C. H., Hung, S. C., Chan, H. S., Gu, H., Lam, W. K., and Huang, L., A Comparative Study of the Cytotoxicity of Silver-Based Dressings in Monolayer Cell, Tissue Explant, and Animal Models, *Wound Repair and Regeneration*, 2007, **15** (1), p: 94.

115. Kim, Y. S., Song, M. Y., Park, J. D., Song, K. S., Ryu, H. R., Chung, Y. H., Chang, H. K., Lee, J. H., Oh, K. H., Kelman, B. J., Hwang, I. K., and Yu, I. J., Subchronic Oral Toxicity of Silver Nanoparticles, *Part Fibre Toxicol*, 2010, **7**, p: 20.

116. Gallardo-Moreno, A. M., Pacha-Olivenza, M. A., Saldaña, L., Pérez-Giraldo, C., Bruque, J. M., Vilaboa, N., and González-Martín, M. L., In Vitro Biocompatibility and Bacterial Adhesion of Physico-Chemically Modified Ti6al4v Surface by Means of Uv Irradiation, *Acta Biomaterialia*, 2009, **5** (1), p: 181.

117. Del Curto, B., Brunella, M. F., Giordano, C., Pedeferri, M. P., Valtulina, V., Visai, L., and Cigada, A., Decreased Bacterial Adhesion to Surface-Treated Titanium, *Int J Artif Organs*, 2005, **28** (7), p: 718.

118. Zhang, F., Zhang, Z., Zhu, X., Kang, E.-T., and Neoh, K.-G., Silk-Functionalized Titanium Surfaces for Enhancing Osteoblast Functions and Reducing Bacterial Adhesion, *Biomaterials*, 2008, **29** (36), p: 4751.

119. Harris, L. G., Tosatti, S., Wieland, M., Textor, M., and Richards, R. G., Staphylococcus Aureus Adhesion to Titanium Oxide Surfaces Coated with Non-Functionalized and Peptide-Functionalized Poly(L-Lysine)-Grafted-Poly(Ethylene Glycol) Copolymers, *Biomaterials*, 2004, **25** (18), p: 4135.

120. Saldarriaga Fernández, I. C., Mei, H. C., Metzger, S., Grainger, D. W., Engelsman, A. F., Nejadnik, M. R., and Busscher, H. J., In Vitro and in Vivo Comparisons of Staphylococcal Biofilm Formation on a Cross-Linked Poly (Ethylene Glycol)-Based Polymer Coating, *Acta biomaterialia*, 2010, **6** (3), p: 1119.

121. Singla, A. K., and Chawla, M., Chitosan: Some Pharmaceutical and Biological Aspects - an Update, *Journal of Pharmacy and Pharmacology*, 2001, **53** (8), p: 1047.

122. Muzzarelli, R., Tarsi, R., Filippini, O., Giovanetti, E., Biagini, G., and Varaldo, P. E., Antimicrobial Properties of N-Carboxybutyl Chitosan, *Antimicrobial agents and chemotherapy*, 1990, **34** (10), p: 2019.

123. Pitt, W. G., Morris, R. N., Mason, M. L., Hall, M. W., Luo, Y., and Prestwich, G. D., Attachment of Hyaluronan to Metallic Surfaces, *Journal of Biomedical Materials Research Part A*, 2004, **68A** (1), p: 95.

124. Kim, I.-Y., Seo, S.-J., Moon, H.-S., Yoo, M.-K., Park, I.-Y., Kim, B.-C., and Cho, C.-S., Chitosan and Its Derivatives for Tissue Engineering Applications, *Biotechnology Advances*, 2008, **26** (1), p: 1.

125. Wilson, L. H., Schumacher, J. F., Finlay, J. A., Perry, R., Callow, M. E., Callow, J. A., and Brennan, A. B., Towards Minimally Fouling Substrates: Surface Grafting and Topography, *Polymer Preprints*, 2005, **46** (2), p: 1312.

126. Sullivan, T., and Regan, F., The Characterization, Replication and Testing of Dermal Denticles of Scyliorhinus Canicula for Physical Mechanisms of Biofouling Prevention, *Bioinspiration & biomimetics*, 2011, **6** (4), p: 046001.

127. Chung, K. K., Schumacher, J. F., Sampson, E. M., Burne, R. A., Antonelli, P. J., and Brennan, A. B., Impact of Engineered Surface Microtopography on Biofilm Formation of Staphylococcus Aureus, *Biointerphases*, 2007, **2** (2), p: 89.

128. Hou, S., Gu, H., Smith, C., and Ren, D., Microtopographic Patterns Affect Escherichia Coli Biofilm Formation on Poly (Dimethylsiloxane) Surfaces, *Langmuir*, 2011, **27** (6), p: 2686.

129. Bers, A. V., and Wahl, M., The Influence of Natural Surface Microtopographies on Fouling, *Biofouling*, 2004, **20** (1), p: 43.

130. Costerton, J. W., Ellis, B., Lam, K., Johnson, F., and Khoury, A. E., Mechanism of Electrical Enhancement of Efficacy of Antibiotics in Killing Biofilm Bacteria, *Antimicrobial agents and chemotherapy*, 1994, **38** (12), p: 2803.

131. Wellman, N., Fortun, S. M., and McLeod, B. R., Bacterial Biofilms and the Bioelectric Effect, *Antimicrobial Agents and Chemotherapy*, 1996, **40** (9), p: 2012.

132. Stoodley, P., DeBeer, D., and Lappin-Scott, H. M., Influence of Electric Fields and Ph on Biofilm Structure as Related to the Bioelectric Effect, *Antimicrobial Agents and Chemotherapy*, 1997, **41** (9), p: 1876.

133. Khoury, A. E., Lam, K., Ellis, B., and COSTERTON, J. W., Prevention and Control of Bacterial Infections Associated with Medical Devices, *ASAIO journal*, 1992, **38** (3), p: 174.

134. Stewart, P. S., Wattanakaroon, W., Goodrum, L., Fortun, S. M., and McLeod, B. R., Electrolytic Generation of Oxygen Partially Explains Electrical Enhancement of Tobramycin Efficacy against Pseudomonas Aeruginosa Biofilm, *Antimicrobial Agents and Chemotherapy*, 1999, **43** (2), p: 292.

135. Kim, Y. W., Ben-Yoav, H., Wu, H. C., Quan, D., Carter, K., Meyer, M. T., Bentley, W. E., and Ghodssi, R. An Enhanced Bacterial Biofilm Treatment Using Superpositioned Electric Field, in *The 7th International Conference on Microtechnologies in Medicine and Biology (MMB)*, Year, Marina del Rey, CA, p: 102.

136. Kim, Y. W., Mosteller, M. P., Meyer, M. T., Ben-Yoav, H., Bentley, W. E., and Ghodssi, R. Microfluidic Biofilm Observation, Analysis, and Treatment (Micro-Boat) Platform, in *Hilton Head Workshop 2012: A Solid-State Sensors, Actuators and Microsystems Workshop*, Year, Hilton Head, SC, p: 233.

137. Geske, G. D., Wezeman, R. J., Siegel, A. P., and Blackwell, H. E., Small Molecule Inhibitors of Bacterial Quorum Sensing and Biofilm Formation, *Journal of the American Chemical Society*, 2005, **127** (37), p: 12762.

138. Junker, L. M., and Clardy, J., High-Throughput Screens for Small-Molecule Inhibitors of Pseudomonas Aeruginosa Biofilm Development, *Antimicrobial agents and chemotherapy*, 2007, **51** (10), p: 3582.

139. Christensen, L. D., van Gennip, M., Jakobsen, T. H., Alhede, M., Hougen, H. P., Høiby, N., Bjarnsholt, T., and Givskov, M., Synergistic Antibacterial Efficacy of Early Combination Treatment with Tobramycin and Quorum-Sensing Inhibitors against Pseudomonas Aeruginosa in an Intraperitoneal Foreign-Body Infection Mouse Model, *Journal of Antimicrobial Chemotherapy*, 2012, p: dks002.

140. Brackman, G., Cos, P., Maes, L., Nelis, H. J., and Coenye, T., Quorum Sensing Inhibitors Increase the Susceptibility of Bacterial Biofilms to Antibiotics in Vitro and in Vivo, *Antimicrobial agents and chemotherapy*, 2011, **55** (6), p: 2655.

141. Roy, V., Meyer, M. T., Smith, J. A. I., Gamby, S., Sintim, H. O., Ghodssi, R., and Bentley, W. E., Ai-2 Analogs and Antibiotics: A Synergistic Approach to Reduce Bacterial Biofilms, *Applied Microbiology and Biotechnology*, 2013, **97** (6), p: 2627.

142. Lowery, C. A., Abe, T., Park, J., Eubanks, L. M., Sawada, D., Kaufmann, G. F., and Janda, K. D., Revisiting Ai-2 Quorum Sensing Inhibitors: Direct Comparison of Alkyl-Dpd Analogues and a Natural Product Fimbrolide, *Journal of the American Chemical Society*, 2009, **131** (43), p: 15584.

143. Roy, V., Smith, J. A., Wang, J., Stewart, J. E., Bentley, W. E., and Sintim, H. O., Synthetic Analogs Tailor Native Ai-2 Signaling across Bacterial Species, *Journal of the American Chemical Society*, 2010, **132** (32), p: 11141.

144. Smith, J. A., Wang, J., Nguyen-Mau, S.-M., Lee, V., and Sintim, H. O., Biological Screening of a Diverse Set of Ai-2 Analogues in Vibrio Harveyi Suggests That Receptors Which Are Involved in Synergistic Agonism of Ai-2 and Analogues Are Promiscuous, *Chemical Communications*, 2009, (45), p: 7033.

145. Gamby, S., Roy, V., Guo, M., Smith, J. A., Wang, J., Stewart, J. E., Wang, X., Bentley, W. E., and Sintim, H. O., Altering the Communication Networks of Multispecies Microbial Systems Using a Diverse Toolbox of Ai-2 Analogues, *ACS Chemical Biology*, 2012, **7** (6), p: 1023.

146. Goeres, D. M., Loetterle, L. R., Hamilton, M. A., Murga, R., Kirby, D. W., and Donlan, R. M., Statistical Assessment of a Laboratory Method for Growing Biofilms, *Microbiology*, 2005, **151** (3), p: 757.

147. Jing, G., Polaczyk, A., Oerther, D. B., and Papautsky, I., Development of a Microfluidic Biosensor for Detection of Environmental Mycobacteria, *Sensors and Actuators B: Chemical*, 2007, **123** (1), p: 614.

148. Richter, L., Stepper, C., Mak, A., Reinthaler, A., Heer, R., Kast, M., Brückl, H., and Ertl, P., Development of a Microfluidic Biochip for Online Monitoring of Fungal Biofilm Dynamics, *Lab on a Chip*, 2007, **7** (12), p: 1723.

149. Zhang, C., Xu, J., Ma, W., and Zheng, W., Pcr Microfluidic Devices for DNA Amplification, *Biotechnology advances*, 2006, **24** (3), p: 243.

150. Jesús-Pérez, N. M., and Lapizco-Encinas, B. H., Dielectrophoretic Monitoring of Microorganisms in Environmental Applications, *ELECTROPHORESIS*, 2011, **32** (17), p: 2331.

151. Melin, J., and Quake, S. R., Microfluidic Large-Scale Integration: The Evolution of Design Rules for Biological Automation, *Annu. Rev. Biophys. Biomol. Struct.*, 2007, **36**, p: 213.

152. Studer, V., Hang, G., Pandolfi, A., Ortiz, M., Anderson, W. F., and Quake, S. R., Scaling Properties of a Low-Actuation Pressure Microfluidic Valve, *Journal of Applied Physics*, 2004, **95** (1), p: 393.

153. Thorsen, T., Maerkl, S. J., and Quake, S. R., Microfluidic Large-Scale Integration, *Science*, 2002, **298** (5593), p: 580.

154. Kim, Y. W., Sardari, S. E., Meyer, M. T., Iliadis, A. A., Wu, H. C., Bentley, W. E., and Ghodssi, R., An Ald Aluminum Oxide Passivated Surface Acoustic Wave Sensor for Early Biofilm Detection, *Sensors and Actuators B: Chemical*, 2012, **163** (1), p: 136.

155. Stepanović, S., Vuković, D., Dakić, I., Savić, B., and Švabić-Vlahović, M., A Modified Microtiter-Plate Test for Quantification of Staphylococcal Biofilm Formation, *Journal of Microbiological Methods*, 2000, **40** (2), p: 175.

156. Kueng, W., Silber, E., and Eppenberger, U., Quantification of Cells Cultured on 96-Well Plates, *Analytical Biochemistry*, 1989, **182** (1), p: 16.

157. Janakiraman, V., Englert, D., Jayaraman, A., and Baskaran, H., Modeling Growth and Quorum Sensing in Biofilms Grown in Microfluidic Chambers, *Annals of Biomedical Engineering*, 2009, **37** (6), p: 1206.

158. Swope, K. L., and Flickinger, M. C., The Use of Confocal Scanning Laser Microscopy and Other Tools to Characterize Escherichia Coli in a High−Cell−Density Synthetic Biofilm, *Biotechnology and bioengineering*, 1996, **52** (2), p: 340.

159. Heydorn, A., Nielsen, A. T., Hentzer, M., Sternberg, C., Givskov, M., Ersbøll, B. K., and Molin, S., Quantification of Biofilm Structures by the Novel Computer Program Comstat, *Microbiology*, 2000, **146** (10), p: 2395.

160. Janknecht, P., and Melo, L. F., Online Biofilm Monitoring, *Reviews in Environmental Science and Biotechnology*, 2003, **2** (2-4), p: 269.

161. Zikmund, A., Ripka, P., Krasny, L., Judl, T., and Jahoda, D. Biofilm Detection by the Impedance Method, in *Biomedical Engineering and Informatics (BMEI), 2010 3rd International Conference on*, Year, p: 1432.

162. Oliver, L. M., Dunlop, P. S. M., Byrne, J. A., Blair, I. S., Boyle, M., McGuigan, K. G., and McAdams, E. T. An Impedimetric Sensor for Monitoring the Growth of Staphylococcus Epidermidis, in *Engineering in Medicine and Biology Society, 2006. EMBS '06. 28th Annual International Conference of the IEEE*, Year, p: 535.

163. Muñoz-Berbel, X., Muñoz, F. J., Vigués, N., and Mas, J., On-Chip Impedance Measurements to Monitor Biofilm Formation in the Drinking Water

Distribution Network, *Sensors and Actuators B: Chemical*, 2006, **118** (1–2), p: 129.

164. Tamachkiarow, A., and Flemming, H., On-Line Monitoring of Biofilm Formation in a Brewery Water Pipeline System with a Fibre Optical Device, *Water Science & Technology*, 2003, **47** (5), p: 19.

165. Bakke, R., Kommedal, R., and Kalvenes, S., Quantification of Biofilm Accumulation by an Optical Approach, *Journal of Microbiological Methods*, 2001, **44** (1), p: 13.

166. Meyer, M. T., Roy, V., Bentley, W. E., and Ghodssi, R., Development and Validation of a Microfluidic Reactor for Biofilm Monitoring Via Optical Methods, *Journal of Micromechanics and Microengineering*, 2011, **21** (5), p: 054023.

167. Subramanian, S., Kim, Y. W., Meyer, M. T., Sintim, H. O., Bentley, W. E., and Ghodssi, R. A Real-Time Bacterial Biofilm Characterization Platform Using a Microfluidic System, in *Hilton Head Workshop 2014: A Solid-State Sensors, Actuators and Microsystems Workshop*, Year, Hilton Head, SC, p: 163.

168. Kim, K. P., Kim, Y.-G., Choi, C.-H., Kim, H.-E., Lee, S.-H., Chang, W.-S., and Lee, C.-S., In Situ Monitoring of Antibiotic Susceptibility of Bacterial Biofilms in a Microfluidic Device, *Lab on a Chip*, 2010, **10** (23), p: 3296.

169. Paredes, J., Becerro, S., and Arana, S., Label-Free Interdigitated Microelectrode Based Biosensors for Bacterial Biofilm Growth Monitoring Using Petri Dishes, *Journal of Microbiological Methods*, 2014, (0), p.

170. Kim, J., Hegde, M., Kim, S. H., Wood, T. K., and Jayaraman, A., A Microfluidic Device for High Throughput Bacterial Biofilm Studies, *Lab on a Chip*, 2012, **12** (6), p: 1157.

171. Radke, S. M., and Alocilja, E. C., Design and Fabrication of a Microimpedance Biosensor for Bacterial Detection, *Sensors Journal, IEEE*, 2004, **4** (4), p: 434.

172. Brady, R. A., Leid, J. G., Camper, A. K., Costerton, J. W., and Shirtliff, M. E., Identification of Staphylococcus Aureus Proteins Recognized by the Antibody-Mediated Immune Response to a Biofilm Infection, *Infection and immunity*, 2006, **74** (6), p: 3415.

173. Meyer, M. T., Design and Implementation of Microfluidic Systems for Bacterial Biofilm Monitoring and Manipulation, in *Department of Bioengineering*2014, University of Maryland, College Park, MD.

174. Kim, Y. W., An Integrated Microsystem for Biofilm Detection and Treatment in *Department of Electrical and Computer Engineering*2014, University of Maryland, College Park, MD.

175. Kim, Y. W., Meyer, M. T., Berkovich, A., Subramanian, S., Iliadis, A. A., Bentley, W. E., and Ghodssi, R., A Surface Acoustic Wave Biofilm Sensor Integrated with a Treatment Method Based on the Bioelectric Effect, *Sensors and Actuators A: Physical*, 2016, **238**, p: 140.

176. Paredes, J., Becerro, S., Arizti, F., Aguinaga, A., Del Pozo, J. L., and Arana, S., Interdigitated Microelectrode Biosensor for Bacterial Biofilm Growth

Monitoring by Impedance Spectroscopy Technique in 96-Well Microtiter Plates, *Sensors and Actuators B: Chemical*, 2013, **178** (0), p: 663.

177. Roberts, B. W., and Olbricht, W. L., The Distribution of Freely Suspended Particles at Microfluidic Bifurcations, *AIChE Journal*, 2006, **52** (1), p: 199.

178. Meyer, M. T., Subramanian, S., Kim, Y. W., Ben-Yoav, H., Gnerlich, M., Bentley, W. E., and Ghodssi, R., Multi-Depth Valved Microfluidics for Biofilm Segmentation, *Journal of Micromechanics and Microengineering*, 2015, **25**, p: 095003.

179. Yang, L., and Bashir, R., Electrical/Electrochemical Impedance for Rapid Detection of Foodborne Pathogenic Bacteria, *Biotechnology Advances*, 2008, **26** (2), p: 135.

180. Gómez, R., Bashir, R., and Bhunia, A. K., Microscale Electronic Detection of Bacterial Metabolism, *Sensors and Actuators B: Chemical*, 2002, **86** (2–3), p: 198.

181. Yang, L., Ruan, C., and Li, Y., Detection of Viable Salmonella Typhimurium by Impedance Measurement of Electrode Capacitance and Medium Resistance, *Biosensors and Bioelectronics*, 2003, **19** (5), p: 495.

182. Yang, L., Li, Y., Griffis, C. L., and Johnson, M. G., Interdigitated Microelectrode (Ime) Impedance Sensor for the Detection of Viable Salmonella Typhimurium, *Biosensors and Bioelectronics*, 2004, **19** (10), p: 1139.

183. Varshney, M., and Li, Y., Double Interdigitated Array Microelectrode-Based Impedance Biosensor for Detection of Viable Escherichia Coli O157:H7 in Growth Medium, *Talanta*, 2008, **74** (4), p: 518.

184. Kim, T., Kang, J., Lee, J.-H., and Yoon, J., Influence of Attached Bacteria and Biofilm on Double-Layer Capacitance During Biofilm Monitoring by Electrochemical Impedance Spectroscopy, *Water Research*, 2011, **45** (15), p: 4615.

185. Kim, S., Yu, G., Kim, T., Shin, K., and Yoon, J., Rapid Bacterial Detection with an Interdigitated Array Electrode by Electrochemical Impedance Spectroscopy, *Electrochimica Acta*, 2012, **82**, p: 126.

186. Winkler, T. E., Ben-Yoav, H., Kelly, D. L., and Ghodssi, R. Microsystem for Particle Counting and Sizing with Tunable Sensitivity and Throughput, in *Hilton Head Workshop 2014: A Solid-State Sensors, Actuators and Microsystems Workshop*, Year, Hilton Head, SC, p: 233.

187. Zang, F., Fan, X. Z., Gerasopoulos, K., Naves, L., Culver, J., and Ghodssi, R. A Nanostructured Impedance Microsensor for the Real-Time Monitoring of Macromolecular Assembly and Elisa-on-a-Chip, in *Hilton Head Workshop 2014: A Solid-State Sensors, Actuators and Microsystems Workshop*, Year, Hilton Head, SC, p: 233.

188. Fan, X. Z., Naves, L., Siwak, N. P., Brown, A., Culver, J., and Ghodssi, R. Virus-Like-Particles for Next Generation Micro/Nano-Biosensors, in *Hilton Head Workshop 2014: A Solid-State Sensors, Actuators and Microsystems Workshop*, Year, Hilton Head, SC, p: 233.

189. Kim, Y. W., Meyer, M. T., Berkovich, A., Iliadis, A. A., Bentley, W. E., and Ghodssi, R. An Integrated Microsystem for Bacterial Biofilm Detection and Treatment, in *The 17th International Conference on Miniaturized Systems for Chemistry and Life Sciences (MicroTAS)*, Year, Freiburg, Germany, p.

190. Pareilleux, A., and Sicard, N., Lethal Effects of Electric Current on Escherichia Coli, *Applied microbiology*, 1970, **19** (3), p: 421.

191. Blenkinsopp, S. A., Khoury, A., and Costerton, J., Electrical Enhancement of Biocide Efficacy against Pseudomonas Aeruginosa Biofilms, *Applied and Environmental Microbiology*, 1992, **58** (11), p: 3770.

192. Caubet, R., Pedarros-Caubet, F., Chu, M., Freye, E., de Belem Rodrigues, M., Moreau, J., and Ellison, W., A Radio Frequency Electric Current Enhances Antibiotic Efficacy against Bacterial Biofilms, *Antimicrobial Agents and Chemotherapy*, 2004, **48** (12), p: 4662.

193. Shirtliff, M. E., Bargmeyer, A., and Camper, A. K., Assessment of the Ability of the Bioelectric Effect to Eliminate Mixed-Species Biofilms, *Applied and Environmental Microbiology*, 2005, **71** (10), p: 6379.

194. Del Pozo, J. L., Rouse, M. S., Euba, G., Kang, C.-I., Mandrekar, J. N., Steckelberg, J. M., and Patel, R., The Electricidal Effect Is Active in an Experimental Model of Staphylococcus Epidermidis Chronic Foreign Body Osteomyelitis, *Antimicrobial agents and chemotherapy*, 2009, **53** (10), p: 4064.

195. Del Pozo, J. L., Rouse, M. S., Mandrekar, J. N., Sampedro, M. F., Steckelberg, J. M., and Patel, R., Effect of Electrical Current on the Activities

of Antimicrobial Agents against Pseudomonas Aeruginosa, Staphylococcus Aureus, and Staphylococcus Epidermidis Biofilms, *Antimicrobial agents and chemotherapy*, 2008, **53** (1), p: 35.

196. Del Pozo, J. L., Rouse, M. S., Mandrekar, J. N., Steckelberg, J. M., and Patel, R., The Electricidal Effect: Reduction of Staphylococcus and Pseudomonas Biofilms by Prolonged Exposure to Low-Intensity Electrical Current, *Antimicrobial agents and chemotherapy*, 2009, **53** (1), p: 41.

197. Giladi, M., Porat, Y., Blatt, A., Shmueli, E., Wasserman, Y., Kirson, E. D., and Palti, Y., Microbial Growth Inhibition by Alternating Electric Fields in Mice with Pseudomonas Aeruginosa Lung Infection, *Antimicrobial Agents and Chemotherapy*, 2010, **54** (8), p: 3212.

198. Sandvik, E. L., McLeod, B. R., Parker, A. E., and Stewart, P. S., Direct Electric Current Treatment under Physiologic Saline Conditions Kills Staphylococcus Epidermidis Biofilms Via Electrolytic Generation of Hypochlorous Acid, *PloS one*, 2013, **8** (2), p: e55118.

199. Del Pozo, J. L., Rouse, M. S., and Patel, R., Bioelectric Effect and Bacterial Biofilms. A Systematic Review, *The International journal of artificial organs*, 2008, **31** (9), p: 786.

200. Van Der Borden, A. J., Van Der Werf, H., Van Der Mei, H. C., and Busscher, H. J., Electric Current-Induced Detachment of Staphylococcus Epidermidis Biofilms from Surgical Stainless Steel, *Applied and Environmental Microbiology*, 2004, **70** (11), p: 6871.

201. Wang, L., Li, J., March, J. C., Valdes, J. J., and Bentley, W. E., Luxs-Dependent Gene Regulation in Escherichia Coli K-12 Revealed by Genomic Expression Profiling, *Journal of Bacteriology*, 2005, **187** (24), p: 8350.

202. Lathi, B. P., Modern Digital and Analog Communication Systems, (Issue), 1990, Oxford University Press, Inc.

203. Kim, Y. W., Subramanian, S., Gerasopoulos, K., Ben-Yoav, H., Wu, H.-C., Quan, D., Carter, K., Meyer, M. T., Bentley, W. E., and Ghodssi, R., Effect of Electrical Energy on the Efficacy of Biofilm Treatment Using the Bioelectric Effect, *Npj Biofilms and Microbiomes*, 2015, **1** (15016), p.

204. Gyurova, A. Y., and Zhivkov, A. M., Influence of the Medium Electrolyte Concentration on the Electric Polarizability of Bacteria Escherichia Coli in Presence of Ethanol, *Colloids and Surfaces B: Biointerfaces*, 2009, **74** (1), p: 23.

205. Bockris, J. O. M., and Reddy, A. K., Modern Electrochemistry, 2000, Kluwer Acadamic/Plenum Publishers, New York.

206. Zwietering, M., De Koos, J., Hasenack, B., De Witt, J., and Van't Riet, K., Modeling of Bacterial Growth as a Function of Temperature, *Applied and Environmental Microbiology*, 1991, **57** (4), p: 1094.

207. Jass, J., Costerton, J., and Lappin-Scott, H., The Effect of Electrical Currents and Tobramycin on Pseudomonas Aeruginosa Biofilms, *Journal of industrial microbiology*, 1995, **15** (3), p: 234.

208. Jass, J., and Lappin-Scott, H. M., The Efficacy of Antibiotics Enhanced by Electrical Currents against Pseudomonas Aeruginosa Biofilms, *Journal of Antimicrobial Chemotherapy*, 1996, **38** (6), p: 987.

209. Freebairn, D., Linton, D., Harkin-Jones, E., Jones, D. S., Gilmore, B. F., and Gorman, S. P., Electrical Methods of Controlling Bacterial Adhesion and Biofilm on Device Surfaces, *Expert review of medical devices*, 2013, **10** (1), p: 85.

210. Toté, K., Berghe, D. V., Maes, L., and Cos, P., A New Colorimetric Microtitre Model for the Detection of Staphylococcus Aureus Biofilms, *Letters in Applied Microbiology*, 2008, **46** (2), p: 249.

211. Paredes, J., Becerro, S., Arizti, F., Aguinaga, A., Del Pozo, J. L., and Arana, S., Real Time Monitoring of the Impedance Characteristics of Staphylococcal Bacterial Biofilm Cultures with a Modified Cdc Reactor System, *Biosensors and Bioelectronics*, 2012, **38** (1), p: 226.

212. Di Biasio, A., and Cametti, C., On the Dielectric Relaxation of Biological Cell Suspensions: The Effect of the Membrane Electrical Conductivity, *Colloids and Surfaces B: Biointerfaces*, 2011, **84** (2), p: 433.

213. Asami, K., Characterization of Heterogeneous Systems by Dielectric Spectroscopy, *Progress in Polymer Science*, 2002, **27** (8), p: 1617.

214. Cametti, C., Dielectric and Conductometric Properties of Highly Heterogeneous Colloidal Systems, 2009, p.

215. Asami, K., Hanai, T., and KoIzumi, N., Dielectric Analysis of Escherichia Coli Suspensions in the Light of the Theory of Interfacial Polarization, *Biophysical journal*, 1980, **31** (2), p: 215.

216. Park, S., Zhang, Y., Wang, T.-H., and Yang, S., Continuous Dielectrophoretic Bacterial Separation and Concentration from Physiological Media of High Conductivity, *Lab on a Chip*, 2011, **11** (17), p: 2893.

217. Korth, B., Rosa, L. F., Harnisch, F., and Picioreanu, C., A Framework for Modeling Electroactive Microbial Biofilms Performing Direct Electron Transfer, *Bioelectrochemistry*, 2015, p.

218. Wu, J., Lian, M., and Yang, K., Micropumping of Biofluids by Alternating Current Electrothermal Effects, *Applied Physics Letters*, 2007, **90** (23), p: 234103.

219. Subramanian, S., Gerasopoulos, K., Sintim, H. O., Bentley, W. E., and Ghodssi, R. A Bacterial Biofilm Combination Treatment Using a Real-Time Microfluidic Platform, in *The 18th International Conference on Solid-State Sensors, Actuators and Microsystems (Transducers)*, Year, Anchorage, AK, p: 2216.

220. Kim, Y. W., Mosteller, M. P., Subramanian, S., Meyer, M. T., Bentley, W. E., and Ghodssi, R., An Optical Microfluidic Platform for Spatiotemporal Biofilm Treatment Monitoring, *Journal of Micromechanics and Microengineering*, 2016, **26** (1), p: 015013.